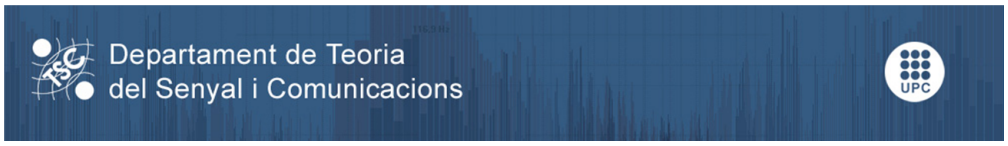

Design and implementation of low complexity adaptive optical OFDM systems for software-defined transmission in elastic optical networks

Ph.D. Thesis dissertation

By

Laia Nadal Reixats

Submitted to the Universitat Politècnica de Catalunya (UPC)

in partial fulfillment of the requirements for the degree of

DOCTOR OF PHILOSOPHY

Barcelona, September 2014

Supervised by Dr. Michela Svaluto Moreolo

Tutor: Gabriel Junyent Giralt

PhD program on Signal Theory and Communications

Abstract

Due to the increasing global IP traffic and the exponential growing demand for broadband services, optical networks are experimenting significant changes. Advanced modulation formats are being implemented at the Digital Signal Processing (DSP) level as key enablers for high data rate transmission. Whereas in the network layer, flexi Dense Wavelength-Division Multiplexing (DWDM) grids are being investigated in order to efficiently use the optical spectrum according to the traffic demand. Enabling these capabilities makes high data rate transmission more feasible. Hence, introducing flexibility in the system is one of the main goals of this thesis. Furthermore, minimizing the cost and enhancing the Spectral Efficiency (SE) of the system are two crucial issues to consider in the transceiver design.

This dissertation investigates the use of Optical Orthogonal Frequency Division Multiplexing (O-OFDM) based either on the Fast Fourier Transform (FFT) or the Fast Hartley Transform (FHT) and flexi-grid technology to allow high data rate transmission over the fiber. Different cost-effective solutions for Elastic Optical Networks (EON) are provided.

On the one hand, Direct Detection (DD) systems are investigated and proposed to cope with present and future traffic demand. After an introduction to the principles of OFDM and its application in optical systems, the main problems of such modulation is introduced. In particular, Peak-to-Average Power Ratio (PAPR) is presented as a limitation in OFDM systems, as well as clipping and quantization noise. Hence, PAPR reduction techniques are proposed to mitigate these impairments. Additionally, Low Complexity (LC) PAPR reduction techniques based on the FHT have also been presented with a simplified DSP.

On the other hand, loading schemes have also been introduced in the analyzed system to combat Chromatic Dispersion (CD) when transmitting over the optical link. Moreover, thanks to Bit Loading (BL) and Power Loading (PL), flexible and software-

defined transceivers can be implemented maximizing the spectral efficiency by adapting the data rate to the current demand and the actual network conditions. Specifically, OFDM symbols are created by mapping the different subcarriers with different modulation formats according to the channel profile. Experimental validation of the proposed flexible transceivers is also provided in this dissertation. The benefits of including loading capabilities in the design, such as enabling high data rate and software-defined transmission, are highlighted.

Resum

Degut al creixement del tràfic IP i de la demanda de serveis de banda ampla, les xarxes òptiques estan experimentant canvis significatius. Els formats avançats de modulació, implementats a nivell de processat del senyal digital, habiliten la transmissió a alta velocitat. Mentre que a la capa de xarxa, l'espectre òptic es dividit en ranures flexibles ocupant l'ample de banda necessari segons la demanda de tràfic. La transmissió a alta velocitat és fa més tangible un cop habilitades totes aquestes funcionalitats. D'aquesta manera un dels principals objectius d'aquesta tesis es introduir flexibilitat al sistema. A demés, minimitzar el cost i maximitzar l'eficiència espectral del sistema són també dos aspectes crucials a considerar en el disseny del transmissor i receptor.

Aquesta tesis investiga l'ús de la tecnologia Optical Orthogonal Frequency Division Multiplexing (OFDM) basada en la transformada de Fourier (FFT) i la de Hartley (FHT) per tal de dissenyar un sistema flexible i capaç de transmetre a alta velocitat a través de la fibra òptica. Per tant, es proposen diferent solucions de baix cost vàlides per a utilitzar en xarxes òptiques elàstiques.

En primer lloc, s'investiguen i es proposen sistemes basats en detecció directa per tal de suportar la present i futura demanda. Després d'una introducció dels principis d' OFDM i la seva aplicació als sistemes òptics, s'introdueixen alguns dels problemes d'aquesta modulació. En particular, es presenten el Peak-to-Average Power Ratio (PAPR) i els sorolls de clipping i de quantització com a limitació dels sistemes OFDM. S'analitzen tècniques de reducció de PAPR per tal de reduir l'impacte d'aquests impediments. També es proposen tècniques de baixa complexitat per a reduir el PAPR basades en la FHT.

Finalment, s'utilitzen algoritmes d'assignació de bits i de potència, Bit Loading (BL) i Power Loading (PL), per tal de combatre la dispersió cromàtica quan es transmet pel canal òptic. Amb la implementació dels algoritmes de BL i PL, es poden dissenyar transmissors i receptors flexibles adaptant la velocitat a la demanda del moment i a les

actuals condicions de la xarxa. En particular, els símbols OFDM es creen mapejant cada portadora amb un format de modulació diferent segons el perfil del canal. El sistema és validat experimentalment mostrant les prestacions i els beneficis d'incloure flexibilitat per tal de facilitar la transmissió a alta velocitat i cobrir les necessitats de l'Internet del futur.

Resumen

Debido al crecimiento del tráfico IP y de la demanda de servicios de banda ancha, las redes ópticas están experimentando cambios significativos. Los formatos avanzados de modulación, implementados a nivel de procesado de la señal digital, habilitan la transmisión a alta velocidad. Mientras que en la capa de red, el espectro óptico se divide en ranuras flexibles ocupando el ancho de banda necesario según la demanda de tráfico. La transmisión a alta velocidad es más tangible una vez habilitadas todas estas funcionalidades. De este modo uno de los principales objetivos de esta tesis es introducir flexibilidad en el sistema. Además, minimizar el coste y maximizar la eficiencia espectral del sistema son también dos aspectos cruciales a considerar en el diseño del transmisor y receptor.

Esta tesis investiga el uso de la tecnologia Optical Orthogonal Frequency Division Multiplexing (OFDM) basada en la transformada de Fourier (FFT) y en la de Hartley (FHT) con tal de diseñar un sistema flexible y capaz de transmitir a alta velocidad a través de la fibra óptica. Por lo tanto, se proponen distintas soluciones de bajo coste válidas para utilizar en redes ópticas elásticas.

En primer lugar, se investigan y se proponen sistemas basados en detección directa con tal de soportar la presente y futura demanda. Después de una introducción de los principios de OFDM y su aplicación en los sistemas ópticos, se introduce el principal problema de ésta modulación. En particular se presentan el Peak-to-Average Power Ratio (PAPR) y los ruidos de clipping y cuantización como limitaciones de los sistemas OFDM. Se analizan técnicas de reducción de PAPR con tal de reducir el impacto de estos impedimentos. También se proponen técnicas de baja complejidad para reducir el PAPR basadas en la FHT.

Finalmente, se utilizan algoritmos de asignación de bits y potencia, Bit Loading (BL) y Power Loading (PL), con tal de combatir la dispersión cromática cuando se transmite por el canal óptico. Con la implementación de los algoritmos de BL y PL, se

pueden diseñar transmisores y receptores flexibles adaptando la velocidad a la demanda del momento y a las actuales condiciones de la red. En particular, los símbolos OFDM se crean mapeando cada portadora con un formato de modulación distinto según el perfil del canal. El sistema se valida experimentalmente mostrando las prestaciones y los beneficios de incluir flexibilidad con tal de facilitar la transmisión a alta velocidad y cubrir las necesidades de Internet del futuro.

Acknowledgments

M'imagino 4 anys enrere i encara no em faig a la idea de que ja hagi arribat aquest dia. El dia en que estic escrivint els agraïments de la tesis. Semblava tan lluny i ja està aquí. El que hagi passat tot tan despresa només és una mostra dels bons anys y les bones experiències que he viscut fins arribar a aquest punt. És per això que voldria agrair a totes les persones que han estat al meu costat i han fet possible aquesta tesis.

Primer de tot vull agrair al CTTC i a tot el personal del centre el seu suport i l'ajuda que m'han oferit durant aquests anys, fent la meva estada al centre més còmoda i especial.

Voldria també agrair a la Michela Svaluto Moreolo, Gabriel Junyent i al Josep Maria Fàbrega per ajudar-me en tot moment. I també a tots els companys del grup d'òptica el Raül Muñoz, Ricard Vilalta, Ricardo Martínez, Ramón Casellas, Arturo Mayoral i Fco. Javier Vílchez.

Quiero agradecer en especial a mi directora de tesis, Michela Svaluto Moreolo, su apoyo y paciencia durante estos años, sin ella no hubiese podido realizar esta tesis. Pero sobre todo gracias por preocuparte siempre por mí.

Agrair també als meus companys i amics del despatx 109 per fer la meva estada al centre millor. Gràcies a: Pol Blasco per organitzar festes al terrat, Angelos Antonopoulos for your patience, Giuseppe Cocco to join the coffee team, Alessandro Acampora for your histories, Moises Espinosa por escucharnos, Vahid Joroughi for your kindness, Musbah Shaat for your advices, Jaime Ferragut per ajudar-nos a entendre millor el BOE, Ana María Galindo per animar-nos sempre i a Laura Martín, Maria Gregori i Jessica Moysen per la vostra amistat i bon humor.

I també gràcies a Miquel Calvo per informar-nos de tot :); gracias a Miguel Ángel Vázquez por tu ayuda; i gràcies a Anica Bukva, Kyriaki Niotaki, Iñaki Estella, Lazar Berbakov, Tatjana Predojev, Biljana Bojovic, Onur Tan, Konstantinos Ntontin, Andrea Bartoli, Daniel Sacristan i Javier Arribas .

Me gustaría agradecer también a Miguel Ángel Lagunas por hacer posible trabajar en el CTTC. También a Ana I. Pérez por haberme guiado al acabar la carrera.

Agradecer al Ministerio de Economia y Competitividad (MINECO), por haber financiado esta investigación.

Schließlich, Ich möchte mich bei Jansen Sander Lars, Michael Eiselt, Helmut Grieβer, Annika Dochman and Jörg-Peter Elbers für Ihre Hilfe wenn ich in ADVA optical networking wäre bedanken.

Moltes gràcies també a la meva família per haver-me ajudat sempre. Sobretot gràcies al meu pare, Julio Nadal, que sé que li hagués fet molta il.lusió compartir aquest moment amb jo. Gràcies a la meva mare, Marina Reixats i a la meva tieta, Pilar Nadal pel seu suport incondicional. Gràcies també a Quimeta Fontelles, Casimiro Reixats, Maria Gramunt, i Sandra Nonell per haver estat al meu costat. Gràcies a Pepita Fierro i Gaspar Murgó per haver-me ajudat tant. Moltíssimes gràcies a Miquel Murgó per estar sempre amb mi, per animar-me en els mals moments i per la teva paciència, gràcies per tot.

Moltes gràcies a Joana Maria Frontera, Lledó Esquerra i Laura Alanís. Tot i que estigueu tan lluny de Barcelona sempre us tinc molt aprop.

Agrair també als meus amics i amigues Elisabet Bosch, Anna Fumàs, Lourdes Monsó, Ione Verdeny, Adriana Pedrico, Bárbara García, Anna Pérez, Maria Cirera, Albert Parra, Pau Guri, Cristina García, Daniel Pérez, Jana Verdeny, Rebeca Escales, Gemma Ribó, Llum Rey, Clàudia Subarroca, Montse Gándara, Vanesa Veras, Jordi Ubach, Oriol Ubach, Miquel Armengol, Jordi Fumàs, Toni Tomàs i Joan Torrecillas.

Gràcies a tots un altre cop!

List of Publications

List of publications associated with this thesis, divided into journals, international and national conferences and master thesis in inverse chronological order.

Journals

(J1) **L. Nadal**, M. Svaluto Moreolo, J.M. Fàbrega, A. Dochhan, H. Grießer, M. Eiselt, J.-Peter Elbers, "DMT Modulation with Adaptive Loading for High Bit Rate Transmission Over Directly Detected Optical Channels", Journal of Lightwave Technology, vol.PP, no.99, pp.1,1, August, 2014.

(J2) **L. Nadal**, M. Svaluto Moreolo, J.M. Fàbrega and G. Junyent, "Low Complexity PAPR Reduction Techniques for Clipping and Quantization Noise Mitigation in Direct-Detection O-OFDM Systems", Optical Fiber Technology (OFT), Volume 20, Issue 3, Pages 208-216, June, 2014.

(J3) M. Svaluto Moreolo, J.M. Fàbrega, F. Vílchez, **L. Nadal** and G. Junyent, "Experimental Demonstration of a Cost-Effective Bit Rate Variable IM/DD Optical OFDM with Reduced Guard Band", Optics Express, n.20, pp.159-164, October, 2012.

International conferences

(C1) M. Svaluto Moreolo, J.M. Fàbrega, **L. Nadal**, F.J. Vílchez, "Optical transceiver technologies for inter-data center connectivity [Invited]", *in Proceedings of International Conference on Transparent Optical Networks (ICTON)*, 6-10 July, 2014, Graz (Austria).

(C2) A. Dochhan, H. Grießer, **L. Nadal**, M. Eiselt, M. Svaluto Moreolo, J.-Peter Elbers, "Discrete Multitone Transmission for Next Generation 400G Data Center Inter-Connections [Invited]", *OECC/ACOFT*, 6-10 Juli, 2014, Melbourne, (Australia).

(C3) A. Dochhan, H. Grießer, **L. Nadal**, M. Eiselt, M. Svaluto Moreolo, J.-Peter Elbers, "Discrete Multitone Transmission in the Presence of Optical Noise, Chromatic Dispersion and Narrow-band Optical Filtering", *ITG Fachtagung Sprachkommunikation*, 24-26 September, 2014, Erlangen (Germany).

(C4) M. Svaluto Moreolo, J. M. Fàbrega, **L. Nadal**, F. J. Vílchez, V. López, and J. P. Fernández-Palacios, "Cost-Effective Data Plane Solutions Based on OFDM Technology for Flexi-Grid Metro Networks Using Sliceable Bandwidth Variable Transponders", *in Proceedings of Optical Network Design and Modeling (ONDM), 19-22 May, 2014, Stockholm (Sweden).*

(C5) A. Dochhan, **L. Nadal**, H. Griesser, M. Eiselt, M. Svaluto Moreolo, and J.-Peter Elbers, "Experimental Investigation of Discrete Multitone Transmission in the Presence of Optical Noise and Chromatic Dispersion", *in Proceedings of Optical Fiber Communication (OFC)*, 9-13 March, 2014, San Francisco, California (USA).

(C6) M. Svaluto Moreolo, J. M. Fàbrega, Fco. J. Vílchez, **L. Nadal**, V. López and G. Junyent, "Experimental Validation of an Elastic Low-Complex OFDM-Based BVT for Flexi-Grid Metro Networks", *in Proceedings of European Conference and Exhibition on Optical Communication (ECOC 2013)*, 22-26 September, 2013, London (United Kingdom).

(C7) **L. Nadal**, M. Svaluto Moreolo, J. M. Fàbrega and G. Junyent, "Adaptive Bit Loading in FHT-based OFDM Transponders for Flexi-Grid Optical Networks", *in Proceedings of International Conference on Transparent Optical Networks (ICTON 2013)*, 23-27 June, 2013, Cartagena (Spain).

(C8) M. Svaluto Moreolo, J. M. Fàbrega, **L. Nadal**, F. Javier Vílchez and G. Junyent, "Bandwidth Variable Transponders Based on OFDM Technology for Elastic Optical Networks", *in Proceedings of International Conference on Transparent Optical Networks (ICTON 2013)*, 23-27 June, 2013, Cartagena (Spain).

(C9) J. M. Fàbrega, M. Svaluto Moreolo, Fco. J. Vílchez, and **L. Nadal**, "Experimental Characterization of a Burst-Enabled O-OFDM Transceiver", *in Proceedings of CLEO/Europe-IQEC*, 12-16 May, 2013, Munich (Germany).

(C10) M. Svaluto Moreolo, J. M. Fàbrega, Fco. J. Vílchez, **L. Nadal** and G. Junyent, "Experimental Demonstration of a Cost-Effective Bit Rate Variable Intensity Modulation and Direct Detection Optical OFDM with Reduced Guard Band", *in Proceedings of 38th European Conference and Exhibition on Optical Communication (ECOC 2012)*, 16-20 September, 2012, Amsterdam (The Netherlands).

(C11) **L. Nadal**, M. Svaluto Moreolo, J. M. Fàbrega, G. Junyent, "Clipping and Quantization Noise Mitigation in Intensity-Modulated Direct Detection O-OFDM Systems based on the FHT", *in Proceedings of 14th International Conference on Transparent Optical Networks (ICTON 2012)*, 2-5 July, 2012, Coventry (UK).

(C12) M. Svaluto Moreolo, J. M. Fàbrega, **L. Nadal**, G. Junyent, "Software-Defined Optical OFDM Transmission Systems: Enabling Elasticity in the Data Plane", *in Proceedings of 14th International Conference on Transparent Optical Networks (ICTON 2012)*, 2-5 July, 2012, Coventry (UK).

(C13) **L. Nadal**, M. Svaluto Moreolo, J. M. Fàbrega, G. Junyent, "Low Complexity Bit Rate Variable Transponders Based on Optical OFDM with PAPR Reduction Capabilities", *in Proceedings of 17th European Conference on Network and Optical Communications (NOC 2012)*, 19-22 June, 2012, Vilanova i la Geltrú,(Spain).

(C14) M. Svaluto Moreolo, J. M. Fàbrega, **L. Nadal**, G. Junyent, "FHT-Based Architectures for Multicarrier Modulation in Direct Detection and Coherent Optical Systems", *in Proceedings of 13th International Conference on Transparent Optical Networks (ICTON 2011)*, 26-30 June, 2011, Stockholm (Sweden).

(C15) **L. Nadal**, M. Svaluto Moreolo, J. M. Fàbrega, G. Junyent, "Comparison of Peak Power Reduction Techniques in Optical OFDM Systems Based on FFT and FHT", *in Proceedings of 13th International Conference on Transparent Optical Networks (ICTON 2011)*, 26-30 June, 2011, Stockholm (Sweden).

National conferences

(N1) **L. Nadal**, M. Svaluto Moreolo and G. Junyent, "Elastic Transponders for Optical Direct Detection OFDM Systems based on the FHT", in Proceedings of 3rd Forum on Ph.D. Research in Information and Communication Technologies, 15 October, 2012, Barcelona.

Master thesis

- **L. Nadal**, "Performance Analysis of Optical OFDM Transmission Systems Using PAPR Mitigation Techniques and Alternative Transforms", Supervisor: M. Savaluto-Moreolo (CTTC), Advisor: Prof. G. Junyent (UPC), April, 2012.

Contents

List of Figures

List of Tables

List of Abbreviations

ACE Active Constellation Extension

ACO-OFDM Asymmetrically Clipped Optical-OFDM

ADC Analog-to-Digital Converter

ADRENALINE All-optical Dynamic REliable Network hAndLINg

IP/Ethernet Gigabit traffic with QoS

AMO-OFDM Adaptively Modulated O-OFDM

APD Avalanche Photo-Detector

ASE Amplified Spontaneous Emission

ASIC Application Specific Integrated Circuits

AWG Arbitrary Waveform Generator

AWGN Additive White Gaussian Noise

BER Bit Error Rate

BL Bit Loading

BPF Band Pass Filter

BPSK Binary Phase-Shift Keying

B2B Back-to-Back

BRAS Broadband Remote Access Servers

BVT Bandwidth Variable Transceiver

BVTx Bandwidth Variable Transmitter

BVRx Bandwidth Variable Receiver

CapEx Capital Expenditure

CCDF Complementary Cumulative Density Function

CCB Chow Cioffi Bingham

CCBMA CCB Margin Adaptive

CCBRA CCB Rate Adaptive

CD Chromatic Dispersion

CML Chirp Managed Lasers

CO-OFDM Coherent Optical OFDM

CP Cyclic Prefix

CSI Channel State Information

DAC Digital-to-Analog Converter

DD Direct Detection

DFB Distributed FeedBack

DML Directly Modulated Laser

DMT Discrete MultiTone

DSB Double-Side Band

DSP Digital Signal Processing

DWDM Dense Wavelength Division Multiplexing

EDFA Erbium Doped Fiber Amplifier

EON Elastic Optical Networks

EML Electro-absorption Modulated Laser

ENOB Effective Number Of Bits

FHT Fast Hartley Transform

FFT Fast Fourier Transform

FEC Forward Error Correction

FPGA Field Programmable Gate Arrays

HD Hard Decision

HS Hermitian Symmetry

IFFT Inverse Fast Fourier Transform

ICI InterCarrier Interference

ISI InterSymbol Interference

IM Intensity-Modulation

LC Low Complexity

LCMA Levin Campello Margin Adaptive

LCRA Levin Campello Rate Adaptive

MA Margin Adaptive

MAN Metro Area Networks

MTU Multi-Tenant Unit

MZM Mach-Zehnder modulator

MCM MultiCarrier Modulation

N-WDM Nyquist WDM

NZDSF Non-Zero Dispersion-Shifted Fiber

OXC Optical Cross-Connect

OFDM Orthogonal Frequency Division Multiplexing

OLT Optical Line Terminal

O-OFDM Optical-OFDM

OpEx Operational Expenditures

OSC Optical Supervisory Channel

OSNR Optical Signal-to-Noise Ratio

PAM Pulse Amplitude-Modulation

PAPR Peak-to-Average Power Ratio

PL Power Loading

PON Passive Optical Network

PS Parallel to Serial

PSK Phase Shift Keying

PTS Partial Transmit Sequence

QAM Quadrature Amplitude Modulation

RA Rate Adaptive

RF Radio Frequency

ROADM Reconfigurable Add-Drop Multiplexer

S-BVT Sliceable BVT

S-BVRx Sliceable BVRx

S-BVRx Sliceable BVRx

SD Soft Decision

SDOT Software-Defined Optical Transmission

SE Spectral Efficiency

SLM SeLective Mapping

SNR Signal-to-Noise Ratio

SP Serial to Parallel

SSB Single-Side Band

SSMF Standard Single Mode Fiber

TI Tone Injection

TIA TransImpedance Amplifier

TL Tunable Laser

TR Tone Reservation

TS Training Symbols

VOA Variable Optical Attenuator

VSB Vestigial-Side Band Transmission

WDM Wavelength Division Multiplexing

WSS Wavelength Selective Switches

1 Introduction

"Technology has advanced more in the last thirty years than in the previous two thousand. The exponential increase in advancement will only continue. Anthropological Commentary The opposite of a trivial truth is false; the opposite of a great truth is also true."

Niels Bohr

1.1 Motivation

The ever increasing demand for communication services and the tremendous growth of global IP traffic are driving the development of novel, high-capacity Elastic Optical Networks (EON). In fact, according to [3] forecast, global IP traffic has increased more than fourfold in the past 5 years, and will increase threefold over the next 5 years. Additionally, data center and cloud IP traffic is increasing drastically every month and the new emerging applications and services such as cloud computing and high quality IP services (VoIP, IPTV, etc.) will also increase in the near future [4]. Specifically, annual global data center IP traffic will reach 7.7 zettabytes by the end of 2017, according to Cisco forecast [4] (see Fig. 1.1).

Dense Wavelength Division Multiplexing (DWDM) are currently being deployed to transport 100 Gb/s per channel using standard fixed-grid [5]. In the conventional fixed spectrum grid, the optical spectrum is divided into separate channels spaced by 50 or 100 GHz as specified by ITU-T standards [6]. DWDM infrastructure leads to an inefficient use of the available resources of the network when the transmitted traffic doesn't occupy the whole allocated optical spectrum. Hence, in order to solve this mismatch of granularities between the client layer and the wavelength layer, DWDM normative has been updated to support finer frequency grids enabling flexible DWDM [6]. Specifically, in order to evolve to a more scalable and flexible grid to efficiently

Figure 1.1: Global data center IP traffic growth. Source: Cisco Global Cloud Index: Forecast and Methodology, 2012 – 2017.

allocate the optical bandwidth resources in EON, frequency slots of 12.5 and 6.25 GHz are defined (further reducing by a factor of 2 the minimum fixed channel spacing of 25 GHz) [7].

The need for high-speed data transmission and the evolution of optical systems towards elastic functionalities and variable bit rates from 10 Gb/s to 100 Gb/s and beyond arises new technical challenges. Single-carrier modulation formats require high symbol rates to enable 100 Gb/s transmission and beyond, that are not technologically feasible in the near future [8]. Hence, advanced modulation formats, such as Optical-OFDM (O-OFDM), and Nyquist WDM (N-WDM) between others are more suitable solutions to fully exploit flexibility at the data plane level in EON. By using multi-carrier modulation formats, high Spectral Efficiency (SE) and high data rate can be achieved while minimizing complexity, power consumption and transceiver cost [9, 10]. In particular, SE can be enhanced by using higher order modulation formats and polarization multiplexing at the expense of the receiver sensitivity and system complexity, respectively. Additionally, Bandwidth Variable Transceiver (BVT) can be designed to fully exploit the flexibility in the data plane level [11]. Flexibility can further be enhanced by slicing the single BVT into several "virtual transceivers" known as Sliceable BVT (S-BVT) [11, 12].

On the one hand, N-WDM enables high SE by using a spectral pulse shaping filter at the transmitter side to allow a narrow subcarrier spacing within the Nyquist frequency limit. Thus, a dense allocation of N-WDM subcarriers is allowed creating a

superchannel. However, significant power penalties arise when the channel frequency spacing is equal to the symbol rate. As a result, Forward Error Correction (FEC) is required to enhance system performance, existing a trade-off between spectral efficiency and InterCarrier Interference (ICI). This transmission scheme becomes an interesting solution for long-haul and ultra long-haul applications.

Although the concept of Orthogonal Frequency Division Multiplexing (OFDM) was first introduced by Chang in 1966 [13], it was not until 1996 that Pan and Green applied this concept to optical communications field [14]. OFDM achieves the same SE as N-WDM when a subcarrier number greater or equal to 64 is used [15]. Despite its late appearance in optics, O-OFDM is arising as one of the most promising technology for designing bit rate and BVT as key enablers for future EON due to its unique data rate/bandwidth scalability and superwavelength and also subwavelength granularity. Additionally, O-OFDM also enables Software-Defined Optical Transmission (SDOT), which allows dynamically adapting or reconfiguring the transmitter and receiver of an optical communication system [9]. SDOT is possible thanks to the advances in Digital Signal Processing (DSP) technology. Advanced multi-level and multi-dimensional modulation formats are supported by OFDM technology providing higher data rate and SE [16]. Hence, OFDM becomes a promising technology to consider in the design of the BVT in EON.

However, high data rate transmission over Standard Single Mode Fiber (SSMF) is affected by fiber impairments such as Chromatic Dispersion (CD) and the bandwidth limitation of some electrical components, such as the Digital-to-Analog Converter (DAC) and the Analog-to-Digital Converter (ADC) [17]. Additionally, DAC and ADC present limited bit resolution which lead to quantization noise. The dynamic range of the converters must be adjusted in order to accommodate the OFDM signal. A major drawback of OFDM systems is the high Peak-to-Average Power Ratio (PAPR) of the transmitted signals, which results in signal distortion. Specifically, high peaks occur when multiple OFDM subcarriers, that could interfere constructively, are superposed. Therefore, the DAC and the ADC must ensure a dynamic range up to the value of the PAPR. A possible way to adjust the dynamic range of the converters to a lower value is to clip the signal [18,19]. Clipping the signal results in clipping noise which also degrades the system performance. Due to all these impairments, hardware limitations and high implementation costs, OFDM technology can not be considered as a near-term solution for EON.

Depending on the application, different O-OFDM schemes can be used to allow high data rate transmission trading cost-effectiveness and performance. Specifically, ultimate performance can be achieved using coherent detection, where the system robustness against CD is enhanced at the expense of increasing the system cost. Alterna-

tively, Direct Detection (DD), which uses simple transmitter and receiver architectures, arises as a potential cost-effective candidate to reduce the cost and complexity of the optical implementation [9, 20]. In a typical implementation, a single modulator and a single photodetector are needed in transmission and reception, respectively, as a real signal is transmitted. The signal processing at the OFDM transmitter/receiver is based on the Fast Fourier Transform (FFT). Nevertheless, the Fast Hartley Transform (FHT) is an alternative transform to the FFT that can also be used to implement the OFDM symbols, further simplifying the complexity of the system [21]. Different transmission architectures can be adopted to transmit real OFDM symbols. However, one of them, the Discrete MultiTone (DMT) attracted attention for the application in optical transmission systems since 2006 [22, 23]. Recently, DMT has been proposed as a low-cost approach for optical transmission of up to 100 Gb/s data using DD and 10G-class components [24]. CD resilience in DD can be enhanced by using optical filters in order to allow Single-Side Band (SSB) and Vestigial-Side Band Transmission (VSB) instead of Double-Side Band (DSB) transmission [25, 26].

In this thesis, cost-efficient adaptive O-OFDM solutions using DD are proposed in order to built novel elastic network architectures to meet the requirements of future EON. The goal is to limit the aforementioned system impairments and enhance the system performance using low complexity DSP in order to drive the use of OFDM technology in EON. PAPR reduction techniques are analyzed to mitigate PAPR, clipping and quantization noise. On the other hand, SDOT and adaptive features are provided by implementing loading algorithms in the transponders. Moreover, Bit Loading (BL) and Power Loading (PL) schemes are also suitable to deal with CD impairment [27]. These solutions can be adopted in elastic Metro Area Networks (MAN) and data center inter-connections using flexible technology, as possible target applications. In particular, FHT-based O-OFDM systems are investigated for MAN. Whereas, DMT systems are analyzed in order to allow elastic high data rate transmission over extended data center connections.

1.2 Thesis Overview

In this section, we present the topic of each chapter and outline the contributions that are included in the present dissertation.

In **Chapter 2**, the state of the art of the present work is introduced. At the beginning of the chapter, an overview of high speed transmission systems and EON is provided. Then, an introduction of OFDM technology and its application in optical systems is shown. A brief description of CD impairment when transmitting over SSMF

is also discussed. Finally, estimation, equalization and synchronization are explained as essential methods to successfully recover the transmitted data at the receiver side.

In **Chapter 3**, the PAPR is presented as one of the major problems of OFDM signals that should be mitigated. Additional drawbacks such as clipping noise and quantization noise are also investigated. Distortionless PAPR reduction techniques based on the FHT are proposed to mitigate all the analyzed impairments. Finally, a performance analysis is provided by means of numerical simulations.

The contributions related to this chapter are contained in the following publications:

- **L. Nadal**, M. Svaluto Moreolo, J.M. Fàbrega and G. Junyent, "Low Complexity PAPR Reduction Techniques for Clipping and Quantization Noise Mitigation in Direct-Detection O-OFDM Systems", Optical Fiber Technology (OFT), Volume 20, Issue 3, Pages 208-216, June, 2014.

- **L. Nadal**, M. Svaluto Moreolo, J.M. Fàbrega, G. Junyent, "Clipping and Quantization Noise Mitigation in Intensity-Modulated Direct Detection O-OFDM Systems based on the FHT", *in Proceedings of 14th International Conference on Transparent Optical Networks (ICTON 2012)*, 2-5 July, 2012, Coventry (UK).

- **L. Nadal**, M. Svaluto Moreolo, J.M. Fàbrega, G. Junyent, "Comparison of Peak Power Reduction Techniques in Optical OFDM Systems Based on FFT and FHT", *in Proceedings of 13th International Conference on Transparent Optical Networks (ICTON 2011)*, 26-30 June, 2011, Stockholm (Sweden).

Chapter 4 deals with BL and PL solutions in O-OFDM systems based on the FHT. A first analysis is performed in Additive White Gaussian Noise (AWGN) channel. Then, DSB transmission is considered over SSMF in a MAN scenario. A first loading approach is proposed for the OFDM-based BVT followed by a further improved loading algorithm suitable to perform the bit and power allocation.

The following publications support the content of this chapter:

- **L. Nadal**, M. Svaluto Moreolo, J.M. Fàbrega and G. Junyent, "Adaptive Bit Loading in FHT-based OFDM Transponders for Flexi-Grid Optical Networks", *in Proceedings of International Conference on Transparent Optical Networks (ICTON 2013)*, 23-27 June, 2013, Cartagena (Spain).

- **L. Nadal**, M. Svaluto Moreolo and G. Junyent, "Elastic Transponders for Optical Direct Detection OFDM Systems based on the FHT", in Proceedings of 3rd Forum on Ph.D. Research in Information and Communication Technologies, 15 October, 2012, Barcelona.

- M. Svaluto Moreolo, J. M. Fàbrega, **L. Nadal**, G. Junyent, "Software-Defined Optical OFDM Transmission Systems: Enabling Elasticity in the Data Plane", *in Proceedings of 14th International Conference on Transparent Optical Networks (ICTON 2012)*, 2-5 July, 2012, Coventry (UK).

- **L. Nadal**, M. Svaluto Moreolo, J.M. Fàbrega, G. Junyent, "Low Complexity Bit Rate Variable Transponders Based on Optical OFDM with PAPR Reduction Capabilities", *in Proceedings of 17th European Conference on Network and Optical Communications (NOC 2012)*, 19-22 June, 2012, Vilanova i la Geltrú,(Spain).

- M. Svaluto Moreolo, J. M. Fàbrega, **L. Nadal**, G. Junyent, "FHT-Based Architectures for Multicarrier Modulation in Direct Detection and Coherent Optical Systems", *in Proceedings of 13th International Conference on Transparent Optical Networks (ICTON 2011)*, 26-30 June, 2011, Stockholm (Sweden).

In **Chapter 5**, an experimental validation of the proposed elastic OFDM-based BVT is provided. Then, a system optimization is provided. Finally, the system performance is assessed for flexi-grid MAN. Moreover, a proof of concept of the BVT being a fundamental building block for future S-BVT is included.

The contributions of this chapter are contained in the following publications:

- M. Svaluto Moreolo, J.M. Fàbrega, **L. Nadal**, F.J. Vílchez, "Optical transceiver technologies for inter-data center connectivity [Invited]", *in Proceedings of International Conference on Transparent Optical Networks (ICTON)*, 6-10 July, 2014, Graz (Austria).

- M. Svaluto Moreolo, J. M. Fàbrega, **L. Nadal**, F. J. Vílchez, V. López, and J. P. Fernández-Palacios, "Cost-Effective Data Plane Solutions Based on OFDM Technology for Flexi-Grid Metro Networks Using Sliceable Bandwidth Variable Transponders", *in Proceedings of Optical Network Design and Modeling (ONDM), 19-22 May, 2014, Stockholm (Sweden).*

- J. Fàbrega, M. Svaluto Moreolo, Fco. J. Vílchez, and **L. Nadal**, "Experimental Characterization of a Burst-Enabled O-OFDM Transceiver", *in Proceedings of CLEO/Europe-IQEC*, 12-16 May, 2013, Munich (Germany).

- M. Svaluto Moreolo, J. M. Fàbrega, Fco. J. Vílchez, **L. Nadal**, V. López and G. Junyent, "Experimental Validation of an Elastic Low-Complex OFDM-Based BVT for Flexi-Grid Metro Networks", *in Proceedings of European Conference and Exhibition on Optical Communication (ECOC 2013)*, 22-26 September, 2013, London (United Kingdom).

- M. Svaluto Moreolo, J. M. Fàbrega, **L. Nadal**, F. Javier Vílchez and G. Junyent, "Bandwidth Variable Transponders Based on OFDM Technology for Elastic Optical Networks", *in Proceedings of International Conference on Transparent Optical Networks (ICTON 2013)*, 23-27 June, 2013, Cartagena (Spain).

- M. Svaluto Moreolo, J. M. Fàbrega, F. Vílchez, **L. Nadal** and G. Junyent, "Experimental Demonstration of a Cost-Effective Bit Rate Variable IM/DD Optical OFDM with Reduced Guard Band", accepted in Optics Express, n.20, pp.159-164, October 2012.

- M. Svaluto Moreolo, J. M. Fàbrega, Fco. J. Vílchez, **L. Nadal** and G. Junyent, "Experimental Demonstration of a Cost-Effective Bit Rate Variable Intensity Modulation and Direct Detection Optical OFDM with Reduced Guard Band", *in Proceedings of 38th European Conference and Exhibition on Optical Communication (ECOC 2012)*, 16-20 September, 2012, Amsterdam (The Netherlands).

In **Chapter 6**, an adaptive cost-effective DMT transponder based on the FFT using DD is presented. The target scenario is data center inter-connections. A loading algorithm is implemented to overcome CD and enhance the system performance.

The content of this chapter is contained in the following publication:

- **L. Nadal**, M. Svaluto Moreolo, J.M. Fàbrega, A. Dochhan, H. Grießer, M. Eiselt, J.-Peter Elbers, "DMT Modulation with Adaptive Loading for High Bit Rate Transmission Over Directly Detected Optical Channels", Journal of Lightwave Technology, vol.PP, no.99, pp.1,1, August, 2014.

In **Chapter 7** the proposed DMT transponder is experimentally validated to enable high data rate transmission over extended data center links. As a second step, optical filtering is analyzed for fixed-grid and flexi-grid technologies.

The publications contained in this chapter are listed here:

- **L. Nadal**, M. Svaluto Moreolo, J.M. Fàbrega, A. Dochhan, H. Grießer, M. Eiselt, J.-Peter Elbers, "DMT Modulation with Adaptive Loading for High Bit Rate Transmission Over Directly Detected Optical Channels", Journal of Lightwave Technology, vol.PP, no.99, pp.1,1, August, 2014.

- A. Dochhan, H. Grießer, **L. Nadal**, M. Eiselt, M. Svaluto Moreolo, J.-Peter Elbers, "Discrete Multitone Transmission for Next Generation 400G Data Center Inter-Connections [Invited]", *OECC/ACOFT, 6-10 Juli, 2014, Melbourne, (Australia).*

- A. Dochhan, H. Grießer, **L. Nadal**, M. Eiselt, M. Svaluto Moreolo, J.-Peter Elbers, "Discrete Multitone Transmission in the Presence of Optical Noise, Chromatic Dispersion and Narrow-band Optical Filtering", *ITG Fachtagung Sprachkommunikation, 24-26 September, 2014, Erlangen (Germany).*

- A. Dochhan, **L. Nadal**, H. Griesser, M. Eiselt, M. Svaluto Moreolo, and J.-Peter Elbers, "Experimental Investigation of Discrete Multitone Transmission in the Presence of Optical Noise and Chromatic Dispersion", *in Proceedings of Optical Fiber Communication (OFC)*, 9-13 March, 2014, San Francisco, California, (USA).

Finally, in **Chapter 8**, the final conclusions of the current thesis and future work are discussed.

2

Background and State of the Art

"The science of today is the technology of tomorrow."

Edward Teller

2.1 High Speed Transmission

Current optical networks must evolve in order to support high data rate transmission and increase the optical capacity to meet the needs of future demand. The electrical bandwidth bottleneck limitation and physical impairments become more severe at the increasing of the data rate. Hence, looking for solutions to support high data rate transmission at the data and control plane levels become a trending topic to enable next generation optical networks. Data rates beyond 100 Gb/s will be required to increase the optical channel capacity and support high rate client interfaces [11]. In fact, 100 Gb/s Ethernet (100 GbE) technology is already standardized by the IEEE and 400 GbE and 1 TbE solutions for Ethernet physical layer are under investigation in order to support the future incoming demand [28]. The need of enhancing the spectral efficiency combined with the newly built data centers and the influence from providers make really difficult to predict the traffic current demand. Intra or short inter data center point-to-point fiber optics interfaces are defined as client optics. Major client optics applications can be general data center and metro inter data center connections which typically cover distances from 10 km up to 40 km of Standard Single Mode Fiber (SSMF) [29]. As a high number of links are required to interconnect all the data centers distributed over an area, simple and low-cost solutions has to be investigated. However, maintaining low cost and high spectral efficiency when high data rate signals are transmitted is certainly not an easy task. The network condition and data rate should be adapted to the traffic demand by implementing flexible and adaptive networks equipped with flexible Bandwidth Variable Transceiver (BVT),

which are key enablers of Elastic Optical Networks (EON) [30, 31]. In [32], 400 Gb/s Wavelength Division Multiplexing (WDM) transmission is demonstrated using Discrete MultiTone (DMT) modulation, which is a special class of Orthogonal Frequency Division Multiplexing (OFDM) systems. Specifically, 100 Gb/s per wavelength data rate is achieved after 5 km of SSMF ensuring a target Bit Error Rate (BER) of 10^{-3}, which can satisfy the short distance connection between data centers. Hence, OFDM also arises as a potential solution for high data rate transmission in short-links scenarios.

Additionally, equipment and device integration can be a future possible solution to reduce the system cost and physical component dimensions. Silicon photonics integration and CMOS with photonics integration are promising technologies under investigation that achieve high power reduction and energy efficiency [33].

2.2 Elastic Optical Networks

EONs arise as a potential solution to deal with high data rates (beyond 100 Gb/s). However, upgrading the current network towards elastic functionalities usually implies additional efforts by the operators. In particular, the deployment of new telecommunications infrastructures and the increasing of the electrical power consumption causes high Capital Expenditure (CapEx) and Operational Expenditure (OpEx), respectively. Hence, the spectral and energy efficiency, the flexibility and the network equipment costs will be crucial parameters to take into account when designing the EON [34]. Highly efficient and adaptive management of the optical spectrum is achieved by using flexi-grid technology [6]. Specifically, fine channel spacings of 12.5 GHz and 6.25 GHz are considered, for the Dense Wavelength Division Multiplexing (DWDM) grid, to adaptively allocate variable-sized frequency slots to bandwidth-variable optical connections, according to the client data rate and the physical conditions of the path. Additionally, the use of advanced optical modulation schemes, such as OFDM, that efficiently use allocated spectrum slots, fully exploit the flexibility enabling Software-Defined Optical Transmission (SDOT) in EON. In fact, SDOT and flexi-grid are considered as technology enablers for high data rate transmission, as well as BVT and flexible spectrum Wavelength Selective Switches (WSS), which can multiplex and switch variable spectral bands. Hence, the flexibility and scalability of the network can be maximized and the cost and energy consumption minimized.

A possible use case of EON using Optical-OFDM (O-OFDM) technology can be Metro Area Networks (MAN), where all these elastic features can be adopted. In particular, MAN is the network segment between the access and the core network. Typically, metro architectures are composed of two main levels of aggregation. The first level of aggregation, called Multi-Tenant Unit (MTU), is in charge of collecting

traffic from the Optical Line Terminal (OLT). Whereas, the second level of aggregation is the access level, which aggregates the traffic from the MTU mainly through direct fiber connections.

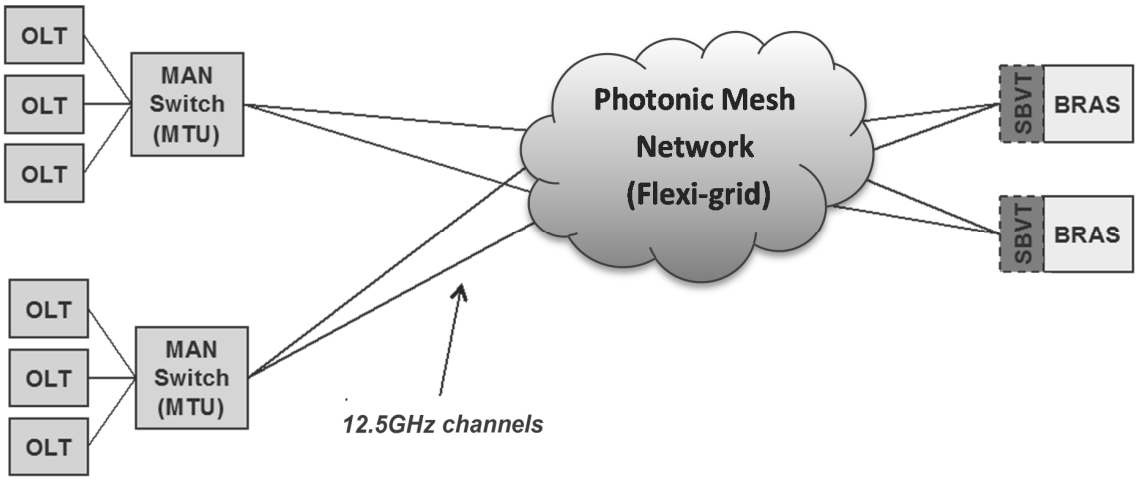

Figure 2.1: Evolutionary flexi-grid MAN scenario with S-BVT at the BRASes.

Nowadays, the IP functionality, such as traffic classification, routing or authentication, is implemented in the Broadband Remote Access Servers (BRAS), which are usually located at the second level of aggregation. Therefore, they are distributed in many sites along the regional area covered by the MAN, causing a high CapEx impact [11]. Lately, main network operators are expanding their photonic mesh to the regional networks, so BRASes could be co-located in fewer locations reducing investment. In fact, as cost effectiveness is an important requirement for the system design, it is desirable to adopt low complex data plane solutions to further minimize the network cost. Additionally, flexi-grid MAN can benefit from the use of BVT and Sliceable BVT (S-BVT) at the BRAS servers, enhancing system's flexibility (see Fig. 2.1).

2.3 Orthogonal Frequency Division Multiplexing

OFDM is a special class of MultiCarrier Modulation (MCM) that consists of transmitting a signal over several lower-rate orthogonal subchannels [9, 35]. The spectrum of individual subcarriers, which has a $sin(x)/x$ form, can overlap due to its orthogonality. As it can be seen in Fig. 2.2, where the different subcarriers that form one OFDM symbol are depicted, each OFDM subcarrier has significant sidelobes over a frequency range which includes many other subcarriers. On the one hand, OFDM presents robustness against channel dispersion and allows an easy phase and channel estimation in a time-varying environment. Thanks to the use of a Cyclic Prefix (CP), the channel dispersion-induced InterSymbol Interference (ISI) and InterCarrier Interference (ICI)

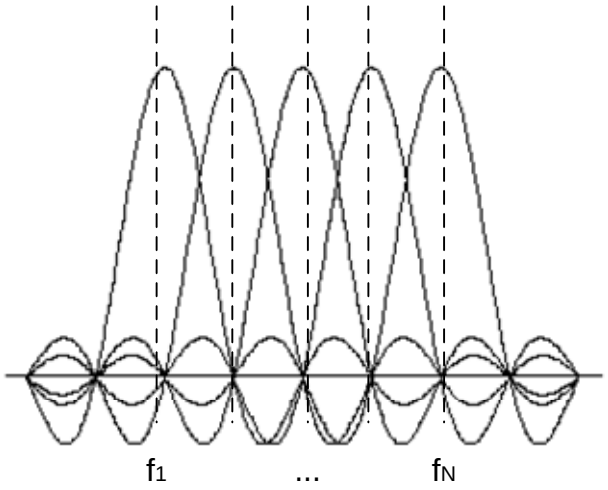

Figure 2.2: OFDM spectrum.

can be resolved [9,36]. The CP is a cyclic redundancy introduced in the OFDM symbol. The elements in the tail of the discrete OFDM signal vector are copied and pasted as a prefix (see Fig. 2.3).

On the other hand, OFDM has disadvantages, such as the high Peak-to-Average Power Ratio (PAPR) and sensitivity to frequency and phase noise [9]. The PAPR problem will be detailed and analyzed in chapter 3. Whereas frequency offset and phase noise appear due to the relatively long OFDM symbol length and they lead to ICI. Frequency estimation and compensation can be implemented at the receiver side to mitigate the frequency offset sensitivity. The phase noise sensitivity can be resolved by careful designing the Radio Frequency (RF) local oscillators.

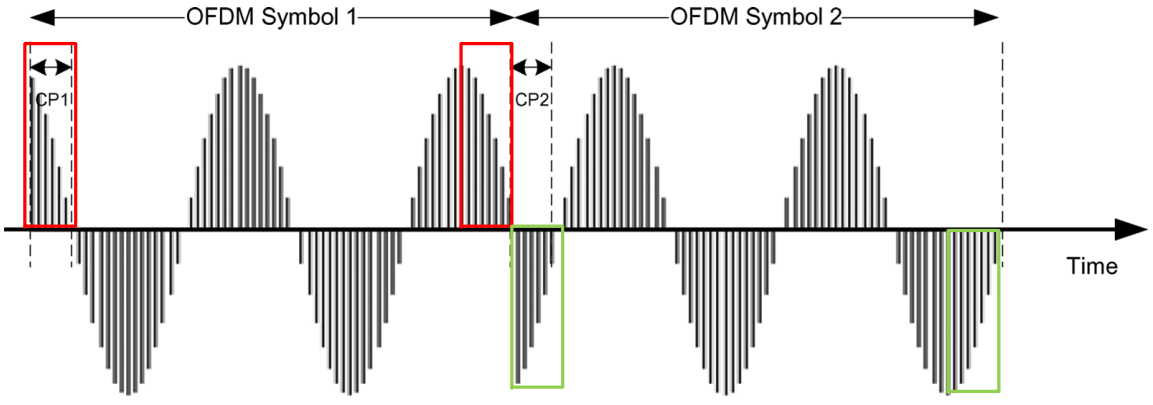

Figure 2.3: Time domain signal of one subcarrier for two OFDM frames using CP.

In order to create the orthogonal subcarriers the Inverse Fast Fourier Transform (IFFT) and the Fast Fourier Transform (FFT) are used for the modulation and de-

modulation of the signal, respectively [37]. The IFFT can be defined as:

$$y_m = \frac{1}{\sqrt{N}} \sum_{n=0}^{N-1} Y_n \; exp(2j\pi mn/N) \quad m = 0, 1, ..., N-1, \tag{2.1}$$

where Y_n indicates the symbol sequence, previously mapped with a M Quadrature Amplitude Modulation (MQAM) or M Phase Shift Keying (MPSK) format, and N represents the number of subcarriers. The symbols have different energy levels when

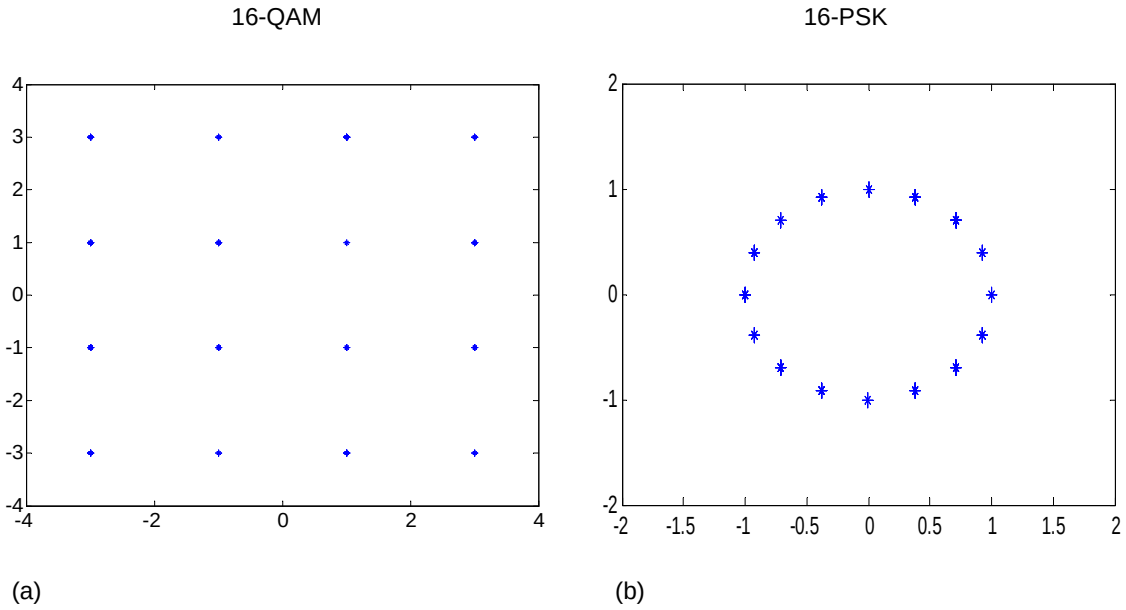

Figure 2.4: (a) 16QAM and (b) 16PSK constellations.

they are mapped into MQAM constellation. Whereas, with mPSK format, they are distributed in a circle of unitary energy [1]. Using MQAM, for a large M, the symbols have more distance between each other and hence, the receiver can recover the signal with less errors. Nevertheless more power is needed to transmit them. For large-size constellations, MPSK format is not suitable, due to the reduced distance between symbols. The constellations of both modulation formats (for 16 symbols) are depicted in Fig. 2.4.

The block diagram of the transmitter is shown in Fig. 2.5 and it is composed by a Serial to Parallel (SP) converter, a mapper, a block to insert the Training Symbols (TS), an IFFT of N points, a block to insert the CP and a Parallel to Serial (PS) converter. With the mapping, a certain number of bits is represented by each mapped symbol. The IFFT block generates an OFDM symbol with N orthogonal subcarriers. Finally the resulting signal is serialized, digital-to-analog converted with a Digital-to-Analog Converter (DAC) and sent through the channel.

At the receiver, Fig. 2.6, the inverse process takes place. Firstly, after the detection

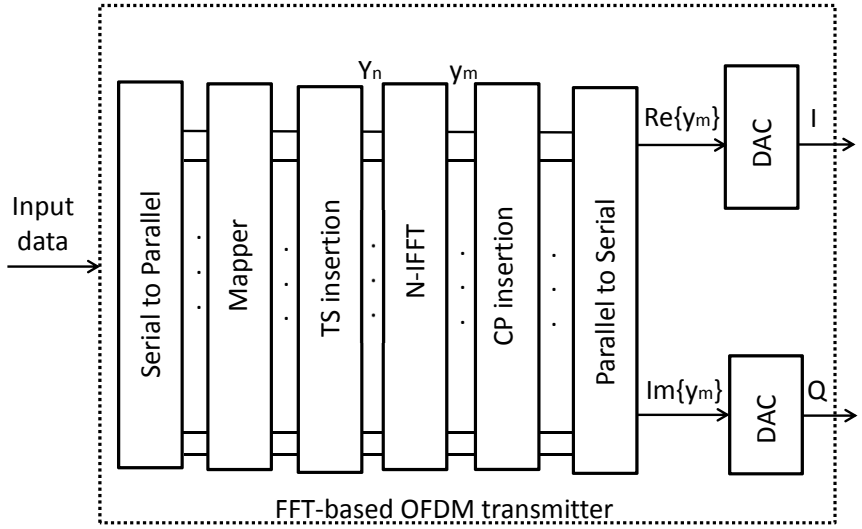

Figure 2.5: Block diagram of the OFDM transmitter based on the FFT.

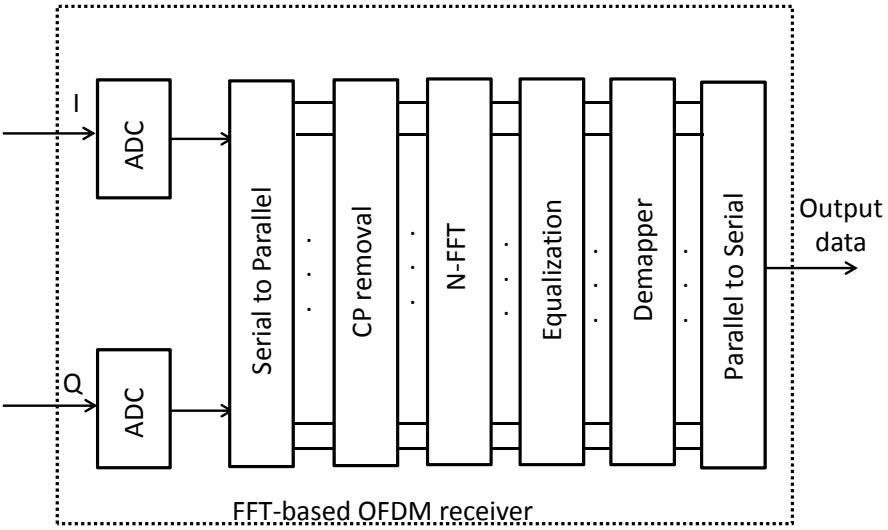

Figure 2.6: Block diagram of the OFDM receiver based on the FFT.

of the signal, the received data is analog-to-digital converted with an Analog-to-Digital Converter (ADC). The resulting digital signal is parallelized in order to remove the CP in the following step. Then, the FFT is implemented and equalization is performed. Finally, the resulting signal is demapped and serialized in order to recover the original bit stream.

2.4 OFDM in Optical Communications

One of the reasons why OFDM has been applied to optical communications is its capability to use high modulation formats to increase the spectral efficiency allowing

high signal-transmission capacities according to the future and growing demand [9,35]. However, the use of high order modulation formats presents lower Optical Signal-to-Noise Ratio (OSNR) tolerance resulting in a shorter distant reach. In order to overcome this limitation, reconfigurable transceivers can be implemented to adapt the system to the current traffic demand and network condition. In fact, O-OFDM has been proposed to cope with upgrades to the next transmission speed in highly reconfigurable networks. It is also a good option for optical long-haul communications specially because it can be designed to be extremely tolerant to Chromatic Dispersion (CD). Additionally, OFDM is a key enabler of future EON as it can be combined with Bit Loading (BL) and Power Loading (PL) [27]. Direct Detection (DD) and coherent detection are two possible optical implementations for receiving the OFDM signal through the optical channel. On the one hand, DD is a very attractive optical implementation due to its low cost and it is suitable for MAN. In such systems, the detection is performed using a single photodetector, as a real signal is transmitted. Additionally, the optical signal can be created with a single laser by directly or externally modulating the electrical signal at the transmitter. DD implementation is explained in more detail in section 2.4.1, as it is the solution adopted in this thesis. On the other hand, Coherent Optical OFDM (CO-OFDM) is an alternative optical implementation which was proposed to combat CD in long haul transmission [22]. It presents better performance than DD-based

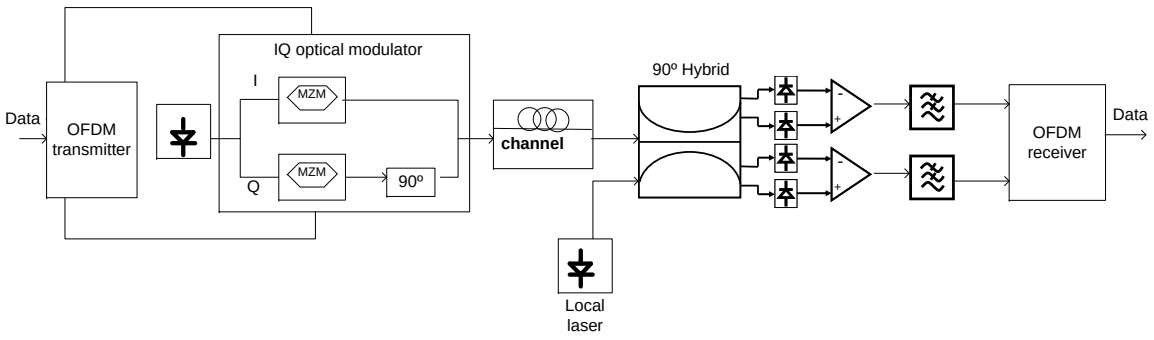

Figure 2.7: Block diagram of a CO-OFDM system.

OFDM in terms of bandwidth efficiency, robustness against fiber dispersion and receiver sensitivity, but it requires higher complexity in the transceiver design than DD systems [9]. Hence, DD scheme result in a more cost-effective solution. According to [38], reduced power consumption can be achieved in either DD or coherent detection when moving towards photonic integration. However, CO-OFDM systems require additional optical components, whose optical performance is so much more demanding than in DD systems. Hence, photonic integration doesn't reduce at all the economic gap between DD and coherent schemes, as the majority of the system's cost is due to the optical components, according to [38]. A typical CO-OFDM block diagram is depicted in

Fig. 2.7. The OFDM in phase and quadrature components of the OFDM complex signal are modulated by using an IQ optical modulator. Then the modulated signal is transmitted to the optical channel. In reception, one laser as local oscillator, a 90º hybrid and 4 balanced photodetectors are needed to recover the signal, 2 for the quadrature and 2 for the in-phase components of the received signal. Finally, both components are filtered and demodulated at the OFDM receiver.

2.4.1 Direct Detection

DD has been presented as a low cost and low complexity optical configuration, which becomes a suitable solution to meet the challenges of this thesis. DD can be used in a broader range of applications due to its transmitter and receiver simplicity. DD variants can be implemented depending on the scenario. On the receiver side, a simple photodetector, which can be either a PIN or an Avalanche Photo-Detector (APD), can be used to directly detect the signal. PIN has lower responsivity and cost than an APD. Despite that the common feature in all possible DD schemes is the use of direct detection at the receiver, alternatives to generate the optical signal exist. Regardless of the implemented transmission architecture, different modulators can be used to perform the electrical-to-optical conversion [39–43]. Specifically, Distributed FeedBack (DFB) laser, Directly Modulated Laser (DML) and Chirp Managed Lasers (CML) directly modulate the electrical signal into the optical domain. DMLs provide high output power and low threshold current [39]. However, it introduces high laser chirp limiting the transmission reach and the achievable bit rate. Alternatively, the electrical real OFDM signal can be externally modulated by using an Electro-absorption Modulated Laser (EML) or a Mach-Zehnder modulator (MZM). EML performance is limited to the fiber length. In contrast, MZM is a typically used external modulator as it presents negligible chirp [9]. Hence, MZM achieves better performance than DML at the expense of increased cost. The MZM creates a Double-Side Band (DSB) spectrum with respect to the optical carrier (f_c), see Fig. 2.8. DSB transmission is very susceptible to chromatic dispersion, however it is simple to implement. Alternatively, Single-Side Band (SSB) was proposed by Schmidt et al. in [25] for chromatic dispersion compensation in DD systems featured by long haul optical fiber links. SSB modulation ensures that the OFDM subcarriers are represented only once by the optical frequencies and avoid CD fading. Optical SSB-OFDM consists of suppressing one of the two OFDM sidebands presented by the real signal. For this purpose, optical filters or more complex schemes are required [25, 44, 45]. Furthermore, a guard band (B_G) equal to the bandwidth of the electrical OFDM signal (B_S) must be considered, reducing the spectral efficiency. Vestigial-Side Band Transmission (VSB) transmission could be seen

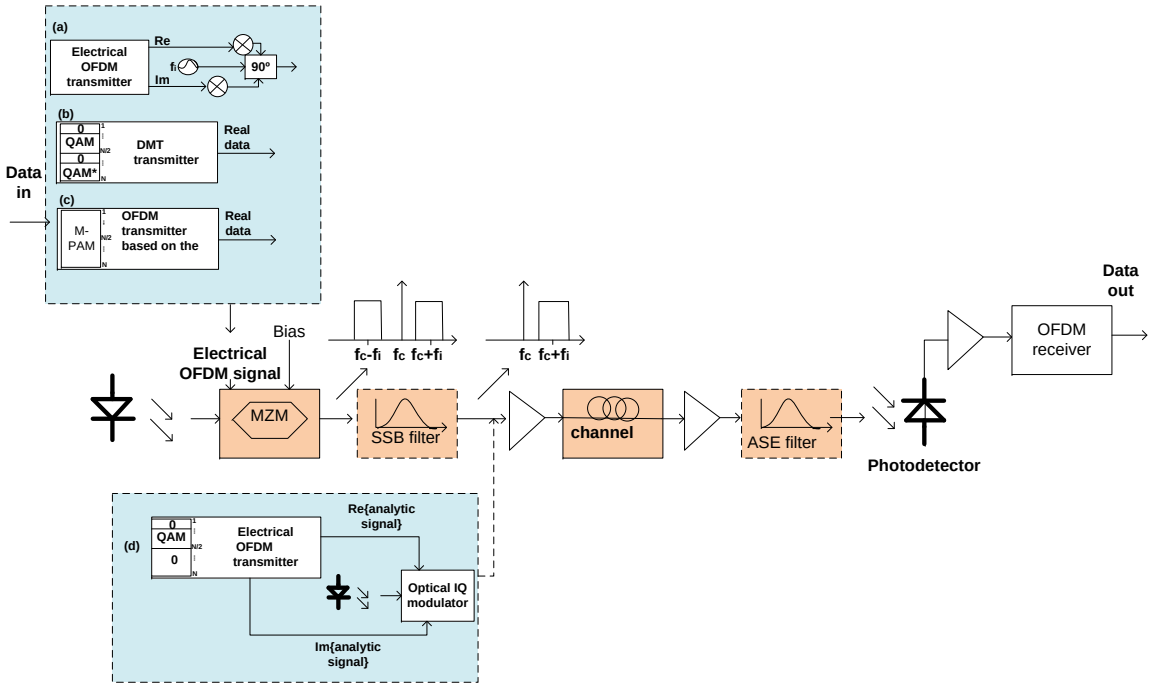

Figure 2.8: Block diagram of a IM/DD system using four different transmission architectures: (a) RF conversion, (b) DMT modulation, (c) FHT tranform and (d) Hilbert transform.

as a variant of SSB modulation. It uses an optical filter, which has not to be centered in the optical carrier [26]. Moreover, depending on the MZM bias point selection, linear field modulation or Intensity-Modulation (IM) can be provided. IM is achieved by biasing the MZM at the quadrature point. Additionally, IM can also be implemented using the aforementioned directly modulated lasers.

DD O-OFDM using IM: AC and DC-biased solutions

When IM is used, the system is less robust against dispersion impairments due to the nonlinear mapping between the OFDM baseband signal and the optical field. In IM systems, using direct laser modulation, the OFDM signal is represented by the optical intensity and not by the optical field. Thus, the transmitted signal must be unipolar. A positive signal can be obtained by applying Asymmetrically Clipped Optical-OFDM (ACO-OFDM) or adding a DC bias to the real OFDM signal generated by a DMT transmitter (DCO-OFDM).

ACO-OFDM ACO-OFDM consists of modulating only the odd subcarriers and set to zero the even ones. Then the signal can be clipped at zero level without any lost of information [46]. The odd frequencies have the property that:

$$Y_n = -Y_{n+N/2}, \tag{2.2}$$

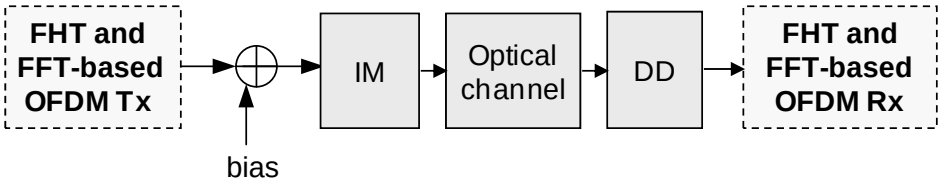

Figure 2.9: Block diagram of a IM/DD system.

where N is the number of subcarriers and $\mathbf{Y}$ is the input vector of the real-valued FFT block. Thus, the useful information in the odd frequencies is redundant and we can cut at zero level without any loss of performance. The clipping noise falls in the even subcarriers, that can be discarded at the receiver side. With this scheme the optical power is substantially reduced, but in contrast it only carries useful information on half of the available signal bandwidth.

DCO-OFDM DCO-OFDM consists of adding a bias (B) to the signal and then clipping it at zero level. The resulting signal from this asymmetrically clipping can be written as:

$$\hat{y}_m = \begin{cases} 0, & y_m + B \leq 0 \\ \\ y_m + B, & y_m + B > 0 \end{cases} \tag{2.3}$$

Alternatively, symmetrically clipping can also be applied. It consists of limiting the amplitude of the signal and then adding a bias equal to this maximum amplitude value in order to ensure a positive signal. The symmetrically clipped digital OFDM signal can be represented by:

$$\hat{y}_m = \begin{cases} y_m, & |y_m| \leq B \\ \\ B \cdot sign(y_m), & |y_m| > B \end{cases} \tag{2.4}$$

where B is also the maximum allowed signal amplitude and it is k times the standard deviation of the signal. The clipping level (C) is defined in decibels as

$$C = 10 \cdot \log_{10}\left(\frac{B^2}{E[|y_m|^2]}\right), \tag{2.5}$$

where $E[|y_m|^2]$ denotes the average signal power of the transmitted signal. Symmetrically clipping is also used to limit the high PAPR of O-OFDM signals. However, clipping the signal introduces a penalty due to the appearance of clipping noise that degrades the performance of the system. Usually, the value of the clipping level is 7 dB [47]. However, when high order modulation formats are used, 7 dB clipping level

is not enough to guarantee a BER lower than 10^{-3}. Higher clipping level values can be applied to the signal for reducing the clipping noise at the expense of increasing the electrical power of the signal [21, 47]. Hence, there is a trade off between power efficiency and noise in the selection of the clipping level or bias.

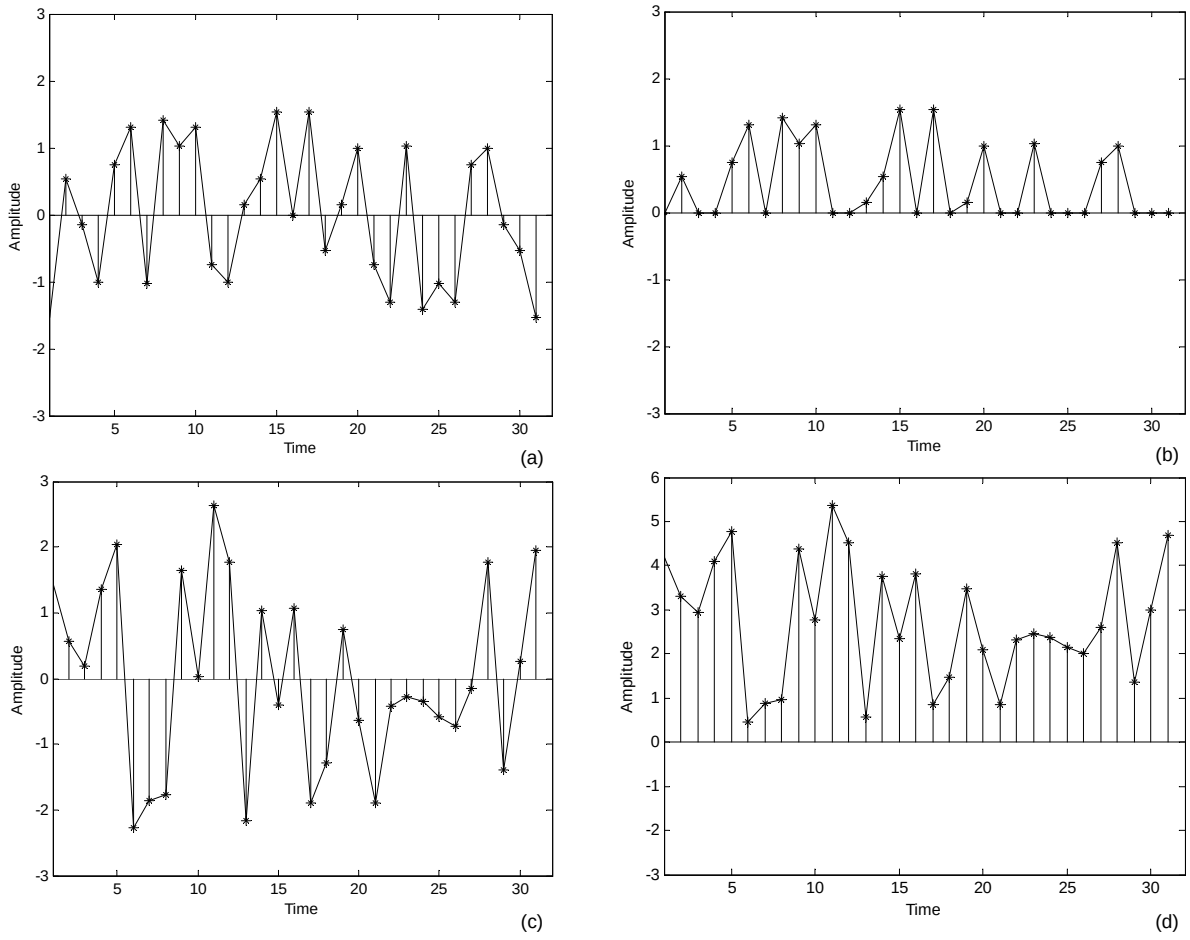

Figure 2.10: Real-valued OFDM time domain signal (a) with only odd subcarriers modulated and (b) clipped to zero level (ACO-OFDM); (c) with all subcarriers modulated and (d) clipped to zero level after adding a bias (DCO-OFDM).

ACO-OFDM and DCO-OFDM comparison Fig. 2.10(a) shows an OFDM frame with only the odd subcarriers modulated (ACO-OFDM). Therefore, as the signal has odd symmetry according to equation (2.2), we can clip the signal without loosing data, as it can be seen in Fig. 2.10(b). In Fig. 2.10(c) it is represented one OFDM frame with all the subcarriers modulated and Fig. 2.10(d) shows the signal clipped to the zero level after adding a bias of twice the standard deviation of the original signal (DCO-OFDM). DCO-OFDM allows transmitting more information than ACO-OFDM with the same bandwidth, implying higher spectral efficiency. However, clipping noise could degrade the transmission. ACO-OFDM can be easily used in adaptive systems using different

modulation formats to transmit the OFDM symbols as an optimum performance with the same design can be achieved [48]. Whereas with DCO-OFDM, the bias must be constantly adjusted depending on the constellation size. Alternatively, the bias can also be fixed according to the highest modulation format at the expense of reduced power efficiency.

Real-valued OFDM symbol generation

As it can be seen in Fig. 2.8 (a), (b), (c) and (d), different transmission architectures can be implemented to create a real OFDM signal. Specifically, a first solution is based on a RF modulation of the OFDM baseband signal, as shown in Fig. 2.8(a). Once the OFDM symbol is digitally generated, the real and imaginary part are converted to the analog domain separately. The next step is to modulate the signal to RF, multiplying the real part by a cosine and the imaginary part by a sine and then adding both signals obtaining a real signal. An oscillator at an intermediate RF frequency, f_i, is required in order to implement the modulation [25].

A second DD scheme is shown in Fig. 2.8(d) and it uses the properties of the Hilbert transform to create a SSB signal without using an optical filter. Modulating the real and imaginary parts of an analytic signal, an optical signal with no-negative frequency components is obtained. In order to have an analytic signal at the output of the IFFT, half of the elements of the input vector must be set to zero.

Discrete Multitone Modulation An alternative scheme to create real OFDM signals with simplified implementation is DMT modulation (see Fig. 2.8(b)). The Hermitian Symmetry (HS) is forced at the input symbols of the IFFT in order to have a real valued signal at the output of the transform [47]. The principle of DMT is depicted in Fig. 2.11. The mapped symbols are divided into N subcarriers. The first half, from input 1 to input $N/2-1$ of the IFFT, carry useful data. Whereas the first and the $N/2$ inputs, the Nyquist frequencies, are set to zero. Then, according to the HS property, the second half of the available inputs carry the flipped complex conjugate version of the first half. As a result, real data is obtained at the output of the IFFT.

$$Y_{N-n} = Y_n^* \quad n = 1, ..., N/2-1. \tag{2.6}$$

Principle of FHT-based O-OFDM in DD systems Finally, the last analyzed option is depicted in Fig. 2.8(c) and it is based on the implementation of the Fast Hartley Transform (FHT) [21]. The FHT is a real trigonometric transform that can be used in OFDM [49, 50] and O-OFDM [21] as an alternative transform to the FFT. It gives real data when the input signal is mapped into a real constellation, such as

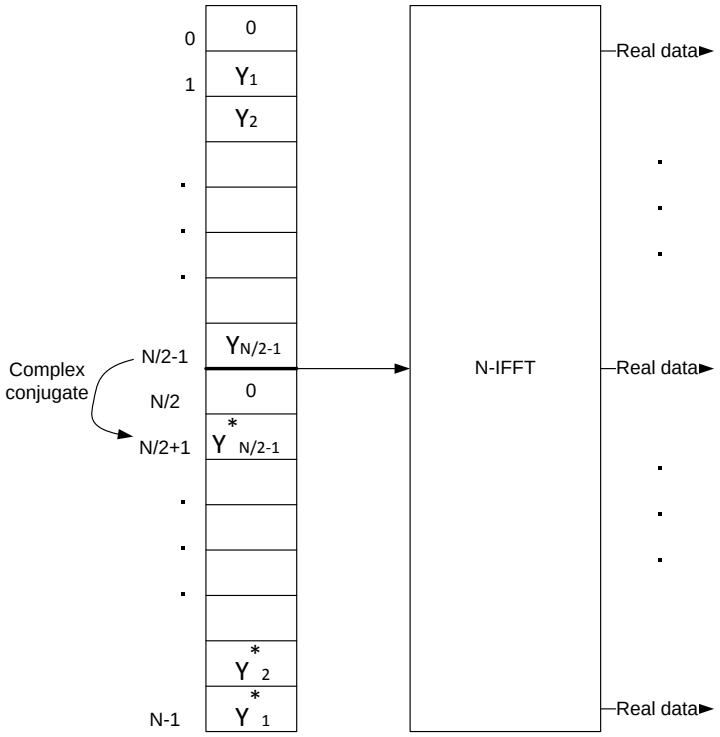

Figure 2.11: Schematic of DMT modulation.

Binary Phase-Shift Keying (BPSK) or M-ary Pulse Amplitude Modulation (MPAM), where M is the constellation size. The FHT allows simplifying the Digital Signal Processing (DSP), as it has the same routine in transmission and reception and does not require to implement the HS. The transmitted discrete signal, x_m can be written as,

$$x_m = \frac{1}{\sqrt{N}} \sum_{n=0}^{N-1} X_n cas(2\pi mn/N) \quad 0 \leq m \leq N-1, \tag{2.7}$$

where $cas(2\pi mn/N) = cos(2\pi mn/N) + sin(2\pi mn/N)$, N is the number of subcarriers of the FHT and X_n is the $n-th$ element of the input vector $\mathbf{X} = [X_0\ X_1\ X_2\ ...\ X_{N-1}]^T$. Since, no symmetry constraint is required, all the subcarriers are filled with data, whereas, when the FFT is used, only half of the subcarriers carry information [47]. Both transforms have similar complexity and the same performance in terms of spectral efficiency and BER [21, 51]. The transform kernels of the FFT and the FHT only differ for the imaginary unit, as the real and imaginary parts of the FFT coincide with the even and the negative odd parts of the FHT, respectively. Due to the kernel structure, the mirror-symmetric sub-bands of the FHT ensure subcarriers orthogonality, resulting in a suitable basis for OFDM modulation. The same spectral efficiency and bit optical power are obtained using the FHT with BPSK, 4PAM and 8PAM formats or either using the FFT with 4QAM, 16QAM and 64QAM formats, respectively, as demonstrated in [52]. A typical DD scheme based on the FHT uses a MZM [51, 53].

2.4.2 Chromatic dispersion in SSMF

Chromatic dispersion is one of the major limitations in transmission over optical fibers [9, 54, 55]. At the increasing of the fiber link length other impairments such as fiber nonlinearities also appear. CD occurs because of short optical pulses enters in the fiber spreading out into a broader temporal distribution which causes signal distortion. Specifically, different spectral components of the pulse travel at slightly different group velocities causing CD. The CD can be expressed as the sum of two contributing factors: the material dispersion and the waveguide dispersion. The dispersion parameter D is defined as

$$D = -\frac{2\pi c}{\lambda^2}\beta_2, \tag{2.8}$$

where c is the light speed, λ is the center wavelength and β_2 represents the dispersion of the group velocity and it is the responsible for pulse broadening. At the increasing of the fiber length (L), CD impact is higher. As a result various subcarriers are highly attenuated. Specifically, the power penalty in decibels introduced by the CD is defined, according to [9, 20, 56] as

$$Penalty = 10log\left|\frac{1}{cos(\frac{\pi LD\lambda^2(f_{CD})^2}{c})}\right|, \tag{2.9}$$

where f_{CD} is the frequency of the subcarrier. According to [20] and equation (2.9), the n-th attenuation peak due to CD (being n any positive integer), appears at the frequency

$$f_{CD}^n = \sqrt{\frac{c(2n-1)/2\lambda^2}{LD}}. \tag{2.10}$$

2.4.3 Channel Estimation and Equalization

Channel estimation is a key process to correctly recover the transmitted data at the receiver side. Different approaches has been presented in the literature to perform channel estimation in OFDM systems [9], which is required for the equalization. Some of them estimate the channel frequency response using consecutive OFDM symbols (TS), whereas in the case of time-variant channels a group of subcarriers (pilot tones) is used. The use of CP, seen in section 2.3, combined with equalization allows a correct recovery of signals distorted by a linear dispersive channel. This represents an overhead in the transmitted signal, which reduces the supported data rate. The total symbol duration is given by the duration of the OFDM symbol and the additional component of the CP length. Generally, the CP is a small fraction of the OFDM symbol, but to be effective should be longer than the delay spread. As the FFT order increases, the impact of CP on the data rate becomes less significant. Generally, a 10% CP is considered in

practical systems. It has been demonstrated that large dispersion tolerance is achieved using long OFDM symbol lengths [57]. Additionally, if the receiver FFT window is aligned with the start of the main symbol period of the first arriving signal and the delay spread, introduced in the system by the channel, is smaller than the CP, then no ICI or ISI occurs.

Periodically inserting training symbols imply also an additional overhead which depends on the total frame length and the number of TS. Using a one tap equalizer, in FFT-based OFDM systems, amplitude and phase errors can be corrected at the received side by performing one complex multiplication for each element. In order to explain the frequency domain equalization we define the IFFT matrix $\mathbf{Q}$, according to [58]:

$$\mathbf{Q} = \frac{1}{\sqrt{N}} \begin{bmatrix} 1 & e^{\frac{j2\pi}{N}(N-1)} & ... & e^{\frac{j2\pi}{N}(N-1)(N-2)} & e^{\frac{j2\pi}{N}(N-1)^2} \\ 1 & e^{\frac{j2\pi}{N}(N-2)} & ... & e^{\frac{j2\pi}{N}(N-2)^2} & e^{\frac{j2\pi}{N}(N-1)(N-2)} \\ . & . & . & . & . \\ . & . & . & . & . \\ . & . & . & . & . \\ 1 & e^{\frac{j2\pi}{N}} & ... & e^{\frac{j2\pi}{N}(N-2)} & e^{\frac{j2\pi}{N}(N-1)} \\ 1 & 1 & ... & 1 & 1 \end{bmatrix} \tag{2.11}$$

Then, the channel output can be expressed in matrix-vector form as:

$$\mathbf{s} = \mathbf{P}\mathbf{y} + \mathbf{n}, \tag{2.12}$$

where $\mathbf{P}$ is the circular channel matrix and $\mathbf{n}$ is the additive noise added by the channel. $\mathbf{P}$ can be decomposed following [58] as $\mathbf{P} = \mathbf{Q}\mathbf{\Omega}\mathbf{Q}^{-1}$. $\mathbf{\Omega}$ is a square diagonal matrix with the eigenvalues of the matrix $\mathbf{P}$ on the diagonal. Hence, from the frequency-domain point of view, the diagonal of the matrix $\mathbf{\Omega}$ can be seen as the FFT of the channel input response. Therefore, it can be estimated using different adaptive signal processing methods with the insertion of TS or pilot tones, as described above. The demodulated signal can be written as $\mathbf{S} = \mathbf{Q}^{-1}\mathbf{s}$. Finally, $\mathbf{S}$ is equalized by multiplying the received data with the inverse of $\mathbf{\Omega}$ in order to recover the transmitted signal. From this first step equalization, decision directed channel estimation is performed by using the equalized data as an input for a second step equalization. Specifically, the equalization matrix is updated and it can be used to retrieve the transmitted data.

On the other hand, when the FHT is used, as each data symbol is transmitted over two mirror-symmetric subcarriers due to the kernel structure of equation (2.7), two correction factors are required for equalizing each vector element at the receiver side to retrieve the transmitted data. However, since the FHT is a real transform and the mapped symbols are real-valued, no complex calculations are needed for the equaliza-

tion processing [58, 59]. In fact, only two real-valued multiplications and one addition per vector element are required to equalize the N received data. Furthermore, it is important to note that, thanks to the FHT symmetry property, if half of the vector elements of the training symbols are set to zero, a simplified channel estimation is possible, as only N real-valued divisions are performed to estimate all the equalization matrix factors [59]. Therefore, this low complexity FHT equalization processing has the same computational load as the equalization processing based on a real-valued FFT, which requires a half-length ($N/2$) equalizer. In fact, taking into account the redundancy of the transmitted symbols in the FFT scheme, due to the HS constraint, the equalization matrix is $N/2$-dimensional, but complex computations (4 real multiplications and 2 additions each tap) are performed to recover the transmitted data and complex divisions are required to estimate the response of each subchannel.

2.4.4 Synchronization in OFDM systems

Different synchronization techniques have been proposed in the literature for OFDM systems [60–63]. In particular, Schmidl & Cox solution is presented in [60] as a robust and rapid method for synchronization in OFDM systems. This algorithm finds an approximation of the starting point of the OFDM symbol by using a TS in which the first half is identical to the second half in the time domain. Thanks to the use of a CP, higher tolerance is achieved in the algorithm solution search. In this thesis, a variation of this algorithm has been implemented transmitting two identical TS to estimate the beginning of the OFDM symbol. This way, these TS can also be used to perform the equalization processing. A timing metric, $M(d)$, as defined in [60], is calculated. The correlation metric $P(d)$ is given by

$$P(d) = \sum_{m=0}^{L_1-1} (r^*_{d+m} r_{d+m+L_1}), \tag{2.13}$$

where L_1 is the length of the symbol, d is a time index corresponding to the first sample in a window of $2*L_1$ samples, r is the received signal and $()^*$ represents the conjugation operation. This operation is performed for all the received OFDM symbols. The energy of the OFDM symbol, $R(d)$, is defined as

$$R(d) = \sum_{m=0}^{N-1} |r_{d+m+N}|^2 \tag{2.14}$$

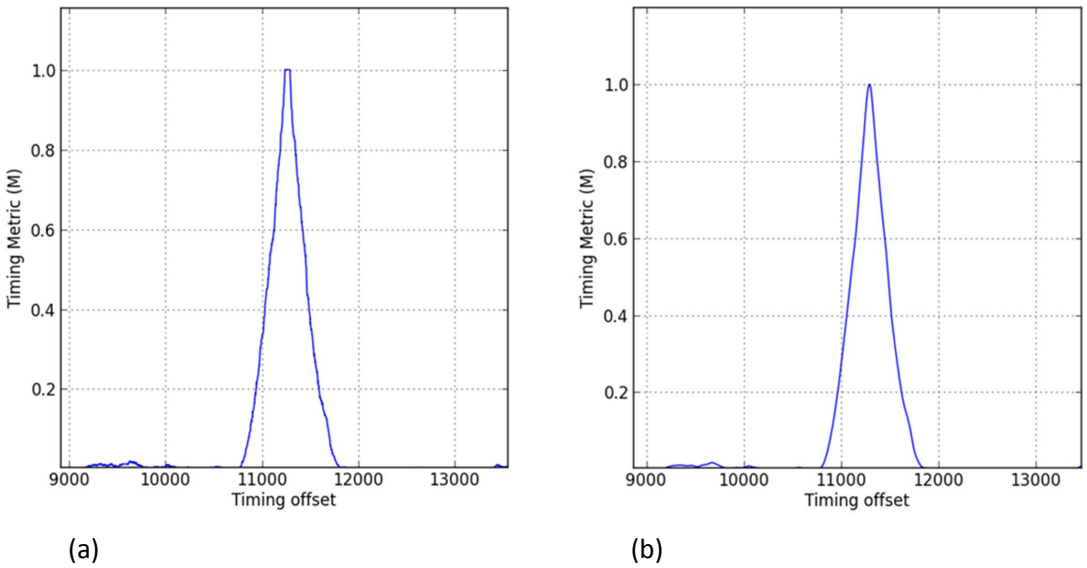

Figure 2.12: Timing metric before (a) and after (b) the average windowing.

Finally the timing metric can be written as

$$M(d) = \frac{|P(d)|^2}{(R(d))^2}. \tag{2.15}$$

The timing metric reaches a plateau with length equal to the difference between the length of the cyclic prefix and the length of the channel impulse response. Any point included in this plateau is a valid shift approximation that give the OFDM symbol beginning. In order to increase the accuracy of the search, an average windowing is used to create a peak at the medium point of the plateau, which is selected as the start of the symbol. As an example, Fig. 2.12 shows the timing metric before (a) and after (b) implementing the average windowing. Specifically, the plateau of the timing metric can be seen in Fig. 2.12(a). Whereas the estimated shift value is depicted in Fig. 2.12(b). Considering $N = 256$, 20 OFDM symbols, a CP of 10% and 16QAM format, the detected shift is around the 11200 sample. Once the symbol beginning is estimated, the received data can be shifted by this number of samples in order to recover the transmitted data.

3

PAPR, clipping and quantization noise mitigation

"Any sufficiently advanced technology is indistinguishable from magic."

Arthur C. Clarke

3.1 Introduction

One of the main drawback of Orthogonal Frequency Division Multiplexing (OFDM) is the high Peak-to-Average Power Ratio (PAPR). Occasionally, the transmitted signal exhibits very high peaks that can cause intermodulation among the subcarriers due to the nonlinearities of devices, such as Mach-Zehnder modulator (MZM), Digital-to-Analog Converter (DAC), Analog-to-Digital Converter (ADC), and the fiber. The OFDM signal must be allocated in the linear part of the transfer function of the MZM. This can be controlled with the selection of the MZM bias point [64]. However, the presence of high PAPR can introduce distortion. Furthermore, the dynamic range of DAC and ADC must be adjusted in order to accommodate the OFDM signal and avoid signal distortion. Hence, a dynamic range up to the value of the PAPR must be ensured and which implies very high values. On the other hand, the limited bit resolution of the DAC and ADC introduces quantization noise to the system.

The problem of PAPR minimization can be solved using an exhaustive search [65]. However, for a feasible system implementation in optical communications, the set of possible solutions must be limited, resulting in a suboptimal solution. Different PAPR reduction techniques have been proposed, in the literature, for optical communications [18, 66–70]. Clipping is the simplest PAPR reduction technique. It consists of limiting the amplitude of the transmitted signal to a maximum allowed value (symmetrically clipping). However, as it will be observed in section 3.2, clipping the signal causes distortion and results in clipping noise, which degrades the system performance [18]. Active Constellation Extension (ACE), Tone Reservation (TR) and Tone Injection (TI)

are another group of PAPR reduction techniques that achieve high PAPR reduction at the expense of high computational complexity and power increase. ACE consists of solving a convex optimization problem to find the optimum or suboptimum extension of the constellation points for minimizing the distance between them and thus reducing the PAPR [66]. TR and TI are based on adding a data-block-dependent time domain signal to reduce the PAPR. So in order to find the data-block that has the best performance, also for these techniques a convex optimization problem must be solved [68]. SeLective Mapping (SLM), interleaving and Partial Transmit Sequence (PTS) are distortionless PAPR reduction techniques that consist of finding an alternative representation of the signal that minimizes the PAPR, by adding transform blocks at the transmitter. In [67], these techniques have been first proposed and analyzed in Additive White Gaussian Noise (AWGN) for Intensity-Modulation (IM)/Direct Detection (DD) systems based on the Fast Hartley Transform (FHT). Coding is another distortionless technique that consists of using codewords to reduce the PAPR. There is a wide range of alternative codewords such as Trellis shaping [71] or Alamouti space-time coding [72]. However, as coding techniques require an exhaustive search to find the best codes, its implementation is very limited when a large number of subcarriers are used. Furthermore, their application to optical systems is limited due to the required complex digital processing at the transmitter. Precoding is a simpler type of coding that consists of multiplying the signal by a matrix to reduce the autocorrelation of the input sequence and thus the PAPR [70]. The precoding matrices can be based on the Hadamard transform [73] or the discrete cosine transform [74].

In this chapter, we consider a DD Optical-OFDM (O-OFDM) system based on the FHT with simplified Digital Signal Processing (DSP) and PAPR reduction capabilities. The main contributions of the chapter are:

- The problem of PAPR, clipping and quantization noise is analyzed in O-OFDM systems based on the FHT.

- Distortionless techniques for minimizing the PAPR, clipping and quantization noise in DD O-OFDM systems based on the FHT are presented. Specifically, Low Complexity (LC)-SLM, PTS and precoding schemes are proposed in order to also reduce the required resources using simple and cost-effective architectures for the design of real-time transceivers scalable to high-speed transmission.

- Symmetrically clipping is combined with the proposed LC distortionless PAPR reduction techniques.

- The PAPR performance of the proposed techniques is analyzed.

- The clipping influence is investigated by first varying the modulation format and last applying the proposed LC PAPR reduction techniques.

- The system performance is evaluated with and without applying the proposed LC schemes in order to investigate the quantization noise impact.

- The performance in IM/DD systems for cost-sensitive applications is evaluated in presence of both clipping and quantization noise. The PAPR reduction is achieved by digital signal processing at the transmitter and thus it is independent from the optical transmission system. So that, the proposed techniques can find application in other optical systems adopting transceivers based on the FHT, such as DD O-OFDM using linear field modulation for long-haul transmission.

The remainder of the chapter is organized as follows. In section 3.2, the PAPR, clipping and quantization noise are presented as limiting factors of the system transmission. An FHT-based O-OFDM system is investigated and the system model is described. Some distortionless PAPR reduction techniques based on the FHT are proposed in section 3.3, as well their equivalent low complexity schemes in section 3.4. In section 3.5, a comparison of the proposed PAPR reduction techniques is provided. Then, in section 3.6, the system performance analysis is provided. Finally, section 3.7 concludes the chapter.

3.2 PAPR, clipping and quantization noise in FHT-based O-OFDM systems

The analyzed DD O-OFDM system based on the FHT is indicated in Fig. 3.1. The input data are parallelized and mapped into Binary Phase-Shift Keying (BPSK) or MPAM format. The resulting symbols are fed into an FHT of N points and then the modulated signal is serialized. Finally, it is symmetrically clipped and digital-to-analog converted. The resulting signal is then modulated with a MZM. As the IM generates an OFDM signal on both sides of the optical carrier frequency, a Double-Side Band (DSB) spectrum is transmitted. Although DD is more robust to dispersion impairments when combined with optical Single-Side Band (SSB) modulation, we use IM with DSB in order to implement a low-cost system, avoiding optical filters or more complex schemes [25]. Furthermore, it has been demonstrated that if IM is performed with an external MZM biased at the quadrature point, the intermodulation products, due to the square law characteristic of the photodetector, are reduced and the guard band can be decreased at the expense of the receiver sensitivity [51, 64]. A guard

band equal to the electrical signal bandwidth ($B_G = B_S$) is considered for correct photodetection. The modulated signal is transmitted over the optical channel.

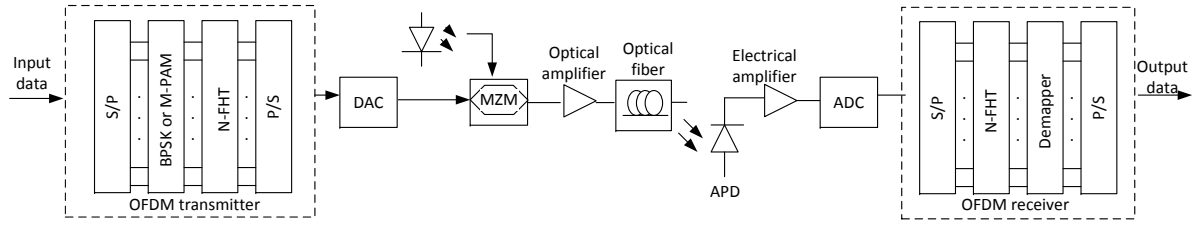

Figure 3.1: Block diagram of a DD O-OFDM system based on the FHT.

At the receiver side, the signal is photodetected with an Avalanche Photo-Detector (APD), electrically amplified and analog-to-digital converted. An APD is selected in order to limit the noise at the receiver side and focus the analysis on PAPR, clipping and quantization noise. Finally, the OFDM demodulation is performed including, serial-to-parallel conversion, FHT processing, demapping and serialization. When an optical link is considered, equalization and synchronization, defined in chapter 2, should also be implemented at the receiver to correctly recover the transmitted data [53]. The transmitted discrete signal, x_m is defined in equation (2.7). When N subcarriers are added in phase a high peak appears, whose power can be N times the average power. The ratio between the maximum peak power and the average power of the OFDM frame is defined as the signal PAPR:

$$PAPR = \frac{\max\limits_{0 \leq m \leq N-1} |x_m|^2}{E[|x_m|^2]}. \tag{3.1}$$

The theoretical limit of PAPR (in dB) can be derived from equation (3.1), giving

$$PAPR = 10 \log_{10} N \tag{3.2}$$

and it only depends on the number of subcarriers [75]. For example, the theoretical maximum of the PAPR in a system with $N = 256$ subcarriers is 24 dB. However, this high value rarely occurs.

One common technique that is used to measure the PAPR is the Complementary Cumulative Density Function (CCDF), defined as

$$CCDF = P_r(PAPR > PAPR_0). \tag{3.3}$$

This function gives the probability that the PAPR exceeds a threshold $PAPR_0$. For calculating the PAPR of the continuous analog signal, Nyquist sampling rate can be used. However, it can occur that the maximum value of the O-OFDM signal may not

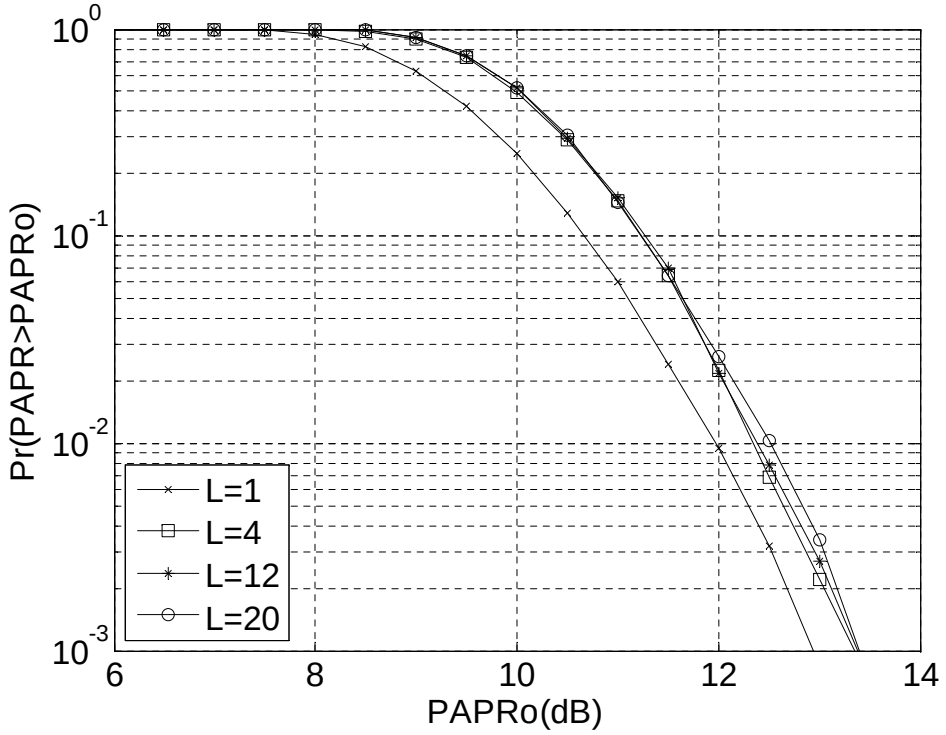

Figure 3.2: CCDF of O-OFDM based on FHT ($N = 256$) for different values of oversampling factor.

be included in the sampled points of the digital version. Therefore, an oversampling factor (L) is needed to consider the missing peaks. The oversampled time domain signal can be written as

$$\tilde{x}_m = \frac{1}{\sqrt{LN}} \sum_{n=0}^{LN-1} X_n cas(2\pi mn/(LN)) \quad 0 \leq m \leq LN-1. \tag{3.4}$$

The PAPR of the L times oversampled time domain signal, can be therefore calculated as

$$PAPR = \frac{\max\limits_{0 \leq m \leq NL-1} |\tilde{x}_m|^2}{E[|\tilde{x}_m|^2]}. \tag{3.5}$$

According to [76], a fourfold oversampling factor ($L = 4$) is enough to consider the missing peaks when the Fast Fourier Transform (FFT) is used. Figure 3.2 shows the CCDF varying the oversampling factor L when the FHT is used. Fig. 3.2 shows that PAPR increases of about 0.5 dB when the oversampling factor is set to 4 in comparison with the case of no oversampling, i.e. $L = 1$. Whereas if the signal is oversampled with greater L factor of 12 or 20, the CCDF of the PAPR is almost the same as the one with $L = 4$. The PAPR also increases with the number of subcarriers, as shown in Fig. 3.3. When the number of subcarriers is set to $N = 256$ the probability that the

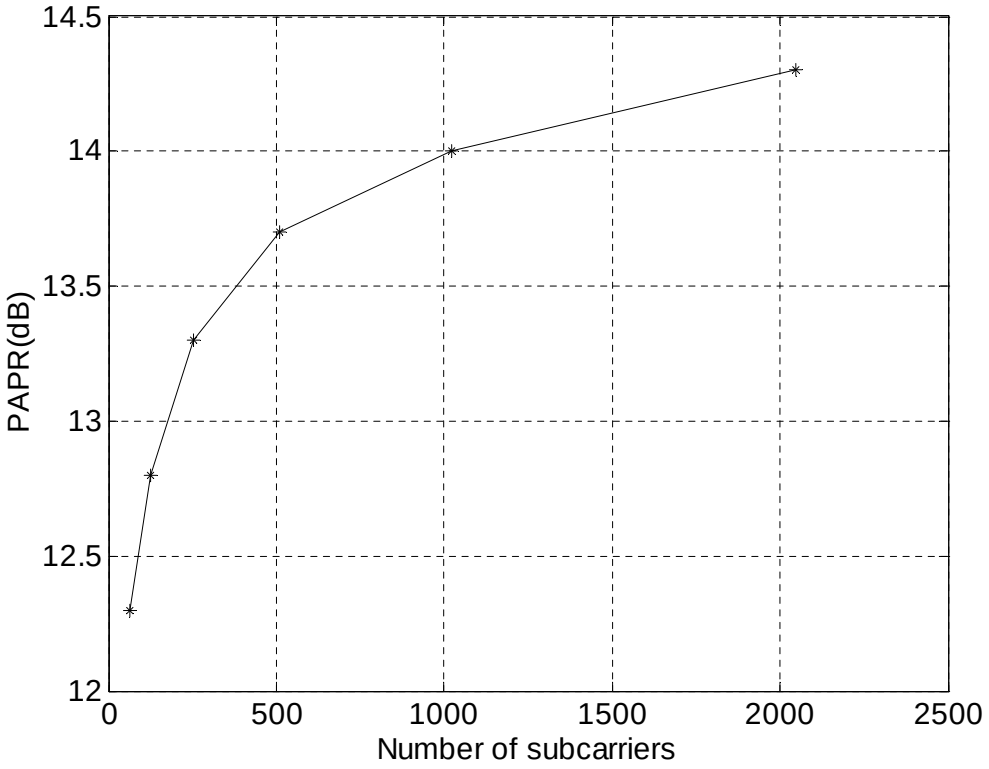

Figure 3.3: PAPR as a function of the number of subcarriers in FHT-based O-OFDM system at a CCDF of 0.1%. The oversampling factor is fixed at 4.

PAPR exceeds 13.3 dB is less than 0.1% whereas with $N = 2048$ the PAPR increases by about 1 dB.

Symmetrically clipping is used to limit the high peaks of power that can occur in OFDM signals. The symmetrically clipped digital FHT-based OFDM signal can be represented by

$$\hat{x}_m = \begin{cases} \tilde{x}_m, & |\tilde{x}_m| \leq B \\ \\ B \cdot sign(\tilde{x}_m), & |\tilde{x}_m| > B \end{cases} \tag{3.6}$$

where B is the maximum allowed signal amplitude and it is defined as k times the standard deviation of the signal ($B = k\sqrt{E[|\tilde{x}(m)|^2]}$) [21]. The clipping level (C) is defined, taking as a reference equation 2.5, in decibels as

$$C = 10 \cdot \log_{10}\left(\frac{B^2}{E[|\tilde{x}_m|^2]}\right), \tag{3.7}$$

where $E[|\tilde{x}_m|^2]$ denotes the average signal power of the oversampled signal. The clipped signal is normalized to a factor of $2B$, which is the peak-to-peak signal amplitude, in order to be adjusted to the dynamic range of the MZM [64]. Additionally, in the OFDM system, the quantization effects due to the digital-to-analog conversion must

be also taken into account. According to [18] and using a uniform quantizer, we consider a step size Δ defined as $\Delta = 2B/(2R-1)$. R is the number of bits of the quantizer that corresponds to the number of binary digits used to represent each sample. The digital signal is quantized using $2R$ amplitude levels ($-B$, B and $-B+q\Delta$ with $q = 1, 2, ..., 2R-2$).

The optimization problem that is tackled in this chapter is the minimization of the OFDM signal PAPR, specified by equation (3.5), in order to limit the signal distortion due to the clipping and to relax the DAC requirements.

3.3 Distortionless PAPR reduction techniques

In this section, we propose to use distortionless PAPR reduction techniques that can be easily applied to O-OFDM systems based on the FHT with simplified DSP, allowing the implementation of low-complexity schemes. SLM, interleaving, PTS and precoding with Hadamard transform are used to design the FHT-based DSP with PAPR reduction capability.

3.3.1 Selective mapping

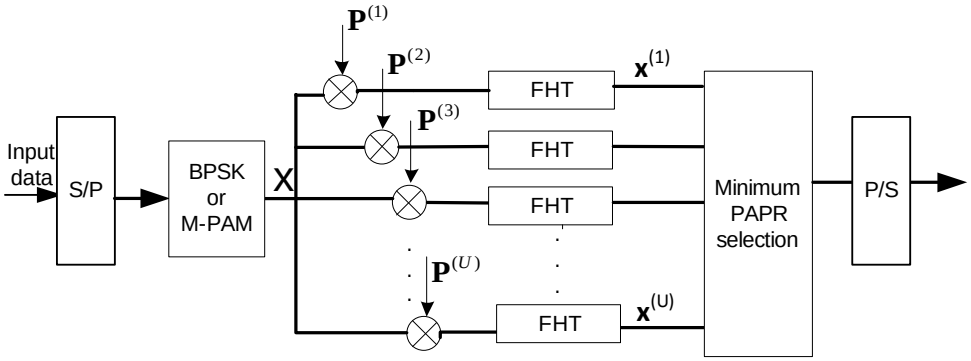

Figure 3.4: Block diagram of SLM PAPR reduction technique using U transform (FHT) blocks in order to create U different signal representations.

SLM consists of generating alternative OFDM frames representing the same information [77]. Each mapped input vector is multiplied by different vectors $\mathbf{P}^{(u)}$ with $u = 1, 2, ..., U$, where U is the number of FHT transform blocks and equal to the number of signal representations. The FHT is applied to the different signal representations, and the $\mathbf{P}^{(u)}$ that provides the minimum PAPR (i.e. equation (3.5)) is selected. Figure 3.4 shows the block diagram of SLM technique. $\mathbf{P}^{(u)}$ has N elements belonging to the set $\{\pm 1\}$, as real data are considered. In order to include the unmodified signal in the set of possible signal representations, all the elements of the first encoding

vector $\mathbf{P}^{(1)}$ are set to one, so that $\mathbf{X}^{(1)} = \mathbf{X} \cdot \mathbf{P}^{(1)} = \mathbf{X}$ (see Fig. 3.4). The choice of these vectors is not restricted to any symmetry constraint. Increasing the number U of signal representations increases the peak power reduction, but also the number of FHT blocks and thus the hardware resources needed for the system implementation. SLM requires $\log_2(U)$ bits of side information for the correct frame reception [65]. Using 4 transform blocks, only 2 bits are required to transmit side information to the receiver. This side information can be carried using 2 pilot tones and this overhead is negligible when compared with DMT systems based on the FFT, where the first and the Nyquist frequencies are set to zero to implement the Hermitian Symmetry (HS).

3.3.2 Interleaving

Interleaving technique consists of permuting or reordering the original data to create different sequences that carry the same information; then the one that provides the minimum PAPR is selected [78]. The original input data vector with N components $\mathbf{X} = [X_0\ X_1\ ...\ X_n\ ...\ X_{N-1}]^T$ becomes $\mathbf{X'} = [X_{\varphi(0)}\ X_{\varphi(1)}\ ...\ X_{\varphi(n)}\ ...\ X_{\varphi(N-1)}]^T$, where the indexes of the vector elements are related by the one-to-one mapping $(n) \rightarrow (\varphi(n))$ and $\varphi(n) \in \{0, 1, ..., N-1\}$ for all n. Also in this case, U number of FHT blocks are required, where U denotes the number of interleavers. Increasing the number of interleavers enhance the system performance at the expense of higher computational complexity. In the particular case of $U = 4$, the required side information is $\log_2 U = \log_2 4 = 2$ bits.

3.3.3 Partial transmit sequence

The main idea of PTS technique is to divide the original frame into different subvectors $\mathbf{X}^{(v)}$ with $v = 1, 2, ..., V$ [79], where V represents the number of required FHT blocks. These subvectors are created such that all the subcarriers positions, which are represented in other subvectors, are set to zero. The total number of zeros at the input of each FHT block is $(V-1)N/V$. A possible choice for the vector partitioning is based on adjacent selection, whereas another implementation is based on a random selection of the subvectors [80]. For example, in the case of $V = 2$ and $N = 8$, the resulting vectors $\mathbf{X}^{(v)}$, obtained after adjacent partitioning $\mathbf{X} = [X_0\ X_1\ X_2\ X_3\ X_4\ X_5\ X_6\ X_7]^T$, is $\mathbf{X}^{(1)} = [X_0\ X_1\ X_2\ X_3\ 0\ 0\ 0\ 0]^T$ and $\mathbf{X}^{(2)} = [0\ 0\ 0\ 0\ X_4\ X_5\ X_6\ X_7]^T$; whereas possible random partitions of $\mathbf{X}$ are $\mathbf{X}^{(1)} = [X_0\ 0\ X_2\ X_3\ 0\ 0\ 0\ X_7]^T$ and $\mathbf{X}^{(2)} = [0\ X_1\ 0\ 0\ X_4\ X_5\ X_6\ 0]^T$. Once the subvector partition is done, the FHT is performed and then the output is multiplied by the components of a weighting vector $\mathbf{p}^{(u)}$. To find the $\mathbf{p}^{(u)}$ that minimizes the PAPR of signal $\mathbf{F}(\mathbf{p}^{(u)})$ an exhaustive search is performed. Finally, the signal is recombined and

transmitted using the optimum $\mathbf{p}^{(u)}$. Due to the linearity of the FHT, we can write

$$\mathbf{F}(\mathbf{p}^{(u)}) = FHT\{\sum_{v=1}^{V} p_v^{(u)} \cdot \mathbf{X}^{(v)}\}$$
$$= \sum_{v=1}^{V} p_v^{(u)} \cdot FHT\{\mathbf{X}^{(v)}\} = \sum_{v=1}^{V} p_v^{(u)} \cdot \mathbf{x}^{(v)} \quad u = 1, ..., U. \tag{3.8}$$

The elements of $\mathbf{p}^{(u)}$ are real values in the set $\{\pm 1\}$, where $p_1^{(u)}$ can be set to 1 reducing

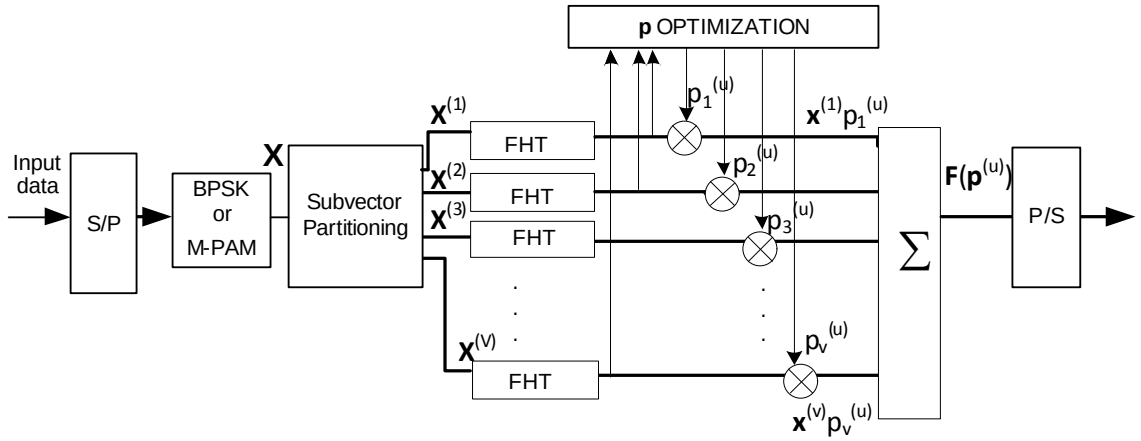

Figure 3.5: Block diagram of PTS PAPR reduction technique using V transform (FHT) blocks.

the complexity of the optimization process without any loss of performance [79]. All the elements of $\mathbf{p}^{(1)}$ are set to 1, in order to consider the original vector. Therefore, the total number of optimization vectors is $2^{(V-1)}$ and it coincides with the total number of signal representations U. The required side information is $(V-1)\log_2(W)$ bits, where W represents the number of possible different values that the components of the vector $\mathbf{p}^{(u)}$ can assume. For example, in the case that the $\mathbf{p}^{(u)}$ components are in the set $\{\pm 1\}$ ($W = 2$) and using 4 FHT blocks ($V = 4$), the required side information is 3 bits. Compared with SLM and interleaving with 4 FHT blocks, PTS needs one additional bit to carry side information.

3.3.4 Precoding with the Hadamard transform

Precoding is another alternative distortionless PAPR reduction technique that consists of multiplying the vector $\mathbf{X}$ by a precoding matrix. Different precoding matrices can be used to reduce the PAPR. Here, we propose to use the Hadamard matrix for optical systems, as it is very easy to compute. The Hadamard transform is based on the Hadamard square matrix ($\mathbf{H}_N$) of dimensions $N \times N$, which elements are +1 or -1 [73].

The Hadamard matrix of 1, 2 and N orders are:

$$H_1 = (1); \quad \mathbf{H}_2 = \frac{1}{\sqrt{2}} \begin{pmatrix} 1 & 1 \\ 1 & -1 \end{pmatrix}$$
$$\mathbf{H}_N = \frac{1}{\sqrt{N/2}} \begin{pmatrix} \mathbf{H}_{N/2} & \mathbf{H}_{N/2} \\ \mathbf{H}_{N/2} & -\mathbf{H}_{N/2} \end{pmatrix}. \tag{3.9}$$

The rows of this matrix are mutually orthogonal, so it is used to lower the correlation relationship of the mapped sequences at the input of the FHT. Therefore, the use of this transform reduces the occurrence of the high peaks, compared to the original OFDM frame, adding low computational complexity. This PAPR reduction technique doesn't need side information as, at the receiver side, the transmitted signal is recovered by applying the inverse of the corresponding Hadamard matrix ($\mathbf{H}_N^{-1}$).

3.4 Low complexity PAPR reduction techniques

In [47], a LC PAPR reduction technique is described for O-OFDM systems based on real valued FFT. Two different symmetries for each transform block are required to implement the scheme. Conversely, here, we use the FHT to implement alternative LC PAPR reduction techniques for O-OFDM without applying any symmetry constraint. The principle of the proposed LC techniques is similar to the standard distortionless PAPR reduction techniques, with the difference that two signal representations of the input signal can be processed in parallel by using a single FHT block, thanks to the properties of this transform [81]. Therefore, the required resources are halved becoming a suitable solution for cost-effective optical implementations. Specifically, in this section we describe the LC-SLM, LC-PTS techniques and LC-SLM with precoding.

3.4.1 Low complexity selective mapping

Low-complexity selective mapping technique, as shown in Fig. 3.6, consists of creating a complex vector, whose real part carries one signal representation while the imaginary part carries another representation of the original data. For example, two weighting vectors $\mathbf{P}^{(u)}$, with $u = 1, 2$, are processed by one FHT block combined to be a single input vector $\mathbf{X}^{(1,2)} = [\mathbf{XP}^{(1)} + j\mathbf{XP}^{(2)}] = [X_0P_0^{(1)} + jX_0P_0^{(2)}, X_1P_1^{(1)} + jX_1P_1^{(2)}, ..., X_{N-1}P_{N-1}^{(1)} + jX_{N-1}P_{N-1}^{(2)})]$. At the output of the FHT, we obtain a complex vector, $\mathbf{x}^{(1,2)} = FHT\{\mathbf{X}^{(1,2)}\} = FHT\{[\mathbf{XP}^{(1)} + j\mathbf{XP}^{(2)}]\} = \mathbf{x}^{(1)} + j\mathbf{x}^{(2)}$. The real part of $\mathbf{x}^{(1,2)}$ is the FHT of the first signal representation and the imaginary part of $\mathbf{x}^{(1,2)}$ is the FHT of the other signal representation. Then the PAPR of both signals is evaluated in order to select the one with minimum peak power. Hence, after the

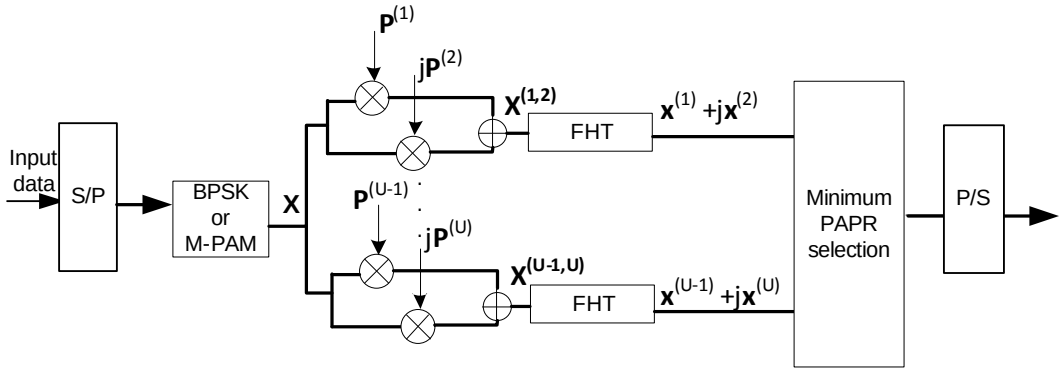

Figure 3.6: Block diagram of LC-SLM PAPR reduction technique applied to an OFDM transmitter based on the FHT.

selection process, only a real-valued signal is transmitted. The same scheme is valid for more transform blocks. Adding one FHT results in two new signal representations. Similarly to SLM, a LC scheme can also be implemented for interleaving technique. Hence, with one FHT block two different signal representations of the transmitted signal can also be processed in parallel. Each signal representation is created with a different interleaver.

3.4.2 Low complexity partial transmit sequences

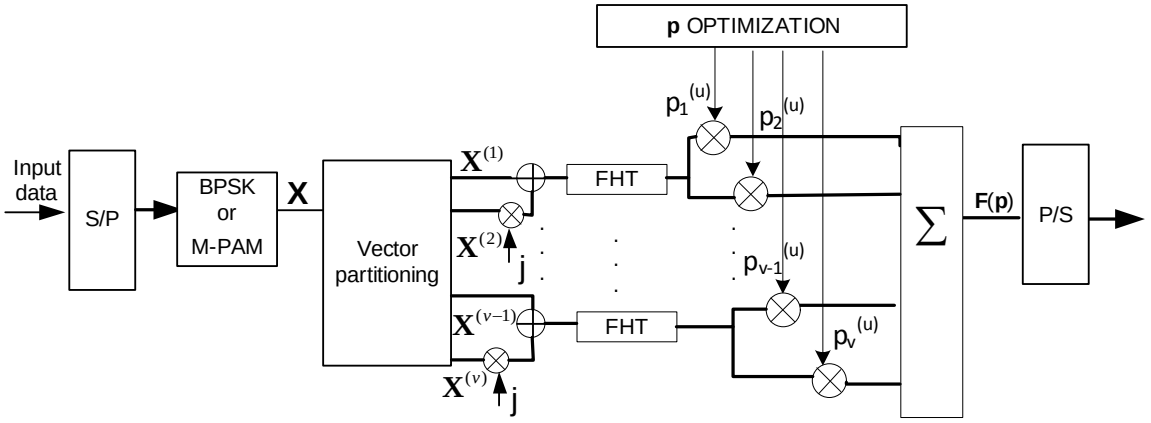

Figure 3.7: Block diagram of LC-PTS PAPR reduction technique applied to an OFDM transmitter based on the FHT.

In Fig. 3.7, the block diagram of the proposed LC-PTS technique is depicted. As in standard PTS technique, the original data are randomly or adjacently divided into subvectors. Then we construct a complex vector whose real part carries one subvector and the imaginary part carries another one. Both subvectors are parallel processed by one FHT block using half of the resources required by the standard technique. Afterwards the FHT outputs are multiplied by a weighting vector $\mathbf{p}^{(u)}$. Finally, the

signal is recombined and the vector $\mathbf{p}^{(u)}$, which has provided the signal with the lowest PAPR, is chosen for signal transmission.

3.4.3 Low complexity SLM with precoding

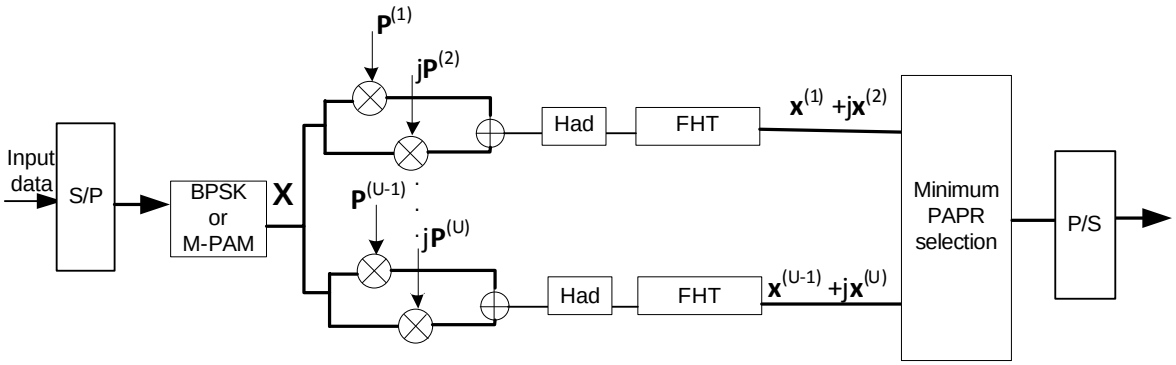

Figure 3.8: Block diagram of LC-SLM with the Hadamard transform precoding applied to an OFDM transmitter based on the FHT.

The Hadamard transform can be used jointly with other PAPR reduction techniques, such as SLM, to obtain higher reduction of the PAPR. Nevertheless, it must be taken into account for the transceiver design that additional transform blocks are used (one at the transmitter for each FHT block and one at the receiver). The signal representations are generated with the LC-SLM scheme and encoded with the Hadamard transform which is performed before implementing the FHT (see Fig. 3.8). So that, the required Hadamard matrix blocks are halved as well as the FHT blocks.

3.5 Comparison of distortionless PAPR reduction techniques

To evaluate the performance of the proposed PAPR reduction techniques, we analyze the CCDF of the O-OFDM system in Fig. 3.1. The transmitter design is adapted in order to implement the proposed techniques as shown in Figs. 3.4, 3.5, 3.6, 3.7 or 3.8. Furthermore, for comparison with the FFT-based O-OFDM system, we analyze the case without applying PAPR reduction techniques when the O-OFDM is based on the FHT. We consider $N = 256$ subcarriers and $L = 4$ oversampling factor. Since real-valued OFDM signals are required, $\mathbf{P}^{(u)}$ and $\mathbf{p}^{(u)}$ vectors have real values in the set $\{\pm 1\}$. Figure 3.9 shows a number of CCDF curves that are computed for OFDM system implementation cases analyzed in this chapter. It can be seen that OFDM signals, modulated with either the FFT or the FHT, present the same PAPR of 13.3 dB

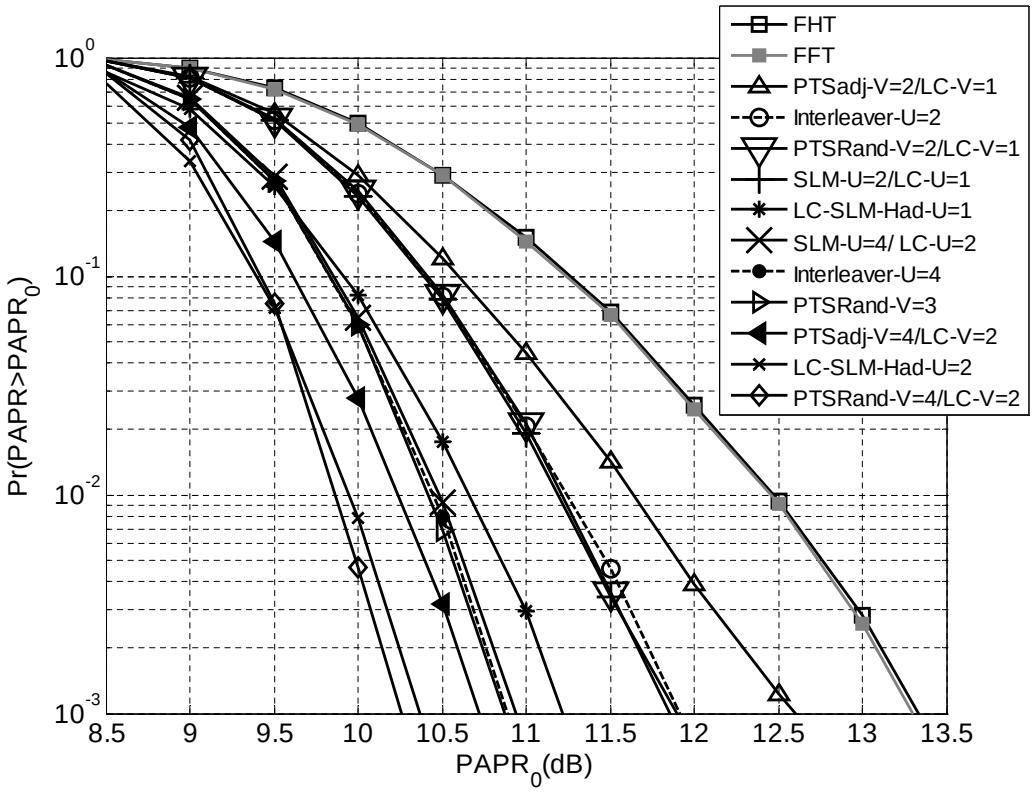

Figure 3.9: CCDF vs. $PAPR_0$ for OFDM signals (for $N = 256$) with and without standard and LC PAPR reduction techniques.

at a CCDF of 0.1%. 2 dB of penalty is obtained, if we compare the achieved result with the PAPR of a complex OFDM signal, according to [82]. LC schemes have the same performance as standard schemes but requires only half transform blocks. In fact, it can be observed that, with $U = 4$ FHT blocks, the standard SLM technique gives a PAPR reduction of 2.4 dB at a probability of 10^{-3}, compared to the unmodified signal PAPR (13.3 dB). The same PAPR reduction is achieved using LC-SLM with $U = 2$ FHT blocks. Using $V = 4$ FHT blocks and applying PTS with adjacent partitions the PAPR reduction is 2.6 dB. PTS with random partitions gives an increased reduction of 3.1 dB. Interleaving technique gives the same performance as SLM using the same number of FHT blocks. The same also occurs in standard OFDM systems based on the FFT, as demonstrated in [65]. It can be also observed that random PTS technique with $V = 3$ blocks gives the same PAPR reduction (2.4 dB) as standard SLM with $U = 4$ transform blocks. Increasing the number of signal representations, better PAPR reduction can be achieved, but it implies using additional transform blocks and this is not suitable for real time applications in optical communications. Hence, we have analyzed the case of using at most 4 FHT blocks corresponding to only 2 FHT for LC schemes. Using SLM, interleaving and PTS with random partitioning and $U = V = 2$ FHT blocks the probability that the PAPR exceeds 11.8 dB is less than 0.1%, resulting

Table 3.1: Comparison of PAPR reduction at 10^{-3} CCDF varying the number of FHT blocks at the transmitter for different distortionless techniques

PAPR technique	**1 FHT**	**2 FHT**	**3 FHT**	**4 FHT**
SLM	-	1.5 dB	-	2.4 dB
Interleaver	-	1.5 dB	-	2.4 dB
PTSadj	-	0.7 dB	-	2.6 dB
PTSRand	-	1.5 dB	2.4 dB	3.1 dB
LC-SLM	1.5 dB	2.4 dB	-	-
LC-PTSadj	0.7dB	2.6 dB	-	-
LC-PTSRand	1.5 dB	3.1 dB	-	-

in a PAPR reduction of 1.5 dB. The same reduction is obtained with LC-SLM with a single FHT block. Using PTS with adjacent partitions, the reduction is 0.7 dB. Similar difference (in dB) between the PAPR reduction values using PTS and SLM has been obtained in OFDM systems based on the FFT, as demonstrated in [2]. Table 3.1 summarizes the results that are obtained by applying the proposed PAPR reduction techniques. These results are presented in terms of PAPR reduction that is estimated at CCDF of 0.1%, and varying the number of FHT blocks at the transmitter.

We also analyze the LC-SLM technique in combination with the Hadamard transform block for precoding. Firstly, we consider the transmitter design that is shown in Fig. 3.8, when only one ($U = 1$) FHT block and only one Hadamard transform block is used. In this case the probability that the PAPR is greater than 11.2 dB is less than 0.1%, corresponding to a 2.1 dB reduction compared with the unmodified signal PAPR. When using two FHT blocks ($U = 2$) and two Hadamard transform blocks this reduction is 2.9 dB. It is important to point out that, at the receiver side, only one FHT block is required when applying distortionless PAPR reduction techniques, whereas, with the proposed precoding technique, one additional Hadamard transform block is needed.

A summary of the proposed distortionless PAPR reduction techniques and the ones that exists on the literature is provided in table 3.2.

Finally, in order to validate some of the results achieved in this section, table 3.3 reports the PAPR reduction, at 10^{-5} BER, achieved in [2], using SLM and PTS techniques in a OFDM system. Despite that the analyzed PAPR reduction techniques in [2] are investigated considering a FFT-based OFDM system, similar PAPR performance to Fig. 3.9 is achieved. From the table, it can be seen that SLM technique presents the same PAPR performance as PTS with random partitions when 2 transform blocks are used. Moreover, PTS with random partition is the technique that achieves the highest PAPR reduction, when considering 4 transform blocks, as also demonstrated in this section when considering the proposed PAPR schemes. However, higher PAPR reduc-

Table 3.2: PAPR techniques overview

PAPR technique	Side Information	Distortionless	Technique's information
Clipping	No	No	Simple technique
ACE	No	Yes	- High computational complexity - Power increase
TR	No	Yes	- High computational complexity - Power increase
TI	No	Yes	- High computational complexity - Power increase
SLM	Yes	Yes	Finds alternative representation of the signal
Interleaver	Yes	Yes	Finds alternative representation of the signal
PTS	Yes	Yes	Finds alternative representation of the signal
Coding	No	Yes	Exhaustive search to find the best code
Precoding	No	Yes	Uses a precoding matrix at the transmitter and at the receiver
LC-SLM	Yes	Yes	Half the number of required transform blocks
LC-PTS	Yes	Yes	Half the number of required transform blocks
LC-SLM-Had	Yes	Yes	Half the number of required transform blocks

Table 3.3: Achieved PAPR reduction at 10^{-5} CCDF varying the number of IFFT blocks at the transmitter for different distortionless techniques in a OFDM system, reported in [2]

PAPR technique	2 IFFT	4 IFFT
SLM	2	3.3 dB
PTSadj	1.2	3.4 dB
PTSRand	2	4.1 dB

tion results are reported in [2], as they are obtained at a target Bit Error Rate (BER) of 10^{-5}.

3.6 Performance analysis

In this section, we numerically analyze the performance of the system shown in Fig. 3.1, by using Matlab software. We first demonstrate that the same performance is achieved in O-OFDM systems based either on the FFT or FHT. Then, the clipping and quantization noise influence on the system performance is evaluated with and without the proposed LC PAPR reduction techniques. Specifically, among the techniques described in sections 3.3 and 3.4, LC-SLM, interleaving and LC-PTS give the highest

PAPR reduction when only one or two FHT blocks are used, respectively, without requiring any additional transform block at the receiver. Hence, from now on, as we only evaluate the LC-PTS with random partitions, we will refer to it simply as LC-PTS. Additionally, as both standard SLM and interleaving techniques have the same performance in terms of PAPR, only the performance of the LC scheme for SLM is analyzed. When LC-SLM or LC-PTS are implemented, the transmitter shown in Fig. 3.1 is replaced by the one shown in Fig. 3.6 with one FHT block or by the transmitter shown in Fig. 3.7 with two FHT blocks, respectively. Finally, the PAPR reduction impact on the system performance is analyzed. For the simulation, we consider 6144 OFDM frames with two possible values of N; $N = 256$ and $N = 512$ points FHT. According to Fig. 3.3, the PAPR increases with the number of subcarriers. The clipping and the

Table 3.4: System parameters

Number of frames	6144
FHT points	256 or 512
Oversampling factor	4
Laser center wavelength	1550 nm
Laser linewidth	10 MHz
PIN responsivity	0.7 A/W
Multiplying factor	7
Overall thermal noise	$12.87{\cdot}10^{-2}$ A/ $\sqrt{Hz}$
Dark current	1 pA
channel	VOA
CP overhead	0%

quantization are modeled for all the simulations according to section 3.2. The MZM is biased at the quadrature point $V_{bias}/V_{\pi} = -0.5$, where V_{bias} is the bias voltage and V_{π} the switching voltage [64]. The laser driving the MZM is modeled as a standard continuous wave laser centered at 1550 nm, with output power 1 mW and 10 MHz linewidth, whose phase is modeled as a Wiener process. The optical channel is replaced by a Variable Optical Attenuator (VOA) to consider a Back-to-Back (B2B) configuration. The receiver is modeled as an APD with 0.7 A/W responsivity, multiplying factor of 7, overall thermal noise value of 12.87×10^{-12} A/ $\sqrt{Hz}$, and dark current of 1 pA. At the receiver, two noise contributions have been considered: the thermal noise, which is modeled as a Gaussian distribution and the shot noise, which is modeled as a Poisson distribution. The former is due to the photodetector and the electrical amplifier; the latter is due to the photoelectric detection. As the thermal noise dominates over the shot noise, the receiver noise can be assumed to have a Gaussian distribution. Finally, the analog-to-digital conversion is modeled with an electrical digital filter of bandwidth equal to the electrical signal bandwidth [21]. The BER evaluation is performed after

the receiver DSP by statistical counting the received bits. The system parameters are summarized in table 3.4.

3.6.1 Comparison using the FFT and the FHT

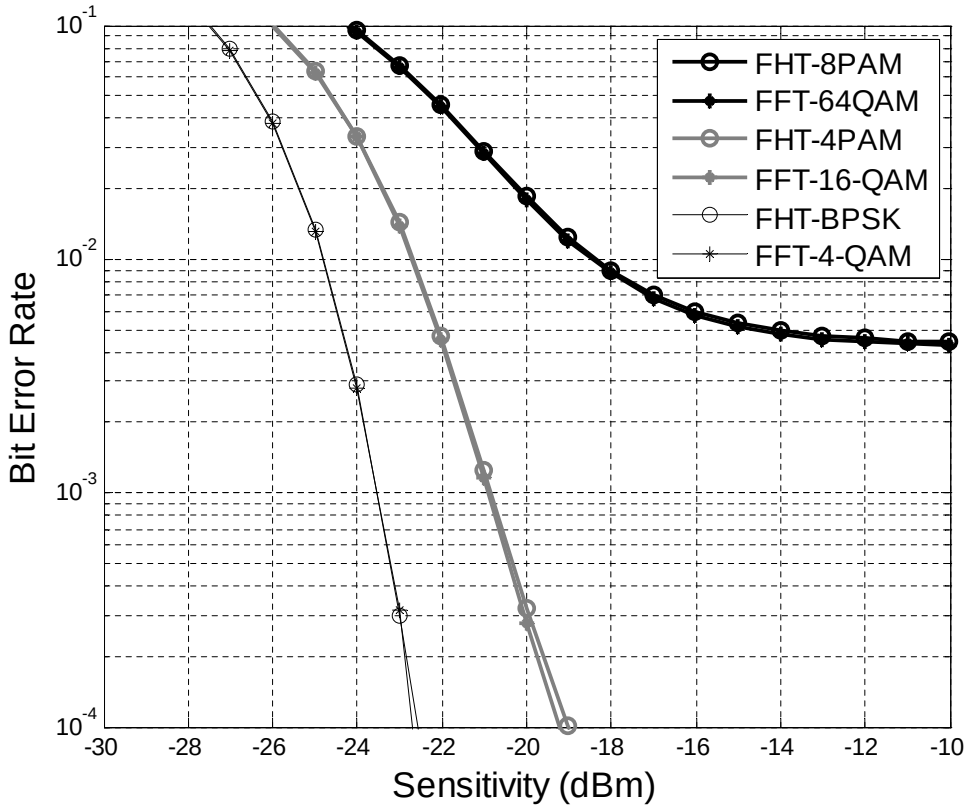

Figure 3.10: Sensitivity performance comparison of DD O-OFDM system based on FFT and FHT.

The system of Fig. 3.1 uses the same FHT block in transmission and reception due to the self-inverse property of this transform (as shown in the DSP transmitter and receiver). Whereas, in the case of a standard O-OFDM system, the FFT modulation and demodulation are performed with the Inverse Fast Fourier Transform (IFFT) and the FFT, respectively. The transmitted data are mapped into different constellations depending on the system implementation that we analyze. In order to transmit the same information bit sequence per parallel processing, an MPAM format (i.e. a real-valued one-dimensional constellation) must be used with the FHT while a two dimensional M^2 quadrature-amplitude modulation (M^2QAM) format is required with the FFT, due to the HS constraint, according to section 2.4.1. Figure 3.10 shows the B2B sensitivity performance of FHT- and FFT-based systems for different constellation sizes and $N = 256$. In the simulations, a randomly generated stream of bits transmitted at 10 Gb/s is considered. A finite DAC resolution of 8 bits and a clipping level of 7 dB

are used in order to take into account the quantization and clipping noise. In Fig. 3.10, it can be seen that both the transforms have the same sensitivity performance. Using the FHT with BPSK format, a receiver input power of −23.55 dBm is needed to ensure a BER of 10^{-3}. The same receiver input power is required to achieve the same target BER with the FFT and 4QAM format. Using 4PAM format and the FHT or 16QAM with the FFT, the required receiver power is 2.65 dB higher to guarantee 10^{-3} BER. Using either the FHT with 8PAM format or the FFT with 64QAM format, a 7 dB clipping level is not enough to ensure a target BER of 10^{-3}, and both the BER curves present a floor above this value.

3.6.2 Clipping noise analysis

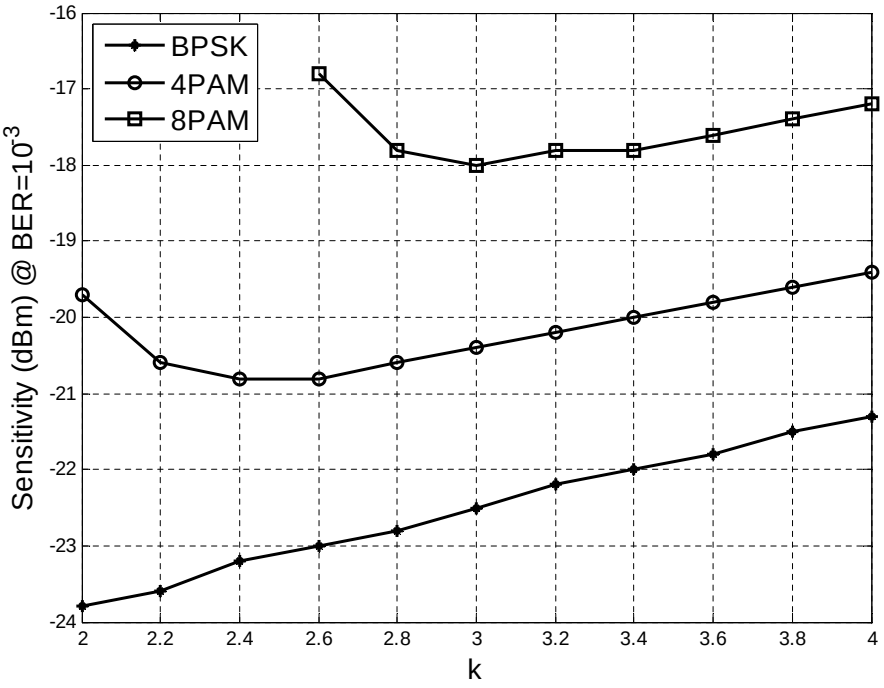

Figure 3.11: Sensitivity performance of the FHT based O-OFDM system of Fig. 3.1 at a target BER of 10^{-3} for different k values using BPSK, 4PAM and 8PAM formats.

Despite being 8PAM the most affected modulation format by system impairments as shown in Fig. 3.10, clipping noise is analyzed also considering BPSK and 4PAM formats without using any PAPR reduction technique. A bit rate of 10 Gb/s and $N = 512$ subcarriers are used. In Fig. 3.11 the sensitivity performance at a BER of 10^{-3} for different values of clipping levels is shown. It is seen that using BPSK format with $k = 2$, which corresponds to a clipping level of $C = 6$ dB according to section 3.2, a target BER of 10^{-3} can be achieved with a sensitivity of −23.6 dBm. Increasing k implies increasing the power of the transmitted signal and the sensitivity required at

the receiver. When 4PAM format is used, a BER of 10^{-3} is also ensured for all the studied values of k. Here, the influence of the clipping noise can be observed for low k values. For 8PAM modulation format, a target BER of 10^{-3} cannot be achieved for a k lower than 2.6 due to the clipping noise. The best sensitivity performance, for 8PAM format, is obtained when $k = 3$.

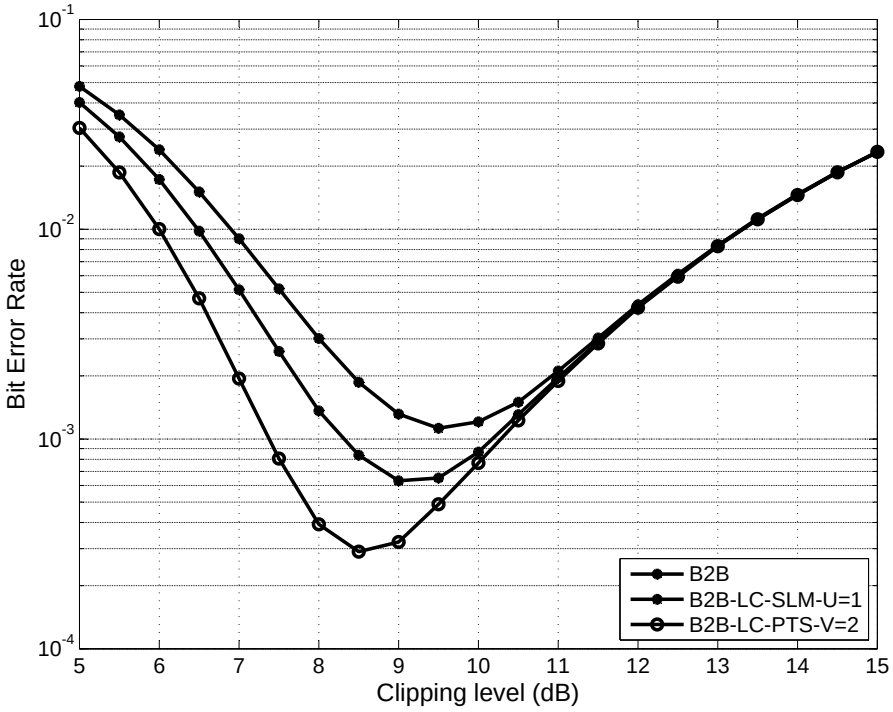

Figure 3.12: BER performance in B2B configuration at a constant receiver input power of -17 dBm versus clipping level for 8PAM O-OFDM ($N = 256$) with and without LC PAPR reduction techniques.

On the other hand, PAPR reduction techniques are applied on the system of Fig. 3.1 in order to enhance the overall performance. Clipping noise is analyzed using 8PAM format and $N = 256$ points FHT. Figure 3.12 shows the BER performance of the B2B O-OFDM system of Fig. 3.1 for different clipping levels at a bit rate of 15 Gb/s. We have analyzed the B2B configuration for a fixed receiver input power of -17 dBm and considering an ideal DAC. Using LC-PTS with 2 FHT blocks at constant receiver power (-17 dBm) and with a clipping level of 7.4 dB, a target BER of 10^{-3} is achieved. Additionally, using a single FHT block with LC-SLM, a target BER of 10^{-3} can be obtained with a clipping level of 8.2 dB. When LC PAPR reduction techniques are not applied, this target BER cannot be achieved with this receiver input power.

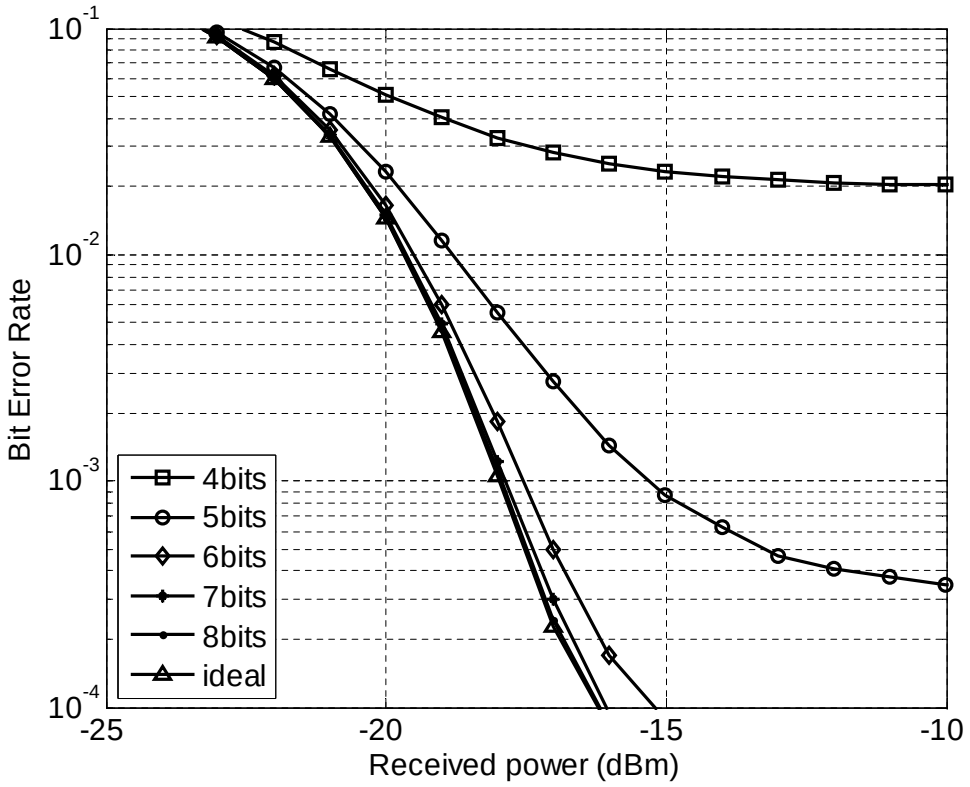

Figure 3.13: Sensitivity performance of the FHT based O-OFDM system of Fig. 3.1 at a target BER of 10^{-3} for different ADC and DAC resolutions using 8PAM format and $k = 3$

3.6.3 Quantization noise analysis

In this section the quantization noise is analyzed. Fig. 3.13 shows the BER performance of the system of Fig. 3.1 for a fixed $k = 3$ and using 8PAM format and $N = 512$. A $k = 3$, which corresponds to a clipping level of $C = 9.5$ dB, has been considered in order to not be limited by the clipping noise. Decreasing the number of bits of the converter introduces higher quantization noise to the system and degrades the performance. It can be seen that for a DAC resolution of 4 bits, the quantization noise is so high that a BER of 10^{-2} cannot be achieved. Moreover, the receiver power penalties at a target BER of 10^{-3} for a resolution of 5 and 6 bits are 2.7 dB and 0.5 dB respectively, when compared with the ideal case for which received power is -18 dBm. Using 7 bits or 8 bits, about the same sensitivity as the ideal case is achieved.

On the other hand, the clipping level is fixed to 9 dB ($k = 2.82$) and an $N = 256$ points FHT is used in order to further evaluate the influence of the quantization noise considering the proposed LC PAPR reduction techniques. In fact, in [47], it is demonstrated that 9 dB is the optimum clipping level when using the FFT with 64QAM, which corresponds to 8PAM format when the FHT is used [52]. Figure 3.14

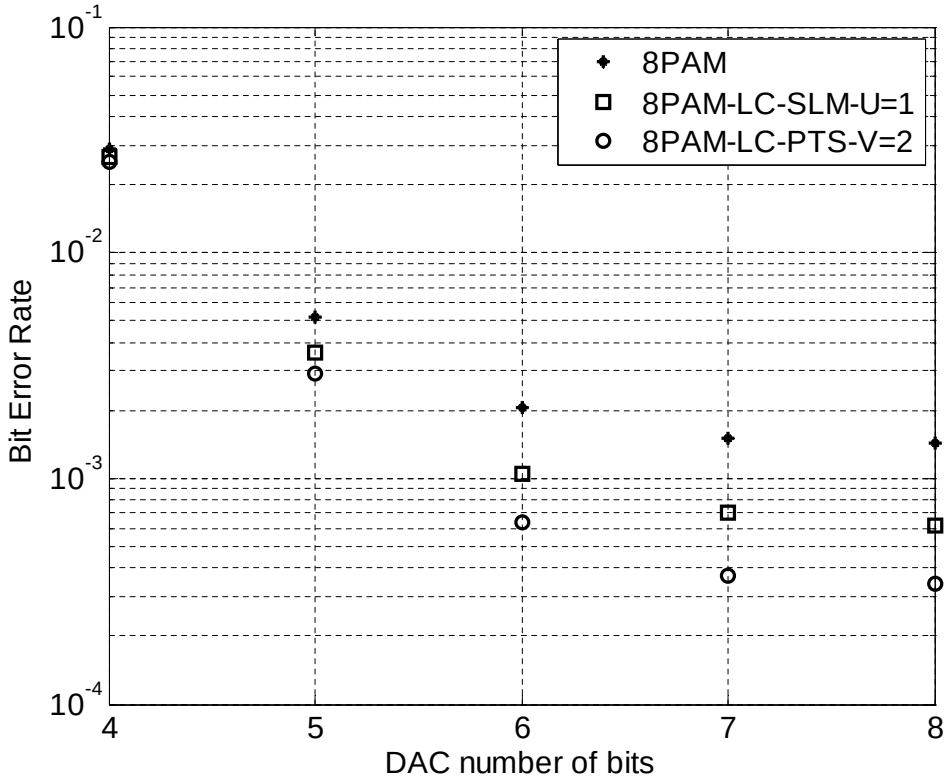

Figure 3.14: BER performance at a constant receiver input power of −17 dBm versus the number of bits of the DAC for 8PAM O-OFDM based on the FHT ($N = 256$) with and without LC PAPR reduction techniques.

shows the BER performance for a fixed receiver input power of −17 dBm when the DAC bit resolution is varying in the range from 4 bits to 8 bits. Applying LC-PTS with 2 FHT blocks a target BER of 10^{-3} can be ensured using a DAC of 6 bit resolution. With LC-SLM, using a single FHT block, the same BER is guaranteed for a DAC of 7 bits. When no PAPR techniques are applied, a BER of 10^{-3} cannot be obtained for this receiver input power.

3.6.4 PAPR reduction impact on the system performance

Here, the BER performance of the O-OFDM system of Fig. 3.1 varying the parameter k for fixed receiver sensitivity (−17 dBm) and using an 8PAM format with $N = 512$ is evaluated in Fig. 3.15. When the number of bits of the DAC decreases, the performance in terms of BER degrades because of the quantization noise. Moreover, the influence of clipping noise can be seen for values of k lower than 3.6. It is also observed that LC-SLM relaxes the constraints on the DAC resolution and allows achieving better performance in terms of clipping noise and power efficiency. In fact, applying the proposed LC-SLM technique, lower BER values can be obtained at fixed bit resolution and lower values

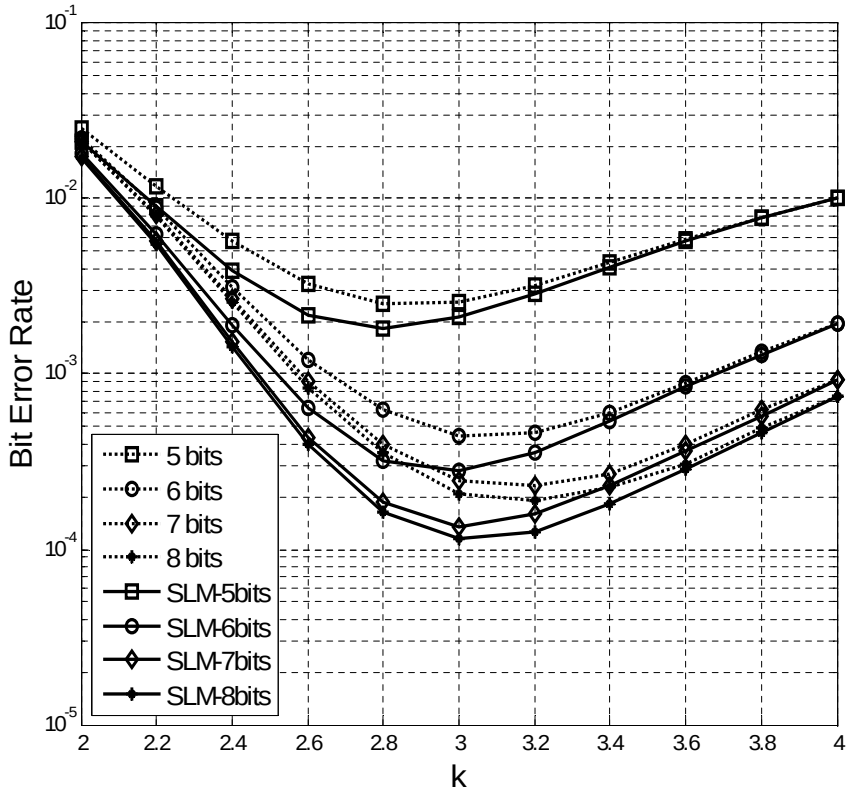

Figure 3.15: BER performance versus k for different DAC resolutions with and without LC-SLM.

of k are required to ensure the same target BER. Additionally, for values of k lower than 2.9 the curve with 6 bits resolution and LC-SLM outperforms the curve obtained using a DAC of 7 bits not applying PAPR reduction techniques. Similarly for k lower than 2.8, using a DAC of 6 bits with LC-SLM, better BER performance is achieved compared to the case of 8 bits converter without applying the proposed technique.

Finally, further simulations are performed to evaluate system performance when LC schemes are applied. Figure 3.16 shows the B2B sensitivity performance of the system of Fig. 3.1 with and without the proposed LC-SLM and LC-PTS schemes and using $N = 256$ points FHT. The receiver input power is measured for a fixed BER of 10^{-3}, varying both the clipping level and the number of bits resolution of the DAC. Applying the proposed techniques, thanks to the mitigation of both the PAPR and clipping noise, the clipping level required to ensure a target BER of 10^{-3} is reduced and the receiver sensitivity is enhanced. Using LC-PTS with 2 FHT blocks and for DAC resolutions of 6 and 8 bits, a clipping level of 7 dB is enough to guarantee 10^{-3} BER. Applying LC-SLM with a single FHT block and for 8 bit DAC resolution, a minimum clipping level of 7.3 dB is needed to ensure the same target BER. Using a DAC of 6 bit resolution the minimum clipping level is increased by 0.1 dB. Whereas, in

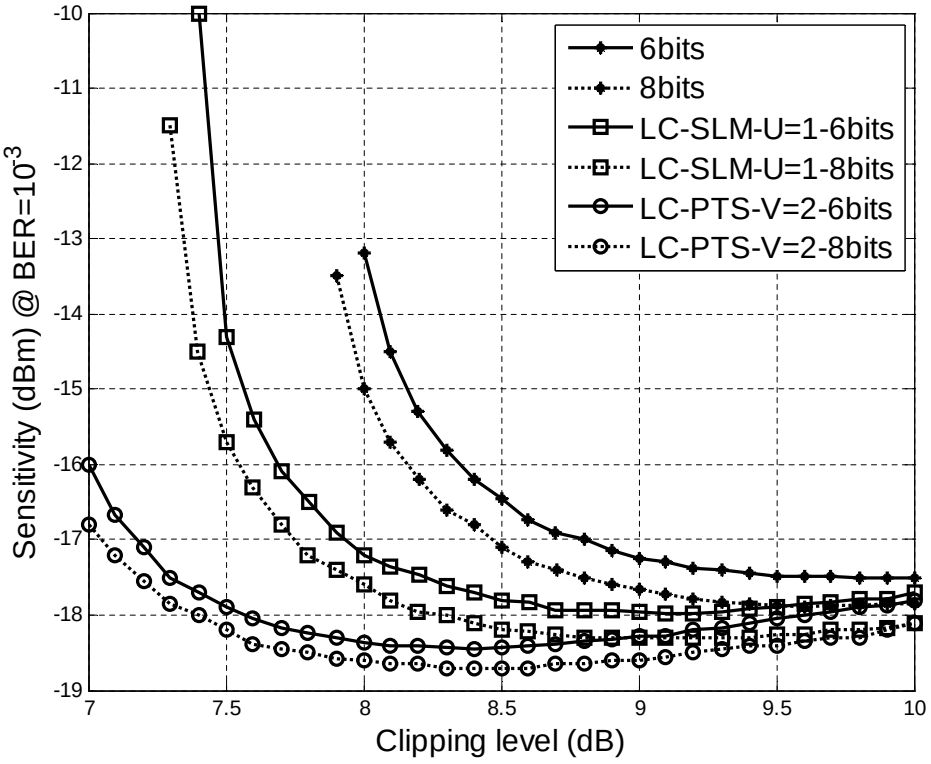

Figure 3.16: Sensitivity performance at a target BER of 10^{-3} for 8PAM O-OFDM system based on the FHT affected by clipping and quantization noise varying the clipping level and using 6 and 8 bit DAC resolutions.

the case of not applying techniques, the required clipping level must be at least 7.9 dB when a DAC of 8 bits is used or 8 dB for a 6 bit DAC resolution. The receiver input power corresponding to 9 dB clipping level and 8 bit DAC, without PAPR reduction, is -17.7 dBm. By applying the proposed techniques, the clipping level required to obtain the same receiver input power is reduced. Specifically, 1 dB and 1.8 dB reduction are obtained, when LC-SLM with a single FHT and LC-PTS with 2 FHT are respectively applied. The clipping noise impact is higher for low values of clipping level. With 8 dB clipping level and compared to the case of not using techniques, for 8 bit DAC resolution, it is demonstrated that applying LC-SLM, the required receiver power for 10^{-3} BER is 2.6 dB lower than the case of not using techniques. Applying LC-PTS with 2 FHT blocks, the reduction is 3.6 dB. Using a 6 bit DAC, the required receiver power decreases 4 dB when LC-SLM is applied and of 5.1 dB when LC-PTS is implemented.

3.7 Summary

In this chapter, we have analyzed standard distortionless PAPR reduction techniques based on the FHT and proposed low complexity schemes. Thanks to the FHT prop-

erties, a simplified DSP can be used and LC techniques can be easily applied without any symmetry constraint. Some of the achieved results are here summarized:

- By applying LC-SLM without any additional transform block at the transmitter, a PAPR reduction of 1.5 dB is obtained. The proposed LC-PTS with random partitions allows achieving the highest PAPR reduction of 3.1 dB using only one additional transform block.

- We have demonstrated that applying LC PAPR reduction techniques in DD O-OFDM systems based on the FHT, the PAPR, the quantization and the clipping noise are mitigated and the required number of resources for implementing standard techniques is halved.

- The performance of the system is improved in terms of receiver sensitivity and power efficiency. At the same time, the constraints on the linear dynamic range of DAC/ADC, drivers and modulators are relaxed thanks to both the symmetrically clipping and PAPR reduction.

- Applying LC PAPR reduction techniques, the required clipping level to guarantee a target BER of 10^{-3} for a fixed receiver input power is reduced.

- We have shown that, for a B2B configuration and using a 6 bit DAC, the required receiver power is 4 dB and 5.1 dB lower, when LC-SLM with a single FHT block and LC-PTS with one additional block are respectively applied.

In the next chapter, loading schemes are investigated in order to cope with Chromatic Dispersion (CD), which appears when transmitting over Standard Single Mode Fiber (SSMF). PAPR is also analyzed when bit loading is implemented. Hence, innovative transceiver designs are proposed to tackle the increasing traffic demand.

4

Design of adaptive FHT-based O-OFDM systems

"There are a lot of things that need to be done to improve communications."

Douglas Feith

4.1 Introduction

Double-Side Band (DSB) transmission arises as a suitable option for the design of low cost transceivers in Direct Detection (DD) Optical-OFDM (O-OFDM) systems based on the Fast Hartley Transform (FHT). DSB modulation doesn't require any optical filter or special modulator to generate the optical signal. Hence, cost-effectiveness is enhanced in contrast with other transmission schemes, such as Single-Side Band (SSB) [17]. However, it is significantly affected by chromatic dispersion, limiting the transmission reach and performance. A possible solution to mitigate this effect is to implement loading schemes by adapting the modulation format of each subcarrier according to the channel profile [83].

Different loading algorithms have been proposed in the literature for O-OFDM systems to overcome the chromatic dispersion effect and optimize the system transmission bandwidth by adapting the bit and power of each subcarrier to the optical channel (see e.g. [27, 84]). These algorithms can be implemented considering different criteria: (i) Bit Error Rate (BER) minimization for fixed data rate and transmit power constraints (ii) Rate maximization for a fixed energy constraint and (iii) Energy minimization at a given data rate [27]. A loading algorithm addressing the problem of BER minimization is proposed in [85]. Cases (ii) and (iii) are usually referred to as Rate Adaptive (RA) and Margin Adaptive (MA) problems, respectively. A well-known algorithm that solves the RA and MA problems is the water-filling [86]. Since the related optimization problems are convex, the water-filling algorithm computes a global

optimal solution (i.e. the minimum of the convex function). However, this algorithm assumes Gaussian symbol distribution, which implies considering infinite granularity in constellation sizes. Hence, a direct implementation in an actual system is not feasible. Alternatively, the Chow Cioffi Bingham (CCB) algorithm is proposed as a discrete loading solution that solves RA and MA optimization problems, assuming integer values for the number of bits assigned to each subcarrier. Specifically, the CCB algorithm, applied to RA and MA problems (CCB Rate Adaptive (CCBRA) and CCB Margin Adaptive (CCBMA), respectively), arrives to a suboptimal solution by rounding the approximated water-filling results [27]. Another discrete loading approach is based on Low Complexity (LC) algorithm, which solves RA and MA problems (Levin Campello Rate Adaptive (LCRA) and Levin Campello Margin Adaptive (LCMA), respectively) using greedy methods. Unlike the suboptimal CCB approach, LC algorithm finds a local optimal solution, as shown in [27] for a InterSymbol Interference (ISI)/Additive White Gaussian Noise (AWGN) channel.

By using loading schemes, a low-cost adaptive O-OFDM transceiver can be designed, becoming a potential solution to be deployed in future Elastic Optical Networks (EON). The initial cost of a Bandwidth Variable Transceiver (BVT) based on Orthogonal Frequency Division Multiplexing (OFDM) technology appears to be higher than a Wavelength Division Multiplexing (WDM) transponder, as additional elements, such as the Digital Signal Processing (DSP) module and the Digital-to-Analog Converter (DAC) should be considered [34]. However, taking into account a realistic network scenario, better performance in terms of Spectral Efficiency (SE) and energy efficiency is achieved when using a OFDM-based BVT transponder [34]. Furthermore, high-speed real-time adaptive OFDM transmission can be achieved using either Application Specific Integrated Circuits (ASIC) or Field Programmable Gate Arrays (FPGA), resulting in reduced energy consumption solutions [87,88]. ASICs are commonly used as they are compact and efficient. However, they require extensive development time and budget. Unlike ASIC, FPGA can be reprogrammed multiple times presenting lower cost and higher degree of flexibility at the expense of higher power consumption.

Here in this chapter, we propose an adaptive transceiver suitable for Metro Area Networks (MAN) where the cost-efficiency is a key issue. Our main contributions are:

- Firstly, we propose a cost-effective bit rate variable transceiver based on DC biased O-OFDM with Peak-to-Average Power Ratio (PAPR) reduction capabilities to mitigate the effects of the clipping noise and increase the power efficiency. The FHT is used to further simplify the DSP. LC-SeLective Mapping (SLM) is introduced in the transceiver design without using additional transform block, hence the system simplicity is preserved. Fine data rate selection can be performed

by implementing Bit Loading (BL). System performance is firstly assessed on AWGN channel.

- An adaptive FHT-based BVT is proposed for flexi-grid MAN. Specifically, the key conclusion of this part of the chapter are:

  - DSB transmission with optimized guard band is demonstrated in a system based on the FHT in the Back-to-Back (B2B) configuration and after links of up to 150 km of Standard Single Mode Fiber (SSMF) using a simple BL scheme. A net data rate of 10 Gb/s for a maximum link of 120 km is transmitted, occupying only one slot of 12.5 GHz or two slots of 6.25 GHz, according to a flexi-grid scenario. Hence, low data rate connections are enabled, which may be used in MAN.
  - Finally, an optimal BL and Power Loading (PL) algorithm is included in the transceiver design in order to further enhance system performance in terms of achieved data rate and spectral efficiency. Although in the optical channel, they might be also subcarrier interference and other nonlinear influences, LCMA algorithm is selected as it is theoretically optimum and minimizes the BER, achieving high data rate transmission.

The remainder of the chapter is organized as follows. In section 4.2, the adaptive FHT-based O-OFDM system model is presented. Furthermore, a performance analysis in the presence of AWGN is provided. As a second step, in section 4.3, the optical components are modeled and a DSB transmission is investigated. The system is characterized and loading schemes are included in the transceiver design. The system performance is evaluated considering simple BL and optimized BL and PL algorithms. Finally, the conclusions are drawn in section 4.4.

4.2 BL in O-OFDM systems based on the FHT

For designing cost-effective bit rate variable transceivers, we propose to use FHT-based modulation and BL. The different subcarriers are mapped with different number of bits providing an efficient use of system resources. An example of adaptive OFDM transmitter and receiver based on the FHT is shown in Fig. 4.1. The input data are mapped using Binary Phase-Shift Keying (BPSK), 4PAM and 8PAM real modulation formats in order to obtain a real-valued FHT-modulated OFDM signal, and then parallelized. The resulting mapped symbols are fed into an $N = 512$ points FHT, serialized and digital-to-analog converted. At the receiver side, the signal is analog-to-digital

converted, parallelized and fed into an FHT. Finally, data are demapped and serialized to recover the original bit stream. The system parameters are summarized in table

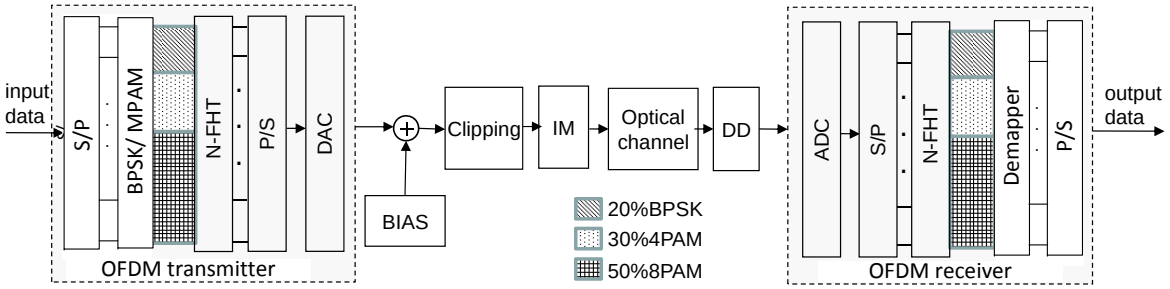

Figure 4.1: Example of adaptive DC biased O-OFDM system based on the FHT.

4.1. BL introduces flexibility to the O-OFDM system enabling fine bit rate selection.

Table 4.1: System parameters

FHT points	512
Oversampling factor	4
B_S	10 GHz
CP length	0
Channel	AWGN

The subcarriers are loaded with symbols mapped with F different modulation formats. We define as p_i the percentage of subcarriers supporting the $i-th$ modulation format, with $i = 1, ..., F$. Hence the total gross bit rate (R_g) can be written as

$$R_g = B_s \sum_{i=1}^{F} p_i n_i, \tag{4.1}$$

where n_i is the number of bits per mapped symbol corresponding to the $i-th$ modulation format (i.e. 1 for BPSK and $\log_2$(M) for MPAM). For example, considering an OFDM electrical signal with $B_S = 10$ GHz, if all the subcarriers are modulated using the same modulation format (uniform bit loading), a bit rate of 10 Gb/s can be transmitted using BPSK, 20 Gb/s using 4PAM and 30 Gb/s using 8PAM. Whereas, applying BL using BPSK, 4PAM and 8PAM, with different p_i, intermediate bit rates can be transmitted according to (4.1). If we consider $p_1 = 20\%$ of symbols modulated with BPSK, $p_2 = 30\%$ modulated with 4PAM and $p_3 = 50\%$ modulated with 8PAM, the achieved gross bit rate is equal to 23 Gb/s. Thus, BL allows to reconfigure the bit rate of the OFDM-based elastic transceivers with a fine granularity.

In order to transmit a positive signal for Intensity-Modulation (IM), a bias (B) is added to the signal. According to section 2.4, B is k times the standard deviation of the signal, and it can be expressed in dB as $10log_{10}(k^2 + 1)$. Hence, a 7 dB bias is twice

the standard deviation, when asymmetrically clipping is performed. As a second step, equally to the case of using the Fast Fourier Transform (FFT) (4.2), the transmitted signal, x_m, is clipped to zero level.

$$\hat{x}_m = \begin{cases} 0, & x_m + B \leq 0 \\ \\ x_m + B & x_m + B > 0 \end{cases} \tag{4.2}$$

Here, the clipping noise also limits the system performance. Using 7 dB bias, OFDM symbols mapped with BPSK and 4PAM formats can be correctly transmitted, whereas the optimum bias to transmit a signal mapped with 8PAM format is 9 dB (see [47, 52] and section 3.6.2). Hence, when BL is implemented, the bias must be adapted to the highest applied modulation format, otherwise it should be constantly adjusted depending on the percentage of subcarriers modulated with high modulation format.

4.2.1 PAPR analysis

Different distortionless PAPR reduction techniques based on the FHT have been proposed and analyzed in chapter 3 to mitigate the effects of the PAPR an other system impairments. Here, the LC-SLM PAPR reduction technique, explained in section 3.4, is implemented in the proposed transceiver of Fig. 4.1 in order to analyze system performance when BL is also used. Fig. 4.2 shows the proposed transmitter introducing LC-SLM technique.

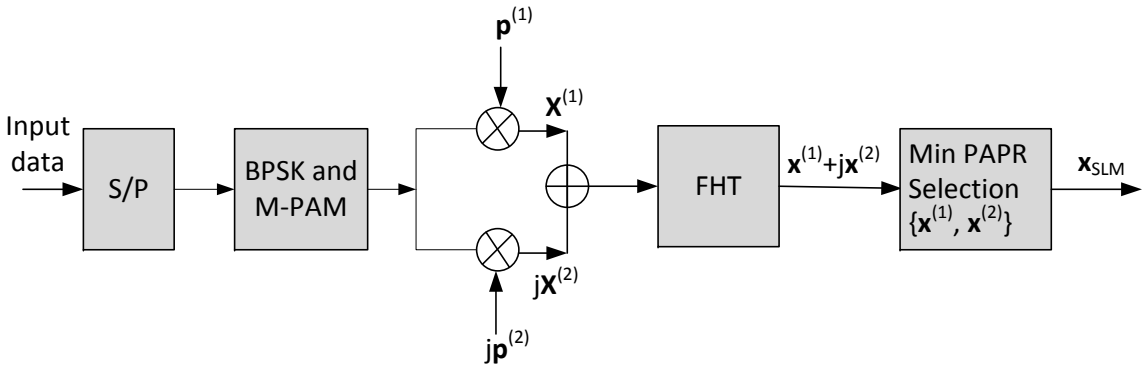

Figure 4.2: OFDM transmitter using LC-SLM PAPR reduction technique with BL and a single FHT block.

The original bit stream is mapped using different percentages of BPSK, 4PAM and 8PAM formats depending on the different bit rate choice. A single FHT of $N = 512$ points is considered, being able to parallel process two signal representations. Finally, the one with minimum PAPR is selected for transmission. The DSP of the FHT-based

O-OFDM system of Fig. 4.1 is modified according to Fig. 4.2 in order to introduce PAPR reduction capabilities.

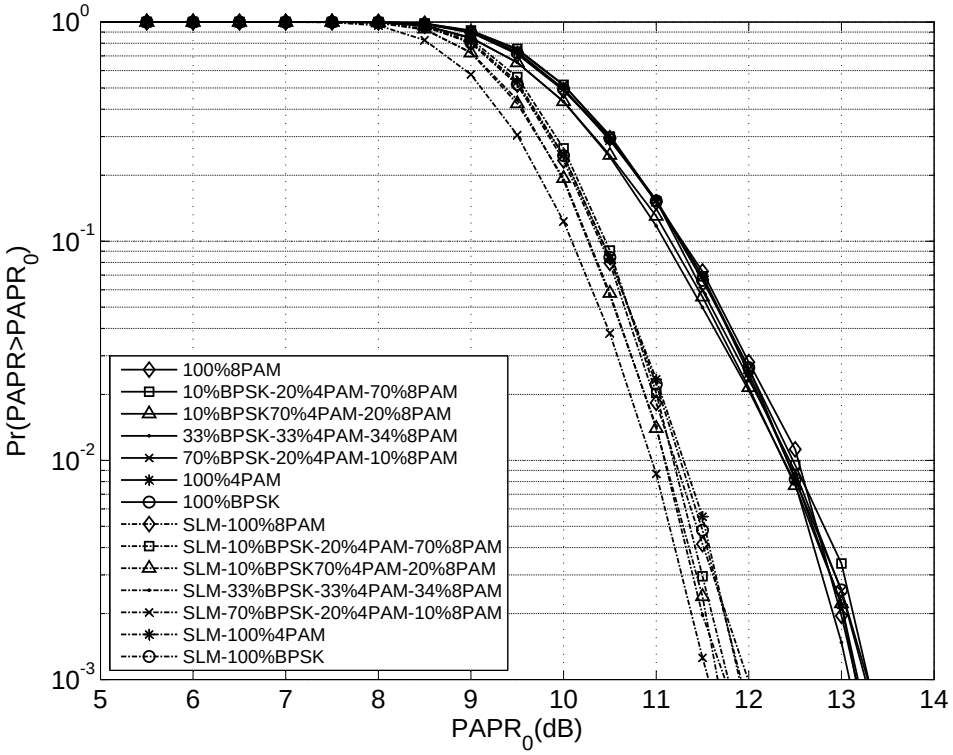

Figure 4.3: PAPR analysis of OFDM signals ($N = 512$) with and without the SLM technique of Fig. 4.2.

In Fig. 4.3, the Complementary Cumulative Density Function (CCDF) of the OFDM signal and after applying the proposed LC-SLM is reported. It is shown that the probability that the PAPR of the OFDM signals with uniform bit loading exceeds 13.7 dB is less than 0.1% when no PAPR technique is used. Whereas using LC-SLM PAPR reduction technique this value is reduced to 12.3 dB. Moreover, when BL is used, the PAPR values differ of only 0.2 dB depending on the selected modulation format type.

4.2.2 Performance evaluation in AWGN

Figure 4.4 shows the BER performance of the proposed O-OFDM system of Fig. 4.1 in AWGN channel using a $7dB$ bias. The best performance in terms of BER is obtained modulating all the symbols with BPSK. The required bit electrical energy normalized to the noise power spectral density (E_b/N_0) is 14.2 dB at a BER of 10^{-3}. In this case, for a 10 GHz signal bandwidth, each subcarrier supports one bit of information and $R_g = 10$ Gb/s. Mapping the bit stream with 4PAM modulation gives a bit rate of

20 Gb/s and the E_b/N_0 required to achieve a BER of 10^{-3} is 19.2 dB. Increasing the number of bits per symbol on each subcarrier, the bit rate increases at the expense of the receiver sensitivity. According to the traffic demand, an intermediate bit rate can be required and the bit rate variable transceiver can be adapted via software (software-defined) at the DSP level. However, in Fig. 4.4, it can be seen that varying the percentages of subcarriers (p_1, p_2 and p_3), which support BPSK, 4PAM and 8PAM formats respectively, the performance can degrade. For example, to obtain a bit rate of 30 Gb/s (with 10 GHz signal bandwidth), 8PAM format is used and the BER curve presents a floor above 10^{-3}. This is due to the clipping noise. In order to avoid the BER floor, a bias value higher than 7dB must be used. If it is increased according to the bit loading scheme, the bit rate variable transceiver would not be fully reconfigurable via software. Thus, the bias must be set to the highest required value for all the configurations, resulting in a power inefficient solution.

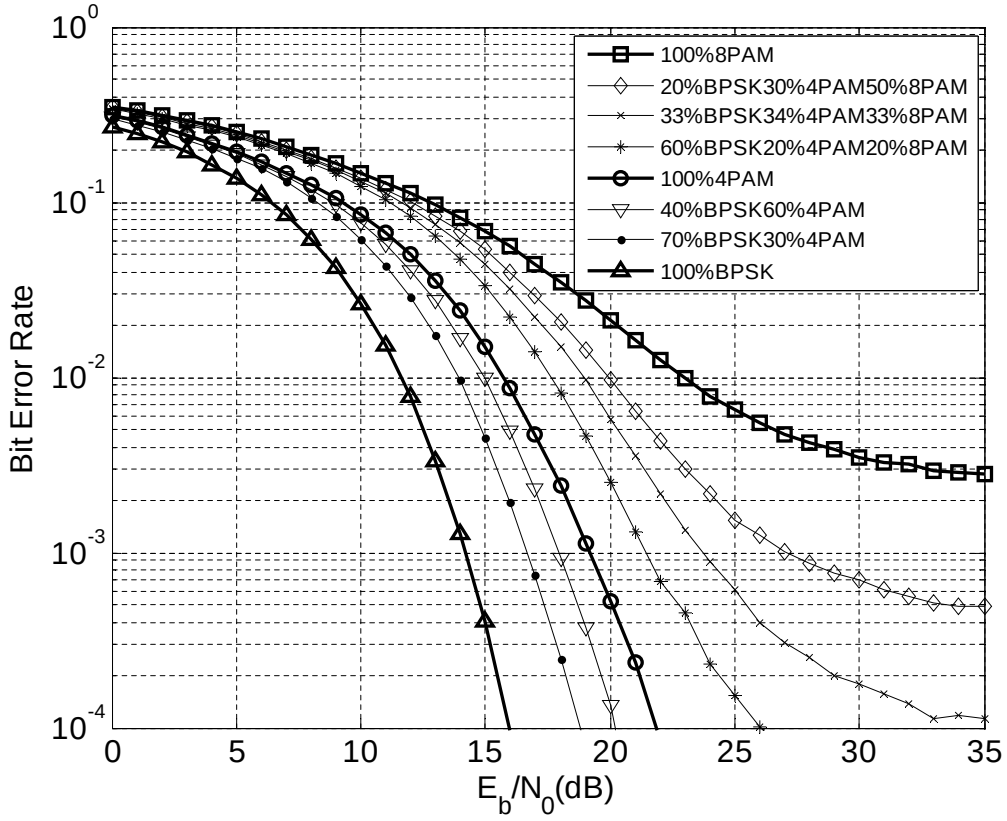

Figure 4.4: BER performance of adaptive DC biased O-OFDM system based on the FHT.

Additionally, different bit loading schemes can provide the same bit rate. For example, a bit rate of 16 Gb/s is achieved using BPSK and 4PAM modulations with percentages of $p_1 = 40\%$ and $p_2 = 60\%$, respectively, or alternatively using BPSK, 4PAM and 8PAM with percentages $p_1 = 60\%$, $p_2 = 20\%$ and $p_3 = 20\%$. It is important

to note that in the first case a lower E_b/N_0 is required and better BER performance is achieved. Therefore, the suitable bit loading must be selected to transmit at the target bit rate with the most power efficient scheme. For example, to obtain a finer granularity between the bit rate provided by the uniform bit loading using BPSK and 4PAM, it is not necessary to introduce 8PAM format. Furthermore, the achieved bit rate, 20 Gb/s, with a bit loading scheme that equally mixes the three different modulation formats ($p_1 = 33\%$, $p_2 = 34\%$ and $p_3 = 33\%$) can be simply obtained by mapping all the transmitted symbols with 4PAM format ($p_2 = 100\%$), requiring a lower E_b/N_0.

A bit rate of 23 Gb/s is obtained with the bit loading scheme of Fig. 4.1, where $p_1 = 20\%$, $p_2 = 30\%$ and $p_3 = 50\%$. In general, increasing the percentage p_3 of subcarriers supporting 8PAM, the required E_b/N_0 increases. Conversely, when reducing this percentage, better performance are achieved at the expense of the bit rate reduction. In Fig. 4.4, it is possible to observe that an average value of E_b/N_0 (between the values corresponding to the two boundary uniform loading using BPSK and 4PAM) is obtained with $p_1 = 70\%$ (instead of 50%) of BPSK-modulated subcarriers. Similarly, when BL is implemented using the three analyzed formats, the BER curves are between the conventional BER curves of uniform bit loading with 4PAM ($p_2 = 100\%$) and 8PAM ($p_3 = 100\%$). This is because the percentage of bits mapped into the $i-th$ modulation format, pb_i, is different from the percentage of subcarriers that support the $i-th$ format, p_i

$$pb_i = \frac{p_i n_i}{\sum_{k=1}^{F} p_k n_k} \qquad for\ i = 1, ..., F \tag{4.3}$$

For example, using BPSK, 4PAM and 8PAM, the approximate percentage of bits modulated in BPSK format is $pb_1 = p_1/(p_1 + 2p_2 + 3p_3)$ and it is independent from the total number of subcarriers. Finally, the performance of the proposed low complexity bit rate variable transceivers with PAPR reduction capabilities is evaluated for DC biased O-OFDM systems based on the FHT. The channel is modeled as an AWGN and the clipping is taken into account as an additional noise source. In adaptive systems using BL, the bit rate is increased at the expense of the receiver sensitivity: as shown in Fig. 4.4, using higher constellation size requires higher electrical energy. Additionally, due to the clipping noise effect, if the bias is not suitably selected, BER floor can occur above the target value. Therefore, we analyze the worst case of uniform bit loading with 8PAM format in order to ensure a correct transmission using different bit loading schemes for achieving a minimum target BER of 10^{-3}. The required bias value must be minimized in order to obtain an efficient adaptive system in terms of power resources. In fact, a fixed bias value is required for adapting the bit loading scheme at the DSP level. Figure 4.5 shows the performance of the system in Fig. 4.1, varying the bias value when the transceiver uses 8PAM with uniform bit loading ($p_3 = 100\%$). The

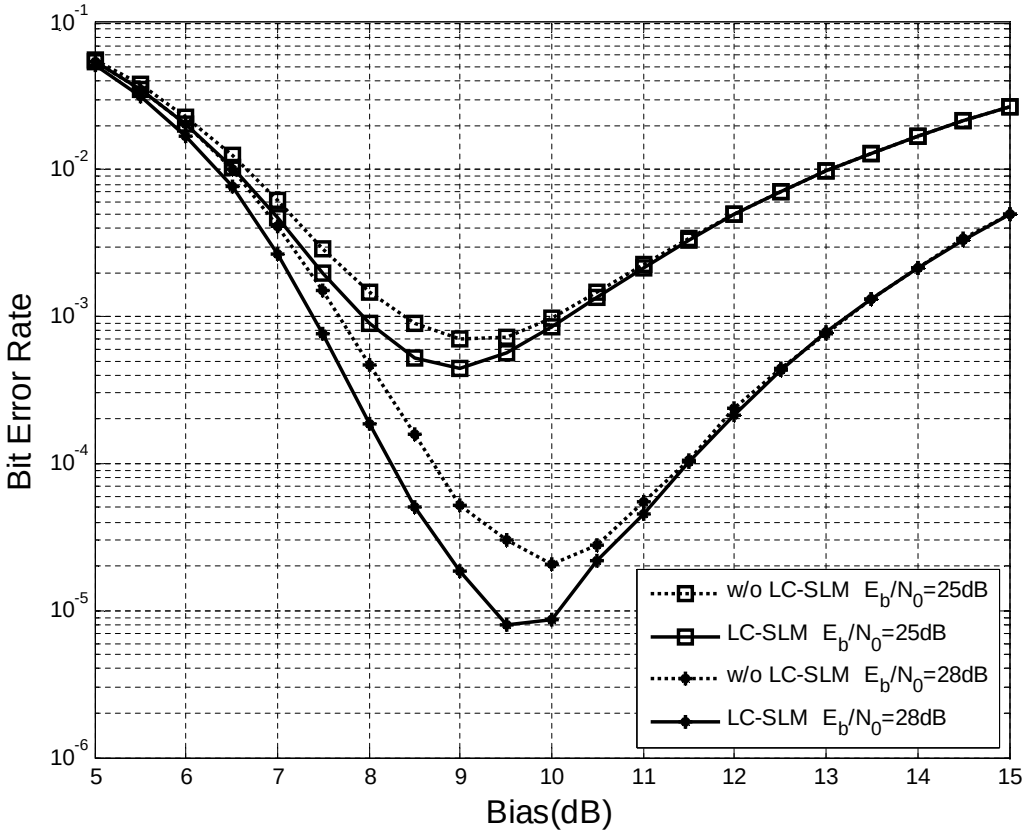

Figure 4.5: BER performance at two constant values of E_b/N_0 versus bias for 8PAM ($p_3 = 100\%$) O-OFDM ($N = 512$) with and without LC-SLM technique.

constant values of E_b/N_0 considered are 25 dB and 28 dB to ensure a BER of 10^{-3} and 10^{-4}, respectively, using 9 dB bias (see Fig. 4.6). In fact, it is demonstrated that 9 dB is the optimum bias using 8PAM format, as seen in Fig. 4.5. It is shown that, using the LC-SLM scheme with one simple transform block, the performance is improved and the required bias value is lowered.

Fixing the E_b/N_0 at 25 dB and using LC-SLM, 10^{-3} BER can be achieved with a minimum bias of 7.9 dB. The same transceiver without PAPR reduction capabilities requires a minimum bias 0.5 dB higher. On the other hand, increasing the electrical energy per bit to 28 dB, 10^{-3} BER is obtained with only 7.4 dB bias, if LC-SLM is applied. This bias value is just 0.4 dB higher than the one required for transmitting at the lowest bit rate using uniform bit loading with $p_1 = 100\%$ BPSK (see Fig. 4.4). When the PAPR reduction technique is not applied, a higher bias of 7.7 dB is needed to achieve the same performance. Additionally, a BER of 10^{-4} is obtained with 8.2 dB bias applying LC-SLM. Whereas, without PAPR reduction technique, the bias increases to 8.7 dB to ensure the same target BER. Furthermore, applying LC-SLM the best performance is obtained with an optimum bias of 9.4 dB. In this case, a BER of 10^{-5} can be achieved, whereas, without PAPR reduction technique, even using the op-

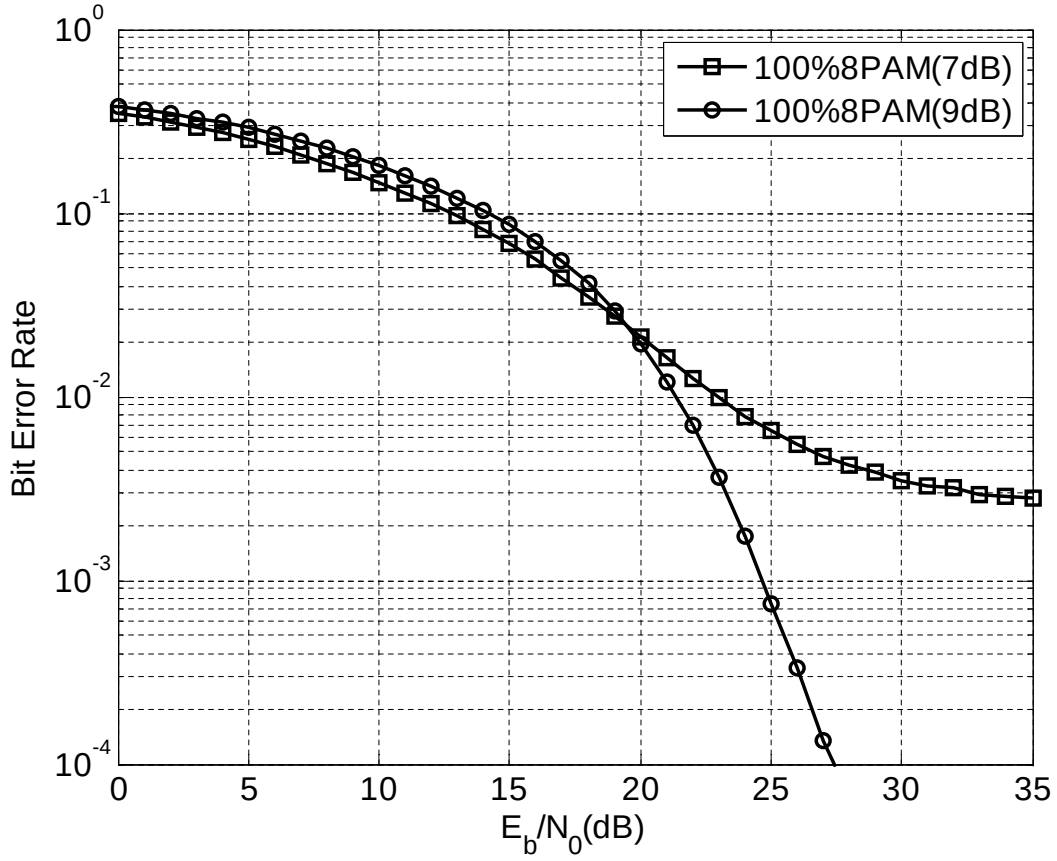

Figure 4.6: BER performance of DC biased O-OFDM system for 8PAM ($p_3 = 100\%$) and using 7 dB and 9 dB bias.

timum bias (10 dB), such a high target BER can not be obtained. Therefore, LC-SLM PAPR reduction technique, using a single transform block, mitigates the clipping noise, improving the BER and enhancing the system power efficiency. The proposed PAPR reduction technique is effective when the clipping noise dominates over the AWGN noise. Depending on the required E_b/N_0, a minimum bias (lower than the one required if SLM is not applied) can be fixed to transmit an O-OFDM signal independently on the percentage of subcarriers filled with 8PAM format, resulting suitable for adaptive schemes. Thus, including LC-SLM technique in the proposed bit rate variable transceiver reduces the value of the bias needed in DCO-OFDM systems. Fixing a bias of 7.4 dB, 10^{-3} BER is ensured for any O-OFDM signal mapped with BPSK, 4PAM, 8PAM format or using BL. Moreover, for a signal bandwidth of 10 GHz, the bit rate ranges from 10 Gb/s to 30 Gb/s according to the different BL schemes.

4.3 Adaptive FHT-based O-OFDM transceivers: DSB transmission

In the previous section, 4.2, the proposed transceiver has been analyzed using BL in AWGN channel. Here, an adaptive transceiver based on the FHT for DD O-OFDM systems is designed and analyzed considering the system model of Fig. 4.7. The input data are parallelized and mapped with uniform loading or BL using real modulation formats. Firstly, a simple BL scheme is considered to achieve distance and rate adaptive capabilities. Then, an optimized BL and PL algorithm is included in the transceiver design.

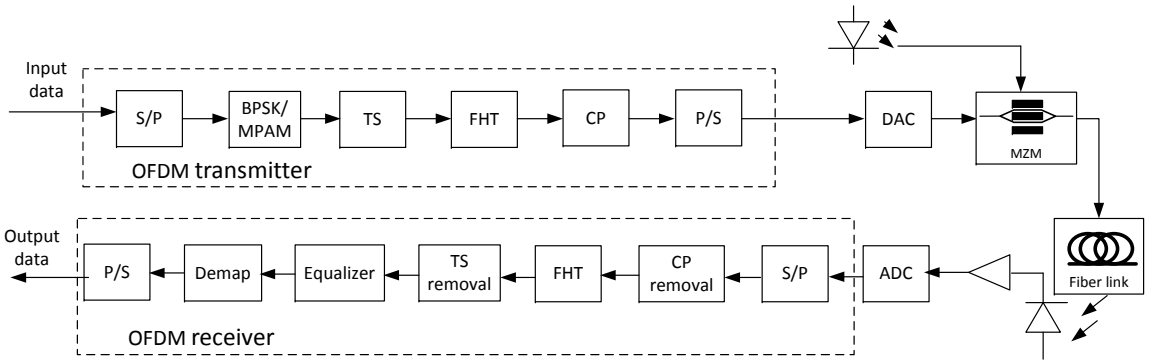

Figure 4.7: Block diagram of the adaptive transceiver based on the FHT.

Table 4.2: System parameters

Transmission	DSB
FHT points	256
B_G	500 MHz
Laser center wavelength	1550 nm
Laser linewidth	1 MHz
PIN Responsivity	0.7 A/W
Overall thermal noise	$12.87{\cdot}10^{-2}$ A/ $\sqrt{Hz}$
Dark current	1 pA
Fiber dispersion coefficient	-20 ps^2/km
Fiber nonlinear coefficient	1.3 $W^{-1}km^{-1}$
Fiber loss factor	0.2 dB/km
CP overhead	10%
TS overhead	0.78% or 1.56%
FEC overhead	7%

After the mapping, the Training Symbols (TS) are added to correctly implement the equalization in reception and the resulting symbols are fed into an $N = 256$ points FHT. The modulated signal is serialized after adding the Cyclic Prefix (CP). Symmetrically clipping is used to limit the PAPR according to equation (3.6). The signal

is digital-to-analog converted considering a uniform quantizer of 8 bit resolution. The electrical signal is then modulated with a Mach-Zehnder modulator (MZM) at the quadrature point ($V_{bias}/V_{\pi} = -0.5$), creating a DSB signal. The laser driving the MZM is modeled as a standard Continuous Wave (CW) laser centered at a wavelength of $\lambda = 1550$ nm, with optimized output power of 1 mW, whose phase is modeled as a Wiener process. Then the modulated optical signal is transmitted over SSMF. The split-step Fourier method is used to model the propagation over the SSMF. We assume a dispersion coefficient of $-20ps^2/km$, a nonlinear coefficient of $1.3W^{-1}km^{-1}$ and a loss factor of 0.2 dB/km. The receiver is modeled as a PIN photodiode with 0.7 A/W responsivity overall thermal noise value of $12.87 \cdot 10^{-2} A/\sqrt{Hz}$, and dark current of 1 pA. After photodetection, the signal is analog-to-digital converted. Finally, the OFDM demodulation is performed, including serial-to-parallel conversion, CP removal, FHT processing, TS removal, equalization, demapping and serialization. Specifically, according to section 2.4.3, a low complexity equalization processing for the FHT, which consists of setting to zero half of the vector elements of the TS, is performed. The system parameters are listed in table 4.2.

As a first step, the proposed system of Fig. 4.7 is characterized without including BL schemes. DSB signals with reduced guard band are transmitted through the fiber link resulting in a cost-effective implementation. An optimum clipping level of 9.5 dB is considered, according to chapter 3. 16 TS are added every 1008 frames, resulting in an overhead of $\delta_{TS} = 1.56\%$, to correctly implement the equalization in reception. An overhead due to the CP ($\delta_{CP} = 10\%$) is used to compensate the ISI. A Forward Error Correction (FEC) overhead of $\delta_{FEC} = 7\%$ is taken into account for a target BER of 10^{-3}. Hence, the total overhead (δ_T) is 19.5%. According to [57], R_n can be calculated as

$$R_n = R_g/((1+\delta_{TS})(1+\delta_{CP})(1+\delta_{FEC})) = R_g/(1+\delta_T). \tag{4.4}$$

In DSB transmission, the received electrical power of each subcarrier is attenuated after optical fiber transmission due to chromatic dispersion causing power fading [20,56] (see section 2.4.2). According to equation (2.10), the first attenuation peak due to CD appears at

$$f_{CD}^0 = \sqrt{\frac{c/2\lambda^2}{LD}}. \tag{4.5}$$

In order to mitigate Chromatic Dispersion (CD) impact on the system performance a total electrical signal bandwidth, $B_T = B_G + B_S$, smaller than f_{CD}^0 can be considered. Hence, the guard band between the electrical signal and the optical carrier should be optimized. Fig. 4.8 shows the BER performance of the system of Fig. 4.7 at the varying of the laser linewidth and the guard band after one fiber span of 80 km. From

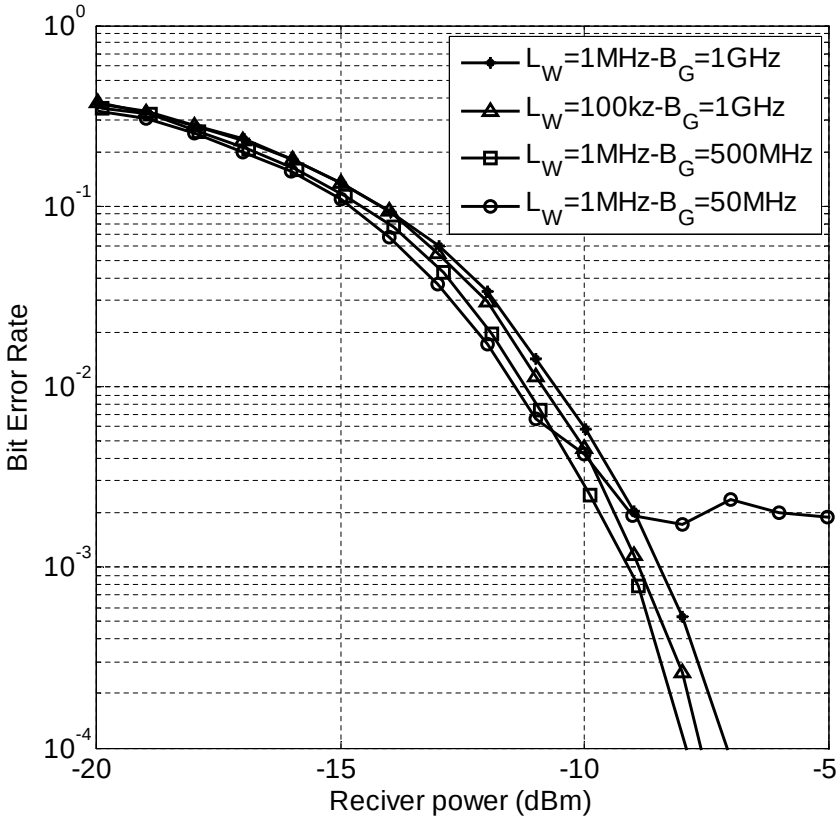

Figure 4.8: BER performance versus receiver power for different laser linewidths and guard band bandwidths.

equation (4.5), f_{CD}^0 is equal to 7 GHz for a fiber link of 80 km. Thus, a B_T lower than 7 GHz should be considered in order to avoid overall performance degradation due to CD. Thus, an OFDM signal bandwidth of $B_S = 6$ GHz is selected considering a guard band of 1 GHz. From Fig. 4.8, it can be seen that using a laser linewidth of 100 kHz with a guard band of $B_G = 1$ GHz and 4PAM format, -8.9 dBm receiver sensitivity is required to ensure a target BER of 10^{-3}. With a broader laser linewidth of 1 MHz for a cost-effective transceiver design, a worst performance is obtained, -9.1 dB higher receiver sensitivity is needed to guarantee the same target BER. Furthermore, reducing the guard band up to 50 MHz floor occurs above 10^{-3} BER. Considering a guard band of 500 MHz with a laser linewidth of 1 MHz, the receiver sensitivity is reduced of 0.5 dB compared to the case of using the narrower linewidth laser and $B_G = 1$ GHz. Hence, a guard band of 500 MHz and a laser linewidth of 1 MHz are selected for the transceiver design and used in all the simulations of the remainder of this chapter, resulting in a cost-effective and spectral efficient implementation.

In order to further characterize the system, CD impact on the received spectra is analyzed. Fig. 4.9(a) and (b) show the received spectra after photodetection in a B2B configuration and after 80 km of SSMF, respectively. Here, a total electrical bandwidth

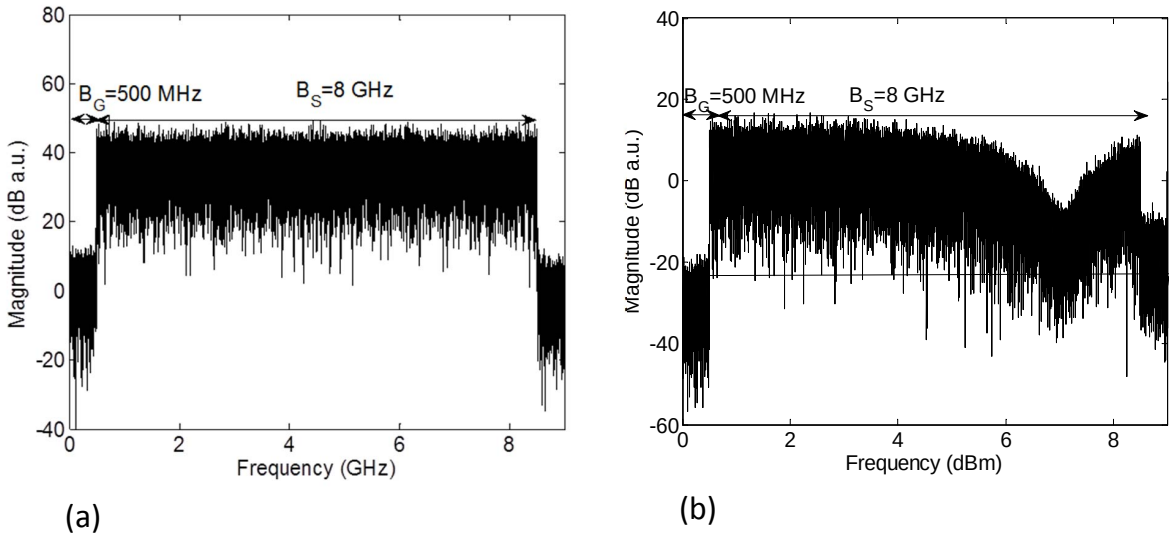

Figure 4.9: Received B2B (a) and after 80 km of fiber (b) spectrum after photodetection of a signal of $B_S = 8$ GHz and $B_G = 500$ MHz with 4PAM.

of 8.5 GHz is considered in order to analyze the system impairments. In Fig. 4.9(a), it is seen that the received B2B spectrum is not degraded. Hence, using such electrical bandwidth, the electronic components do not limit the system performance. However, after 80 km SSMF, the first attenuation peak due to CD appears at $f_{CD}^0 = 7$ GHz according to equation 4.5. Hence, as the occupied B_T is higher than f_{CD}^0 the frequencies around 7 GHz are highly attenuated as it can be seen in Fig. 4.9(b). Therefore, an analysis of the maximum bandwidth that can be transmitted ensuring a target BER of 10^{-3} after 80 km of SSMF is performed (as shown in Fig. 4.10).

Fig. 4.10 shows that using 8 PAM format a maximum signal bandwidth of $B_S = 4GHz$ can be transmitted. Whereas, using 4PAM format a B_S up to 7 GHz can be considered to ensure 10^{-3} BER. Finally, mapping the data with a more robust format such as BPSK a signal of $B_S = 8$ GHz can be correctly received even though the sub-carriers around 7 GHz are highly attenuated due to the CD (see Fig. 4.9(b)). Variable data rates are obtained at the varying of the OFDM bandwidth and the modulation format achieving different system performance in terms of receiver sensitivity. In the inset of Fig. 4.10, it is shown the suitable modulation format, and the related signal bandwidth, to be used to achieve a required data rate. Steps of 1 GHz for B_S have been considered. According to [57], the SE is defined as the relation between the net data rate and the optical bandwidth ($SE = R_n/B_o$). BPSK format is selected to be used when gross data rates up to 3 Gb/s are transmitted. However, 4PAM format results in a more spectral efficient solution when data rates between 4 Gb/s and 6 Gb/s are achieved. For higher data rates and up to 12 Gb/s, 8PAM format enhances SE at the expense of higher receiver sensitivity requirement. Finally when 13 Gb/s and 14 Gb/s

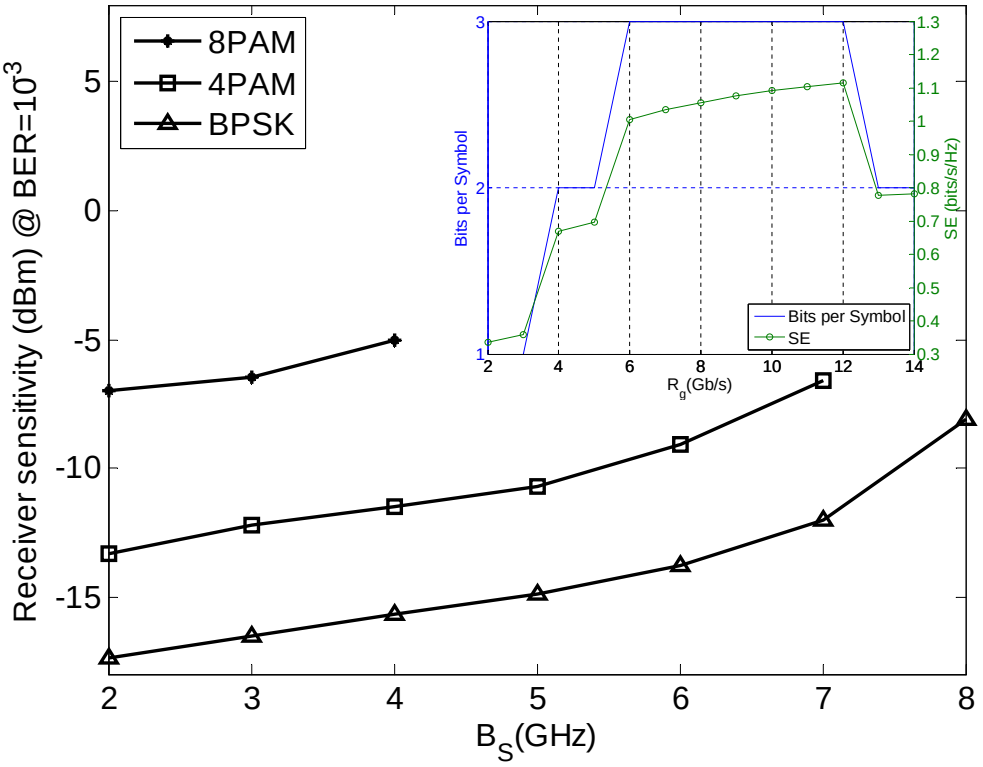

Figure 4.10: Sensitivity performance at a BER 10^{-3} and after 80 km of fiber at the varying of the OFDM signal bandwidth. In the inset of the figure, optimum modulation format and SE for a required gross bit rate.

are achieved 4PAM format is preferable.

As a last step to characterize the system, the transmission reach of the proposed transceiver of Fig. 4.7 is analyzed. A maximum $B_S = 9.5$ GHz an 10 GHz bandwidth electronic components are considered. Figure 4.11 shows the maximum reach and the required receiver sensitivity for a target BER of 10^{-3} at the varying of the modulation format. A maximum gross data rate of 28.5 Gb/s ($R_n = 23.8$) can be obtained after 20 km with 8PAM format. Using 4PAM format, a gross bit rate of 19 Gb/s after a fiber link of 50 km can be transmitted. Using a more robust modulation format such as, BPSK up to 60 km of fiber with a gross data rate of 9.5 Gb/s is achieved.

4.3.1 Performance analysis using BL

Here, a simple BL scheme is included in the system model of Fig. 4.7 to achieve fine data rate selection and limit CD. A maximum B_S of 5.5 GHz is analyzed in this section, as it corresponds to an optical bandwidth of $B_o = 2(B_G + B_S) = 12$ GHz, which perfectly fits in 1 slot of flexi-grid MAN. With a guard band of $B_G = 500$ MHz, the optical bandwidth of the DSB signal occupies only 1 GHz more than the corresponding SSB signal, where a guard band equal to the electrical signal bandwidth must be considered

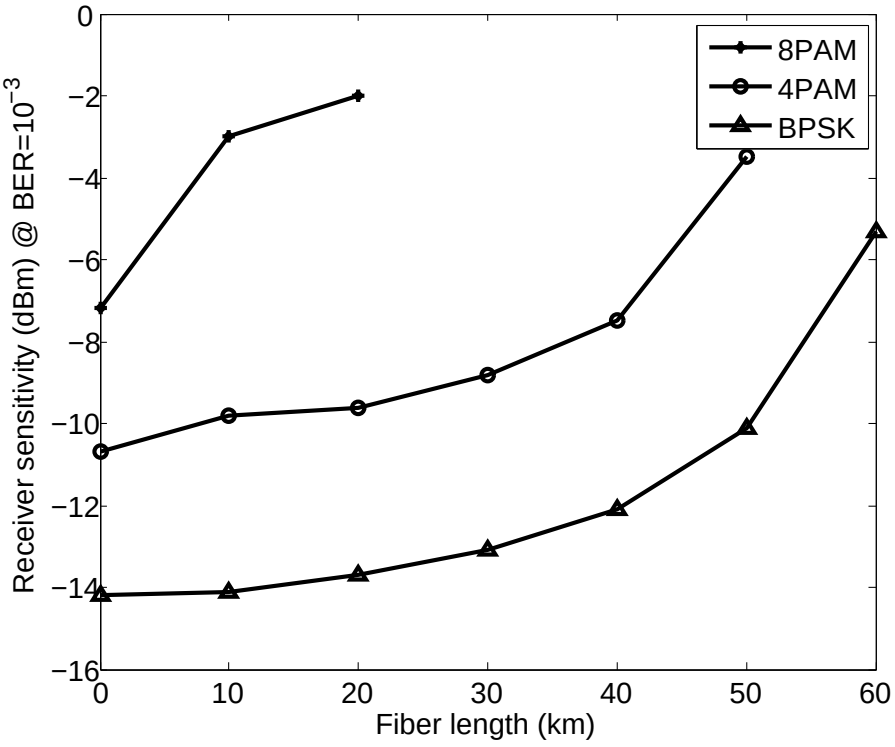

Figure 4.11: Receiver sensitivity to achieve a target BER of 10^{-3} versus fiber length for BPSK, 4PAM and 8PAM format.

for correct photodetection [17]. The gross data rate, in equation 4.1, can be re-defined as

$$R_g = B_s \sum_{i=1}^{F} \frac{[2q_i N/2]n_i}{N}, \tag{4.6}$$

where q_i is the percentage of subcarriers supporting the i-th modulation format for F different formats and with $i = 1, ..., F$. [.] represent the approximation to the nearest integer and n_i is the number of bits per mapped symbol, corresponding to the i-th modulation format (i.e. 1 for BPSK and $log_2(M)$ for MPAM). In order to calculate the net data rate, here in the simulations, we have considered $\delta_{CP} = 10\%$, $\delta_{TS} = 0.78\%$ and $\delta_{FEC} = 7\%$. Thus, the total overhead is 18.6%. However, considering also that the Nyquist frequency is set to zero, which implies an additionally overhead of 0.39%, the total overhead is 19.1%. R_n can be calculated according to equation 4.4.

Initially, BL is implemented considering BPSK, 4PAM and 8PAM according to the channel profile. Additionally, the mirror-symmetric subcarriers of the FHT are also taken into account (see Fig. 4.7). In fact, due to the kernel structure, the mirror-symmetric sub-bands of the FHT ensure subcarriers orthogonality as seen in section 2.4.1. Hence, they must be mapped into the same modulation format. It is worth noting that, the FHT allows achieving the same degrees of freedom in terms of flexibility as

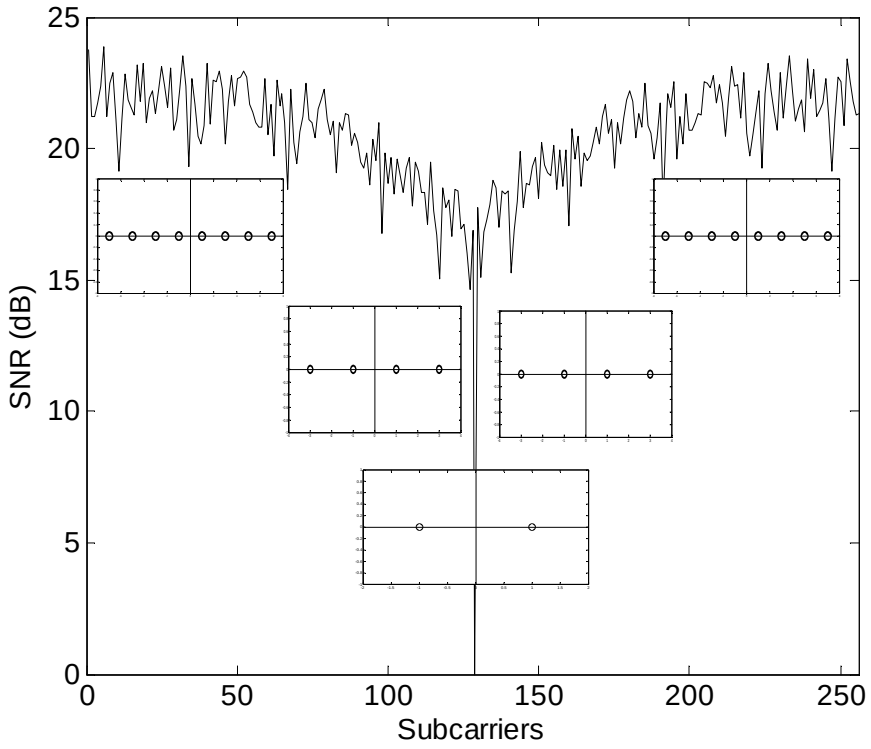

Figure 4.12: SNR per subcarrier of a signal of $B_S = 5.5$ GHz after 120 km of SSMF.

the FFT with Hermitian Symmetry (HS). With the FFT, each symbol is redundant, due to the complex conjugate constraint, and the real and imaginary parts of one independent symbol, corresponding to two real-valued symbols when FHT modulation is performed, belong to the same modulation format. Figure 4.12 shows the Signal-to-Noise Ratio (SNR) of $N = 256$ OFDM subcarriers, after a fiber link of 120 km. It is seen that the central subcarriers are more affected by the channel impairments. Hence, the most robust format, BPSK, must be assigned to those subcarriers. Similarly, due to FHT mirror symmetric effects the first group and last group of subcarriers must be mapped with the same format and as they present the highest SNR, they are filled with 8PAM format. The remaining subcarriers are mapped with 4PAM format.

Table 4.3: Table of different BL schemes and corresponding achievable reach. R_g has been approximated

$\mathbf{B_s}$ **(GHz)**	**%BPSK**	**%4PAM**	**%8PAM**	$\mathbf{R_g}$ **(Gb/s)**	$\mathbf{R_n}$ **(Gb/s)**	**Link (km)**
5.5	0	0	100	16.5	13.85	60
5.5	10	60	30	12	10	120
5	10	40	50	12	10	100
4.5	0	40	60	12	10	70
4	0	0	100	12	10	70
5	0	100	0	10	8.4	150

Figure 4.13 shows the required receiver sensitivity to achieve a target BER of 10^{-3} for different links and using uniform loading and the proposed BL scheme as defined in table 4.3. Steps of 10 km are considered to calculate the sensitivities of the figure. The percentage of subcarriers modulated with a particular format is determined by the required bit rate. Whereas the distribution of the modulation formats into the subcarriers are fixed by the channel profile (see Fig. 4.12). The total number of simulated bits is 2^{19}.

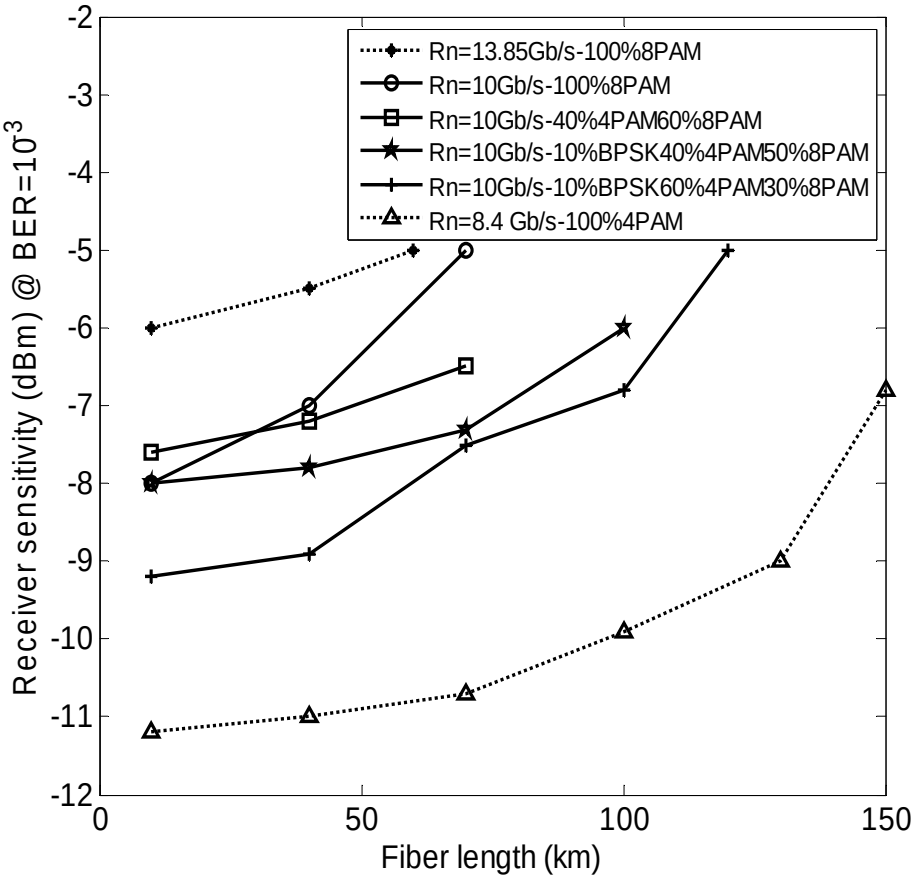

Figure 4.13: Receiver sensitivity at a target BER of 10^{-3} for different links and BL schemes.

Firstly, we have analyzed the case of transmitting a net bit rate of 10 Gb/s, which can be achieved using either uniform loading or BL. In Fig. 4.13, it is seen that the most power efficient BL scheme is the one that uses 10% BPSK, 60% 4PAM and 30% 8PAM and guarantees a target BER of 10^{-3} up to 120 km of fiber. Other BL schemes, combining two and three modulation formats, have also been analyzed, as shown in table 4.3. However, as they use a higher percentage of 8PAM format, a higher receiver sensitivity is required to ensure 10^{-3} BER and the reach is reduced. A net data rate of 10 Gb/s can be transmitted using uniform loading with 8PAM format and $B_S = 4$ GHz

achieving a target BER of 10^{-3} up to 70 km. When all the subcarriers are mapped with 4PAM format $R_n = 10$ Gb/s cannot be achieved occupying only 12.5 GHz, as it requires an electrical bandwidth of 6 GHz, and hence, an optical bandwidth of 13 GHz. A gross data rate of $R_g = 10$ Gb/s, corresponding to a net data rate of 8.4 Gb/s, is obtained with 4PAM uniform bit loading and a $B_S = 5$ GHz ($B_o = 11$ GHz). In this case, 10^{-3} BER is achieved for a maximum link of 150 km with a received power of -6.8 dBm. Finally, the case of transmitting at a maximum net data rate of 13.85 Gb/s, is analyzed by mapping all the subcarriers into 8PAM format with $B_S = 5.5$ GHz. In this case, a target BER of 10^{-3} is ensured up to 60 km of SSMF at the expense of the receiver sensitivity.

4.3.2 Performance analysis using optimized BL and PL algorithm

As it has been shown at the beginning of the chapter, at the increase of the fiber length the power fading effect due to CD increases, degrading the system performance. Hence an optimized BL and PL algorithm is included in the proposed transceiver of Fig.4.7 to further combat CD limitation. Specifically, LCMA algorithm, which consists of finding the optimal bit and power allocation for each subcarrier according to the channel profile for a fixed bit rate is applied [27, 83]. The basic concept of this iterative algorithm is that each increment of information is placed onto the subcarrier that requires less incremental energy for its transmission. In order to solve the MA problem, the LC algorithm finds an efficient symbol distribution by performing an exhaustive search [27]. The resulting bit distribution is defined as efficient when the energy cannot be further reduced by any other loading scheme. Finally, the algorithm verifies that the correct number of bits is transmitted according to the target data rate, giving a local optimal solution.The gap approximation of the SNR, Γ, is used in order to relate the number of bits per symbol and the required SNR to achieve a target error probability in a straightforward manner, simplifying the bit loading algorithm [27]. In particular, according to [89], an initial value of $\Gamma = 9.8$ dB is used to calculate the energies of each subcarrier. After applying the loading algorithm, the resulting margin will give the real gap and the related probability of error that can be achieved. The algorithm is adapted to MPAM format according to [27].

Firstly, the SNR of each subcarrier is estimated and plotted in Fig. 4.14, after one span of 80 km of SSMF and at a fixed receiver sensitivity of -13 dBm. A $\delta_T = 19.5\%$ is considered in the simulations and R_n can be calculated according to equation 4.4. In order to see the effect of CD in the transmission, different signal bandwidths have been used and only half of the subcarriers ($N = 128$) are plotted to avoid redundancy

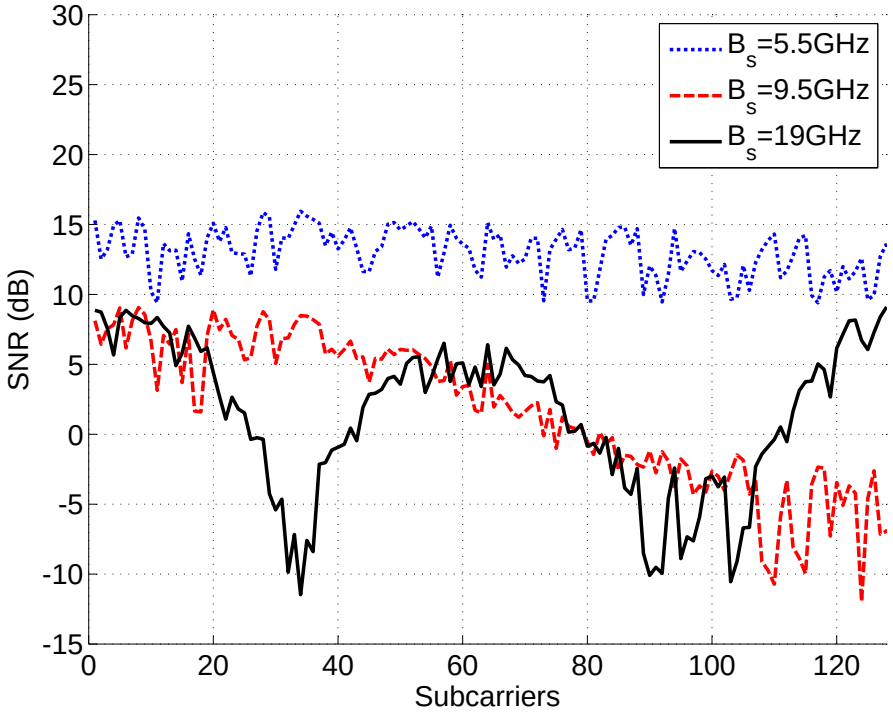

Figure 4.14: SNR estimation vs number of subcarriers for different electrical signal bandwidths at −13 dBm receiver sensitivity after 80km of SSMF.

due to FHT symmetry. Specifically, $B_S = 5.5$ GHz, $B_S = 9.5$ GHz and $B_S = 19$ GHz, which occupy 1, 2 and 3 frequency slots of 12.5 GHz, respectively, are simulated. From Fig. 4.14 it can be seen that using $B_S = 5.5$ GHz, the subcarriers are not degraded as $f_{CD}^0 = 7$ GHz is higher than the electrical signal bandwidth. Whereas, using $B_S = 9.5$ GHz, which is higher than f_{CD}^0, the subcarriers at higher frequency are attenuated due to CD. Additionally, using $B_S = 19$ GHz, two attenuation peaks, due to the CD affects the transmission. In this last case, loading algorithms become essential in order to enable the transmission, as the subcarriers which are highly affected by CD will degrade the overall system performance.

Fig. 4.15 show the bit and power loading for half of the subcarriers after applying LCMA using $B_s = 19$ GHz, as it is more affected by CD. The maximum assigned modulation format is 8PAM, which corresponds to the subcarriers that present the highest SNR values (see Fig. 4.14). The subcarriers more affected by CD don't carry data as it can be seen in Fig. 4.15(left). Similarly, for the power loading scheme, no power is assigned to the same group of subcarriers as shown in Fig. 4.15(right). Subcarriers with intermediate SNR performance are loaded with BPSK and 4PAM depending also on the target data rate.

Fig. 4.16 shows the performance of the system in Fig. 4.7 after applying LCMA. The spectral efficiency and gross data rate are reported for a target BER of 10^{-3}.

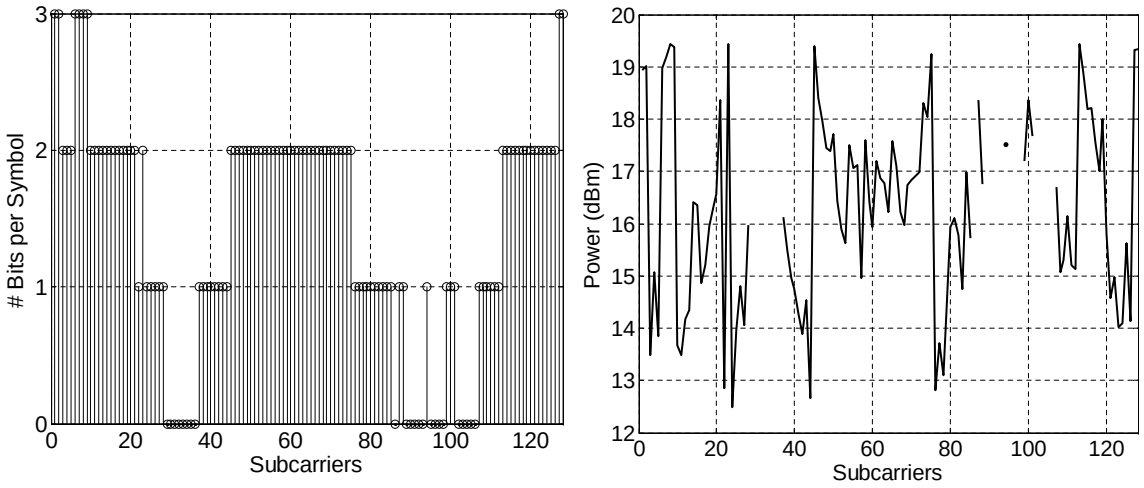

Figure 4.15: Bit and power allocation vs number of subcarriers considering a B_s = 19 GHz at 27 Gb/s after 80 km of SSMF.

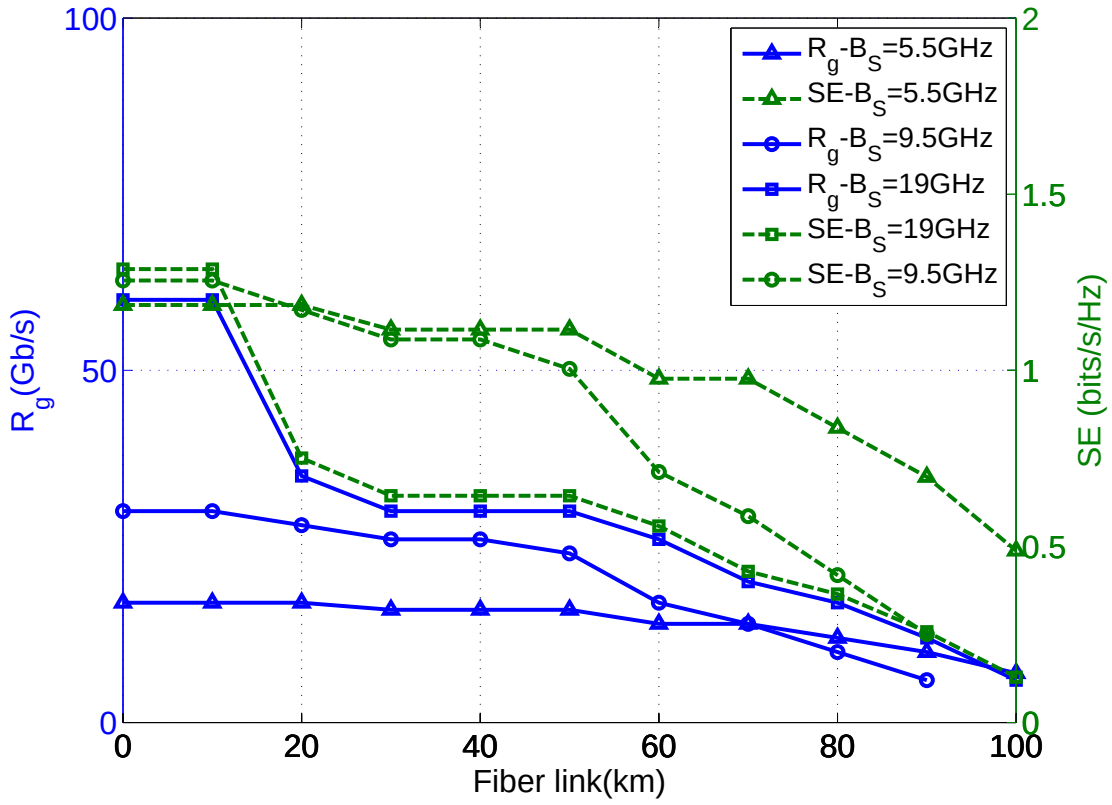

Figure 4.16: Maximum R_g and corresponding SE vs different fiber link for different signal bandwidths to ensure 10^{-3} BER.

Using B_S = 19 GHz outperforms the cases of considering lower bandwidths in terms of achieved data rate at the expense of SE, as 3 frequency slots of 12.5 GHz are occupied. However, in the B2B configuration and after 10 km of SSMF both data

rate and SE are maximized. Specifically, up to 60 Gb/s is successfully transmitted with a SE of 1.29 bits/s/Hz after 10 km of SSMF enabling high data rate transmission in a MAN scenario. Conversely, when $B_G = 5.5$ GHz is used, CD impact is lower. However, at the increase of the fiber length the maximum transmitted data rate to ensure 10^{-3} BER is reduced, as higher modulation formats are required to ensure a target data rate. Specifically, a maximum data rate of 17 Gb/s is achieved up to 20 km of SSMF. Occupying such a low bandwidth, SE is enhanced and a SE around 1 bits/s/Hz can be maintained up to 70 km of SSMF. Finally, when $B_S = 9.5$ GHz is occupied, intermediate performance in terms of maximum achieved data rate and SE is obtained. This case can be compared with uniform loading (see Fig. 4.11) where the same bandwidth is occupied. It is seen that higher data rates and longer fiber reaches are achieved when LCMA is applied. Specifically, with uniform loading a maximum data rate of 28.5 Gb/s is achieved with a SE of 1.19 bits/s/Hz up to 20 km of SSMF (see Fig. 4.11) Whereas, using the same $B_S = 9.5$ GHz applying the loading algorithm, a higher data rate of 30 Gb/s is achieved in the B2B configuration and after 10 km of SSMF with a enhanced SE of 1.25 bits/s/Hz.

A single channel has been taken into account in the simulations. However, it is worth mentioning that cost-effectiveness can be further enhanced when sharing optical components, such as the optical fiber or optical amplifiers among a multitude of WDM channels and multitude of WDM channels and additional system impairments appear such as interchannel crosstalk. The crosstalk is caused due to the interference between subcarriers and the sidelobes of the neighboring WDM channels. Hence, the WDM channel spacing is compost of the OFDM signal bandwidth and a guard band to reduce the power penalty introduced by the interchannel crosstalk. Increasing the number of subcarriers, a larger suppression of the sidelobes can be achieved, allowing to use a reduced guard band between WDM channels without increasing the crosstalk [36].

4.4 Summary

In this chapter, loading schemes have been analyzed and proposed to be used as a solution to combat CD effect and achieve fine data rate in DD O-OFDM systems based on the FHT. The main results from the first scenario, where an AWGN channel is considered, are summarized below:

- Loading capabilities allow fine data rate selection.
- By applying BL in combination with the proposed LC-SLM, the performance in terms of BER and power efficiency is improved as we achieve to mitigate the PAPR and the clipping noise of the system.

The system has been characterized and a simple BL scheme has been introduced in the transceiver design considering the optical channel. Some of the obtained results are listed here:

- DSB signals are transmitted with reduced guard band using BL, resulting in a spectral efficient solution.
- A net data rate of 10 Gb/s is obtained using BL, ensuring a target BER of 10^{-3} up to 120 km.
- Additionally, a net data rate of 13.85 Gb/s is achieved up to 60 km, occupying 1 single slot of 12.5 GHz or two of 6.25 GHz.

Finally, an optimized loading algorithm is included in the BVT, arising as a suitable cost-effective solution for MAN. From the presented simulations we conclude that:

- Up to 16PAM modulation format is used to implement loading schemes, enabling fine bit rate transmission and distance adaptive capabilities.
- 60 Gb/s data rate is achieved after 10 km of SSMF ensuring 10^{-3} BER and enabling high data rate transmission in a MAN scenario.
- 30 Gb/s transmission can be achieved up to 40 km of SSMF using BL and PL.

In the next chapter, an experimental validation of the proposed adaptive cost-effective transceiver is provided. The analyzed solution can find application in MAN. Despite being a promising solution to overcome CD, loading schemes introduce complexity in the DSP. Additionally, PAPR reduction techniques become more effective in long-haul optical systems where fiber nonlinearities are a major problem. In fact, in such scenario the nonlinearity penalty due to the fiber could be reduced after applying PAPR reduction techniques [66]. However, the simplest technique to limit the PAPR (i.e. symmetrically clipping) will be used in all the following simulations and experiments, as long-haul is not the target scenario. The clipping level will be selected depending on the higher modulation format according to the analysis performed in chapter 3.

5

Implementation of FHT-based O-OFDM systems

"We're still in the first minutes of the first day of the Internet revolution."

Scott Cook

5.1 Introduction

A cost-effective Bandwidth Variable Transceiver (BVT) has been proposed using Direct Detection (DD) for a Metro Area Networks (MAN) scenario. In this chapter, an experimental validation of the proposed adaptive Optical-OFDM (O-OFDM) system based on the Fast Hartley Transform (FHT) is provided. Below, we summarize the main contributions of this chapter:

- An Intensity-Modulation (IM)/DD optical system based on OFDM modulation with FHT processing is experimentally demonstrated, achieving similar sensitivity performance as the one obtained with Fast Fourier Transform (FFT)-based O-OFDM.

- We experimentally demonstrate that it is possible to enhance the spectral efficiency, increasing the bit rate by reducing the guard band. This allows designing a bit rate variable IM/DD transmission system, resulting in a suitable cost-effective solution for elastic networks.

- We analyze the Back-to-Back (B2B) system at different bit rates, varying the guard band, and evaluate the sensitivity penalty after 25 km of Standard Single Mode Fiber (SSMF).

- A cyclic extension and increased number of Training Symbols (TS) are considered to enhance the performance of the bit rate variable FHT-based O-OFDM system at the expense of additional overhead.

- The proposed cost-effective BVT in section 4.3 is experimentally validated in the ADRENALINE testbed [90]. Different Broadband Remote Access Servers (BRAS) locations in a MAN have been emulated according to section 2.2, also analyzing the system performance.

- Given the unique subwavelength granularity offered by the OFDM, Bit Loading (BL) schemes are implemented for rate and distance adaptive transmission in MAN.

- The proposed BVT can be the fundamental building block for future Sliceable BVT (S-BVT) [11, 12], where e.g. an array of sub-transmitters with 10 Gb/s capacity each, generates OFDM signals with tunable optical carriers that can be aggregated to be routed as variable data flows towards different nodes [91]. A proof of concept of this advanced elastic feature is also provided.

The rest of the chapter is organized as follows. In section 5.2, the proposed experimental setup of a bit rate variable FHT-based O-OFDM system is presented. The guard band bandwidth is varied in order to enhance system performance. Further simulations are performed with optimized parameters. In section 5.3, loading capabilities are included in the design of the transceiver. The proposed solution is tested in a metro scenario (ADRENALINE testbed). Finally, section 5.4 concludes the chapter.

5.2 Bit rate variable O-OFDM system with reduced guard band

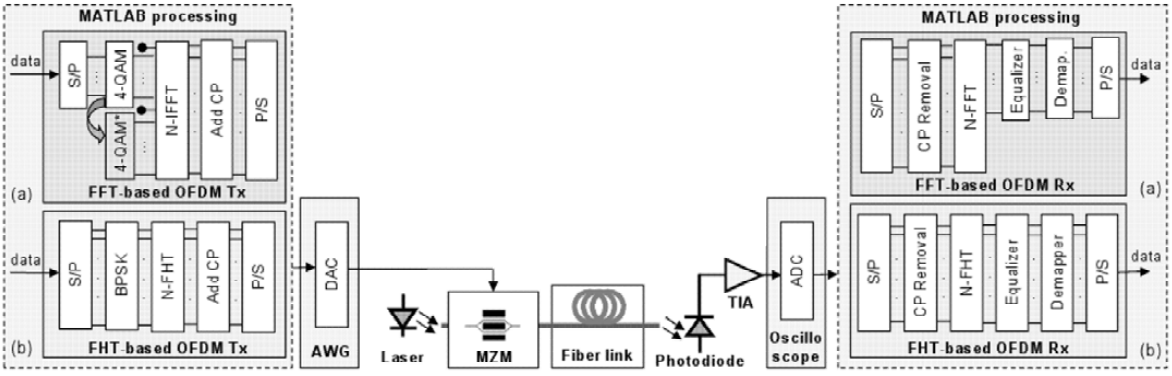

Figure 5.1: Experimental set-up for optical OFDM systems using IM/DD and (a) FFT-based (b) FHT-based processing.

The experimental set-up is described in Fig. 5.1(b). The Digital Signal Processing (DSP) at the transmitter/receiver is performed off-line using Matlab software. A

Table 5.1: System parameters

Transmission	DSB
FHT points	64
Number of frames	5120
Number of TS	2 TS every 512 frames
B_T	10 GHz
Laser center wavelength	1550.92 nm
AWG sampling rate	24 GS/s
Channel	VOA and SSMF
Oscilloscope sampling rate	50 GS/s
CP length	0
TS overhead	0.4%
FEC overhead	7%

stream of data randomly generated is mapped into Binary Phase-Shift Keying (BPSK) format and modulated by an N-FHT with $N = 64$ subcarriers. The baseband signal is up-converted to an intermediate frequency to create the guard band, initially set to equal the bandwidth of the OFDM signal and then varied to accommodate variable OFDM signal bandwidths. The real-valued OFDM digital signal (only in-phase component), with electrical bandwidth $B_T = B_G + B_S$, is loaded into an arbitrary waveform generator, which generates an analog signal at 24 GS/s. The analog Radio Frequency (RF) signal modulates an external Mach-Zehnder modulator (MZM) biased at the quadrature point ($0.5V_\pi$) and driven by a tunable laser source at 1550.92 nm. At the output of the transmitter, the optical power is measured to be +1.8 dBm. The optical fiber link is a SSMF (G.652). At the receiver side, the transmitted signal is detected by a PIN photodiode and amplified with a TransImpedance Amplifier (TIA). The data is captured by using a real-time oscilloscope at a sampling rate of 50 GS/s and then down-converted, demodulated, equalized and demapped off-line with Matlab. The total number of transmitted and analyzed OFDM frames is 5120. Every 512 frames, two training symbols are inserted for synchronization and further equalization. As the FHT can outperform the FFT in terms of robustness against channel delay spread [92], the Cyclic Prefix (CP) is not added in this first experimental assessment, so that the total overhead is 7.4%, due to forward error correction (7% Forward Error Correction (FEC)) and training symbols insertion (0.4%) [57]. The system parameters are summarized in table 5.1

5.2.1 Comparison using the FFT and the FHT

In order to experimentally validate the performance of the proposed system, we compare it with an O-OFDM system transmitting real-valued signals based on FFT. We

consider a stream of bit randomly generated and mapped into either BPSK or 4QAM and modulated by N-FHT or N-Inverse Fast Fourier Transform (IFFT) with $N = 64$, respectively (see Fig.5.1(a)). In fact, to transmit with the same spectral efficiency, FFT-based systems require higher constellation size than FHT-based OFDM, due to the Hermitian Symmetry (HS) constraint [93]. A maximum electrical bandwidth $B_T = 10$ GHz is considered, given the limitation of the Arbitrary Waveform Generator (AWG) filter. Using $B_G = 5$ GHz a maximum bit rate of 5 Gb/s is transmitted

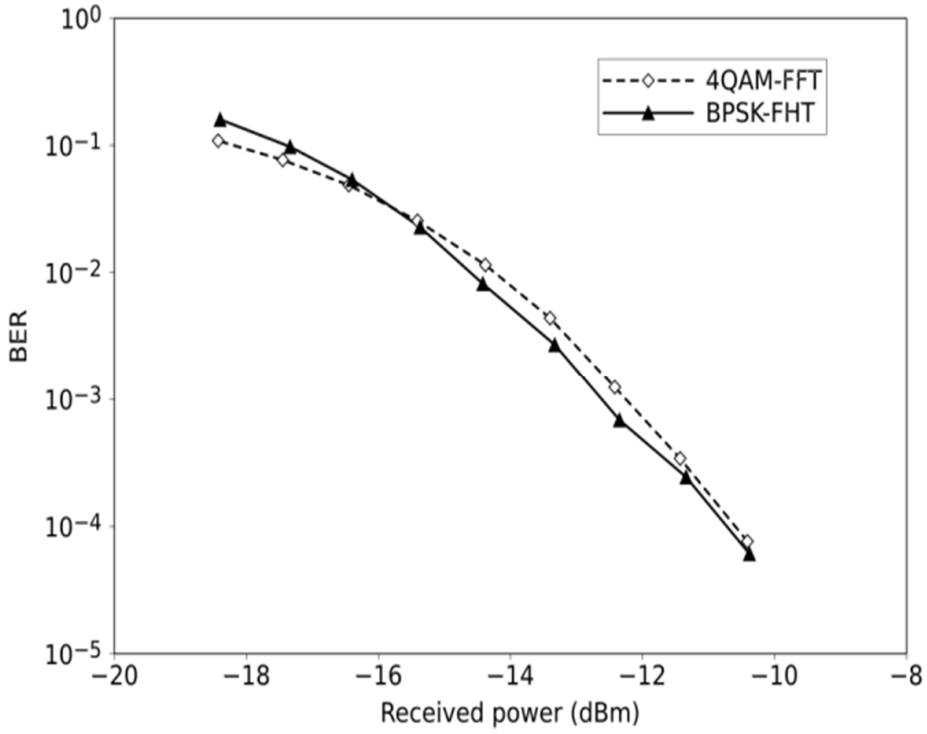

Figure 5.2: Sensitivity performance of the O-OFDM back-to-back system for FHT and FFT processing at 5 Gb/s.

using either 1D modulation (BPSK) with FHT or bidimensional modulation (4QAM) with FFT. For the sensitivity performance analysis of the B2B O-OFDM systems based on FFT and FHT, the fiber link is replaced by a Variable Optical Attenuator (VOA). Thus, measuring the optical power at the PIN input, sensitivity curves are obtained. Results are shown in Fig. 5.2. As it can be observed, the experimental Bit Error Rate (BER) curves of the O-OFDM using DSP based on FFT and FHT are in good agreement, according to the theoretical results (see Fig. 3.10 and [21]). At a target BER of 10^{-3}, assuming an enhanced FEC with 7% overhead, the FHT-based O-OFDM presents a sensitivity of -12.7 dBm and the FFT-based O-OFDM -12.4 dBm.

5.2.2 Performance analysis

As the MZM is biased at the quadrature point, the spectral efficiency of the proposed low complexity system of Fig. 5.1(b) can be enhanced by reducing the guard band [93]. Therefore, at fixed total bandwidth and modulation format (BPSK), the transmitted bit rate can be increased, by decreasing the guard band and increasing the OFDM signal bandwidth. We have first analyzed the sensitivity performance at 10^{-3} BER,

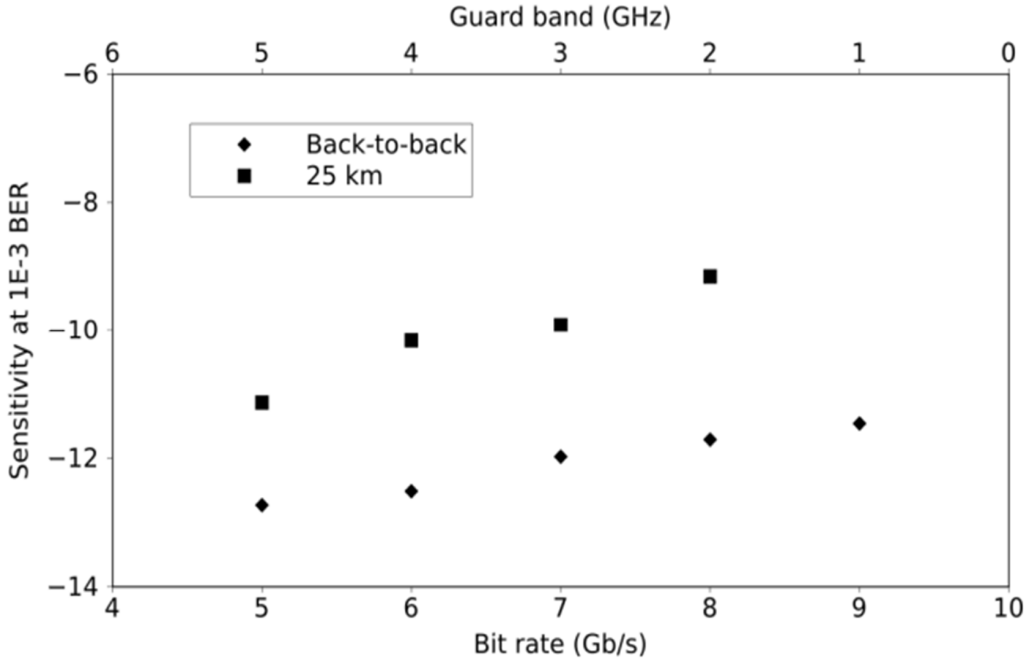

Figure 5.3: Sensitivity at 10^{-3} BER of the B2B system and after 25 km of SSMF, varying bit rate and guard band.

considering a fixed bandwidth $B_T = 10$ GHz and variable bit rate from 5 Gb/s to 9 Gb/s, reducing B_G from 5 GHz to 1 GHz. The experimental results are shown in Fig. 5.3. In the B2B system, the required received power for obtaining 10^{-3} BER at 9 Gb/s and 8 Gb/s is -11.5 dBm and -11.7 dBm, respectively. Thus, the sensitivity penalty corresponding to 80% and 60% bit rate increasing is 1.2 dB and 1 dB, respectively. We have then evaluated the performance of the system in Fig. 5.1(b) after 25 km SSMF. In this case, the sensitivity penalty measured for the same target BER, compared to the B2B system, is 1.6 dB at 5 Gb/s without B_G reduction. This penalty can be also due to the used equalization, selected to minimize the overhead and the computational complexity. The penalty for 6 Gb/s, 7 Gb/s and 8 Gb/s, compared to the corresponding B2B cases, ranges from 2.1 dB to 2.6 dB, while transmission at 9 Gb/s could not be achieved. The sensitivity penalty for varying the bit rate from 5 Gb/s to 8 Gb/s and reducing the required guard band up to 75% (from 8 GHz to

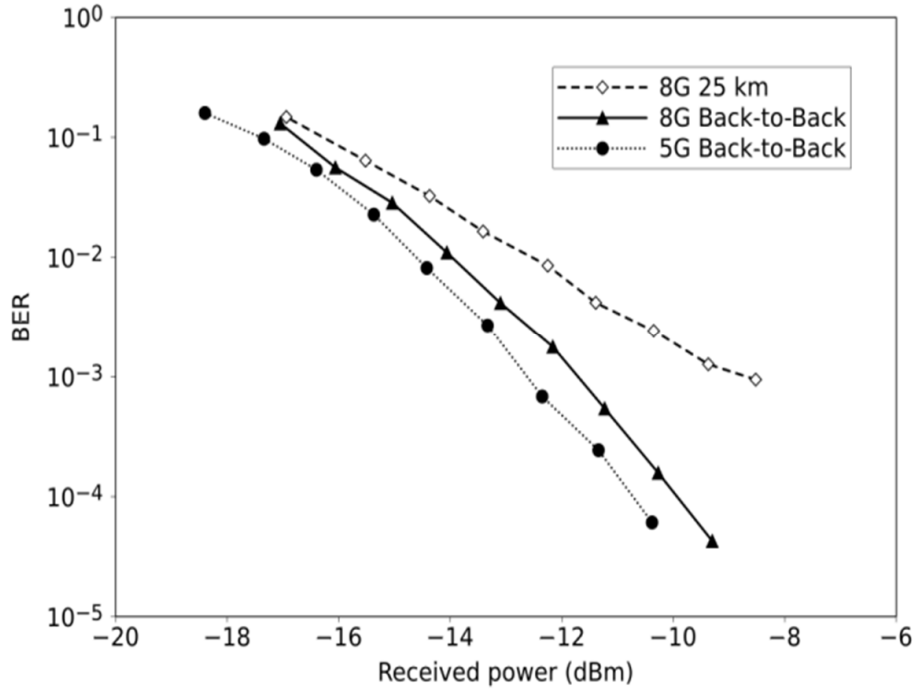

Figure 5.4: BER versus received power at 5 Gb/s (B2B) and 8 Gb/s (B2B and after 25 km).

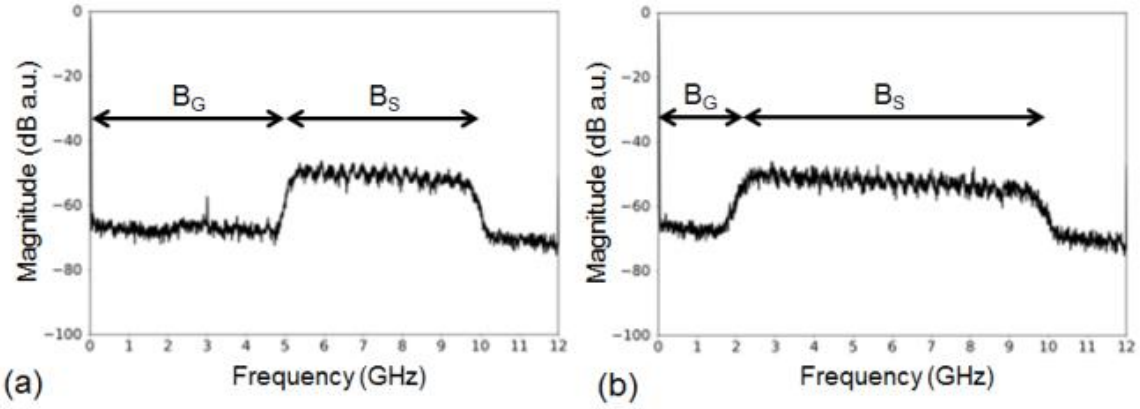

Figure 5.5: Received spectra after photodetection for B2B transmission at (a) 5 Gb/s ($B_G = B_S = 5$ GHz) and (b) 8 Gb/s ($B_G = 2$ GHz, $B_S = 8$ GHz).

2 GHz) is 2 dB. In Fig. 5.4, the measured BER curves versus the received power for 8 Gb/s transmission in the B2B case and after 25 km of SSMF are reported. The 5 Gb/s B2B system performance without guard band reduction is also reported.

Fig. 5.5 shows the B2B transmitted spectra after photodetection of the proposed variable bit rate FHT-based O-OFDM at 5 Gb/s (no B_G reduction) and 8 Gb/s (75% B_G reduction). Thanks to the optimal MZM biasing, low intermodulation products are evidenced. For an optimal spectral resources allocation, B_T can be varied, reducing

B_G also for lower bit rate transmission, resulting in a bandwidth and bit rate variable system. The spectral efficiency can be further enhanced using higher 1D modulation.

5.2.3 System Optimization

In order to enhance the performance of the proposed bit rate variable system, we propose to optimize the transceiver design. For this purpose, we adopt the low complexity channel estimation described in Sec. 2.4.3, and include a digital symmetrical clipping at the transmitter for limiting the Peak-to-Average Power Ratio (PAPR) of the OFDM signal. The clipping value has been selected in order to minimize the clipping noise. According to our theoretical and numerical study (section 3.6, [19,52]), it has been set to a value slightly greater than twice the signal standard deviation, considered optimal for a BPSK format; moreover, it has been previously tested in the experimental set-up for the B2B case. The overhead due to the training symbols has been increased from 0.4% to 1.6% and a 10% of cyclic extension has been added to cope with inter-channel interference and inter-symbol interference. According to Eq. (4.4), the total overhead considered in this case is 19.6% and the corresponding gross data rate is 10.8 Gb/s.

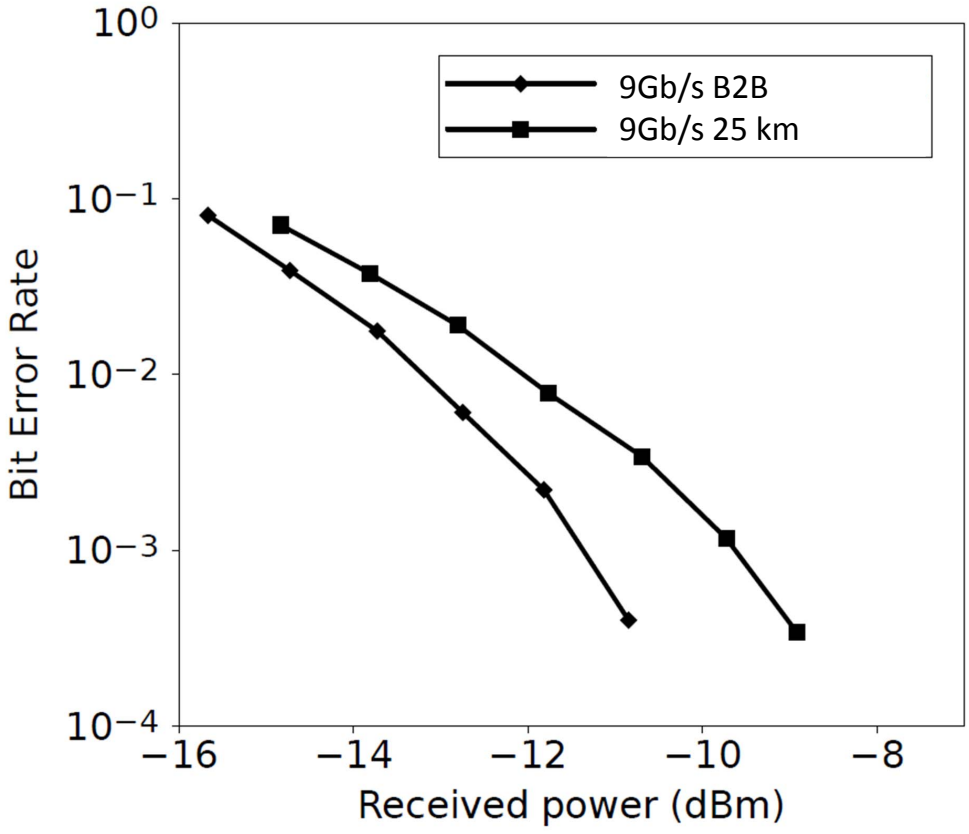

Figure 5.6: BER versus received power at 9 Gb/s using the optimized bit rate variable transceiver.

Table 5.2: Optimized system parameters

Transmission	DSB
FHT points	64
Number of frames	5120
Number of TS	2 TS every 512 frames
B_T	10 GHz
Laser center wavelength	1550.92 nm
AWG sampling rate	24 GS/s
Oscilloscope sampling rate	50 GS/s
CP overhead	10%
TS overhead	1.6%
FEC overhead	7%

The optimized bit rate variable transceiver has been tested in the experimental set-up of Fig. 5.1(b). The simulations parameters are listed in table 5.2. In Fig. 5.6, the measured BER curves versus the received power in the B2B case and after 25 km of SSMF are reported. It can be seen that the transmission at 9 Gb/s, corresponding to the maximum bandwidth reduction (1 GHz), over 25 km of SSMF has been achieved. Furthermore, the sensitivity penalty measured at the target BER of 10^{-3} is 1.6 dB.

5.3 Elastic OFDM-based BVT

Here, the proposed elastic BVT, in chapter 4, based on low-complexity DSP using the FHT for distance adaptive transmission in flexi-grid metro networks is experimentally validated in the ADRENALINE testbed [90]. Double-Side Band (DSB) modulation is implemented, as it requires a simpler and lower-cost transceiver design [53]. It has been demonstrated that using an external MZM biased at the quadrature point the required guard band can be reduced enhancing the spectral efficiency (see section 5.2, [53]). However, this scheme is more affected by the CD, in fact, self-cancellation between carriers of the two sidebands of the DSB spectrum can occur, limiting the achievable reach. A more robust DSB transmission can be obtained by reducing the spectral occupancy of the OFDM signal as seen in chapter 4, so that the carriers of the two sidebands experiment lower power fading due to CD, according to formula (4.5). This way the same spectral efficiency as Single-Side Band (SSB) modulation can be achieved. According to the analysis performed in section 4.8, a laser with linewidth of the order of MHz and a guard band of 500 MHz is considered.

The experimental set-up is shown in Fig. 5.7. The DSP at the transmitter/receiver is performed off-line using Matlab software. A stream of randomly generated data is mapped into 1D constellation (BPSK or/and 4PAM) and modulated by an FHT with

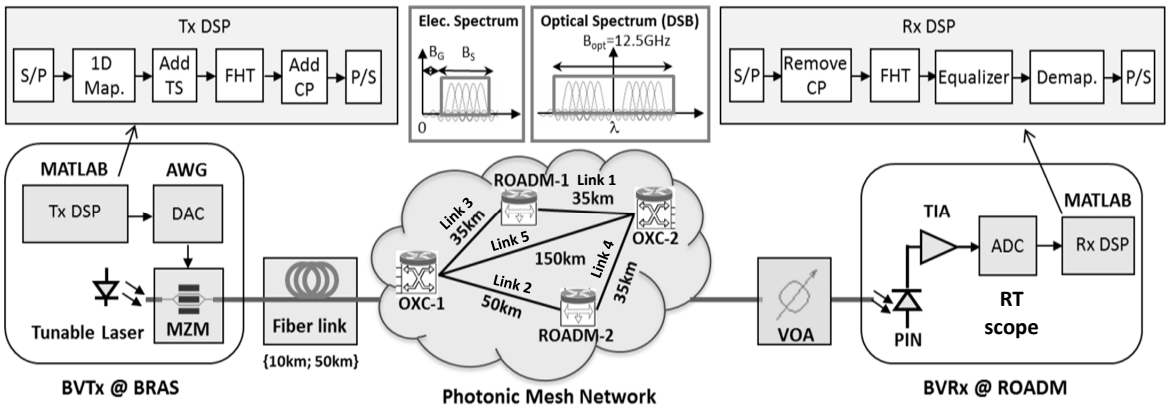

Figure 5.7: BVT schematic and experimental set-up

$N = 64$ subcarriers. The real-valued OFDM digital signal is loaded into an AWG, which generates an analog signal at 12 GS/s. The analog OFDM signal modulates an external MZM biased at the quadrature point and driven by a tunable laser source at $\lambda = 1550.12$ nm. The maximum B_S is 5 GHz and the total electrical bandwidth, including the guard band, is $B_T = 5.5$ GHz. The resulting DSB optical spectrum is $B_{opt} = 11$ GHz, which perfectly fit within a 12.5 GHz flexi-grid channel, as shown in the inset of Fig. 5.7. At the receiver side, the transmitted signal is detected by a PIN photodiode. The data is captured by a real-time oscilloscope at a sampling rate of 50 GS/s and then down-converted, demodulated, equalized and demapped off-line with Matlab. 8 half-length TS are considered for equalization (see section 2.4.3 and [53]); they are inserted each 512 OFDM frames resulting in an overhead of 1.56%. A 10% CP is also considered. In order to assume a target BER of 10^{-3}, a FEC with 7% overhead is taken into account. Thus, the resulting total overhead is 19.54%. For sensitivity measurements, a VOA is used. The fiber link is a SSMF (G.652), whose length is varied in order to emulate different BRAS locations (e.g. 10 km or 50 km), according to section 2.2. The ADRENALINE testbed represents a 4-nodes mesh metro network. Specifically, it consists of two Optical Cross-Connect (OXC)s and two Reconfigurable Add-Drop Multiplexer (ROADM)s, interconnected with 5 different links from 35 km up to 150 km, as indicated in Fig. 5.7. Specifically, links 1, 2, 3, and 4 have 6 available channels spaced 100 GHz. Whereas link 5 it is designed to support transmission of 13 channels 50 GHz spaced. In the set-up, we assume that the rate/Bandwidth Variable Transmitter (BVTx) is located at the BRAS and the Receiver (BVRx) at the ROADM. In table 5.3, the system parameters are shown.

Table 5.3: Optimized system parameters

Transmission	DSB
FHT points	64
Number of TS	8 half-length TS every 512 frames
B_G	500 MHz
Maximum B_S	5 GHz
Laser center wavelength	1550.12 nm
AWG sampling rate	12 GS/s
Oscilloscope sampling rate	50 GS/s
CP overhead	10%
TS overhead	1.56%
FEC overhead	7%

5.3.1 Experimental assessment in the ADRENALINE testbed

We assess the performance of the proposed BVT using BL according to section 4.3. We analyze two modulation formats (BPSK and 4PAM) at 5 GBaud/s ($B_S = 5$ GHz), giving 5 Gb/s and 10 Gb/s, respectively. Fine bit rate selection is achieved using BL. An 8 Gb/s connection is obtained by mapping the 40% of the subcarriers with BPSK and the 60% to 4PAM. This target rate is also obtained by reducing the electrical signal bandwidth to 4 GHz and using only 4PAM format. In all the experiments, the BER is measured by error counting up to 1000 errors. First, we analyze the B2B case. Fig. 5.8

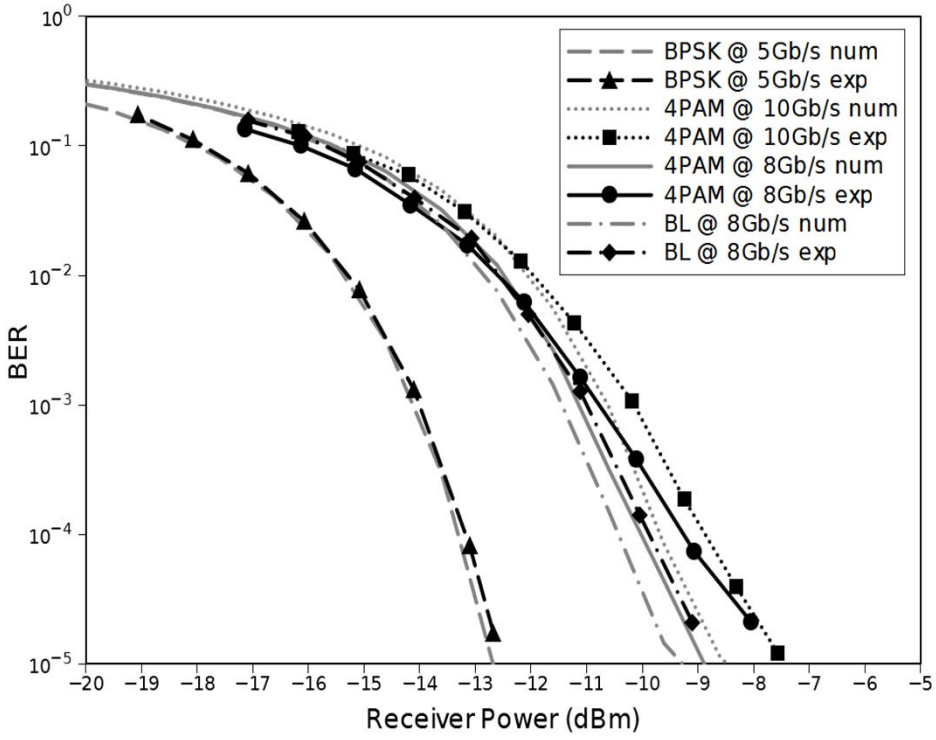

Figure 5.8: B2B performance for variable BVT formats

shows the experimental BER curves (black lines with markers) versus the receiver power, compared to the simulated ones (gray lines). It can be observed that the BPSK curves at 5 Gb/s are in good agreement. The measured sensitivity at 10^{-3} BER is -14 dBm, the numerical result is -14.1 dBm. When using multilevel modulation, the experimental curves present approximately 0.5 dB of penalty (at the target BER) with respect to the corresponding numerical curves. The measured received power at 10^{-3} BER is -10.1 dBm and -10.6 dBm for the 4PAM format at 10 Gb/s and 8 Gb/s; the BL scheme at 8 Gb/s shows better performance, requiring -10.9 dBm of receiver power.

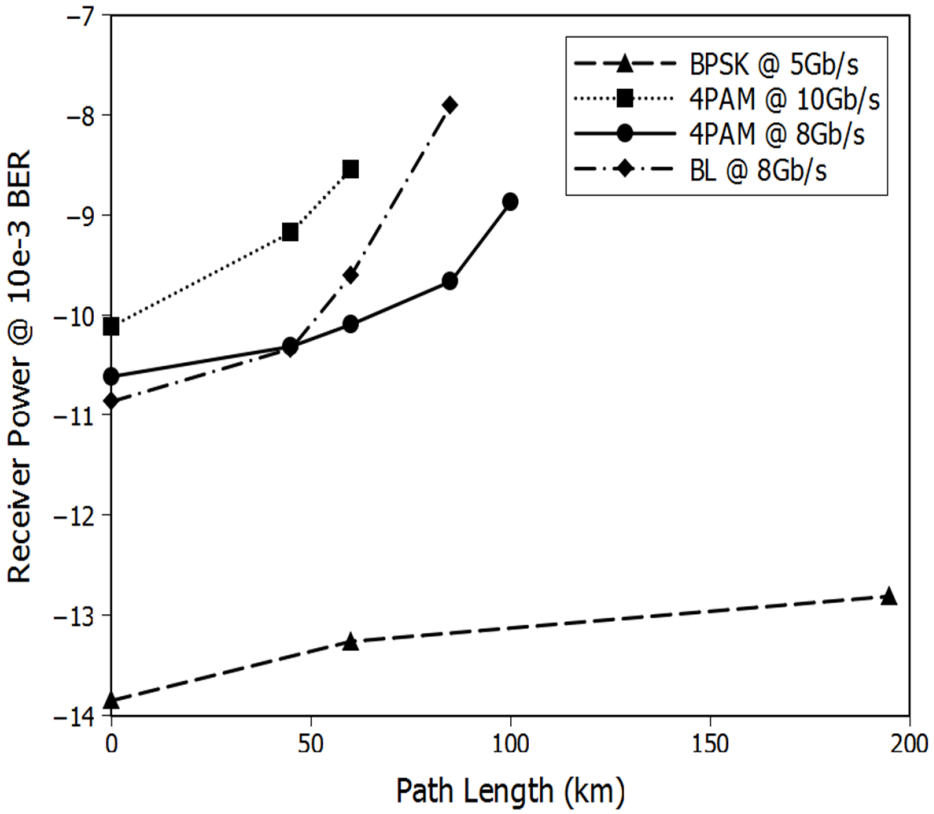

Figure 5.9: BVT performance at different optical paths

Then, we validate the BVT in the experimental set-up described in Fig. 5.7. The optical OFDM signal is routed towards one of the network ROADM through optical paths of 2 hops (via OXC-1). Connections of 45 km, 60 km, 85 km and 100 km are tested. Results in terms of receiver sensitivity at 10^{-3} BER are shown in Fig. 5.9. BPSK is the most robust modulation format. Thus, it is also successfully transmitted to ROADM-2 through a 3 hops path (via OXC-1 and OXC-2) of length 195 km. Compared to the sensitivity (at the target BER) required for the 2 hops path of length 60 km (-13.26 dBm), a penalty of only 0.45 dB is measured. 4PAM format, with the same

bandwidth occupancy, doubles the spectral efficiency at the expense of the receiver sensitivity and the achievable reach. The required receiver power for a BER of 10^{-3} is -8.54 dBm, considering a path of 60 km with 2 hops.

For distance-adaptive transmission assessment, we analyze the connections at 8 Gb/s. As the subcarriers at the edge of the signal present lower Signal-to-Noise Ratio (SNR) (due to channel impairments), they are loaded with BPSK symbols. We compare this BL scheme at 8 Gb/s ($B_{opt} = 11$ GHz), with uniform 4PAM format and reduced bandwidth occupancy ($B_{opt} = 9$ GHz). The BL scheme has better performance up to a reach of 45 km (2 hops). For longer path, in order to cope with the accumulated CD, it is convenient to obtain the same bit rate by reducing the signal bandwidth and select the same modulation format (4PAM) for all the subcarriers. This connection can be successfully established through an optical path with 2 hops of length 100 km, requiring a receiver sensitivity of -8.87 dBm. The longest 2 hops path supporting BL at 8 Gb/s is 85 km; a BER of 10^{-3} is achieved with a receiver power of -7.9 dBm. This results in a penalty of 1.76 dB compared to the sensitivity of 4PAM format at the same bit rate.

5.3.2 Proof of concept of a S-BVT

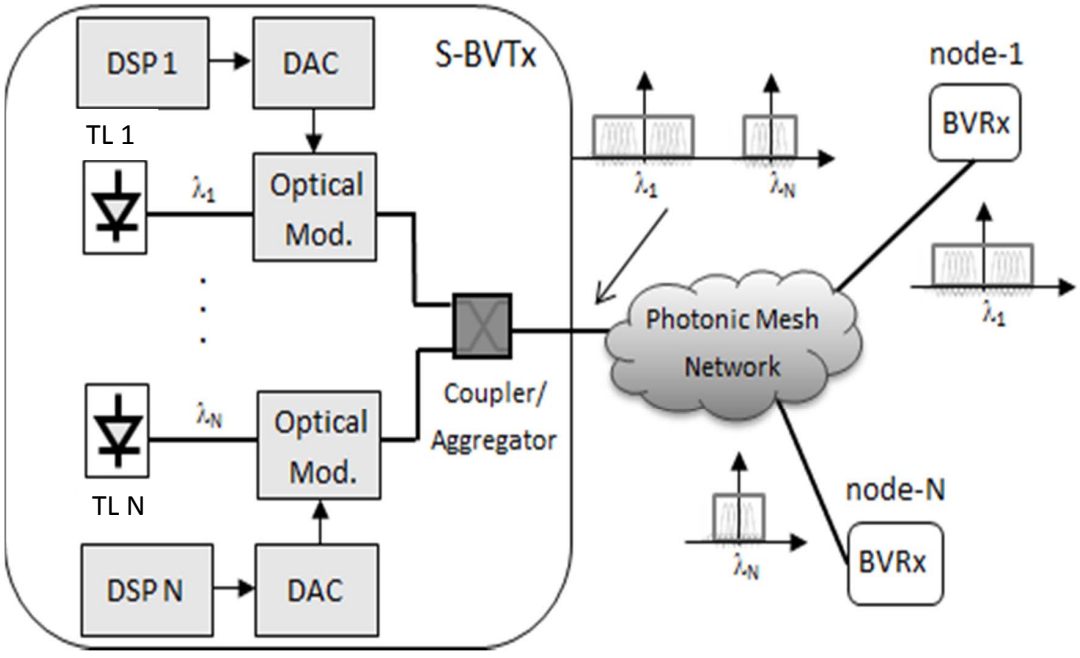

Figure 5.10: S-BVT architecture

The proposed BVT in section 4.3 can be considered as a building block for designing a S-BVT, as shown in Fig. 5.10. Specifically, the transceiver consists of a set of virtual

transceivers able to generate a flow of great capacity, which can be suitably sliced as multiple flows direct towards different destination nodes [11]. A possible architecture is described in Fig. 5.10, where an array of bandwidth variable sub-transmitters generate Orthogonal Frequency Division Multiplexing (OFDM) signals centered at different optical carriers, according to the wavelength selected at the Tunable Laser (TL) [91]. Multi-band OFDM signals can be transmitted with cost-effective DD scheme reducing the cost of the implementation. This architecture can found application in flexi-grid MAN, and it can be used at the BRAS node (see chapter 2). The total S-BVT capacity is given by the contribution of all the sub-transmitters. The aggregated flow at the node can be routed as sliced data flows with less capacity towards different destination nodes, as shown in Fig. 5.10. Specifically, at the destination node, the (sliced) data flow is received to be correctly demapped. In case of receiving an aggregated data flow at the Sliceable BVRx (S-BVRx), it is distributed to the sub-receiver array and parallel processed [91].

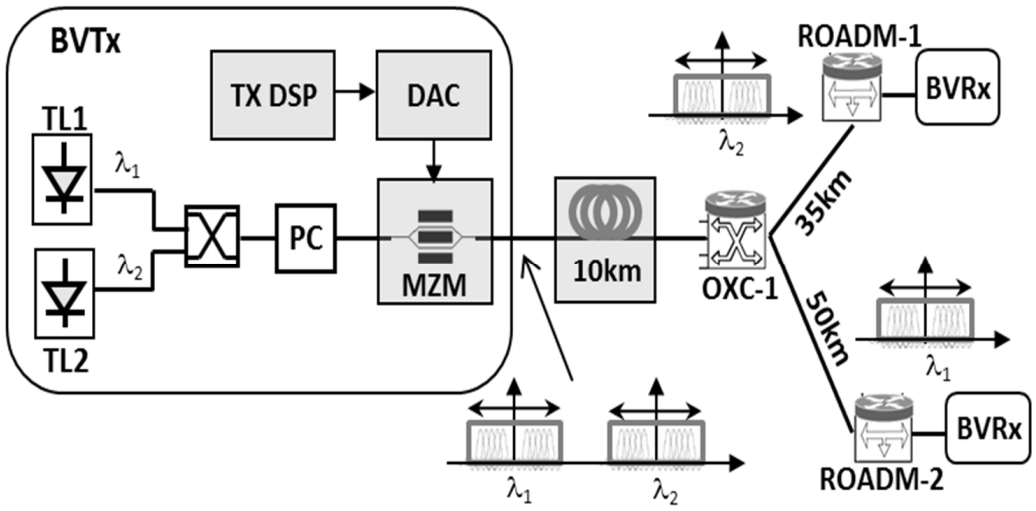

Figure 5.11: Set-up for S-BVT proof of concept

In order to prove this capability, the set-up in Fig. 5.11 is implemented. Two data flows, consisting of two optical OFDM signals at half of the maximum rate capacity of the BVT, are generated using two TL sources at $\lambda_1 = 1550.12$ nm and $\lambda_2 = 1550.92$ nm. BPSK format and electrical bandwidth of 5 GHz are selected at the transmitter DSP. As the modulation is performed by a single MZM, two identical signals at 5 Gb/s with optical bandwidth of 11 GHz are obtained. After passing the first hop (10 km), at the OXC-1, they are sent towards ROADM-1 and ROADM-2, through the link of 35 km and 50 km, respectively. Both signals have been correctly detected. For a BER of 10^{-3}, the measured receiver power at ROADM-1 (signal at λ_2) is -13.1 dBm and the Optical Signal-to-Noise Ratio (OSNR) is 34.7 dB. At ROADM-2 (signal at λ_1), the

receiver power is −13.35 dBm and the OSNR is 35.43 dB.

5.4 Summary

In this chapter, we have experimentally demonstrated an O-OFDM BVT based on FHT processing suitable for cost-sensitive applications. The main conclusions are summarized below:

- It has been experimentally validated an O-OFDM system based on BPSK FHT processing showing that similar performance to a 4QAM FFT-based system, in terms of receiver sensitivity and spectral efficiency, can be achieved using DSP with lower complexity.

- We have implemented a cost-effective bit rate variable system by varying the guard band, with a fixed modulation format. We have demonstrated:

  - 60% bit rate increasing, corresponding to 75% reduction of the required guard band, can be achieved with a sensitivity penalty of 1 dB in a B2B transmission and 2 dB after 25 km SSMF.

  - It is shown that a variable bit rate, from 5 Gb/s to 8 Gb/s, can be transmitted using BPSK format and low complex processing, with up to 75% reduction of the required guard band, over 25 km SSMF for a BER of 10^{-3}.

- We have optimized the proposed transceiver at the expense of additional overhead, showing that:

  - Up to 80% bit rate increasing, corresponding to 89% reduction of the required guard band, can be achieved with a sensitivity penalty of 1.6 dB after 25 km SSMF compared to the B2B transmission, when including a cyclic prefix extension.

  - Up to 9 Gb/s can be transmitted over a 25 km SSMF link thanks to the improved transceiver design.

- Finally, the optimized BVT has been presented as suitable cost-effective solution for Elastic Optical Networks (EON). The main results are:

  - The proposed BVT based on OFDM with DSB and DD has been experimentally validated in MAN scenario. The modulation format and bandwidth occupancy (within 12.5 GHz channel) are selected at the DSP by software.

- Distance-adaptive connections at variable rates from 5 Gb/s to 10 Gb/s are tested. BPSK at 5 Gb/s is supported up to 195 km link (3hops) in the ADRENALINE testbed.
- By reducing the signal spectrum with 4PAM format, more robust transmission than using adaptive bit loading is obtained at 8 Gb/s up to 100 km and 2 hops in the ADRENALINE testbed.
- To provide higher capacity and flexibility, the BVT is used as a building block for future sliceable transceiver.

6

Design of adaptive FFT-based DMT systems

"Technology has become as ubiquitous as the air we breathe, so we are no longer conscious of its presence."

Godfrey Reggio

6.1 Introduction

In this chapter, a high data rate adaptive Discrete MultiTone (DMT) transceiver using a Direct Detection (DD) optical implementation based on Mach-Zehnder modulator (MZM) featured with Levin Campello Margin Adaptive (LCMA) is implemented to allow connectivity between data centers. The LCMA algorithm is selected to be implemented in the transceiver Digital Signal Processing (DSP), as it is shown that this loading strategy outperforms the loading algorithm according to Chow Cioffi Bingham (CCB) [27]. Several DMT systems, that can be applied in data center scenarios, are found in the literature. Single-Side Band (SSB) transmission is proposed as a solution to deal with Chromatic Dispersion (CD), allowing long-haul transmission in DMT systems at the expense of increasing system complexity and the appearance of higher amount of non-linear subcarrier mixing distortions in lower frequency range [25]. Alternatively to SSB modulation, other solutions for high data rate transmission over fiber have been presented. As an example, in [84] a simplified on-off loading for 42.8 Gb/s over a 80 km span with optical pre-amplification is proposed to mitigate CD. Specifically, it is shown by means of simulations that loading can be an adequate alternative to SSB. On the other hand, significant limitations due to CD appear when working in the wavelength range of 1550 nm, as demonstrated in [94] for different types of modulators. In [95], optical pre-compensation is used to overcome this effect and to reach 80 km with 2×50 Gb/s. Recent research focuses on DMT for client side applications in the O-band. Using non-linear Volterra equalization, a transmission of

101 Gb/s on a single channel over 80 km is possible [96]. Additionally, 469 Gb/s on four channels have been demonstrated over 30 km [97]. In [20], a detailed study by means of simulation is performed comparing various DMT systems with optimized Bit Loading (BL) and Power Loading (PL) transmitting at 10.7 Gb/s. In [98], an experimental demonstration of the transmission of a DMT system using Levin Campello Rate Adaptive (LCRA) algorithm is performed. 19 Gb/s and 9.7 Gb/s are achieved over 25 km and 100 km, respectively. A later study shows a 50 Gb/s transmission over 20 km of Standard Single Mode Fiber (SSMF) with a Directly Modulated Laser (DML) laser and suboptimal bit and power loading [99]. Finally, in [24], 100 Gb/s transmission using suboptimal BL and PL is achieved after 10 km SSMF using a DML. Hence, DMT becomes a potentially low-cost approach for Nx100 Gb/s Dense Wavelength Division Multiplexing (DWDM) inter-data center interconnects over distances beyond 40 km.

The main contributions of the chapter are listed below:

- A MZM is selected because it presents negligible chirp. Hence, the required Optical Signal-to-Noise Ratio (OSNR), to ensure a target Bit Error Rate (BER) and a certain transmission reach, is lowered.
- A baseband signal is transmitted allowing a simpler implementation when compared with other transmission systems such as SSB modulation [25].
- The system performance is assessed by means of simulation at different data rates ranging from 20 Gb/s to 112 Gb/s.
- OSNR measurements have been performed, analyzing links of 50 km and 80 km, beyond the distances found in the literature.
- It is shown that LCMA presents superior performance compared to CCB.
- The BER performance and the achievable reach of the proposed system is investigated, evidencing the improvement over bandwidth variable uniform loading and taking into account the channel response and transmission impairments.
- We demonstrate that using the presented design guidelines, the proposed adaptive transceiver can be adopted as a solution for major client optics applications, providing a possible extension of the link reach between data centers.

The rest of the chapter is detailed here. In section 6.2, the DMT transceiver design is described, giving the guidelines for the fundamental DSP blocks implementation. The performance analysis of the system is presented in section 6.3. Specifically, system limitations are analyzed and LCMA algorithm is included in the design. A comparison of the proposed transceiver with suboptimal loading such as CCB and with uniform loading scheme is also included. Finally, the conclusions are drawn in section 6.4.

6.2 Adaptive DMT transceiver design

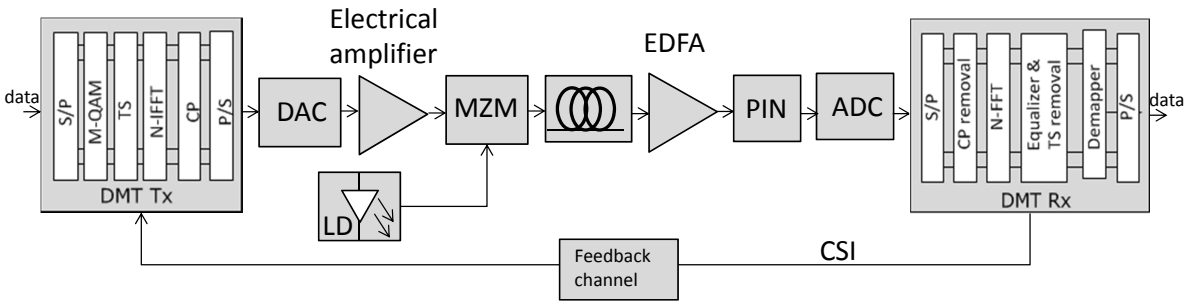

Figure 6.1: DMT system model. The DSP modules at the DMT transmitter/receiver (Tx/Rx) are detailed.

Fig. 6.1 shows the system model of the proposed adaptive DMT transceiver. The input data are parallelized and mapped onto the subcarriers using the same modulation format (uniform bit loading) or different formats per subcarrier (bit loading). Binary Phase-Shift Keying (BPSK) and MQAM are considered. The constellations of the analyzed formats have been implemented according to [1] and are indicated in Fig. 6.2. Then, Training Symbols (TS) are added for synchronization and channel estimation in reception. The resulting signal is fed into an N points Inverse Fast Fourier Transform (IFFT), forcing Hermitian Symmetry (HS) to create the DMT symbols. At the increase of N, a finer granularity can be obtained, as a larger number of subcarriers can be mapped with different modulation formats. Thus, the system flexibility is enhanced. Then a Cyclic Prefix (CP) is added to cope with channel dispersion-induced InterSymbol Interference (ISI) and InterCarrier Interference (ICI). The CP must be chosen considering a trade-off between system performance and CP overhead [36]. However, when the DMT symbol size increases, the impact of CP overhead on the data rate is reduced. Additionally, symmetrical clipping is performed to limit the Peak-to-Average Power Ratio (PAPR) using a C, defined in equation (2.5) [19] and [100]. The clipping level must be selected according to the highest modulation format, in order to limit the clipping noise at the expense of increasing the power of the signal [18]. The serialized data are digital-to-analog converted with a Digital-to-Analog Converter (DAC) and modulated onto the optical carrier by means of a MZM. External modulation is used, in contrast to alternative implementations based on direct laser modulation, such as [98], where the DMT signal is directly modulated with a Distributed FeedBack (DFB) laser. Then, the optical signal is transmitted over the fiber channel. CD limits the system performance when transmitting over the fiber. SSMF or other optical fibers with lower dispersion coefficients such as Non-Zero Dispersion-Shifted Fiber (NZDSF) can be used as optical channel. Nevertheless, SSMF

is considered for our analysis as it is the most critical case in terms of CD impact and it is deployed in most of major client optics applications [29]. At the receiver side, the DMT signal is detected with a PIN photodiode whereas in [98] an Avalanche Photo-Detector (APD) is used as Passive Optical Network (PON) is the target application. Then, the resulting signal is analog-to-digital converted and synchronized. Specifically, the variant of Schmidl & Cox's algorithm, explained in section 2.4.4, is implemented. Finally, the signal is demodulated, equalized, and demapped.

An initial channel estimation can be performed by transmitting a probe DMT signal mapped with uniform loading. The Signal-to-Noise Ratio (SNR) of each subcarrier is estimated at the receiver side and sent back to the transmitter as Channel State Information (CSI) through the feedback channel (see Fig.6.1) [9]. The feedback channel can be realized over the inverse channel of a bidirectional system setup (with usually a pair of fibers, but also a single fiber is possible). Also an Optical Supervisory Channel (OSC), which is a dedicated low rate optical channel at a different wavelength can be used as it is present in many systems. The CSI is used to implement the LCMA loading algorithm at the transmitter side. Conversely, in other implementations LCRA is more appropriate. For example in [98], LCRA is adopted since direct modulation of DFB laser is implemented for a PON scenario.

LCMA algorithm has been introduced in section 4.3.2. However, here some modifications are performed. Specifically, the algorithm is adapted in order to take into account non-squared constellations by scaling the resulting energies of each subcarrier by a factor k_{MQAM}. In [27], LCMA is applied considering squared MQAM constellations. When squared constellations are considered, the scaling factor is one. Alternatively, for non-squared constellations, the scaling factors are obtained taking as a reference the power of the QPSK format. In particular, the normalized mean powers of the different modulation formats can be calculated according to [1]. Thus, the normalized mean power of BPSK ($\bar{P}_{BPSK}$) and 4 QAM format ($\bar{P}_{4QAM}$) are 1 and 2, respectively implying a power ratio of $\bar{P}_{BPSK}/\bar{P}_{4QAM} = 1/2$. On the other hand, the relation between both formats in terms of energy is $(2^{b_{BPSK}} - 1)/(2^{b_{4QAM}} - 1) = (2^1 - 1)/(2^2 - 1) = 1/3$, where b_{4QAM} and b_{BPSK} are the number of bits per symbols of the 4QAM and BPSK formats, respectively. Hence, the scaling factor of BPSK format is $k_{BPSK} = 3/2$. Following this, the resulting scaling factors for 8QAM, 32QAM, and 128QAM formats are $k_{8QAM} = 9/7$, $k_{32QAM} = 30/31$, and $k_{128QAM} = 123/127$, respectively. CCB algorithm is also implemented to solve the Margin Adaptive (MA) problem, for comparison with Low Complexity (LC) solution. In particular, CCB algorithm first computes the water-filling solution considering the SNR of the subcarriers, a tentative margin and Γ. Then, the resulting bit distribution is approximated by rounding the bit number values, according to the data rate constraint. As a last step, the energy is recalculated

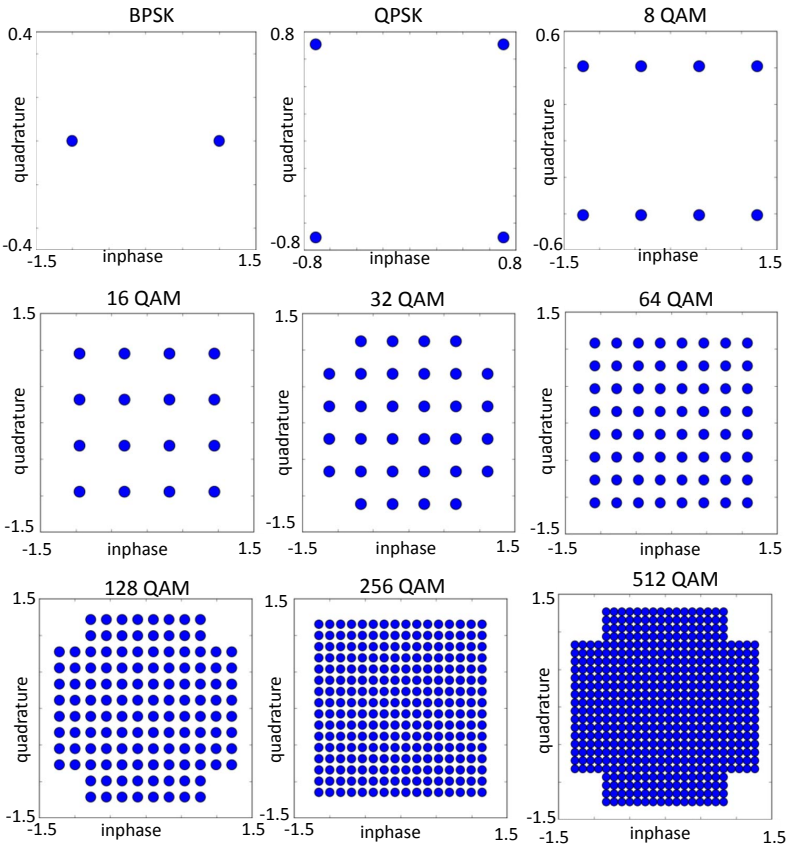

Figure 6.2: BPSK and rectangular QAM constellations implemented at the transmitter [1].

also including the scaling factors. It is worth mentioning that, if suboptimal CCB Margin Adaptive (CCBMA) is used in the transceiver DSP for reducing the computational complexity, the same parameters as in the LC case, namely the initial Γ and scaling factors, can be used.

Finally, in a real implementation, network information will be provided once at the beginning of the transmission. Since the optical channel changes very slowly, the latency due to the round trip for the CSI will not be a problem. Hence, latency will be related with the optical path setting. On the other hand, Forward Error Correction (FEC) will also affect the latency as transmission delays for FEC encoding and decoding occur. Thus, different FEC schemes can be considered: Hard Decision (HD)-FEC, which has an overhead $\delta_{FEC} = 7\%$, and Soft Decision (SD)-FEC with $\delta_{FEC} = 20\%$ [5,101]. Depending on the used FEC coding scheme, a different target BER is allowed. Specifically, for the HD-FEC, the target BER is 10^{-3} [5]. Whereas SD-FEC gives a target BER of $1.9 \cdot 10^{-2}$ [102]. Additionally, other FEC can be used depending on latency and performance requirements [5, 103].

6.3 Performance analysis

In order to analyze the proposed DMT transceiver described in section 6.2 and used in the system of Fig. 6.1, Python software is used. BPSK and MQAM formats are considered, with $M = 2^q$ and q variable between 2 and 9 according to the implemented loading algorithm (see Fig. 6.2) [1]. 5 TS are added every 119 symbols to estimate the channel at the receiver side; 2 of them are also used for frame synchronization. Thus, the overhead due to the TS is 4%. The 124 DMT symbols are statistically independent and constitute a DMT frame which is repeatedly transmitted. As motivated in section 6.2, an $N = 2048$ points IFFT is implemented considering that half of the subcarriers are used to force HS. A maximum of 852 subcarriers carry data in order to introduce an oversampling factor, $L = 1.2$, for avoiding aliasing in the filtering process. A CP of 1.56% is considered. Then, according to [18], the DMT signal is symmetrically clipped using a clipping level of $C = 12$ dB. A model of the spectral behavior of a high speed CMOS 8 bits resolution DAC working at 64 GS/s is considered for digital-to-analog conversion [104]. Hence, the corresponding maximum DMT electrical signal bandwidth is 26.67 GHz ($B_s = \frac{64GS/s}{2 \cdot L}$). The optical carrier is set to 192.5 THz, and the MZM is biased at the quadrature point. The peak-to-peak drive level has been adjusted to be about the 90% of V_π. The optical link is emulated with a SSMF (G.652). The split-step Fourier method is used to model the propagation over the SSMF with a dispersion coefficient of 17 ps/nm/km, a nonlinear coefficient of 1.37 $W^{-1}km^{-1}$ and 0.2 dB/km attenuation. The power at the input of the fiber is 5 dBm. Amplified Spontaneous Emission (ASE) noise is modeled adding white optical noise. The OSNR is defined in a 12.5 GHz bandwidth. At the receiver, a variant of Schmidl & Cox's method is considered for frame synchronization, as defined in section 2.4.4. One tap equalization with decision directed channel estimation is implemented (see section 2.4.3). The BER is calculated using error counting. Bits are transmitted until at least 100 errors occur. System parameters used in simulations are summarized in table 6.1.

Considering a minimum FEC overhead of 7% and also taking into account the overhead due to CP and TS a total overhead of 13% is needed. When SD-FEC is implemented, the total overhead increases up to 26.7%. All the bit rates in this chapter are gross data rates which include the overhead due to FEC. The overhead due to CP and TS is not part of the gross data rate. Hence, the net data rates can be calculated as $R_n = R_g/(1 + \delta_{FEC})$ according to [57].

In order to evaluate the system limitations, the SNR of each subcarrier is estimated in the Back-to-Back (B2B) configuration by implementing decision directed channel estimation, as explained in section 2.4.3. An initial channel estimation is performed by sending 5 TS and using uniform loading with 16 QAM format at 100 Gb/s. An OSNR

Table 6.1: System parameters

Modulation format	BPSK to 512QAM
FFT points	2048 (max. used 852)
Number of TS	5 TS every 124 frames
DAC sampling rate	64 GS/s
DAC bandwidth	13 GHz
DAC number of bits	8 bits
Laser center frequency	192.5 THz
Input power of the fiber	5 dBm
Fiber dispersion coefficient	17 ps/nm/km
Fiber nonlinear coefficient	1.37 $W^{-1}km^{-1}$
Fiber loss factor	0.2 dB/km
Clipping ratio	12 dB
CP overhead	1.56%
TS overhead	4%

of 31 dB is used in the estimation to limit the ASE noise influence and analyze other system impairments. In Fig. 6.3(a) it is shown that the 3 dB bandwidth of the DAC (13 GHz) is limiting the system, as the high frequency subcarriers present low values of SNR. In Fig. 6.3(b), the BER and number of errors per subcarrier is drawn for the B2B configuration. It can be observed that the last group of subcarriers presents more errors and high BER values, which causes the overall system performance degradation. In a second step, the same analysis is performed after 50 km of SSMF. Fig. 6.4(a) shows the channel estimation after 50 km of SSMF using 16 QAM format at 100 Gb/s. It can be seen that CD also limits the system performance. As a result various subcarriers are highly attenuated. According to equation (2.10), the first attenuation peak (f_{CD}^{1}) occurs around 8.53 GHz which correspond to the subcarrier 274. In Fig. 6.4(b) the number of errors and the BER per subcarrier after the fiber link are reported. It can be seen that the subcarriers affected by CD also present a high number of errors and BER values around 10^{-1}. In fact, each subcarrier suffers different power fading, depending on accumulated CD and the frequency of the subcarrier [17, 20]. It is shown that 100 Gb/s can not be transmitted, ensuring 10^{-3} BER, by using uniform loading for a DMT signal with 26.67 GHz bandwidth (neither in B2B configuration nor after 50 km of SSMF) due to system impairments that degrade the performance.

In order to asses the system impairments mitigation capability of LCMA, this DSP functionality is applied to the system of Fig. 6.1. The resulting bit and power allocation, after applying LCMA in a B2B configuration, can be seen in Fig. 6.5(a) and Fig. 6.5(b), respectively. In Fig. 6.5(a), it is shown that the first group of subcarriers, which present high values of SNR, are mapped with a 64 QAM format. It can also be seen that the modulation format order decreases with the reduction of the SNR. The last subcarriers

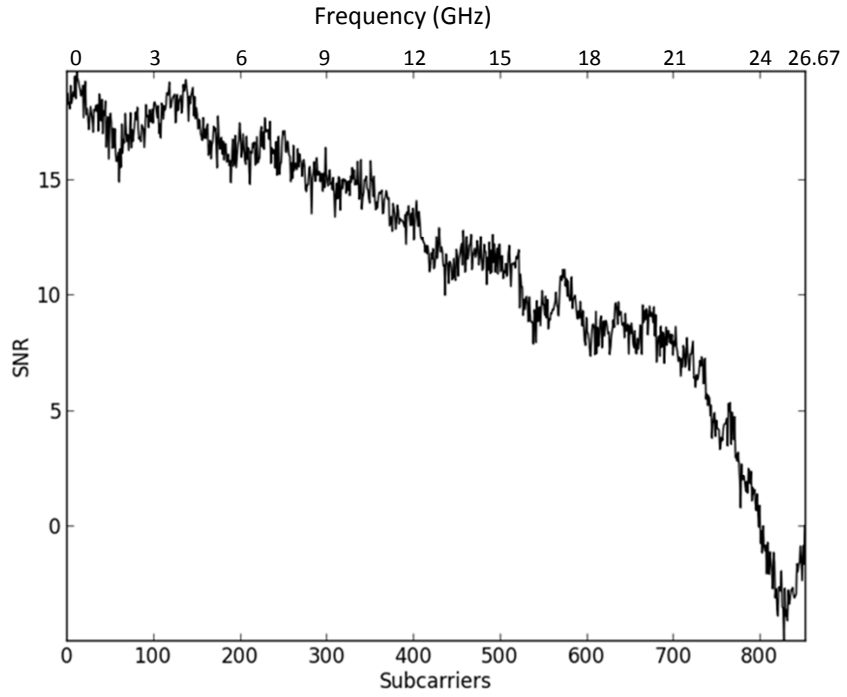

(a)

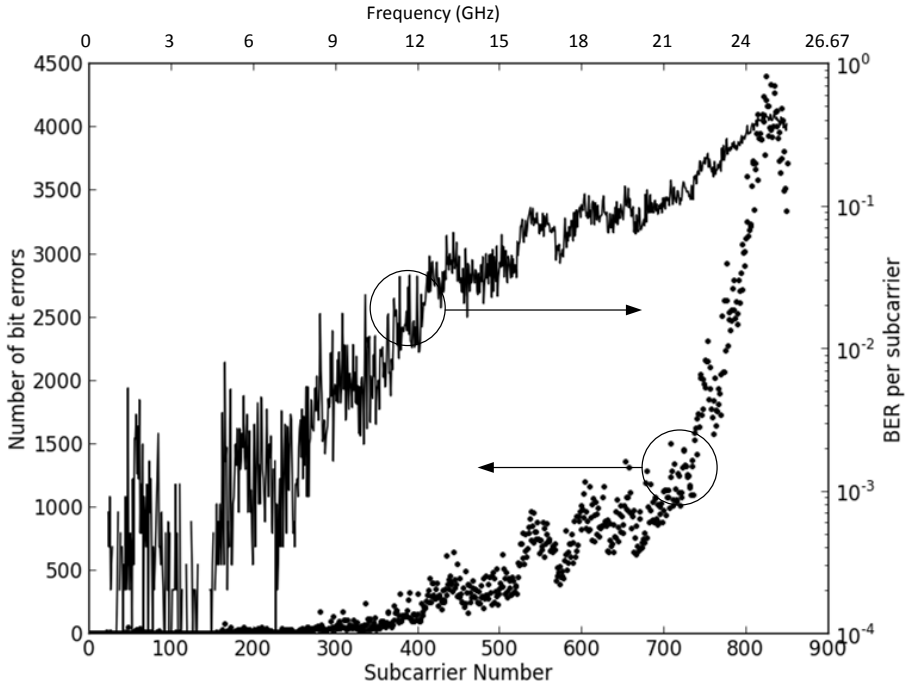

(b)

Figure 6.3: (a) SNR estimation of an optical B2B channel and (b) BER (solid line) and number of errors (dotted line) per subcarrier transmitting 8441920 bits at 100 Gb/s with 16 QAM (Uniform bit loading) in the B2B configuration. The estimation time is 89.75 s.

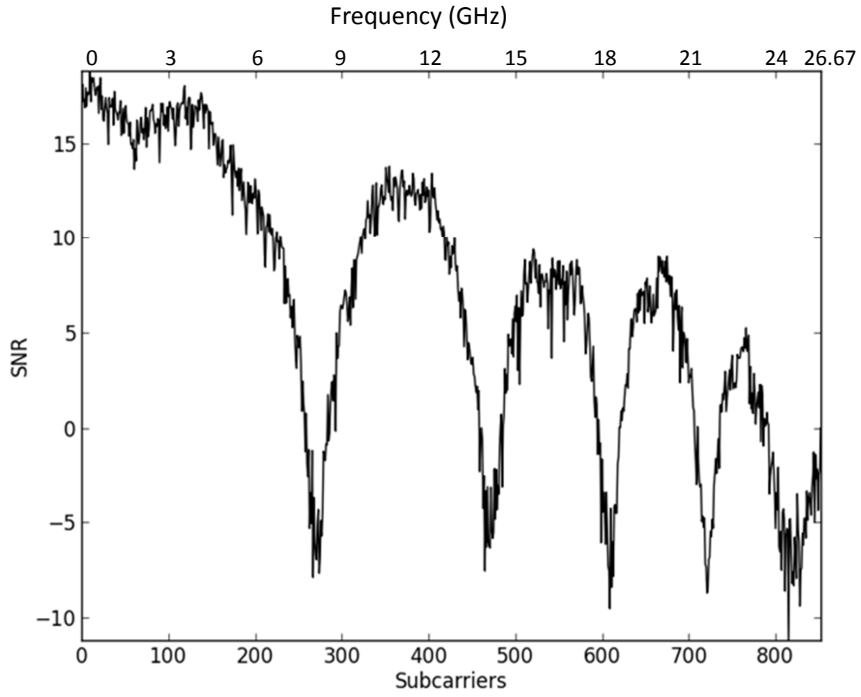

(a)

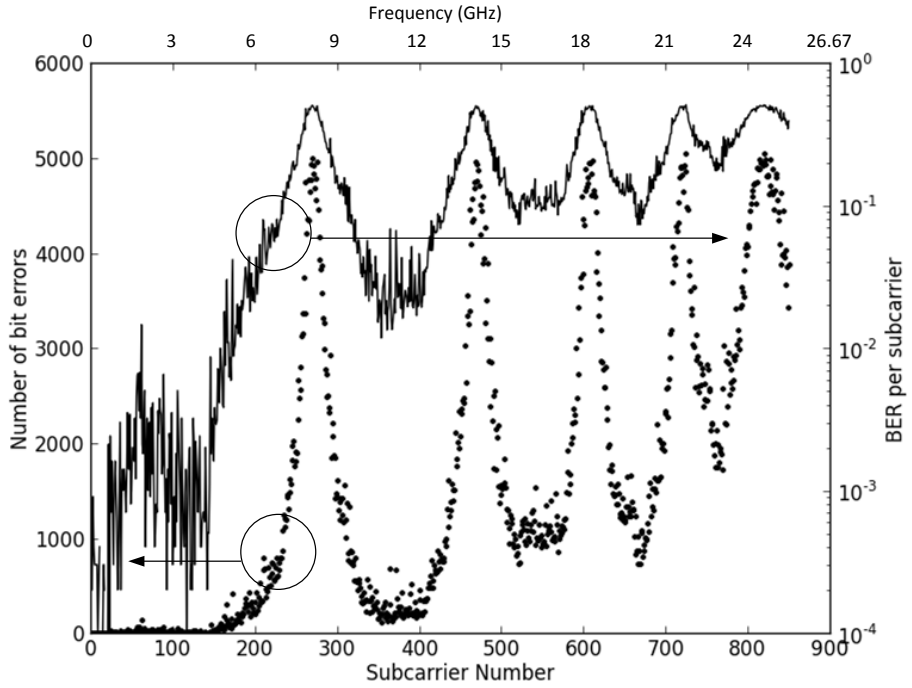

(b)

Figure 6.4: (a) SNR estimation after 50 km of SSMF fiber and (b) BER (solid line) and number of errors (dotted line) per subcarrier transmitting 8441920 bits at 100 Gb/s with 16 QAM (Uniform bit loading) after 50 km of SSMF fiber. The estimation time is 466.21 s.

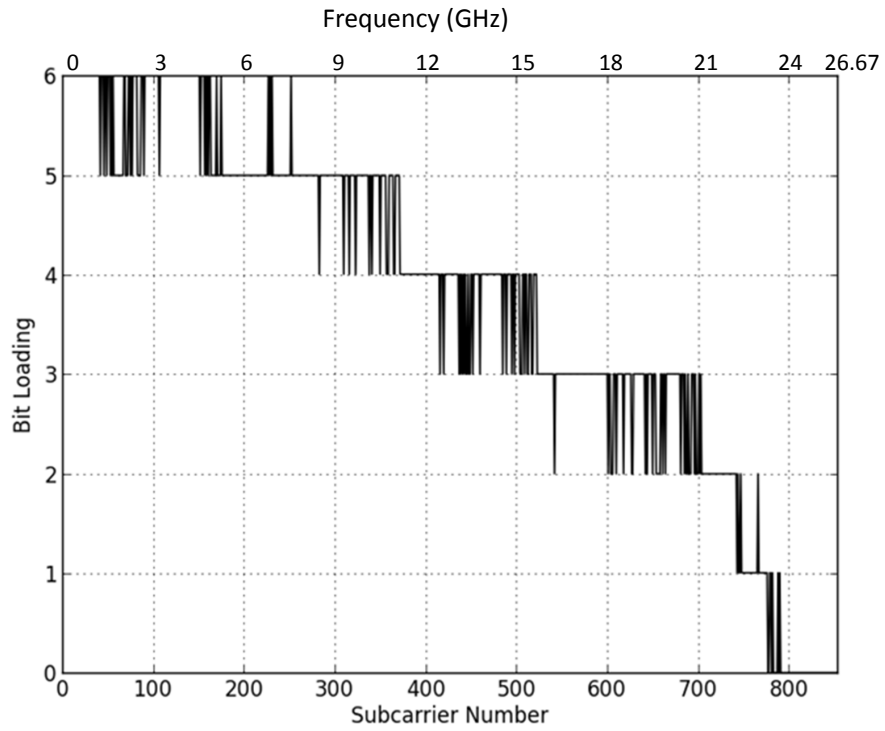

(a)

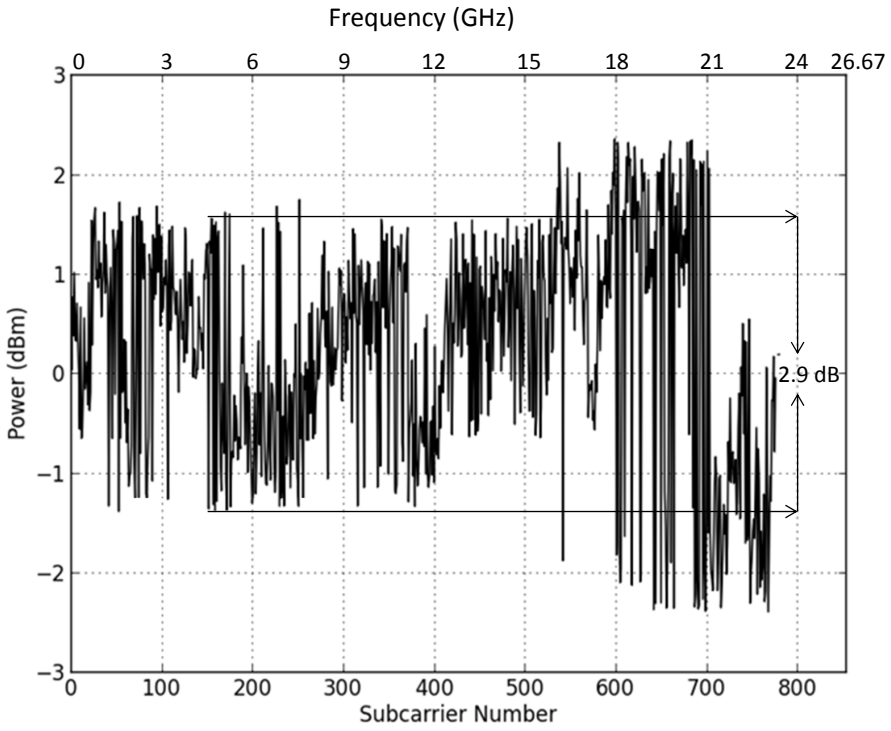

(b)

Figure 6.5: (a) Bit loading and (b) power loading using LCMA at 100 Gb/s in the B2B case.

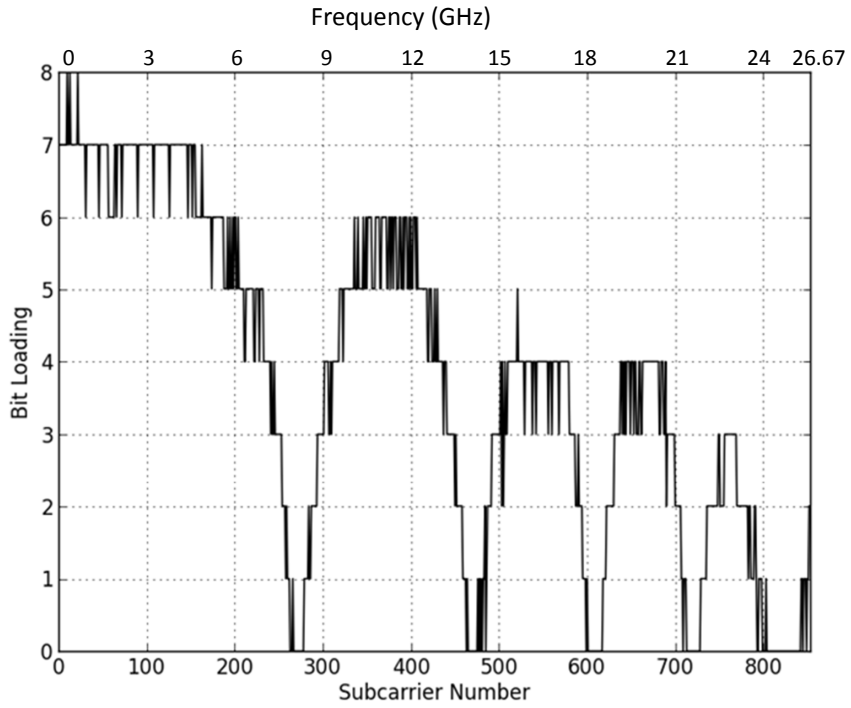

(a)

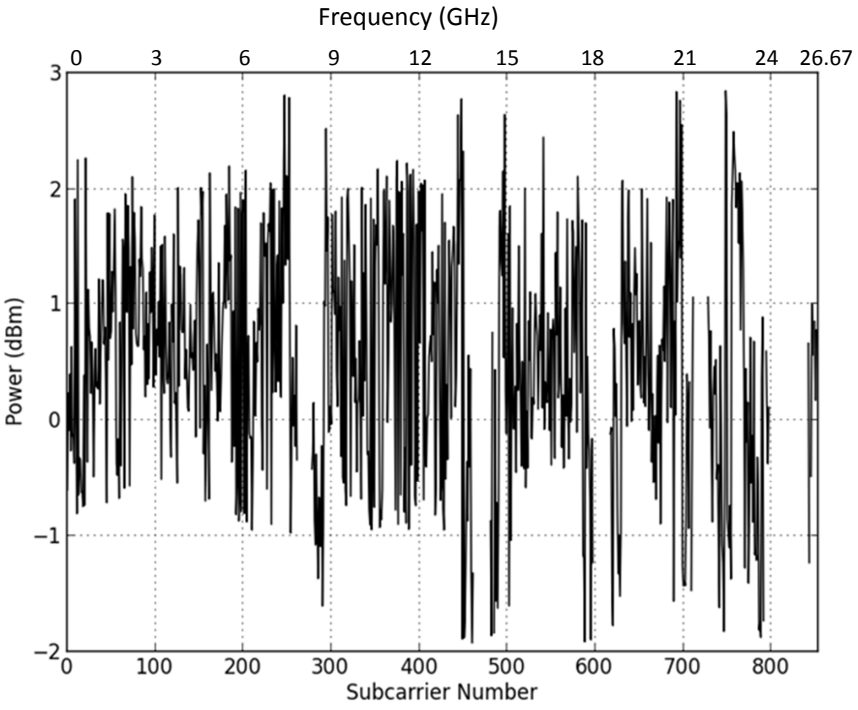

(b)

Figure 6.6: (a) Bit loading and (b) power loading using LCMA for 100 Gb/s after 50 km of SSMF.

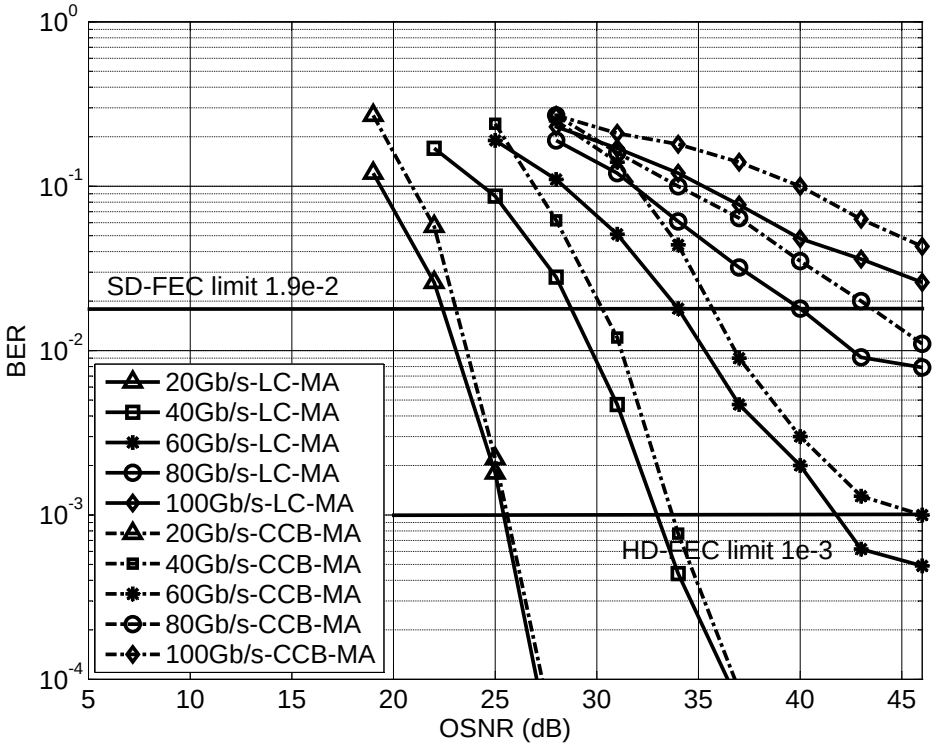

Figure 6.7: BER performance comparison using LCMA and CCBMA algorithms vs OSNR for various bit rates after 50 km of SSMF.

that are affected by the DAC bandwidth limitation, do not carry data and their power is set to zero after applying LCMA (see Fig. 6.5(b)). The change of the modulation format can also be seen in terms of power in Fig. 6.5(b). As an example, in Fig. 6.5(a), subcarrier 159 is mapped into a 32QAM format, whereas subcarrier 160 is mapped into 64QAM. According to [27] and considering the scaling factors of both formats (defined in section 6.2), this change of modulation format corresponds to about 3 dB energy-gain. In fact, in Fig. 6.5(b) it can be observed that the power corresponding to subcarrier 159 and 160 varies from -1.4 dBm to 1.5 dBm, respectively. Finally, figures 6.6(a) and 6.6(b), show the bit and power loading distribution per subcarrier, respectively, after applying LCMA considering a fiber link of 50 km of SSMF. It can be seen that the frequencies affected by CD do not carry data and hence, no power is assigned to these subcarriers. Power variation can also be seen in Fig. 6.6(b), corresponding to the change from one modulation format to another (see Fig. 6.6(a)).

In order to take into account both the DAC and CD effects, the BER performance of the proposed system of Fig. 6.1 is analyzed considering a SSMF link of 50 km. Firstly, LCMA performance is compared with CCBMA in order to show the superior performance over the suboptimal algorithm. In particular, Fig. 6.7 shows the BER performance using both loading algorithms. It can be seen, that LCMA outperforms

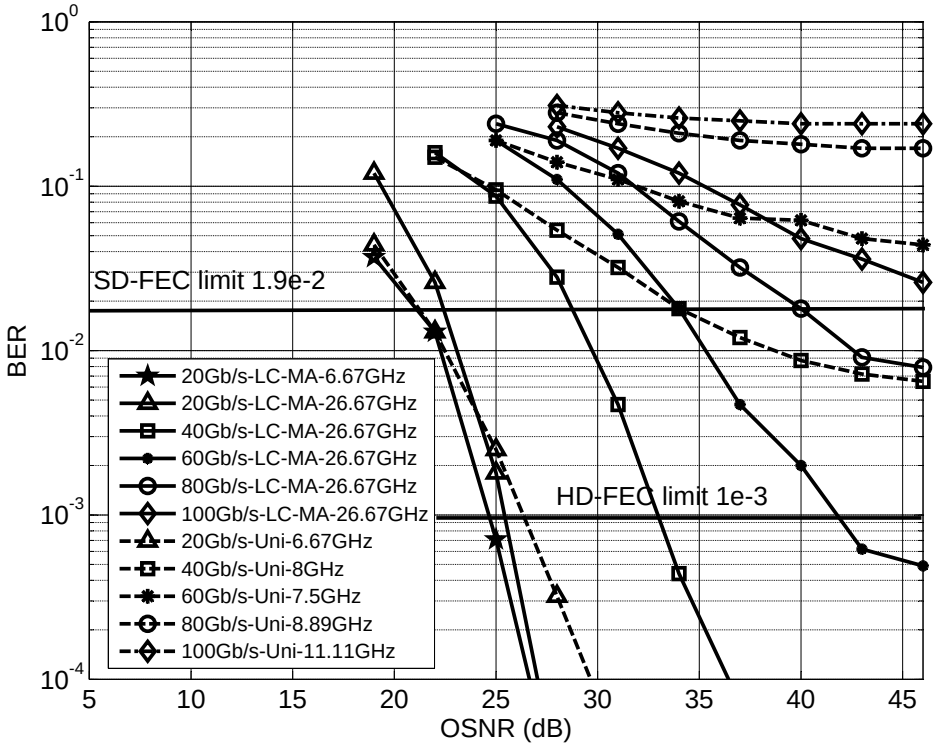

Figure 6.8: BER performance comparison using LCMA and uniform loading vs OSNR for various bit rates after 50 km of SSMF.

the CCBMA algorithm in terms of required OSNR to achieve a target BER for all the analyzed cases. Specifically, applying LCMA, a BER of 10^{-3} is ensured for 60 Gb/s with about 4 dB less OSNR than in CCBMA case. Moreover, using LCMA up to 80 Gb/s can be achieved for a target BER of $1.9 \cdot 10^{-2}$ given an OSNR of 40 dB. Whereas, 43 dB OSNR is needed to ensure the same data rate at this target BER after CCBMA algorithm. For the rest of this chapter the LCMA algorithm is used to perform BL and PL.

Table 6.2: Achievable reach, required OSNR for 10^{-3} BER, maximum assigned number of bits per symbol and effective signal bandwidth using LCMA at different gross data rates

Rate (Gb/s)	**Reach (km)**	**OSNR (dB)**	**Max. # bits/symb**	**B_s (GHz) Effective**
20	150	26	4	20.9
40	150	36	5	23.9
60	70	49	5	24.8
80	20	43	6	22.5
100	10	55	7	26.6

Fig. 6.8 shows the BER performance versus required OSNR using LCMA evidencing

Table 6.3: Achievable reach, f_{CD}^1, required OSNR for 10^{-3} BER, signal bandwidth and modulation format used to implement uniform loading at different gross data rates

Rate (Gb/s)	**Reach (km)**	$\mathbf{f_{CD}^1}$ **(GHz)**	**OSNR (dB)**	$\mathbf{B_s}$ **(GHz)**	**Format**
20	140	5.1	40	4	32 QAM
40	40	9.5	41	8	32 QAM
60	20	13.5	47	10	64 QAM
80	10	19.1	40	16	32 QAM
100	0	24.3	40	20	32 QAM

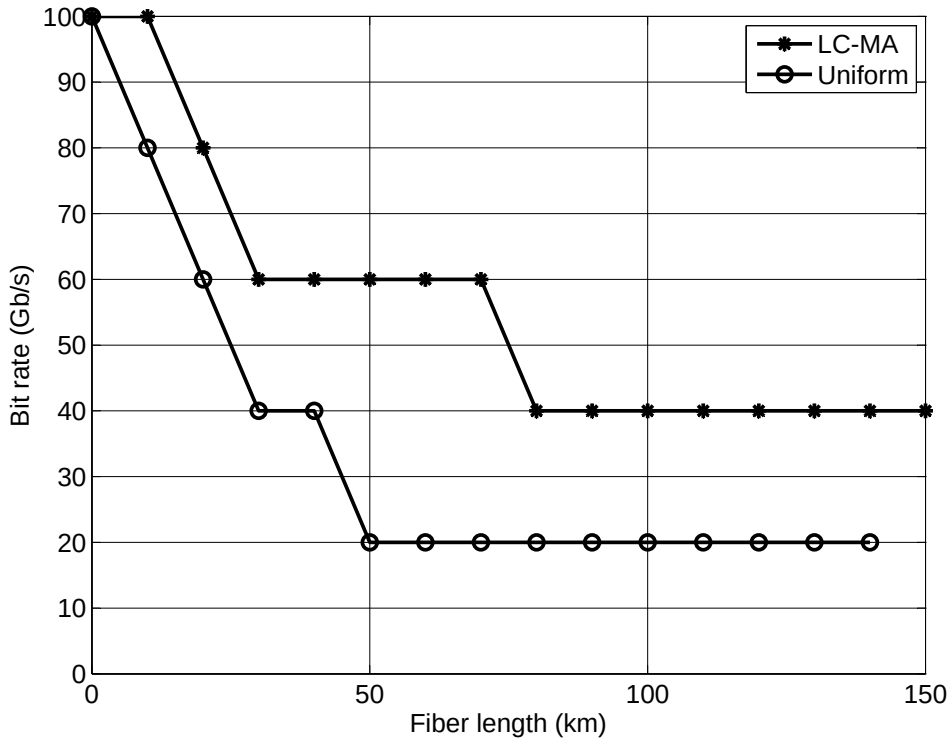

Figure 6.9: Achievable data rate for a target BER of 10^{-3} using LCMA algorithm and uniform loading for different fiber links.

the improvement over the uniform approach. For uniform loading at a fixed data rate, the modulation format and signal bandwidth combination is selected to require lowest OSNR at 10^{-3} target BER. The values are obtained through exhaustive simulations. Furthermore, B_s is chosen under the constraint of fixing a B_s lower than the frequency where the first attenuation peak due to CD (f_{CD}^1) appears. This value is updated for each fiber link. Hence, when a 50 km SSMF is considered, signal bandwidths lower than 8.53 GHz should be selected for uniform loading according to Fig. 6.4(a) and equation (2.10). As a result, in order to transmit at 20 Gb/s over 50 km of SSMF, and ensuring a target BER of 10^{-3}, a signal bandwidth of 6.67 GHz and 8 QAM modulation

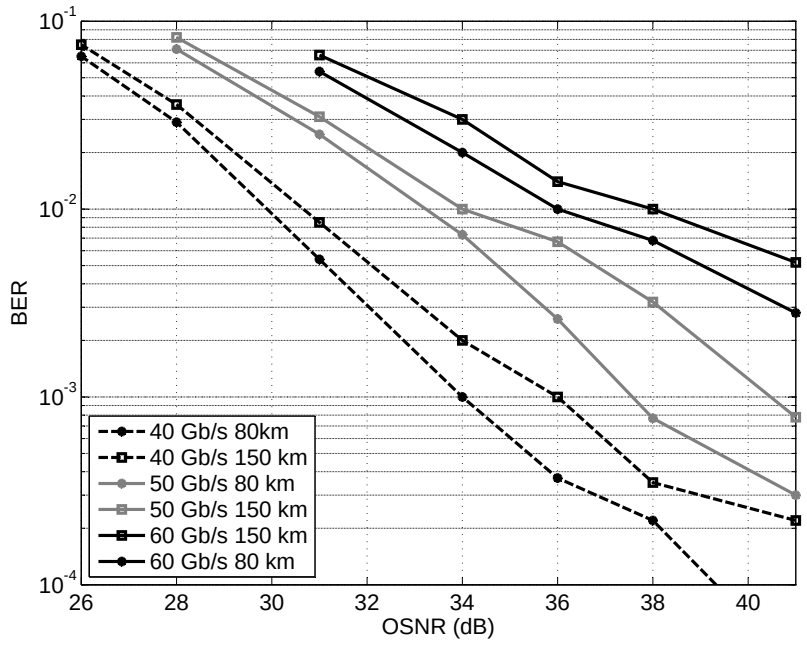

Figure 6.10: BER performance using LCMA vs OSNR for 40 Gb/s, 50 Gb/s and 60 Gb/s after 80 km and 150 km of SSMF.

format for all subcarriers can be used requiring 26 dB OSNR. Other possibilities to achieve 20 Gb/s holding the 8.53 GHz maximum bandwidth restriction, could be 16 QAM with 5 GHz signal bandwidth or higher constellation formats with reduced signal bandwidths. However, these alternatives require a higher OSNR to ensure the same target BER of 10^{-3}. From Fig. 6.8, it can be seen that applying LCMA with a $B_s = 26.67$ GHz at 20 Gb/s achieves better performance than uniform in the cases where a BER lower than 10^{-2} is obtained. In order to outperform uniform loading for any BER value, when a low data rate is transmitted, LCMA should be applied with a reduced signal bandwidth. As a result, it is seen in Fig. 6.8 that transmitting at 20 Gb/s using the same bandwidth than in the uniform case, $B_s = 6.67$ GHz, LCMA requires in all cases less OSNR than uniform loading to ensure the same target BER. On the other hand, in order to transmit at higher data rates, LCMA is applied with a $B_s = 26.67$ GHz. Specifically, up to 60 Gb/s transmission is obtained using LCMA ensuring a target BER of 10^{-3} with 42 dB OSNR. The same target BER can only be guaranteed up to 20 Gb/s when uniform loading is used. Considering a BER threshold of $1.9{\cdot}10^{-2}$ up to 80 Gb/s can be transmitted using LCMA with 40 dB OSNR. Conversely, with uniform loading up to 40 Gb/s transmission is achieved ensuring the same target BER of $1.9 \cdot 10^{-2}$ with 34 dB, $B_S = 8$ GHz and 32 QAM format.

Finally, in Fig. 6.9 the achievable data rate at 10^{-3} BER of the proposed transceiver of Fig. 6.1 using LCMA and the uniform loading scheme is analyzed for different fiber

links. Data rate steps of 20 Gb/s are considered. Additionally, Table 6.2 shows the maximum achieved reach for different data rates, the required OSNR to ensure 10^{-3} BER, the maximum assigned number of bits per symbols per subcarrier and effective signal bandwidth according to LCMA. Table 6.3 also includes the frequency of the first notch f_{CD}^{1} and the optimum combinations of modulation format and signal bandwidth for a particular link at a fixed data rate. Please note that for 60 Gb/s, 64 QAM is the selected uniform format as the OSNR is minimized for a target BER of 10^{-3}. In fact, 60 Gb/s transmission using 32 QAM would be more affected by both CD and DAC bandwidth limitation, as a $B_s = 12$ GHz is required. A maximum link length of 150 km of SSMF has been considered, as long haul applications are not the target of the present work. From Fig. 6.9, it can be seen that with the increase of the fiber link LCMA can transmit at a higher data rate than uniform loading for the same target BER of 10^{-3}. Specifically, LCMA allows 100 Gb/s transmission over 10 km of SSMF ensuring a target BER of 10^{-3}, whereas with uniform bit and power loading 100 Gb/s can not be transmitted and in the B2B configuration an OSNR of 40 dB is required, considering a signal bandwidth of 20 GHz and 32 QAM format. Additionally, 20 Gb/s transmission is ensured after 140 km of SSMF with 40 dB OSNR and using uniform loading with a signal bandwidth of 4 GHz and the 32 QAM format. On the other hand, according to Fig. 6.9 and Table 6.2, using LCMA algorithm, the data rate is doubled for the same fiber link of 140 km, achieving 40 Gb/s transmission. Furthermore, this data rate can be maintained up to 150 km of SSMF with a required OSNR of 36 dB ensuring 10^{-3} BER and occupying an effective $B_s = 23.9$ GHz.

Considering finer data rate steps of 10 Gb/s, the results presented in Fig. 6.10 have been obtained. It is shown that using LCMA, up to 50 Gb/s can be transmitted over 150 km of SSMF at the same target BER with 41 dB OSNR. Also 80 km of SSMF has been considered in the analysis of Fig. 6.10, as it is a possible extended reach for data center connections. In particular, 50 Gb/s can be transmitted over 80 km of SSMF ensuring a target BER of 10^{-3} with about 37 dB OSNR. As latency is also related to the adopted FEC scheme, using a simpler FEC coding with 10^{-4} target BER, such as the Reed-Solomon RS(255,239) code, the system latency can be reduced [103]. Considering this target BER, up to 40 Gb/s can be transmitted over 80 km of SSMF with 39 dB OSNR.

6.4 Summary

In this chapter we have designed a cost-effective DMT transceiver with adaptive loading capabilities using a DD optical implementation. The main conclusions are summarized below.

- Simulations show that using loading schemes, system impairments such as fiber CD and DAC bandwidth limitations are mitigated enabling high data rate transmission.
- The LCMA solution outperforms the CCBMA loading algorithm in terms of required OSNR for a fixed target BER.
- The LCMA scheme achieves higher data rate and reach compared with bandwidth variable uniform loading optimized according to the transmission impairments.
- 50 Gb/s can be transmitted beyond 80 km of SSMF, enabling high data rate transmission over an extended link reach between data centers.
- Reducing the gross data rate, longer inter data center connections can be covered.
- It is demonstrated that the provided guidelines allow designing adaptive cost-effective transceivers capable of coping with the transmission of high volumes of data, resulting potential candidates to enable connectivity between data centers.

In the following chapter, experimental validation of the proposed DMT transceiver is provided. Furthermore, optical filtering is analyzed in terms of required OSNR to achieve a target BER and reach, for fixed-grid and flexi-grid scenarios.

7 Implementation of FFT-based DMT systems

"Technology feeds on itself. Technology makes more technology possible."

Alvin Toffler

7.1 Introduction

This chapter provides an experimental validation of the proposed Discrete MultiTone (DMT) transceiver of section 6.2, in presence of optical noise and CD. Moreover, optical filtering is analyzed in fixed-grid and flexi-grid networks. We summarized the main novel contribution in the list below:

- The proposed adaptive DMT transceiver using Levin Campello Margin Adaptive (LCMA) is experimentally validated in a Back-to-Back (B2B) configuration and after 50.5 km and 82.1 km of Standard Single Mode Fiber (SSMF).
- The numerical simulations, obtained considering the system model of chapter 6, have been compared with the experimental results evidencing good agreement in presence of transmission impairments.
- High data rates can be achieved using LCMA, but at the expense of a strong optical carrier and thus a high Optical Signal-to-Noise Ratio (OSNR) requirement.
- Optical filtering is implemented using optical tunable filters. The optimum filter position is found for different fiber links. 100 GHz and 36 GHz filter bandwidths are used for a fixed-grid and a flexi-grid network, respectively.
- Chow Cioffi Bingham (CCB) suboptimal loading algorithm is used in order to simplify the Bit Loading (BL) and Power Loading (PL) search.

- The performance in terms of reach and required OSNR to achieve a target Bit Error Rate (BER) is experimentally investigated after applying optical filtering.

The remainder of the chapter is organized as follows. In section 7.2, the experimental set up is shown. Moreover, the achieved numerical and experimental results are compared. In section 7.3, optical filtering is analyzed. The system performance considering the proposed solutions is included. Finally the chapter concludes with section 7.4.

7.2 Experimental validation of the adaptive DMT transceiver

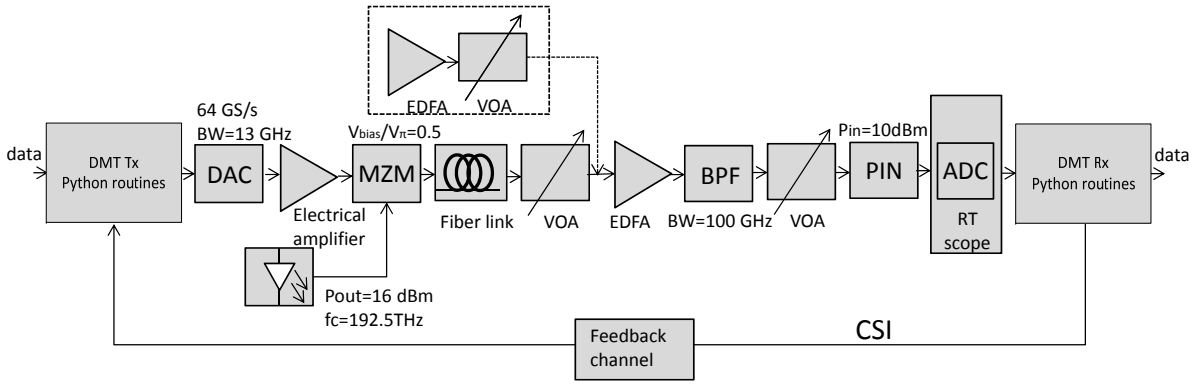

Figure 7.1: Experimental set-up.

Fig. 7.1 shows the set-up that has been used for the experimental assessment of the adaptive transceiver proposed in chapter 6. The signal processing has been performed offline using Python software. The Tx and Rx Digital Signal Processing (DSP) modules are the same used in simulation (as described in section 6.2). A commercial 8 bits resolution Digital-to-Analog Converter (DAC) running at 64 GS/s has been used for the experimental validation [104]. A signal bandwidth of 26.67 GHz is considered and the optical carrier is set to 192.5 THz. The Mach-Zehnder modulator (MZM) is biased at the quadrature point and it is suited for 40 GHz bandwidth signals. A single span of SSMF of 50.5 km and 82.1 km with 0.2 dB/km attenuation is used. The launch power into the SSMF is set to 5 dBm. Erbium Doped Fiber Amplifier (EDFA) are added to the system to perform OSNR measurements. In order to measure high OSNR values only the inline EDFA is needed, whereas to achieve low values of OSNR a second EDFA (dashed box in Fig. 7.1) is added for additional noise loading. A bandpass filter of 100 GHz bandwidth is used to limit the Amplified Spontaneous Emission (ASE) noise

Table 7.1: System parameters

Modulation format	BPSK to 512QAM
FFT points	2048 (max. used 852)
Maximum B_S	26.67 GHz
Number of TS	5 TS every 124 frames
DAC sampling rate	64 GS/s
DAC bandwidth	13 GHz
Driver bandwidth	30 GHz
MZM bandwidth	40 GHz
Laser center frequency	192.5 THz
PIN bandwidth	50 GHz
Oscilloscope sampling rate	80 GS/s
Oscilloscope bandwidth	29.4 GHz
Clipping ratio	12 dB
CP overhead	1.56%
TS overhead	4%

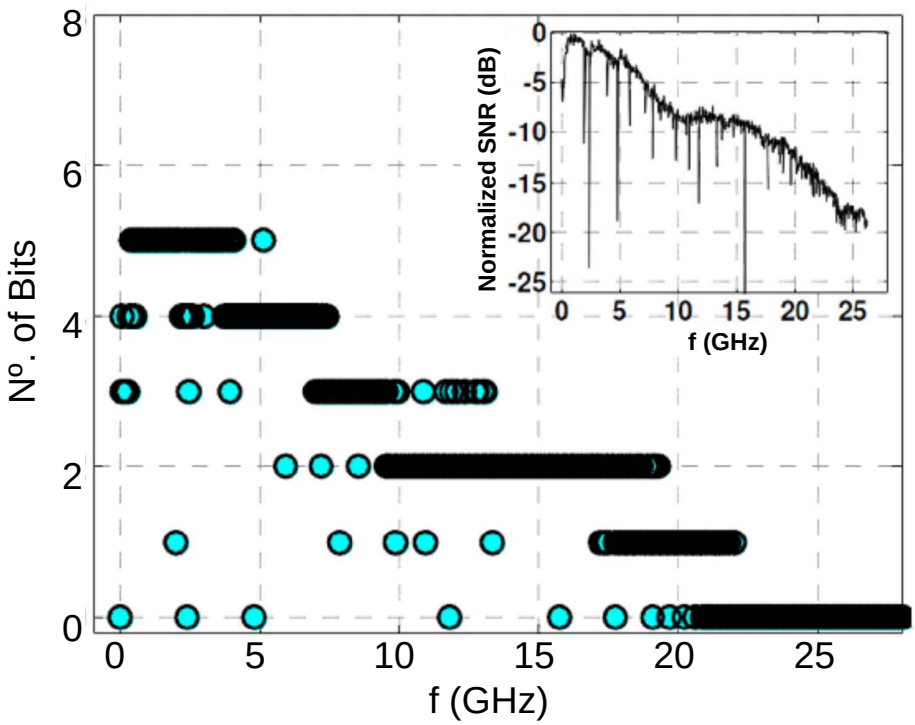

Figure 7.2: Bit loading using LCMA for 56 Gb/s and the estimated SNR (inset) in the B2B configuration.

for optical-to-electrical conversion. At the reception, a 50 GHz PIN photodiode is used and its input power is fixed at 10 dBm using a Variable Optical Attenuator (VOA). The photodetected signal is captured by an 80 GS/s real-time oscilloscope with 29.4 GHz bandwidth. The SNR per subcarrier is estimated for each value of OSNR in order to perform the loading algorithm. The experimental system parameters are summarized

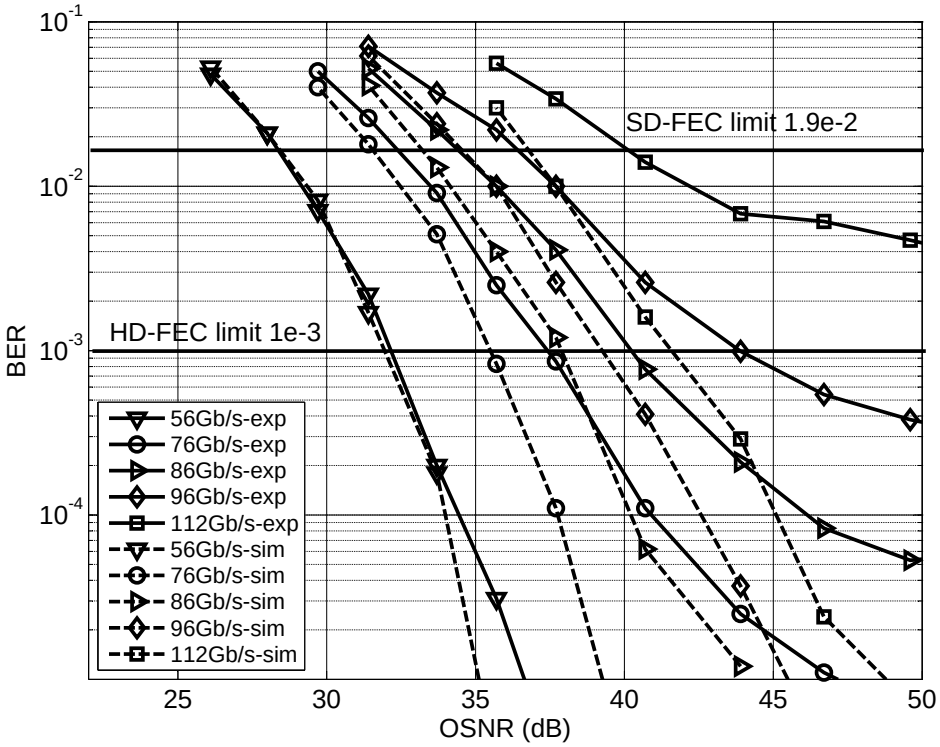

Figure 7.3: Experimental and numerical BER curves for different data rates and OSNR values in the B2B configuration.

in table 7.1.

The estimated SNR per subcarrier in the B2B configuration and the corresponding bit and power loading for 56 Gb/s are shown in Fig. 7.2. In Fig. 7.3, the obtained experimental results are compared to the numerical BER curves of the proposed adaptive DMT transceiver using LCMA algorithm vs the OSNR in a B2B system configuration. From the figure, it can be seen that up to 96 Gb/s is experimentally achieved (considering a target BER of 10^{-3}) for 44 dB OSNR. Additionally, at the expense of using an increased overhead, 112 Gb/s is demonstrated with 40 dB OSNR for a target BER of $1.9 \cdot 10^{-2}$. Using a simpler FEC scheme, 86 Gb/s is achieved at 10^{-4} BER. In general, lower OSNR values are required in the simulations to achieve a certain target BER, when comparing with experimental results. The difference between the experimental and numerical curves becomes higher at the increase of the data rate. This effect is mainly due to the fact that in the experiments the nonlinearity impairments caused by the electronic and optoelectronic devices, such as the MZM, the drivers and the Effective Number Of Bits (ENOB) of the converters, highly degrade the system performance especially when high order constellations are used. Specifically, the ENOB of the DAC used in the experiments is 6.5 [104]. Whereas, ideally the ENOB of the converters should be 8 in order to reduce the difference between experimental and

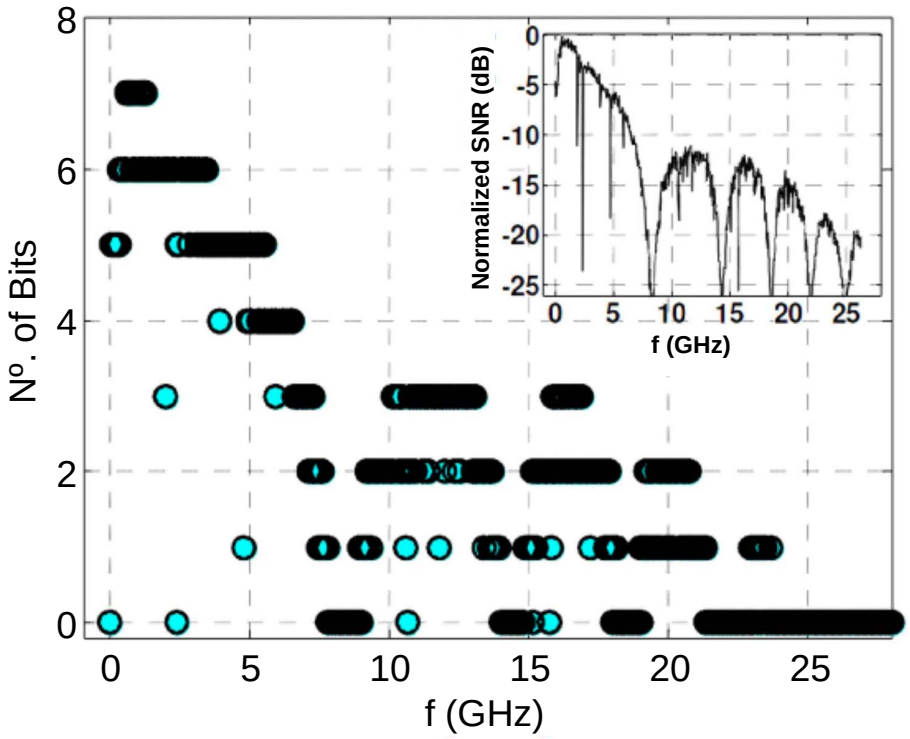

Figure 7.4: Bit loading using LCMA for 56 Gb/s and the estimated SNR (inset) after 50.5 km of SSMF.

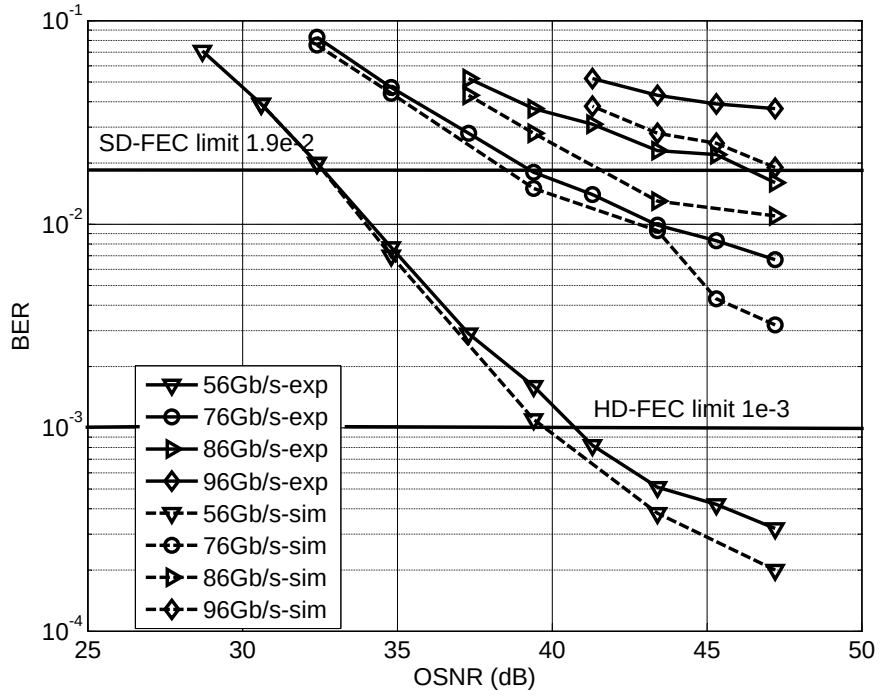

Figure 7.5: Experimental and numerical BER curves for different data rates and OSNR values after 50.5 km of SSMF.

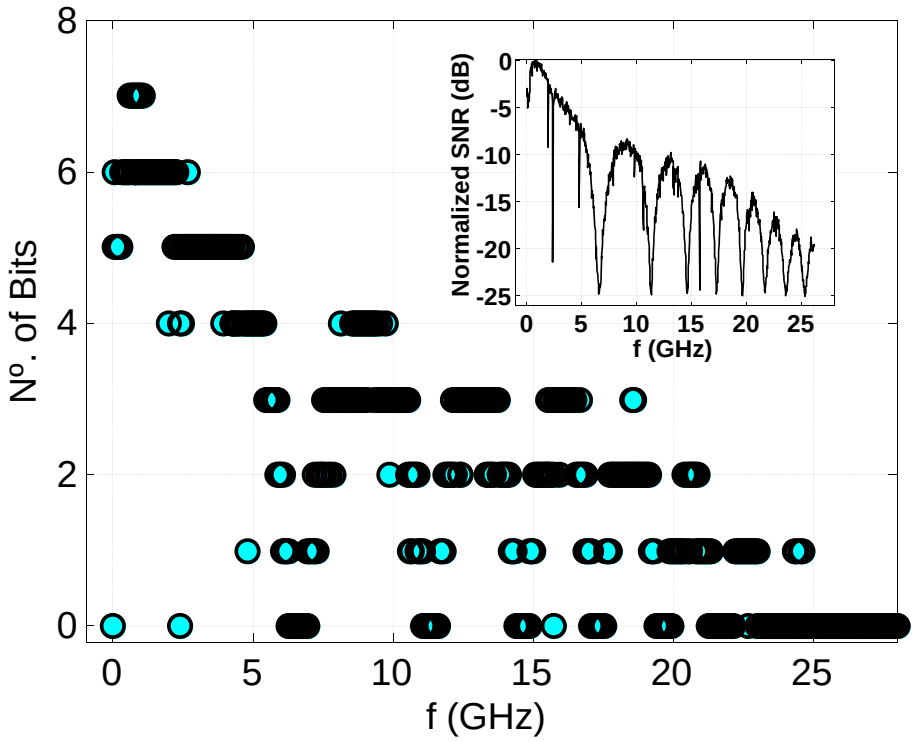

Figure 7.6: Bit loading using LCMA for 56 Gb/s and the estimated SNR (inset) after 82.1 km of SSMF.

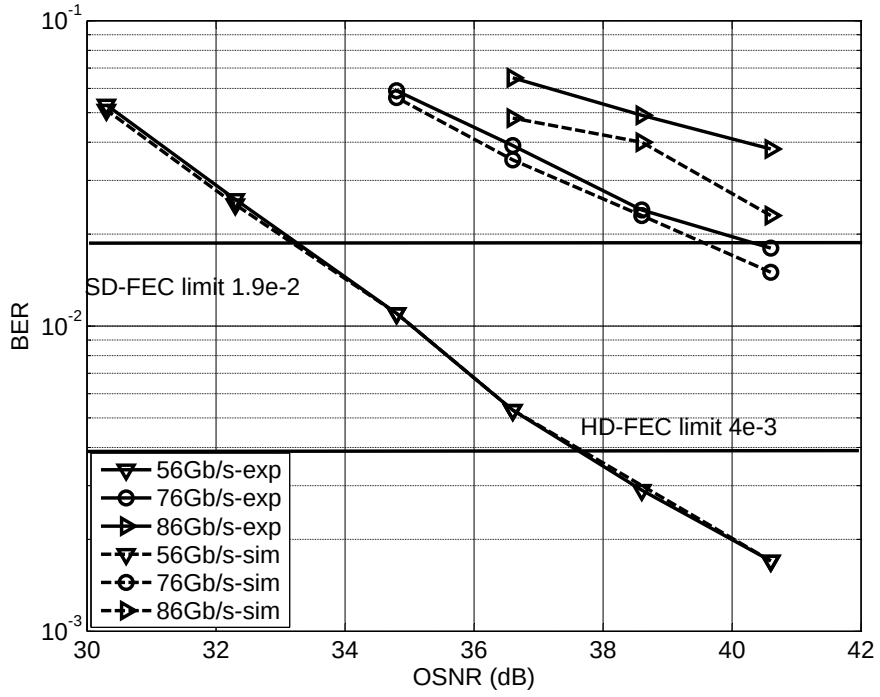

Figure 7.7: Experimental and numerical BER curves for different data rates and OSNR values after 82.1 km of SSMF.

numerical curves. In fact, a 14-bit DAC with a conversion rate of up to 12 GS/s is commercialized by Fujitsu [105]. Additionally, experimental results are more affected by the MZM nonlinearities, as in simulation the peak-to-peak drive level of the MZM has been adjusted to be about the 90% of V_π.

Additional experiments have been performed in order to analyze the system robustness against CD and evaluate the BER performance of the proposed adaptive transceiver considering 50.5 km and 82.1 km of SSMF, as possible extended links suitable for inter data center connections. In the inset of Fig. 7.4 the estimated SNR after 50.5 km of SSMF is depicted. In the figure, it is also shown the resulting BL after applying LCMA for 56 Gb/s. Fig. 7.5 shows the obtained BER curves at data rates varying between 56 Gb/s and 96 Gb/s after 50.5 km of SSMF for different OSNR values. Considering Hard Decision (HD)-Forward Error Correction (FEC), 56 Gb/s gross data rate (which corresponds to a net data rate of 52.3 Gb/s) is transmitted. Specifically, to ensure a BER of 10^{-3}, the OSNR requirement for this data rate is 41 dB OSNR (1 dB more than in simulation), as it can be seen in Fig. 7.5. Considering a target BER of $1.9 \cdot 10^{-2}$, up to 86 Gb/s is transmitted over 50.5 km of fiber with an OSNR of 46 dB. Fig. 7.7 shows the BER performance for different data rates after 82.1 km of SSMF. At that distance, 56 Gb/s transmission cannot be achieved for a target BER of 10^{-3} with the analyzed OSNR values. As it can be seen in the inset of Fig. 7.6, after 82.1 km of SSMF the signal bandwidth is highly affected by CD. According to the estimated Signal-to-Noise Ratio (SNR), the corresponding BL for 56 Gb/s using LCMA is depicted in Fig. 7.6. However, using a different code to implement HD-FEC with 7% overhead, such as two interleaved extended BCH(1020,988), $4 \cdot 10^{-3}$ BER can be considered according to [6]. At this BER value, 56 Gb/s can be successfully transmitted with 37 dB OSNR as numerically and experimentally demonstrated in Fig. 7.7. Moreover, with an OSNR of 40 dB up to 76 Gb/s can be experimentally transmitted for $1.9 \cdot 10^{-2}$ target BER. In these last analysis, where the fiber link is considered, simulations are closer to the experiments as the chromatic dispersion dominates over the MZM nonlinearities.

7.3 Analysis of optical filters impact

In this section, the impact of optical filtering is analyzed considering tuneable optical filters in the proposed DMT system of chapter 6. 56 Gb/s DMT transmission is investigated as it enables 100 Gb/s and 400 Gb/s transmission, by combining 2 or 4 channels, required to deal with the huge amount of traffic between data centers interconnections (see section 2.1). Figure 7.8 shows the proposed DMT experimental setup. The DMT Tx and Rx DSP modules are the same described in section 6.2. The signal

is generated offline with Python routines. A suboptimal algorithm is used to reduce the computational complexity of the solution search. Specifically, CCB algorithm is used to implement BL and PL, according to the estimated SNR of the channel [27,89]. The system parameters are listed in table 7.2.

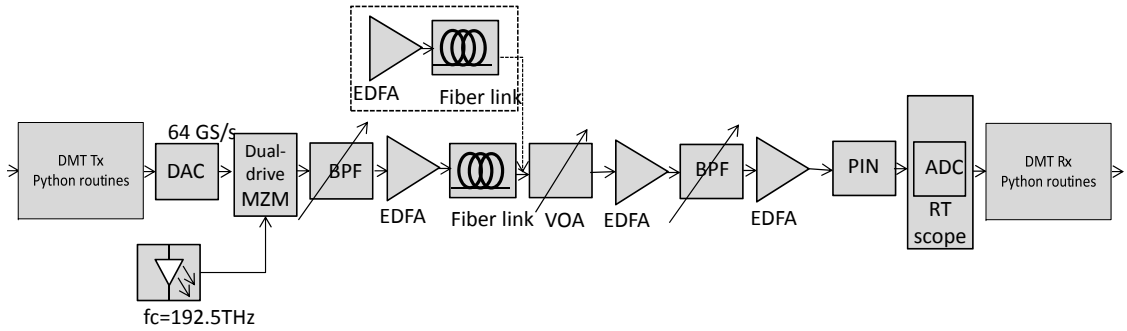

Figure 7.8: Experimental setup.

Table 7.2: System parameters

Modulation format	BPSK to 512QAM
FFT points	2048 (max. used 974)
Maximum B_S	30.44 GHz
Number of TS	5 TS every 124 frames
DAC sampling rate	64 GS/s
DAC bandwidth	13 GHz
Driver bandwidth	30 GHz
MZM bandwidth	40 GHz
Laser center frequency	192.5 THz
Fiber launch power	5 dBm
Tuneable filter BW	36 GHz or 100 GHz
PIN bandwidth	50 GHz
Oscilloscope sampling rate	80 GS/s
Oscilloscope bandwidth	29.4 GHz
Clipping ratio	9 dB
CP overhead	1.56%
TS overhead	4%

In a first step, uniform loading is performed by mapping all the subcarriers with 16QAM format and equal power in order to estimate the SNR of the channel. A 2048 points Inverse Fast Fourier Transform (IFFT) is implemented, where only half of the subcarriers carry data due to the Hermitian Symmetry (HS) constraint. Considering that the Nyquist frequency is set to zero, the number of usable subcarriers is reduced to 1023. Furthermore, a maximum of 974 carriers are modulated in order to introduce oversampling to support aliasing filtering. Hence, a maximum signal bandwidth of

30.44 GHz is considered. A DMT frame consists of 5 Training Symbols (TS), for channel estimation and synchronization, followed by 119 data symbols. The net data rate is 56 Gb/s without including the training symbols and the cyclic prefix which is set to 1/64 of the symbol duration. The DMT time signal is symmetrically clipped with a clipping ratio of 9 dB to reduce the Peak-to-Average Power Ratio (PAPR). The clipping level is optimized together with the MZM bias voltage to achieve a minimum OSNR requirement at a 10^{-3} BER. The clipped signal is loaded to a high-speed DAC with 64 GS/s. Then, the DMT signal is modulated onto a continuous wave carrier at 192.5 THz frequency, using a dual-drive MZM (suitable for 40 Gb/s signals) and the differential outputs of the DAC. The single-ended output of the DAC is around 450 mV peak-to-peak, offering the possibility of linear modulation of the electrical field with sufficient amplitude in differential mode to omit an electrical driver. The signal is then fed into a tunable optical bandpass filter. In particular, 100 GHz is selected considering a fixed-grid network and 36 GHz for a flexi-grid network. After filtering, the signal is amplified by an EDFA and transmitted over up to two fiber spans with varying lengths. Single-span configuration lengths from 10.8 km to 101 km of

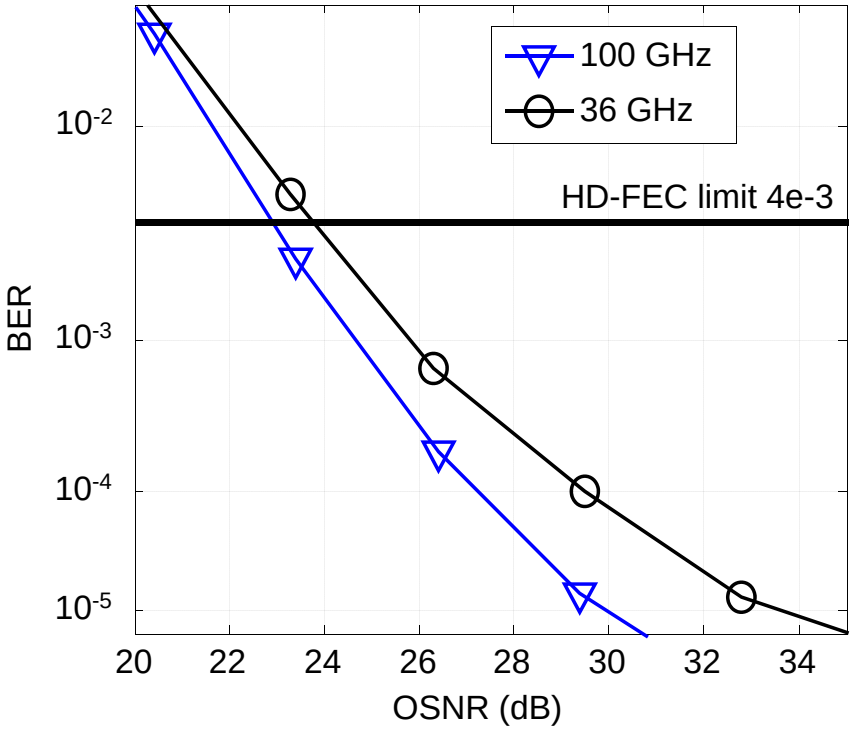

Figure 7.9: BER vs. OSNR for 56 Gb/s in B2B configuration.

SSMF are considered. Two dual-span configurations are taken into account: one with 162.1 km transmission length in total (80.7 km+81.4 km) and one with 202 km length (101 km+101 km). An additional EDFA is considered before the second span of fiber.

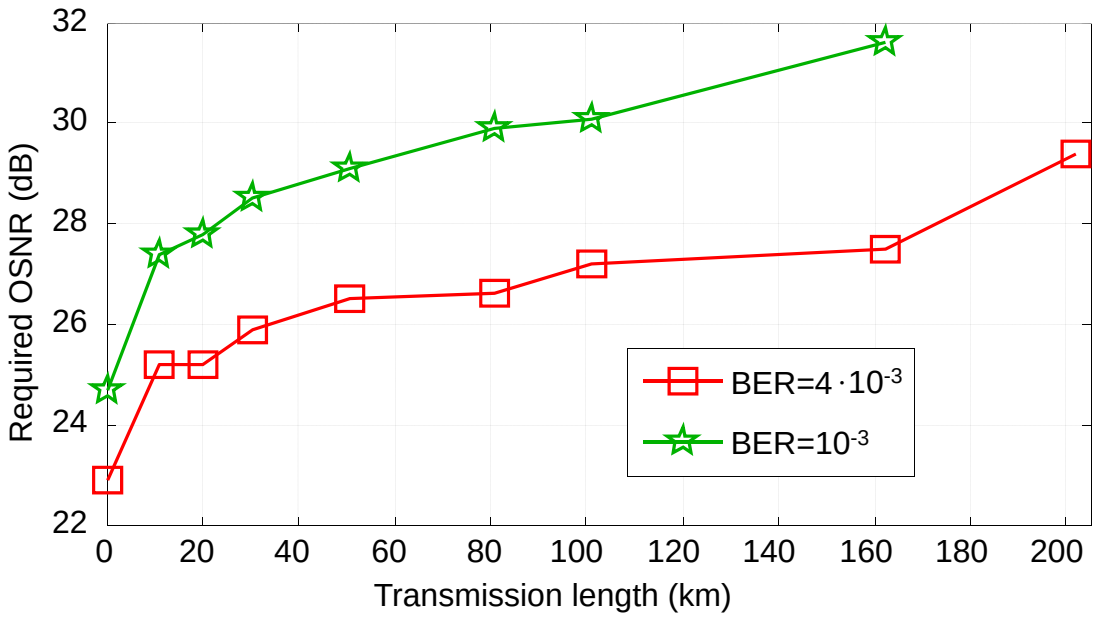

Figure 7.10: Required OSNR at $4 \cdot 10^{-3}$ and 10^{-3} BER vs. transmission length.

The fiber launch power is set to 5 dBm. The transmitted signal is attenuated and amplified to vary the OSNR in order to measure it in this point, and then filtered again by a tunable bandpass filter at the receiver side. The settings of the second filter are always identical to those of the first one. Since the allowed input power to the filter is limited and the receiver PIN photodiode requires an optical power as high as 10 dBm (TransImpedance Amplifier (TIA) is not used), the filtered signal needs to be amplified again. After detection with a wideband PIN photodiode the signal is digitized by an 80 GS/s real-time oscilloscope with 29.4 GHz bandwidth. The detected signal is offline processed in Python routines. Specifically, at the receiver side, the proposed variant of Schmidl-Cox synchronization algorithm, in section 2.4.4, are applied. The Fast Fourier Transform (FFT) is implemented and all overheads are removed. One tap equalization with decision directed channel estimation is applied according to the method detailed in section 2.4.3. Finally, the symbols are properly demapped for Monte Carlo type error counting.

As a first step, optical filtering is achieved by centering both Band Pass Filter (BPF) of Fig. 7.8 at the carrier frequency of 192.5 THz. Figure 7.9 shows the BER vs. the OSNR for B2B transmission. Considering HD-FEC with 7% overhead, about 24 dB OSNR is required to ensure $4 \cdot 10^{-3}$ BER using a 36 GHz filter. The same target BER can be achieved with 0.9 dB less OSNR using a broader filter bandwidth of 100 GHz OSNR. However, considering a target BER of 10^{-3} the penalty in terms of OSNR of using a 100 GHz filter instead of a 36 GHz one, increases up to 1.1 dB. In order to evaluate Chromatic Dispersion (CD) effect in the proposed system of Fig. 7.8 when

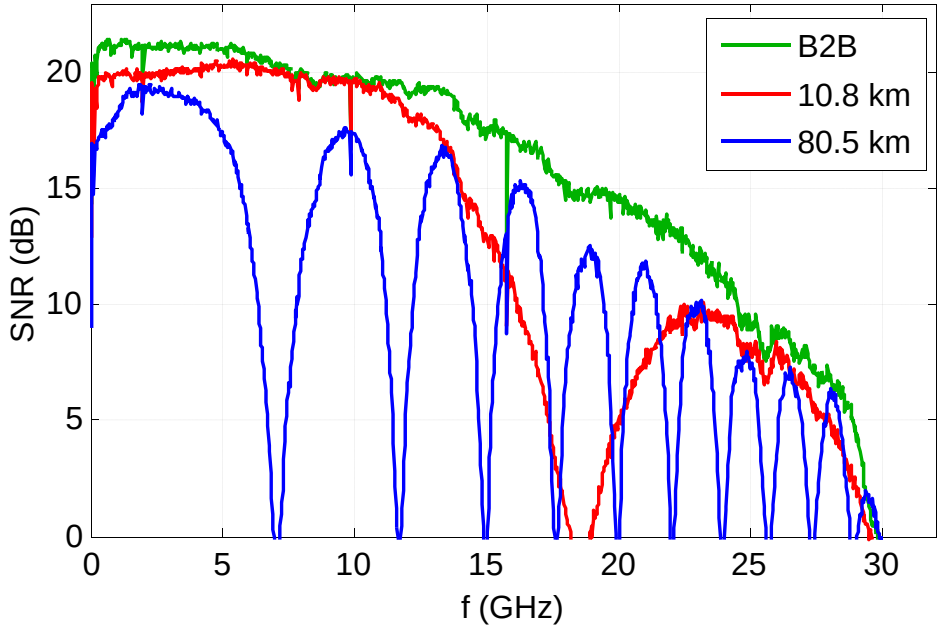

Figure 7.11: Estimated SNR for B2B, 10.8 km and 80.5 km of SSMF using 100 GHz filters.

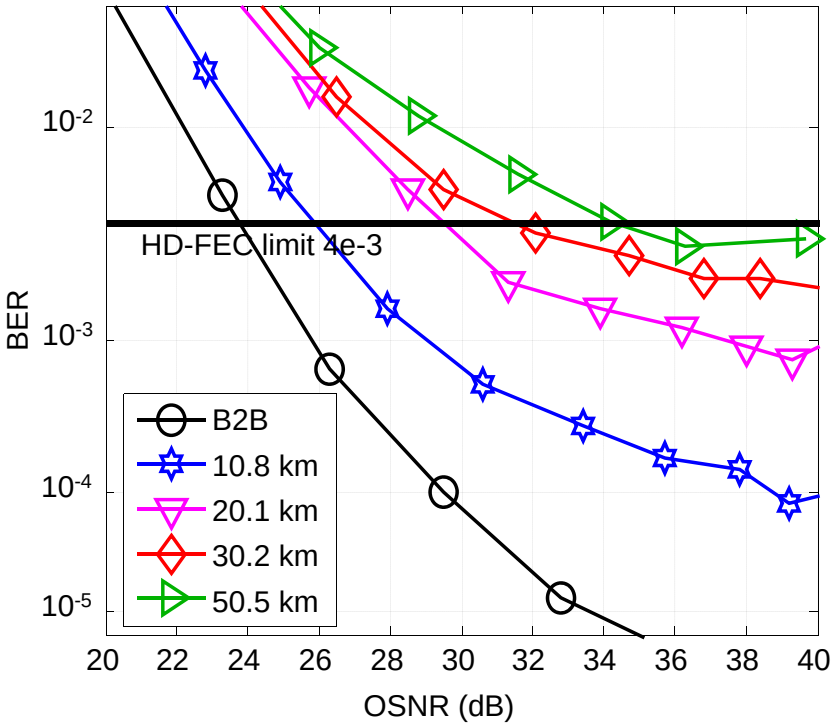

Figure 7.12: BER vs. OSNR for different transmission lengths using 36 GHz filters.

using optical filters, the system performance in terms of OSNR is evaluated in Fig. 7.10 after different fiber links. Both tuneable filters of Fig. 7.8 are centered at the carrier wavelength and have a 100 GHz bandwidth. Thus, considering this high bandwidth, the Double-Side Band (DSB) signal is not affected by filtering, but the ASE noise

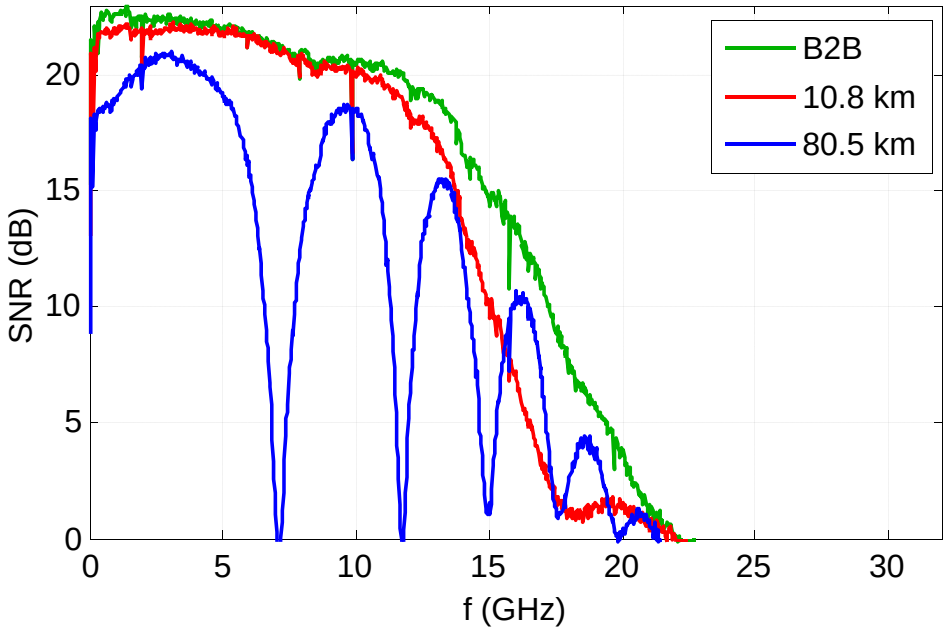

Figure 7.13: Estimated SNR for B2B, 10.8 km and 80.5 km of SSMF using 36 GHz filters.

of the EDFAs is sufficiently suppressed. Fiber links between 10.8 km and 202 km are analyzed. In case of 162.1 km and 202 km, two spans of similar length with an amplifier in between are used. From figure 7.10, it can be seen that, at the increase of the fiber link, higher OSNR is required to ensure a target BER of either 10^{-3} or $4 \cdot 10^{-3}$, due to the CD effect. 56 Gb/s can be transmitted ensuring 10^{-3} and $4 \cdot 10^{-3}$ target BER after 162.1 and 202 km of SSMF, respectively. In order to illustrate the effect of CD on the optical signal, the estimated SNR in the B2B configuration and after 10.8 km and 80.5 km of SSMF is depicted in Fig. 7.11. The effect of power fading can be also observed, as higher frequency subcarriers are more severely attenuated.

Alternatively, Fig. 7.12 shows the BER performance vs. OSNR up to 50.5 km of SSMF and using 36 GHz filters. It can be seen that the influence of CD is higher at the increase of the fiber link. Specifically, 10^{-3} BER can be achieved after 20.1 km of SSMF with 38 dB OSNR. However, this target BER can not be ensured when a fiber link of 30.2 km is considered. Using a different FEC code, $4 \cdot 10^{-3}$ BER can be achieved after 50.5 km of SSMF with 34 dB OSNR. Using a narrower filter enhances spectral efficiency at the expense of system performance degradation in terms of achievable reach.

Additionally, the filtering impact on the spectrum can be seen in Fig. 7.13, showing the estimated SNR in the B2B configuration and after 10.8 and 80.5 km of SSMF, using filter bandwidths of 36 GHz.

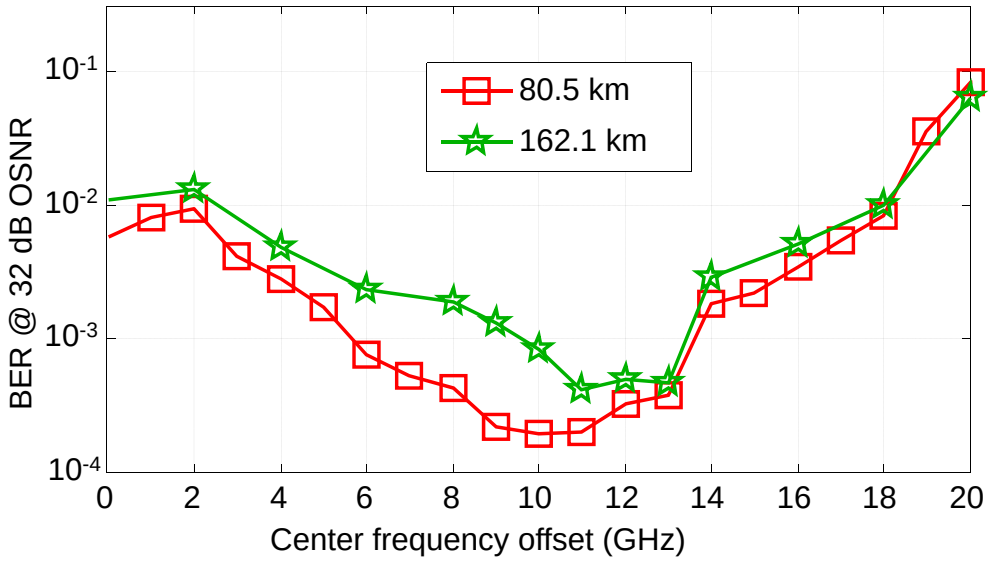

Figure 7.14: BER at OSNR of 32 dB vs. center frequency offset using VSB filtering.

7.3.1 Comparison of DSB and VSB filtering

Here, DSB filtering is compared with Vestigial-Side Band Transmission (VSB) filtering. In order to implement VSB, the tunable filters of Fig. 7.8 are shifted from the carrier frequency of the optical signal with 1 GHz steps in order to find the optimum filter center frequency. Fig. 7.14 shows the measured BER vs. the filter detuning, considering a fixed OSNR of 32 dB. The filters at the beginning and at the end of the transmission line are tuned simultaneously. The detuning is performed for two transmission reaches, one span of 80.5 km and two spans of 162.1 km in total.

From the figure, it can be seen that a BER below 10^{-3} can be achieved after 80.5 km and 162.1 km of SSMF, by choosing the suitable center frequency offset. Thus, a detuning of 10 GHz is selected when fiber links of 80.5 km or 101 km are considered. Whereas, a 12 GHz offset is fixed for 162.1 km and 202 km links, according to Fig. 7.14. The BER performance of DSB transmission and using VSB filtering is analyzed for different OSNR values after 80.5 km and 101 km of SSMF in Fig. 7.15(left) and Fig. 7.15(right), respectively. The tuneable filters of Fig. 7.8 are fixed to 36 GHz bandwidth when VSB filtering is considered and to 100 GHz bandwidth for DSB transmission. In this last case, 100 GHz filters are selected instead of 36 GHz ones as it has been demonstrated, that longer reaches can be achieved. From Fig. 7.15, it can be seen that implementing asymmetrically clipping spectral efficiency is enhanced as narrower filters are used and the OSNR performance is improved compared to the broadband transmission. This improvement can be explained with Fig. 7.16, where the estimated SNR of the DSB (0 GHz detuning) and VSB signals (10 GHz and 18 GHz detuning) after 80.5 km of SSMF is shown. Using a center frequency offset of 10 GHz, which is optimum for the

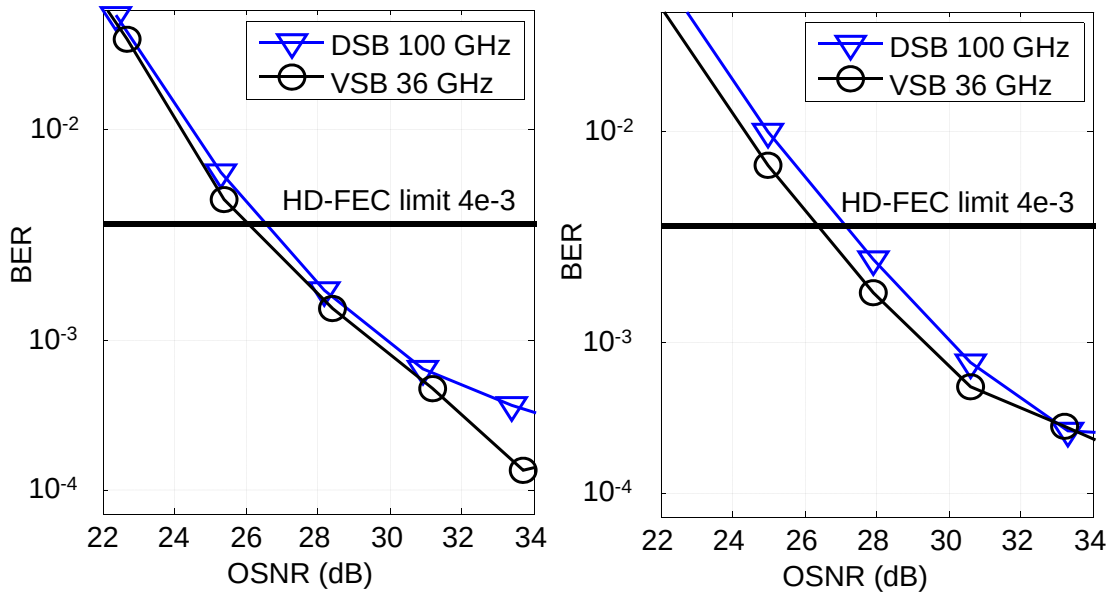

Figure 7.15: BER vs. OSNR after (left) 80.5 km of SSMF and (right) 101 km SSMF for a 100 GHz symmetrically and asymmetrically filtered signal.

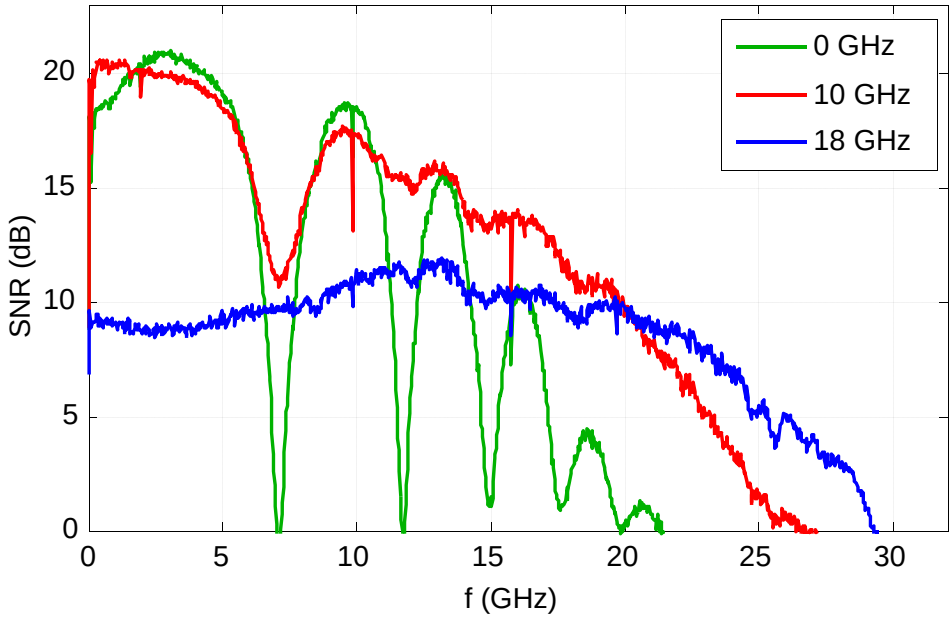

Figure 7.16: Estimated SNR for 0, 10 and 18 GHz of filter detuning and 80.5 km of SSMF.

analyzed link, CD is limited when comparing with the case of not doing any detuning. Furthermore, the BER performance comparison between DSB and VSB filtering after 162.1 km and 202 km fiber links is shown in Fig. 7.17(left) and Fig. 7.17 shows(right), respectively. Considering these fiber links, the optimum detuning of the tuneable filters of Fig. 7.8 are shifted to 12 GHz, according to Fig. 7.14. Hence, enhanced BER

performance in terms of OSNR after both fiber links is achieved by using VSB filtering when comparing with DSB transmission. Specifically, VSB filtering with 12 GHz detuning and 36 GHz filters requires 2 dB less OSNR, to ensure $4 \cdot 10^{-3}$ BER, than DSB transmission with 100 GHz filters.

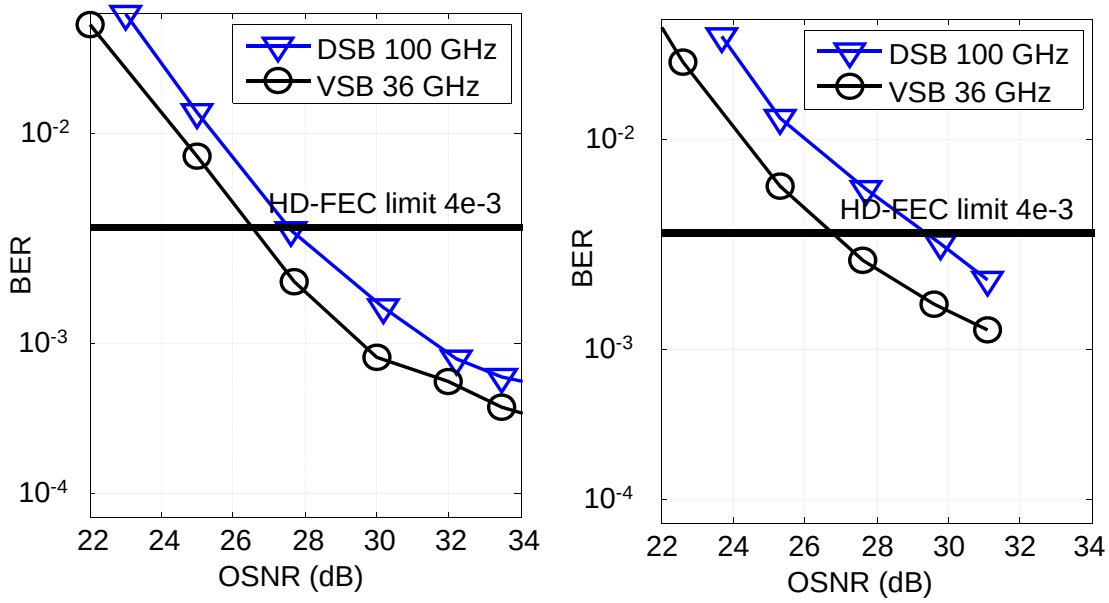

Figure 7.17: BER vs. OSNR after (left) 162.5 km of SSMF and (right) 202 km SSMF for a 100 GHz DSB and VSB signal.

The obtained results indicate that DMT is not only a solution for very short distances below 10 km, but also for short metro distances of up to 200 km with available OSNR slightly above 30 dB. However, in a network, the optical signal undergoes several nodes and several filters, causing the well-known cascaded effect. This effect will introduce different power penalties. Specially in a flexi-grid scenario, low data rate transmission will become highly affected when cascading low bandwidth filters. Hence, in order to limit the performance degradation due to the cascade filtering effect, the bandwidth and number of filters considering a certain fiber link should be analyzed [106].

7.3.2 Adaptive DMT systems performance

Here, the system performance in terms of BER is evaluated for different data rates. Initially, only the receiver of Fig.7.8 includes an optical filter of 100 GHz bandwidth to reduce the optical noise. It is worth mentioning that for enabling 400 Gb/s transmission, 112 Gb/s using 4 channels or 56 Gb/s using 8 channels can be considered. However, to analyze the performance at the increase of the rate, 76 Gb/s, 86 Gb/s and 96 Gb/s are also evaluated.

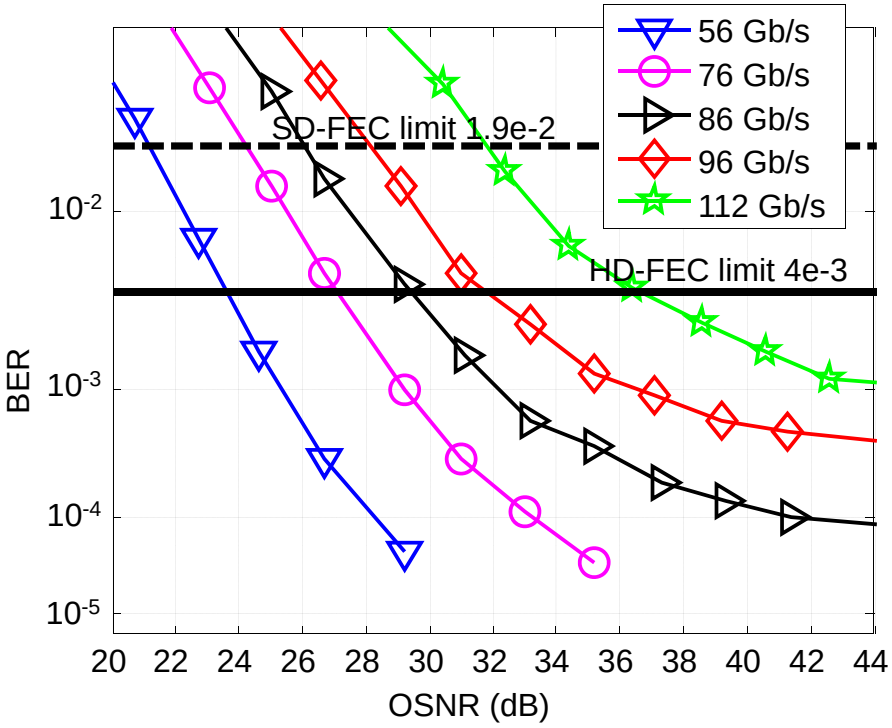

Figure 7.18: BER vs. OSNR for different data rates in a B2B configuration.

Specifically, in Fig. 7.18, the BER vs. OSNR at data rates ranging from 56 Gb/s to 112 Gb/s in the B2B configuration is depicted. It can be seen that 112 Gb/s can be transmitted ensuring a BER of $4 \cdot 10^{-3}$ with 38 dB OSNR. Additionally, in Fig. 7.19 the BER performance is analyzed after 81.6 km of SSMF. It can be shown that the transmission over 81.6 km increases the OSNR requirement. In particular, considering 56 Gb/s and the HD-FEC limit, about 4 dB more OSNR is required when comparing with the B2B case (from 23.5 dB to 27.7 dB). Moreover, HD-FEC limit can be ensured after 81.6 km of SSMF up to 76 Gb/s with 34 dB OSNR. Increasing the FEC overhead, 96 Gb/s transmission is experimentally validated ensuring the Soft Decision (SD)-FEC limit of $1.9 \cdot 10^{-2}$ with 36 dB OSNR.

To further investigate the effect of CD, the data rate is fixed to 56 Gb/s and the transmission distance is varied up to 200 km. Tunable optical filters are used, as a next step, before and after the transmission line. Both filters are set to equal bandwidths. Fig. 7.20 shows the required OSNR to ensure a target BER of $4 \cdot 10^{-3}$ when transmitting at 56 Gb/s and using 100 GHz and 36 GHz filters for different fiber links. $4 \cdot 10^{-3}$ BER can be ensured up to 50 km of SSMF with 34 dB OSNR for a DSB transmission. However increasing the filter bandwidth up to 100 GHz, the transmission reach is enhanced to 200 km ensuring the same target BER with 29 dB OSNR. Similar performance to DSB transmission using 100 GHz filters, in terms of achievable reach,

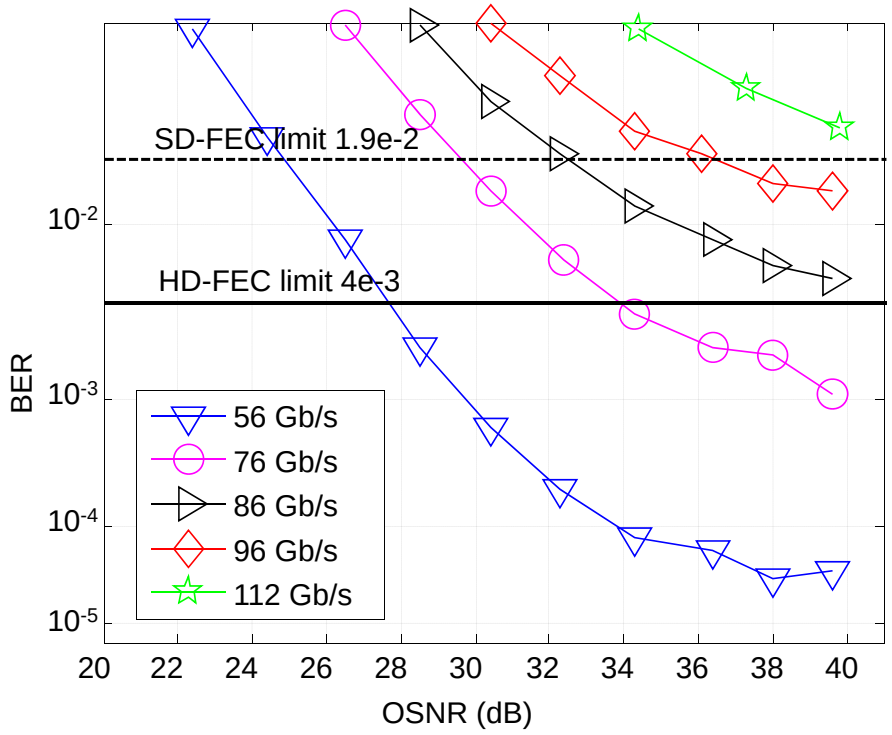

Figure 7.19: BER vs. OSNR for different data rates after 81.6 km of SSMF.

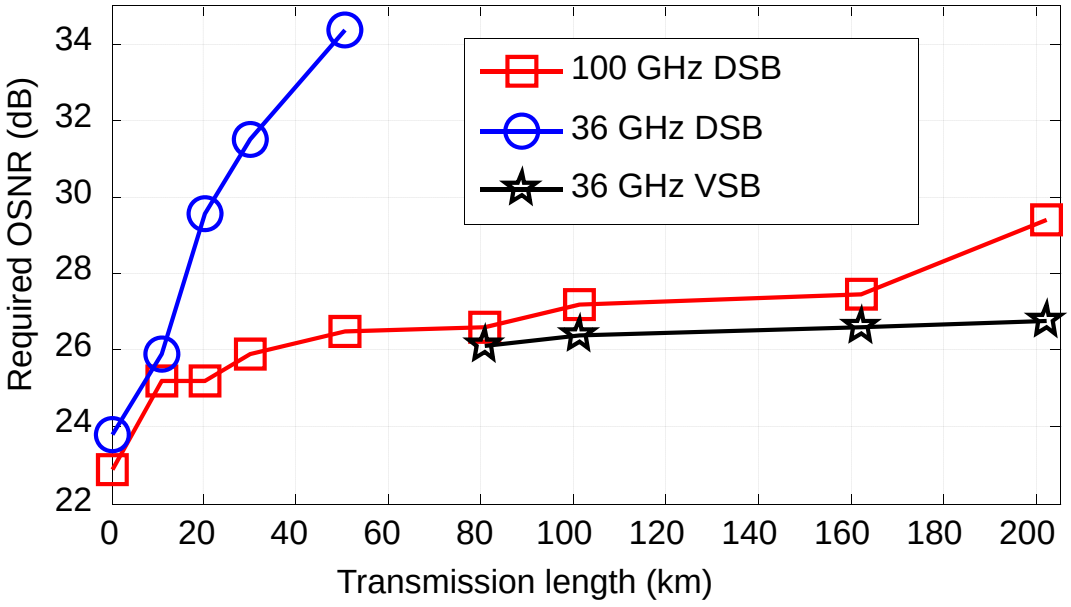

Figure 7.20: Required OSNR for $4 \cdot 10^{-3}$ BER vs. transmission reach at 56 Gb/s.

is obtained when VSB filtering is implemented with 36 GHz filters. Specifically, it is demonstrated that 56 Gb/s could be transmitted over up to 200 km of SSMF with about 27 dB OSNR. Hence, VSB filtering becomes a suitable solution to enhance both system performance and spectral efficiency. Additionally, from Fig. 7.20 it can be seen,

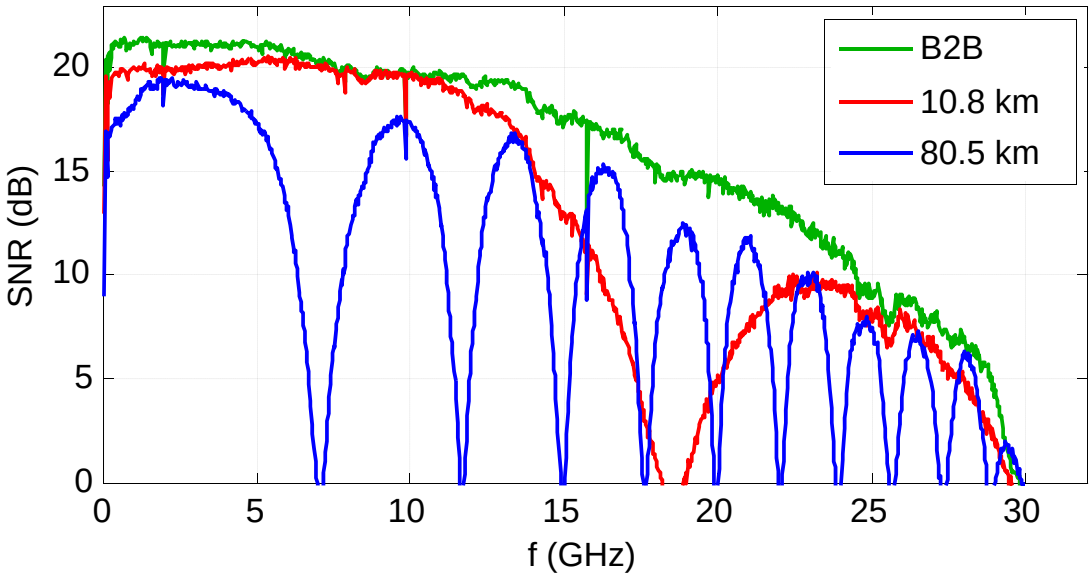

Figure 7.21: Estimated SNR for various SSMF lengths and 100 GHz filters.

that the highest penalty in terms of required OSNR to ensure $4 \cdot 10^{-3}$ BER, occurs after 20 km of fiber. This is due to the fact that CD occurs within the optical spectrum. For higher amounts of CD, the notches move closer together, but also have steeper edges so that the usable bandwidth is not significantly further decreased. This effect is illustrated in Fig. 7.21, where the estimated SNR using 100 GHz tuneable filters for the B2B, 10.8 km and 80.5 km of SSMF is depicted.

7.4 Summary

Here, in this chapter we have experimentally assessed high data rate DMT transmission based on the FFT over SSMF fiber using loading algorithms to overcome CD. Specifically, on the first part of the chapter we have demonstrated that:

- Numerical results are in good agreement with experimental ones at the presence of CD.
- An optical transmission of 56 Gb/s DMT (including 7% FEC overhead) over a dispersive and optically amplified link of up to 80 km of SSMF can be experimentally achieved.

Further experiments have been performed by transmitting DSB and VSB signals using optical filters achieving lower OSNR requirements and longer reach. CCB loading algorithm has been included in the transceiver design. The main conclusions from this chapter are listed below:

- VSB filtering with optimal detuned filters of 36 GHz bandwidth outperforms DSB transmission with either 36 GHz or 100 GHz filter bandwidths in terms of system performance.
- 56 Gb/s DMT transmission over up to 200 km of SSMF without optical dispersion compensation using VSB filtering with 36 GHz filters is experimentally demonstrated. Hence, combining 2 or 8 channels to a superchannel, 100 Gb/s or 400 Gb/s signals can be transmitted over high capacity flexi-grid network links as used for inter-data center interconnects.
- 96 Gb/s DMT transmission over 81.6 km of SSMF with VSB filters of 36 GHz bandwidth is experimentally validated.

8 Conclusions and future work

"The most compelling reason for most people to buy a computer for the home will be to link it to a nationwide communications network. We're just in the beginning stages of what will be a truly remarkable breakthrough for most people - as remarkable as the telephone."

Steve Jobs

This chapter concludes the present thesis, highlighting the main contributions of each chapter and providing guidelines for future investigation. Specifically, section 8.1 contains a summary of the conclusions extracted from this work. Finally, section 8.2 remarks the open investigation lines related to the current dissertation.

8.1 Conclusions

In this thesis we have proposed cost-effective solutions based on Direct Detection (DD), designing Digital Signal Processing (DSP)-enabled software-defined systems based on Orthogonal Frequency Division Multiplexing (OFDM) for Elastic Optical Networks (EON), limiting the Peak-to-Average Power Ratio (PAPR) and Chromatic Dispersion (CD). Adaptive Bandwidth Variable Transceiver (BVT) transceivers based on the Fast Hartley Transform (FHT) have been numerically and experimentally validated in a Metro Area Networks (MAN) scenario. Whereas, high speed Discrete MultiTone (DMT) transmission has been demonstrated over extended data center links. In the following we provide a summary of the main contributions for each of the chapters.

In **Chapter 3** we have introduced the PAPR problem as well as the clipping and quantization noise. The proposed low complexity PAPR reduction techniques based on the FHT mitigated all these impairments.

Thanks to the use of the FHT, low complexity distortionless PAPR reduction techniques have been easily applied to the system without any symmetry constraint. Additionally, the required number of transform blocks to create the OFDM symbols have been halved.

It has been seen that there is a trade off between PAPR mitigation and computational complexity. Thus, a solution using a single FHT block has been proposed without adding additional complexity to the DSP. Symmetrically clipping has also been included in the system model to further enhance the system performance. We have demonstrated that the proposed Low Complexity (LC) schemes with a single transform block allow mitigating the PAPR, clipping and quantization noise.

The proposed LC techniques have improved the system performance in terms of receiver sensitivity and power efficiency. At the same time, the constraints on the linear dynamic range of Digital-to-Analog Converter (DAC)/Analog-to-Digital Converter (ADC), drivers and modulators have been relaxed.

Hence, it has been demonstrated that PAPR reduction techniques limit the influence of such system impairments typical from an Optical-OFDM (O-OFDM) DD system. However, in order to do not highly increase the system complexity, the simplest PAPR reduction technique, which is the symmetrically clipping, has been selected to perform the numerical and experimental analysis of the subsequent chapters.

In **Chapter 4** and **Chapter 5**, we have proposed a BVT for rate and distance-adaptive transmission using Bit Loading (BL). The FHT has been selected to reduce the DSP complexity as allows a direct implementation of the real OFDM symbols without requiring any symmetry constraint. A first study in Additive White Gaussian Noise (AWGN) channel has been provided. Additionally, we have dealt with CD as the dominant limiting factor of Double-Side Band (DSB) transmission over Standard Single Mode Fiber (SSMF) in O-OFDM DD systems.

Loading schemes have resulted in a promising solution to overcome CD impairment when transmitting over SSMF. Improved system performance has been achieved by mapping the different subcarriers with different modulation formats and powers according to the channel profile.

The use of DSB modulation has further reduced the cost and complexity of the system implementation. Additionally, the guard band between the optical carrier and the OFDM signal has been reduced, enhancing the spectral efficiency and increasing the data rate.

The performance assessment of the proposed solution in a photonic mesh net-

work is also one major achievement of the present dissertation. As the target scenario can be flexi-grid MAN, the transceiver has been experimentally validated in the ADRENALINE testbed. It has been also proposed as a fundamental building block for future sliceable BVT. Specifically, a proof of concept of this capability has been experimentally demonstrated.

In **Chapter 6** and in **Chapter 7**, a DMT transceiver based on the Fast Fourier Transform (FFT) has been proposed to deal with the increasing traffic demand between data centers. CD and optical noise have been limited thanks to the application of loading algorithms. The FFT has been adopted to achieve fine granularity in the loading implementation. In fact, it enables the use of non-squared constellations such as 8QAM, 32QAM, 128QAM and 512QAM in the creation of the OFDM symbols.

High data rate transmission has been numerically and experimentally achieved covering fiber links up to 80 km of SSMF, resulting in a promising solution for data centers connections.

Optical filtering has been analyzed for fixed-grid and flexi-grid networks. The optical noise influence has been limited and the system performance has been enhanced in terms of achieved reach and required Optical Signal-to-Noise Ratio (OSNR) to ensure a target Bit Error Rate (BER). Optimal detunings for the VSB filters have been found for the analyzed links, achieving high data rate transmission over extended data center links.

The proposed solution has been experimentally validated, targeting next generation 400G data center inter-connections.

In general, either the FHT or the FFT can be used to create the OFDM symbols in a DD system. Both transforms achieve similar performances and enable the use of loading schemes, arising as suitable cost-effective solutions for EON.

8.2 Future work

The main open lines of investigation to continue the work performed in this dissertation are indicated in the following points:

- In order to further optimize the proposed DD system to overcome CD when transmitting over fiber, Single-Side Band (SSB) modulation can be performed. SSB transmission can be an interesting topic to study and exploit in O-OFDM based on either the FHT or the FFT. Despite requiring an additional optical

filter at the transmitter, better results in terms of achieved reach and supported data rate could be obtained.

- The proposed distortionless PAPR reduction techniques could be included in the adaptive transceiver. LC-SeLective Mapping (SLM) and LC-Partial Transmit Sequence (PTS) technique, using a single transform blocks, could be selected to limit the system complexity when also loading algorithms are implemented. An analysis of performance versus cost should be performed for targeting cost-sensitive applications.

- A FHT-based DMT system could be implemented, including loading algorithms, and compared to the FFT-based approach.

- Other work extensions can be performed by implementing OFDM-based solutions to support wireless signals delivery over high capacity optical networks.

- Additionally, an alternative investigation line is based on the coherent O-OFDM implementation, which can provide high data rate transmission in core networks at the expense of increased system complexity and cost.

Bibliography

[1] J. G. Proakis and M. Salehi, *Digital Communications*. McGraw-Hill Higher Education, 2008.

[2] S. H. Muller and J. B. Huber, "A comparison of peak power reduction schemes for OFDM," *IEEE Global Telecommunications Conference (GLOBECOM)*, pp. pp. 1–5, November 1997.

[3] Cisco, "Cisco visual networking index: Forecast and methodology," 2013. [Online]. Available: http://www.cisco.com/c/en/us/solutions/collateral/service-provider/ip-ngn-ip-next-generation-network/white_paper_c11-481360.pdf

[4] ——, "Cisco global cloud index: Forecast and methodology, 2012-2017," 2013. [Online]. Available: http://www.cisco.com/c/en/us/solutions/collateral/service-provider/global-cloud-index-gci/Cloud_Index_White_Paper.pdf

[5] "ITU-T recommendation G.975.1," 2004.

[6] I.-T. R. G.694.1, "Spectral grids for WDM applications: DWDM frequency grid," February 2012.

[7] M. Jinno, B. Kozicki, H. Takara, A. Watanabe, Y. Sone, T. Tanaka, and A. Hirano, "Distance-adaptive spectrum resource allocation in spectrum-sliced elastic optical path network [topics in optical communications]," *IEEE Communications Magazine*, vol. 48, no. 8, pp. 138–145, August 2010.

[8] E. Lach and W. Idler, "Modulation formats for 100g and beyond," *Optical Fiber Technology*, vol. 17, no. 5, pp. 377 – 386, 2011, 100G and Beyond. [Online]. Available: http://www.sciencedirect.com/science/article/pii/S1068520011001027

[9] W. Shieh and I. Djordjevic, *OFDM for Optical Communications*. Elsevier,USA, 2010.

[10] I. Tomkos, E. Palkopoulou, and M. Angelou, "A survey of recent developments on flexible/elastic optical networking," in *International Conference on Transparent Optical Networks (ICTON)*, July 2012, pp. 1–6.

[11] O. Gerstel, M. Jinno, A. Lord, and S. Yoo, "Elastic optical networking: a new dawn for the optical layer?" *IEEE Communications Magazine*, vol. 50, no. 2, pp. 12–20, February 2012.

[12] N. Amaya, G. S. Zervas, B. R. Rofoee, M. Irfan, Y. Qin, and D. Simeonidou, "Field trial of a 1.5 tb/s adaptive and gridless oxc supporting elastic 1000-fold all-optical bandwidth granularity," *Optics Express*, vol. 19, no. 26, pp. 235–241, December 2011. [Online]. Available: http://www.opticsexpress.org/abstract.cfm?URI=oe-19-26-B235

[13] R. W. Chang, "Synthesis of band-limited orthogonal signals for multichannel data transmission," *Bell System Technical Journal*, vol. 45, no. 10, pp. 1775–1796, August 1966. [Online]. Available: http://dx.doi.org/10.1002/j.1538-7305.1966.tb02435.x

[14] Q. Pan and R. Green, "Bit-error-rate performance of lightwave hybrid AM/OFDM systems with comparison with AM/QAM systems in the presence of clipping impulse noise," *IEEE Photonics Technology Letter*, vol. 8, no. 2, pp. 278–280, February 1996.

[15] R. Schmogrow, M. Winter, M. Meyer, D. Hillerkuss, S. Wolf, B. Baeuerle, A. Ludwig, B. Nebendahl, S. Ben-Ezra, J. Meyer, M. Dreschmann, M. Huebner, J. Becker, C. Koos, W. Freude, and J. Leuthold, "Real-time nyquist pulse generation beyond 100 gbit/s and its relation to ofdm," *Opt. Express*, vol. 20, no. 1, pp. 317–337, Jan 2012. [Online]. Available: http://www.opticsexpress.org/abstract.cfm?URI=oe-20-1-317

[16] X. Zhou and J. Yu, "Multi-level, multi-dimensional coding for high-speed and high-spectral-efficiency optical transmission," *J. Lightwave Technol.*, vol. 27, no. 16, pp. 3641–3653, Aug 2009. [Online]. Available: http://jlt.osa.org/abstract.cfm?URI=jlt-27-16-3641

[17] B. Lin, J. Li, H. Yang, Y. Wan, Y. He, and Z. Chen, "Comparison of DSB and SSB transmission for OFDM-PON," *Journal of Optical Communications and Networking (JOCN)*, vol. 4, no. 11, pp. 94–100, March 2012.

[18] E. Vanin, "Performance evaluation of intensity modulated optical OFDM system with digital baseband distortion," *Optics Express*, vol. 19, no. 5, pp. 4280–4293, 2011.

[19] L. Nadal, M. Svaluto Moreolo, J. M. Fabrega, and G. Junyent, "Clipping and quantization noise mitigation in intensity-modulated direct detection O-OFDM systems based on the FHT," in *International Conference on Transparent Optical Networks (ICTON)*, 2012.

[20] D. Barros, S. Wilson, and J. Kahn, "Comparison of orthogonal frequency-division multiplexing and pulse-amplitude modulation in indoor optical wireless links," *IEEE Transaction on Communications*, vol. 60, no. 1, pp. 153 –163, January 2012.

[21] M. Moreolo, R. Muñoz, and G. Junyent, "Novel power efficient optical OFDM based on hartley transform for intensity-modulated direct-detection systems," *Journal of Lightwave Technology*, vol. 28, no. 5, pp. 798 –805, March 2010.

[22] W. Shieh and C. Athaudage, "Coherent optical orthogonal frequency division multiplexing," *Electronics Letter*, vol. 42, no. 10, pp. 587 – 589, May 2006.

[23] A. Lowery and J. Armstrong, "Orthogonal-frequency-division multiplexing for dispersion compensation of long-haul optical systems," *Optics Express*, vol. 14, no. 6, pp. 2079–2084, March 2006. [Online]. Available: http://www.opticsexpress.org/abstract.cfm?URI=oe-14-6-2079

[24] W. Yan, T. Tanaka, B. Liu, M. Nishihara, L. Li, T. Takahara, Z. Tao, J. Rasmussen, and T. Drenski, "100 Gb/s optical IM-DD transmission with 10G-class devices enabled by 65 GS/s CMOS DAC core," in *Optical Fiber Communication Conference and Exposition and the National Fiber Optic Engineers Conference (OFC/NFOEC)*, 2013.

[25] B. Schmidt, A. Lowery, and J. Armstrong, "Experimental demonstrations of electronic dispersion compensation for long-haul transmission using direct-detection optical OFDM," *Journal of Lightwave Technology*, vol. 26, no. 1, pp. 196 –203, January 2008.

[26] A. Dochhan, L. Nadal, H. Griesser, M. Eiselt, M. Svaluto Moreolo, and J. P. Elbers, "Discrete multitone transmission in the presence of optical noise, chromatic dispersion and narrow-band optical filtering," in *ITG Fachtagung Sprachkommunikation*, September 2014.

[27] J. Cioffi, *Data Transmission Theory.* Chapter 4 of Course text for EE379A-B and EE479. [Online]. Available: www.stanford.edu/group/cioffi/book/

[28] "IEEE standard for ethernet," *IEEE 802.3*, December 2012.

[29] C. Cole, "Beyond 100G client optics," *IEEE Communications Magazine*, vol. 50, no. 2, pp. 58–66, February 2012.

[30] C. Cole, I. Lyubomirsky, A. Ghiasi, and V. Telang, "Higher-order modulation for client optics," *IEEE Communications Magazine*, vol. 51, no. 3, pp. 50–57, March 2013.

[31] P. Winzer, "Beyond 100G Ethernet," *IEEE Communications Magazine*, vol. 48, no. 7, pp. 26–30, 2010.

[32] Y. Qiao, Q. Li, and Y. Ji, "400 gbps WDM transmission over short range with discrete multi-tone," *Optik - International Journal for Light and Electron Optics*, no. 0, pp. –, 2014. [Online]. Available: http://www.sciencedirect.com/science/article/pii/S003040261400761X

[33] D. Guckenberger, S. Abdalla, C. Bradbury, J. Clymore, P. de Dobbelaere, D. Foltz, S. Gloeckner, M. Harrison, S. Jackson, D. Kucharski, Y. Liang, C. Lo, M. Mack, G. Masini, A. Mekis, A. Narasimha, M. Peterson, T. Pinguet, J. Redman, S. Sahni, B. Welch, K. Yokoyama, and S. Yu, "Advantages of CMOS photonics for future transceiver applications," in *European Conference and Exhibition on Optical Communication (ECOC)*, Sept 2010, pp. 1–6.

[34] J. Vizcaino, Y. Ye, V. Lopez, F. Jimenez, R. Duque, and P. Krummrich, "Cost evaluation for flexible-grid optical networks," in *IEEE Globecom Workshops (GC Wkshps)*, Dec 2012, pp. 358–363.

[35] J. Armstrong, "OFDM: From copper and wireless to optical," in *Optical Fiber Communication Conference and Exposition and the National Fiber Optic Engineers Conference (OFC/NFOEC)*, February 2008, pp. 1–27.

[36] H. Takahashi, A. Al Amin, S. Jansen, I. Morita, and H. Tanaka, "Highly spectrally efficient DWDM transmission at 7.0 b/s/Hz using 8x65.1-gb/s coherent PDM-OFDM," *Journal of Lightwave Technology*, vol. 28, no. 4, pp. 406–414, February 2010.

[37] P. Duhamel and M. Vetterli, "Improved fourier and hartley transform algorithms: Application to cyclic convolution of real data," *International Conference*

on Acoustics, Speech and Signal Processing (ICASSP), vol. 35, no. 6, pp. 818 – 824, June 1987.

[38] Infinera, "Coherent DWDM technologies," in *White paper*, 2012.

[39] D. Torrientes, P. Chanclou, F. Laurent, S. Tsyier, Y. Chang, B. Charbonnier, and C. Kazmierski, "10Gbit/s for next generation PON with electronic equalization using un-cooled 1.55 μm directly modulated laser," in *European Conference on Optical Communication (ECOC)*, 2009.

[40] R. Giddings, E. Hugues-Salas, and J. Tang, "Experimental demonstration of record high 19.125Gb/s real-time end-to-end dual-band optical OFDM transmission over 25km SMF in a simple EML-based IMDD system," *Opt. Express*, vol. 20, no. 18, pp. 20 666–20 679, August 2012. [Online]. Available: http://www.opticsexpress.org/abstract.cfm?URI=oe-20-18-20666

[41] M. Chacinski, U. Westergren, L. Thylen, B. Stoltz, J. Rosenzweig, R. Driad, R.-E. Makon, J. Li, and A. Steffan, "ETDM transmitter module for 100-Gb/s ethernet," *IEEE Photonics Technology Letter*, vol. 22, no. 2, pp. 70–72, 2010.

[42] L. A. Neto, P. Chanclou, N. Brochier, N. Genay, J. luc Barbey, B. Charbonnier, S. Gosselin, A. Gharba, F. Saliou, M. Ouzzif, C. Aupetit-Berthelemot, J. L. Masson, E. Grard, and V. Rodrigues, "10Gb/s over 513km uncompensated SSMF link using direct modulation and direct detection." Optical Society of America, 2011, p. We.8.B.3. [Online]. Available: http://www.opticsinfobase.org/abstract.cfm?URI=ECOC-2011-We.8.B.3

[43] S. Chandrasekhar, C. Doerr, L. Buhl, D. Mahgerefteh, Y. Matsui, B. Johnson, C. Liao, X. Zheng, K. McCallion, Z. Fan, and P. Tayebati, "Flexible transport at 10-Gb/s from 0 to 675km (11,500 ps/nm) using a chirp-managed laser, no DCF, and a dynamically adjustable dispersion-compensating receiver," in *Optical Fiber Communication Conference and Exposition and the National Fiber Optic Engineers Conference (OFC/NFOEC)*, vol. 6, 2005.

[44] B. Schmidt, A. Lowery, and L. Du, "Low sample rate transmitter for direct-detection optical OFDM," in *Optical Fiber Communication Conference (OFC)*, March 2009, pp. 1–3.

[45] B. J. Schmidt, A. J. Lowery, and J. Armstrong, "Experimental demonstrations of 20 Gbit/s direct-detection optical OFDM and 12 Gbit/s with a colorless transmitter," in *Optical Fiber Communication Conference and Exposition and the National Fiber Optic Engineers Conference (OFC/NFOEC)*, 2007, p. PDP18.

[46] X. Liang, W. Li, W. Ma, and K. Wang, "A simple peak-to-average power ratio reduction scheme for all optical orthogonal frequency division multiplexing systems with intensity modulation and direct detection," *Optics Express*, vol. 17, no. 18, pp. 15 614–15 622, 2009. [Online]. Available: http://www.opticsexpress.org/abstract.cfm?URI=oe-17-18-15614

[47] R. Lee, Breyer, Boom, and Koonen, "High-speed transmission over multimode fiber using discrete multitone modulation," *Journal of Optical Networking*, vol. 7, no. 2, p. 183, 2008. [Online]. Available: http://repository.tue.nl/649709

[48] J. Armstrong and B. Schmidt, "Comparison of asymmetrically clipped optical OFDM and DC-biased optical OFDM in AWGN," *IEEE Communications Letter*, vol. 12, no. 5, pp. 343 –345, May 2008.

[49] R. N. Bracewell, "Discrete hartley transform," *Journal of the Optical Society of America*, vol. 73, no. 12, pp. 1832–1835, December 1983. [Online]. Available: http://www.opticsinfobase.org/abstract.cfm?URI=josa-73-12-1832

[50] P. Duhamel, "Implementation of "split-radix" FFT algorithms for complex, real, and real-symmetric data," *International Conference on Acoustics, Speech and Signal Processing (ICASSP)*, vol. 34, no. 2, pp. 285 – 295, April 1986.

[51] M. Svaluto Moreolo, J. M. Fabrega, F. J. Vilchez, L. Nadal, and G. Junyent, "Experimental demonstration of a cost-effective bit rate variable intensity modulation and direct detection optical OFDM with reduced guard band," *European Conference on Optical Communication (ECOC)*, September 2012.

[52] M. Svaluto Moreolo, "Performance analysis of DHT-based optical OFDM using large-size constellations in AWGN," *IEEE Communications Letter*, vol. 15, no. 5, pp. 572 –574, 2011.

[53] M. S. Moreolo, J. M. Fàbrega, F. J. Vílchez, L. Nadal, and G. Junyent, "Experimental demonstration of a cost-effective bit rate variable IM/DD optical OFDM with reduced guard band," *Optics Express*, vol. 20, no. 26, pp. 159–164, December 2012. [Online]. Available: http://www.opticsexpress.org/abstract.cfm?URI=oe-20-26-B159

[54] G. P. Agrawal, *Fiber-Optic Communication Systems*. John Wiley and Sons, 2012.

[55] ——, *Nonlinear Fiber Optics*. Elsevier, 2007.

[56] B. Lin, J. Li, H. Yang, Y. Wan, Y. He, and Z. Chen, "Comparison of DSB and SSB transmission for OFDM-PON," *Journal of Optical Communications and Networking (JOCN)*, vol. 4, no. 11, pp. 94–100, November 2012. [Online]. Available: http://jocn.osa.org/abstract.cfm?URI=jocn-4-11-B94

[57] S. L. Jansen, B. Spinnler, I. Morita, S. Randel, and H. Tanaka, "100GbE: QPSK versus OFDM," *Optical Fiber Technology*, vol. 15, pp. 407 – 413, 2009.

[58] C. Wang, C. Chang, J. Fan, and J. Cioffi, "Discrete Hartley transform based multicarrier modulation," in *IEEE International Conference on Acoustics, Speech and Signal Processing (ICASSP)*, vol. 5, 2000, pp. 2513 – 2516.

[59] D. Wang, D. Liu, F. Liu, and G. Yue, "A novel DHT-based ultra-wideband system," in *IEEE International Symposium on Communications and Information Technologies (ISCIT)*, vol. 50, 2005, pp. 172–184.

[60] T. Schmidl and D. Cox, "Robust frequency and timing synchronization for OFDM," *IEEE Transaction on Communications*, vol. 45, no. 12, pp. 1613–1621, December 1997.

[61] H. Minn and V. Bhargava, "A simple and efficient timing offset estimation for OFDM systems," in *IEEE Vehicular Technology Conference (VTC)*, vol. 1, 2000, pp. 51–55.

[62] P. H. Moose, "A technique for orthogonal frequency division multiplexing frequency offset correction," *IEEE Transactions on Communications*, vol. 42, no. 10, pp. 2908–2914, October 1994.

[63] S. D. Choi, J. M. Choi, and J. H. Lee, "An initial timing offset estimation method for OFDM systems in rayleigh fading channel," in *IEEE Vehicular Technology Conference (VTC)*, September 2006, pp. 1–5.

[64] J. Leibrich, A. Ali, H. Paul, W. Rosenkranz, and K.-D. Kammeyer, "Impact of modulator bias on the OSNR requirement of direct-detection optical OFDM," *IEEE Photonics Technology Letter*, vol. 21, no. 15, pp. 1033 –1035, August 2009.

[65] S. H. Han and J. H. Lee, "An overview of peak-to-average power ratio reduction techniques for multicarrier transmission," *IEEE Wireless Communications*, vol. 12, no. 2, pp. 56 – 65, 2005.

[66] B. Krongold, Y. Tang, and W. Shieh, "Fiber nonlinearity mitigation by PAPR reduction in coherent optical OFDM systems via active constellation extension," in *European Conference on Optical Communication (ECOC)*, 2008, pp. 1 –2.

[67] L. Nadal, M. Svaluto Moreolo, J. M. Fabrega, and G. Junyent, "Comparison of peak power reduction techniques in optical OFDM systems based on FFT and FHT," in *International Conference on Transparent Optical Networks (ICTON)*, no. We.A1.5, 2011.

[68] L. Chen, B. Krongold, and J. Evans, "A tone reservation-based optical OFDM system for short-range IM/DD transmission," *Journal of Lightwave Technology*, vol. volume 29, no. 24, pp. pp.3824 –3833, 2011.

[69] E. Vanin, "Signal restoration in intensity-modulated optical ofdm access systems," *Optics Letter*, vol. 36, pp. 4338–4340, 2011.

[70] B. Ranjha and M. Kavehrad, "Precoding techniques for PAPR reduction in asymmetrically clipped OFDM based optical wireless system," in *SPIE*, vol. 8645, 2013.

[71] B. Goebel, S. Hellerbrand, N. Haufe, and N. Hanik, "PAPR reduction techniques for coherent optical OFDM transmission," in *International Conference on Transparent Optical Networks (ICTON)*, 2009, pp. 1 –4.

[72] M. El Tabach, P. Tortelier, R. Pyndiah, and O. Bouchet, "On free-space optic communication with alamouti-type coding and direct detection," in *International Symposium on Wireless Pervasive Computing*, 2008, pp. 740 –743.

[73] J.-K. Sang-Woo and Heung-Gyoon, "PAPR reduction of the OFDM signal by the SLM-based WHT and DSI method," in *IEEE TENCON*, 2006, pp. 1 –4.

[74] I. Baig and V. Jeoti, "DCT precoded SLM technique for PAPR reduction in OFDM systems," in *International Conference on Intelligent and Automation Systems (ICIAS)*, June 2010, pp. 1 –6.

[75] H. Taga, "A theoretical study of OFDM system performance with respect to subcarrier numbers," *Optics Express*, vol. 17, no. 21, pp. 18 638–18 642, October 2009.

[76] C. Tellambura, "Computation of the continuous-time PAR of an OFDM signal with BPSK subcarriers," *IEEE Communications Letter*, vol. 5, no. 5, pp. 185 –187, May 2001.

[77] R. Bäuml, R. F. H. Fischer, and J. B. Huber, "Reducing the peak-to-average power ratio of multicarrier modulation by selected mapping," *Electronics Letter*, vol. volume 32, pp. pp.2056–2057, 1996.

[78] A. Jayalath and C. Tellambura, "Reducing the peak-to-average power ratio of orthogonal frequency division multiplexing signal through bit or symbol interleaving," *Electronics Letter*, vol. volume 36, no. no.13, pp. 1161 –1163, June 2000.

[79] S. Muller and J. Huber, "OFDM with reduced peak-to-average power ratio by optimum combination of partial transmit sequences," *Electronics Letter*, vol. volume 33, no. no.5, pp. 368 –369, February 1997.

[80] ——, "A novel peak power reduction scheme for OFDM," in *IEEE International Symposium on Personal, Indoor and Mobile Radio Communications (PIMRC)*, vol. 3, September 1997, pp. 1090 –1094.

[81] M. Svaluto Moreolo, L. Nadal, J. M. Fabrega, and G. Junyent, "FHT-based architectures for multicarrier modulation in direct detection and coherent optical systems," in *International Conference on Transparent Optical Networks (ICTON)*, no. We.A1.1, 2011.

[82] S. A. Aburakhia, E. F. Bradan, and D. A. Mohamed, "Distribution of the PAPR for real-valued OFDM signals," in *International Conference on Information Technology (ICIT)*, June 2009.

[83] Q. Yang, W. Shieh, and Y. Ma, "Bit and power loading for coherent optical OFDM," *IEEE Photonics Technology Letters*, vol. 20, no. 15, pp. 1305 –1307, August 2008.

[84] H. Paul and K. D. Kammeyer, "Subcarrier selection for IM/DD OFDM systems," in *European Conference on Optical Communication (ECOC)*, 2009, p. P3.11.

[85] R. F. H. Fischer and J. Huber, "A new loading algorithm for discrete multitone transmission," in *Communications: The Key to Global Prosperity Global Telecommunications Conference, GLOBECOM*, vol. 1, November 1996, pp. 724–728.

[86] G. Gallager, *Information Theory and Reliable Communication*. Wiley, 1969.

[87] R. Schmogrow, M. Winter, D. Hillerkuss, B. Nebendahl, S. Ben-Ezra, J. Meyer, M. Dreschmann, M. Huebner, J. Becker, C. Koos, W. Freude, and J. Leuthold, "Real-time ofdm transmitter beyond 100 gbit/s," *Opt. Express*, vol. 19, no. 13, pp. 12 740–12 749, Jun 2011. [Online]. Available: http://www.opticsexpress.org/abstract.cfm?URI=oe-19-13-12740

[88] C. Kachris, E. Giacoumidis, and I. Tomkos, "Energy-efficiency study of optical ofdm in data centers," in *Optical Fiber Communication Conference and Exposition and the National Fiber Optic Engineers Conference (OFC/NFOEC)*, March 2011, pp. 1–3.

[89] P. Chow, J. Cioffi, and J. A. C. Bingham, "A practical discrete multitone transceiver loading algorithm for data transmission over spectrally shaped channels," *IEEE Transaction on Communications*, vol. 43, no. 234, pp. 773–775, 1995.

[90] R. Munoz, C. Pinart, R. Martinez, J. Sorribes, G. Junyent, and A. Amrani, "The adrenaline testbed: integrating GMPLS, XML, and SNMP in transparent DWDM networks," *IEEE Communications Magazine*, vol. 43, no. 8, pp. 40–48, August 2005.

[91] M. Jinno, Y. Sone, H. Takara, A. Hirano, K. Yonenaga, and S. Kawai, "Ip traffic offloading to elastic optical layer using multi-flow optical transponder," in *European Conference and Exposition on Optical Communications*. Optical Society of America, 2011, p. Mo.2.K.2.

[92] R. Merched, "On ofdm and single-carrier frequency-domain systems based on trigonometric transforms," *IEEE Signal Processing Letters*, vol. 13, no. 8, pp. 473–476, August 2006.

[93] A. Ali, J. Leibrich, and W. Rosenkranz, "Spectral efficiency and receiver sensitivity in direct detection optical-ofdm," in *Optical Fiber Communication Conference (OFC)*, 2009.

[94] T. Takahara, T. Tanaka, M. Nishihara, Y. Kai, L. Li, Z. Tao, and J. C. Rasmussen, "Discrete multi-tone for 100 Gb/s optical access networks," in *Optical Fiber Communication Conference and Exposition and the National Fiber Optic Engineers Conference (OFC/NFOEC)*, 2014, p. M2I.1.

[95] T. Takahara, T. Tanaka, M. Nishihara, L. Lei, T. Zhenning, and J. Rasmussen, "100 gb/s (2×50 Gb/s) transmission over 80 km using 10 gb/s class DML," in *Opto-Electronics and Communications Conference (OECC)*, July 2012, pp. 417–418.

[96] W. Yan, L. Li, B. Liu, H. Chen, Z. Tao, T. Tanaka, T. Takahara, J. C. Rasmussen, and T. Drenski, "80 km IM-DD transmission for 100 Gb/s per lane enabled by DMT and nonlinearity management," in *Optical Fiber Communication Conference and Exposition and the National Fiber Optic Engineers Conference (OFC/NFOEC)*, 2014, p. M2I.4.

[97] T. Tanaka, M. Nishihara, T. Takahara, W. Yan, L. Li, Z. Tao, M. Matsuda, K. Takabayashi, and J. C. Rasmussen, "Experimental demonstration of 448 gbps+ DMT transmission over 30 km SMF," in *Optical Fiber Communication Conference and Exposition and the National Fiber Optic Engineers Conference (OFC/NFOEC)*, 2014, p. M2I.5.

[98] C. Milion, T. Duong, N. Genay, E. Grard, V. Rodrigues, B. Charbonnier, J. Le Masson, M. Ouzzif, P. Chanclou, and A. Gharba, "High bit rate transmission for NG-PON by direct modulation of DFB laser using discrete multi-tone," in *European Conference on Optical Communication (ECOC)*, September 2009, pp. 1–2.

[99] T. Tanaka, M. Nishihara, T. Takahara, L. Li, Z. Tao, and J. Rasmussen, "50 Gbps class transmission in single mode fiber using discrete multi-tone modulation with 10G directly modulated laser," in *Optical Fiber Communication Conference and Exposition and the National Fiber Optic Engineers Conference (OFC/NFOEC)*, 2012.

[100] S. Randel, F. Breyer, S. C. J. Lee, and J. Walewski, "Advanced modulation schemes for short-range optical communications," *IEEE Jornal of Selected Topics in Quantum Electronics*, vol. 16, no. 5, pp. 1280–1289, September 2010.

[101] T. Mizuochi, Y. Konishi, Y. Miyata, T. Inoue, K. Onohara, S. Kametani, T. Sugihara, K. Kubo, T. Kobayashi, H. Yoshida, and T. Ichikawa, "Fpga based prototyping of next generation forward error correction," in *European Conference on Optical Communication (ECOC)*, 2009.

[102] G. Zhang, L. Nelson, Y. Pan, M. Birk, C. Skolnick, C. Rasmussen, M. Givehchi, B. Mikkelsen, T. Scherer, T. Downs, and W. Keil, "3760km, 100G SSMF transmission over commercial terrestrial DWDM ROADM systems using SD-FEC," in *Optical Fiber Communication Conference and Exposition and the National Fiber Optic Engineers Conference (OFC/NFOEC)*, March 2012, pp. 1–3.

[103] "ITU-T recommendation G.975," 2000.

[104] Fujitsu, "Leia 55 65 GSa/s 8-bit DAC," *Fact sheet*. [Online]. Available: http://www.fujitsu.com/downloads/MICRO/fme/documentation/c60.pdf

[105] ——, "CMOS 14-bit MB86066 anakin DAC." [Online]. Available: http://phys.org/news/2012-02-fujitsu-world-fastest-cmos-bit.html

[106] M. Chochol, J. Fabrega, M. Svaluto Moreolo, and G. Junyent, "Optical filter cascading effects in a phase modulated coherent optical ofdm transmission system based on hartley transform," in *Transparent Optical Networks (ICTON), 2012 14th International Conference on*, July 2012, pp. 1–4.